

Sheffield Hallam University

Incipient corrosion in concrete repair.

PEET, Matthew.

Available from the Sheffield Hallam University Research Archive (SHURA) at:

<http://shura.shu.ac.uk/20216/>

A Sheffield Hallam University thesis

This thesis is protected by copyright which belongs to the author.

The content must not be changed in any way or sold commercially in any format or medium without the formal permission of the author.

When referring to this work, full bibliographic details including the author, title, awarding institution and date of the thesis must be given.

Please visit <http://shura.shu.ac.uk/20216/> and <http://shura.shu.ac.uk/information.html> for further details about copyright and re-use permissions.

CITY CAMPUS, HOWARD STREET
SHEFFIELD S1 1WB

101 755 598 2



Fines are charged at 50p per hour

- JUN 2005

17.00

SHEFFIELD HALLAM UNIVERSITY
LIBRARY CENTRE
100, FORD STREET,
SHEFFIELD S1 1WB.

REFERENCE

ProQuest Number: 10700861

All rights reserved

INFORMATION TO ALL USERS

The quality of this reproduction is dependent upon the quality of the copy submitted.

In the unlikely event that the author did not send a complete manuscript and there are missing pages, these will be noted. Also, if material had to be removed, a note will indicate the deletion.



ProQuest 10700861

Published by ProQuest LLC (2017). Copyright of the Dissertation is held by the Author.

All rights reserved.

This work is protected against unauthorized copying under Title 17, United States Code
Microform Edition © ProQuest LLC.

ProQuest LLC.
789 East Eisenhower Parkway
P.O. Box 1346
Ann Arbor, MI 48106 – 1346

Incipient Corrosion in Concrete Repair

Matthew Peet

A thesis submitted in partial fulfilment of the requirements of
Sheffield Hallam University for the degree of Doctor of Philosophy

October 2003



Acknowledgement

The author would like to acknowledge the help of the staff of the School of Construction, now School of Environment and Development, at Sheffield Hallam University in the preparation of this thesis. In particular I would like to thank Prof. P.S. Mangat for his guidance and supervision of the project and Dr. P. Lambert for his help in reviewing and editing the final thesis.

I would also like to thank the technicians in the School of Environment and Development for their help in the experimental work in the project, in particular Geoff Harwood and Bob Skelton in the Concrete Laboratory at the University.

I would also like to thank my wife for giving me the love, encouragement and sacrifice, that gave me the courage and determination to *finally* complete the thesis.

Abstract

One of the main causes of deterioration of reinforced concrete structures is the corrosion of the reinforcement. This may be as a result of carbonation or chloride diffusion into the concrete. During the lifetime of any reinforced concrete structure it is likely to require maintenance and repair. Repair materials are used as a form of "corrosion prevention" on deteriorated areas of a structure. The properties of the repair material offer maximum protection to the steel at the repair. Combining two cementitious materials with different properties can create a difference in oxygen or chloride concentration between two materials, creating a galvanic cell. Matching the physical properties of the repair and substrate materials may mitigate the corrosion of the reinforcement. The theoretical and experimental work to support the idea of matching properties is currently limited.

This project has examined the effect of combining repair and substrate materials with different physical properties on the corrosion of reinforcement embedded in these materials. The initial part of the experimental programme examined the physical properties of typical repair and substrate materials to quantify the range of the properties. This concentrated on mass-transport properties such as, the density, porosity, permeability, chloride diffusion and resistivity of each material. The electrochemical compatibility of the materials was measured using potentiodynamic polarisation measurements. This showed that steel embedded in materials with lower permeability coefficients had lower corrosion potentials. The permeability and chloride concentration in the materials were used to produce test specimens with range of differences in cell potentials between the steel embedded in the repair and substrate materials. The specimens of the different repair substrate combinations were exposed to a saline solution for twelve months. Measurements of the resistivity, half-cell potentials and corrosion currents of the specimens monitored with time assess the corrosion rate of the specimens. Two methods were used to measure corrosion currents, impedance spectroscopy and linear polarisation resistance.

The half-cell potential measurements indicated that a low permeability material would be anodic when combined with a high permeability material, which would be cathodic. The corrosion current of the material identified as anodic by half-cell potentials was higher for larger mismatch in permeability. This indicated a higher corrosion rate in the anodic material for substrate repair combinations that result in large differences in half-cell potentials. This would suggest that a galvanic cell was formed due to oxygen concentration differences between the repair and substrate materials.

The results from the experimental work were used to model the distribution of current between the anodic and cathodic sites. The model shows that it is the difference in potential that has the greatest influence on the current flowing in the cell and the resistivity of the material controls the distribution of the current within the cell. This indicated that corrosion would be concentrated at the interface between the repair and substrate material with the low permeability material being anodic. The study shows that the corrosion resulting from a disparity in properties between repair and substrate materials is likely to be small. However higher corrosion rates may occur at the interface between repair and substrate that may require additional corrosion protection systems to be used. Matching the permeabilities of materials would not be practical, as permeability has been found to change with time altering the match between repair and substrate.

Incipient Corrosion in Concrete Repair

Table of Contents

Contents	i
List of Figures	v
List of Table	xi
1. Introduction	1
1.1 SCOPE OF RESEARCH	3
1.2 SCOPE OF CURRENT WORK	3
1.3 THESIS STRUCTURE	4
2. Literature Review	6
2.1 REPAIR MATERIALS	6
2.1.1 Nature of Repair Materials	10
2.1.2 Properties of Repair Materials	12
2.1.3 Effect of Property Mismatch	14
2.2 CORROSION OF REINFORCEMENT IN CONCRETE	20
2.2.1 Electrochemistry of Corrosion	20
2.2.2 Passivity of Steel in Concrete	28
2.2.3 Carbonation	30
2.2.4 Chloride Induced Corrosion	32
2.2.5 Chloride Induced Macro-cell Corrosion	36
2.2.6 Differential Aeration	42
2.3 MASS TRANSPORT IN CONCRETE	47
2.3.1 Porosity	47
2.3.2 Permeability	50
2.3.3 Chloride Diffusion	55
2.3.4 Oxygen Diffusion	63
2.4 MODELLING OF CORROSION IN REINFORCED CONCRETE	66
2.5 ELECTROCHEMICAL TEST METHODS	70
2.5.1 Half-cell Potentials	72
2.5.2 Potentiodynamic and Potentiostatic Polarisation Curves	75
2.5.3 Linear Polarisation Resistance	79
2.5.4 Impedance Spectroscopy	83
2.5.5 Galvanic Corrosion Currents	92
2.5.6 Resistivity	95
2.5.7 Other Techniques	99
3. Introduction to experimental work	100
3.1 INTRODUCTION	100
3.2 AIMS AND OBJECTIVES OF THE EXPERIMENTAL PROGRAMME	101
3.3 EXPERIMENTAL PROGRAMME	102

Table of Contents

3.4	TEST MATERIALS	103
3.4.1	<i>Repair Materials</i>	103
3.4.1.1	<i>Repair Material A</i>	103
3.4.1.2	<i>Repair Material B</i>	105
3.4.1.2	<i>Repair Material C</i>	105
3.4.2	Substrate Concrete Mixes	106
3.4.2.1	<i>Ordinary Portland Cement</i>	107
3.4.2.2	<i>Sand</i>	108
3.4.2.3	<i>Coarse Aggregate</i>	110
4.	Physical Properties of substrate and repair materials	111
4.1	INTRODUCTION	111
4.2	POROSITY	111
4.2.1	Introduction	111
4.2.2	Experimental Procedure	112
4.2.2.1	<i>Test Materials</i>	112
4.2.2.2	<i>Test Specimens</i>	112
4.2.2.3	<i>Experimental Technique</i>	113
4.2.2.4	<i>Calculations</i>	113
4.2.3	Results and Discussion	116
4.2.4	Conclusions	117
4.3	PERMEABILITY	120
4.3.1	Introduction	120
4.3.2	Permeater Apparatus	120
4.3.3	Operating Parameters	123
4.3.4	Experimental Conditions	124
4.3.5	Darcy Coefficient of Permeability	128
4.3.6	Materials and Test Specimens	128
4.3.7	Results and Discussion	130
4.3.7.1	<i>Permeability of Test Materials</i>	130
4.3.7.2	<i>Level of Mismatch in Materials</i>	131
4.3.8	Conclusions	134
4.4	CHLORIDE DIFFUSION	139
4.4.1	Test Materials	139
4.4.2	Test Specimen Preparation	139
4.4.3	Test Method for Chloride Contamination and pH	140
4.4.4	Chloride Diffusion Coefficients	143
4.4.5	Results and Discussions	148
4.4.6	Conclusions	150
4.5	RESISTIVITY	152
4.5.1	Introduction	152
4.5.2	Experimental Procedure	152
4.5.2.1	<i>Test Materials</i>	152
4.5.2.2	<i>Test Specimens</i>	153
4.5.2.3	<i>Experimental Techniques</i>	154
4.5.3	Results and Discussions	154
4.5.4	Conclusions	155

Table of Contents

4.6	DISPARITY IN PROPERTIES BETWEEN REPAIR AND SUBSTRATE MATERIALS	157
4.6.1	Introduction	157
4.6.2	Porosity and Permeability	158
4.6.3	Permeability and Chloride Diffusion Coefficient	160
4.6.4	Conclusions	163
5.	Corrosion Testing	164
5.1	CORROSION TESTING (DESTRUCTIVE) POTENTIODYNAMIC POLARISATION CURVES	164
5.1.1	Introduction	164
5.1.2	Test Specimens	164
5.1.3	Test Method	165
5.1.4	Results	171
5.1.5	Discussion	177
5.1.5.1	<i>Interpretation of Measured Polarisation Curves</i>	177
5.1.5.2	<i>Corrosion Rate Calculation from Polarisation Curves</i>	180
5.1.6	Conclusions	183
5.1	CORROSION TESTING (NON DESTRUCTIVE)	185
5.1.1	Introduction	185
5.1.2	Materials	185
5.1.3	Test Specimen	186
5.1.4	Test Specimen Repair – Substrate Combinations	189
5.1.5	Corrosion Tests	192
5.3	LINEAR POLARISATION RESISTANCE MEASUREMENTS	193
5.3.1	Introduction	193
5.3.2	Test Method	194
5.3.3	Analysis of Results	204
5.3.3.1	<i>Case 1: Both Repair and Substrate of Low Permeability</i>	205
5.3.3.2	<i>Case 2: Low Permeability Repair and High Permeability Substrate</i>	205
5.3.3.3	<i>Case 3 & 4: Case 2: High Permeability Repair and Low Permeability Substrate</i>	206
5.3.3.4	<i>Case 5 & 6: Case 2: High Permeability Repair and High Permeability Substrate</i>	207
5.3.4	Conclusions	209
5.4	IMPEDANCE SPECTROSCOPY	210
5.4.1	Introduction	210
5.4.2	Impedance Spectroscopy Test Method	211
5.4.3	Analysis of Impedance Spectroscopy Data	215
5.4.3.1	<i>Equivalent Circuits</i>	216
5.4.3.2	<i>Selection of Appropriate Equivalent Circuit</i>	218
5.4.3.3	<i>Analysis of Equivalent Circuit used in Present Study</i>	221
5.4.3.4	<i>Data Analysis by the fitting of Semi-circles</i>	227
5.4.4	Results	229
5.4.5	Discussion	236
5.4.6	Conclusions	239

Table of Contents

5.5	RESISTIVITY MEASUREMENTS	240
5.5.1	Method	241
5.5.2	Results	243
5.5.3	Discussion	243
5.5.4	Conclusions	255
5.6	POTENTIAL MEASUREMENTS	256
5.6.1	Method	257
5.6.2	Results	257
5.6.3	Discussion	261
5.6.4	Conclusions	264
5.7	COMPARISON OF CORROSION CURRENTS	265
5.7.1	Introduction	265
5.7.2	Analysis of Results	265
5.7.2.1	<i>Comparison of Corrosion Currents obtained for different Repair-Substrate Combinations</i>	269
5.7.3	Conclusions	279
6.	Analysis of the Effect of Disparity in Material Properties on Reinforcement Corrosion	280
6.1	INTRODUCTION	280
6.2	EFFECT OF DISPARITY IN PROPERTIES ON RESISTIVITY	281
6.3	EFFECT OF DISPARITY IN PROPERTIES ON CORROSION POTENTIALS	289
6.3.1	Introduction	289
6.3.2	Effect of Permeability on Corrosion Potential	290
6.3.3	Effect of Chloride Concentration on Corrosion Potential	293
6.3.4	Creation of a Macrocell due to the Disparity in Properties	295
6.4	EFFECT OF DISPARITY IN PROPERTIES ON CORROSION CURRENTS	301
6.6	CONCLUSIONS	311
7.	Factors Affecting the Galvanic Cell	312
7.1	INTRODUCTION	312
7.2	MODELLING WORK FOR REPAIR MACROCELL	314
7.2.1	Theory	314
7.2.2	Validity of Experimental Data	318
7.3	SIGNIFICANCE OF MODELLING WITH RESPECT TO CONCRETE REPAIR	331
7.3.1	Effect of a Large Disparity in Permeability of Repair and Substrate	332
7.3.2	Effect of a Match in Permeability between Repair and Substrate	334
7.3.3	Effect of Repair and Substrate Resistivity on the size of the Macrocell	335
7.4	SUMMARY AND CONCLUSIONS	338

Table of Contents

8.	Summary and Conclusion	341
8.1	PHYSICAL AND ELECTROCHEMICAL PROPERTIES OF REPAIR AND SUBSTRATE MATERIALS	341
8.2	CORROSION OF THE TEST SPECIMENS	342
8.2	DISPARITY IN PROPERTIES BETWEEN REPAIR AND SUBSTRATE MATERIALS ON CORROSION OF THE REINFORCEMENT STEEL.	344
8.4	MODELLING THE EFFECT OF DISPARITY	345
9.	Further Work	347
10.	References	350

List of Figures

2. Literature Review

2.1	Typical Repair Costs	8
2.2	Comparison of one hit repair to multiple repairs on design life.	9
2.3	Corrosion mechanism due to macro-cell action before and after patch repair.	19
2.4	Pourbaix diagram for the Fe-H ₂ O system.	23
2.5	Influence of chloride on Fe-H ₂ O system.	23
2.6	Evans diagram for types of corrosion control.	27
2.7	Schematic anodic polarisation curve for chloride contaminated concrete	38
2.8	Differential aeration mechanism	46
2.9	Illustration of porosity and permeability.	49
2.10	Service life model.	66
2.11	Polarisation curve extrapolation	75
2.12	Anodic polarisation curve showing active –passive transition.	76
2.13	Theoretical and measured polarisation curves.	78
2.14	Linearity of polarisation curves.	79
2.15	Equivalent circuits and resulting Nyquist diagrams.	86
2.16	Flow diagram for evaluating experimental impedance results.	87
2.17	Equivalent circuits used to represent corrosion in reinforced concrete.	90
2.18	Resistivity electrode arrangement.	96

3. Introduction to Experimental Work

3.1	Particle size distribution for Ketton OPC.	107
3.2	Grading curve for Belmoor sand	109
3.3	Grading curve for coarse aggregate	110

4. Physical Properties of substrate and repair materials

4.1	Change in porosity between 28 days and 12 months.	119
4.2	Schematic of permeater	122
4.3	Effect of head pressure on permeability coefficient.	127
4.4	Change in permeability of test materials between 28 days and 12 months.	136
4.5	Comparison of water permeability data for concretes and repair materials.	137
4.6	Permeability match between repair and substrate materials.	138
4.7	Schematic of the specimen used for chloride analysis.	142
4.8	Chloride concentration at steel over 12 months exposure.	151
4.9	Trends in porosity and resistivity properties.	156
4.10	Relationship between porosity and resistivity measurements.	156
4.11	Trends in permeability and chloride diffusion coefficients	161
4.12	Chloride diffusion coefficients against permeability.	161

5. Corrosion Testing

5.1	Test Specimen	167
5.2	Schematic diagram of Test Equipment.	168
5.3	Anodic polarisation curve showing active-passive transition.	169
5.4	Theoretical and measured polarisation curves	170
5.5	Typical polarisation curve for a repair material.	172
5.6	Average polarisation curves.	173
5.7	The relationship between E_{CORR} and permeability.	174
5.8	Repeated cathodic sweeps on material A	175
5.9	Relationship between anodic Tafel constant and permeability.	176
5.10	Polarisation curve showing Tafel extrapolation.	182

List of Figures

5.11	Experimental arrangement	188
5.12	Schematic of IR drop.	195
5.13	Effect of IR Compensation on Corrosion Current: 0.4 w/c Substrate with Repair material A	198
5.14	Corrosion Current with Time Relationship: 0.8 w/c Substrate with Repair material A	199
5.15	Corrosion Current with Time Relationship: 0.4 w/c Substrate with Repair material B	200
5.16	Corrosion Current with Time Relationship: 0.4 w/c Substrate with Repair material C	201
5.17	Corrosion Current with Time Relationship: 0.8 w/c Substrate with Repair material B	202
5.18	Corrosion Current with Time Relationship: 0.8 w/c Substrate with Repair material C	203
5.19	Impedance against frequency plot for 0.4 w/c substrate.	212
5.20	Frequency against phase angle theta for 0.4 w/c substrate.	213
5.21	Nyquist plot for 0.4 w/c substrate	214
5.22	Flow diagram for evaluating experimental impedance results	217
5.23	Equivalent circuit from Wheat [25].	219
5.24	Equivalent circuit from Sagoe-Crentsil et al [21]	219
5.25	Equivalent circuit used in present study.	221
5.26	Sample data fitted to equivalent circuit using complex number non linear least square method.	225
5.27	Comparison of corrosion rates calculated using different measurement techniques for material B combined with 0.8w/c.	226
5.28	Randles equivalent circuit.	227
5.29	Nyquist plot from the Randles equivalent circuit.	228
5.30	Material A with 0.4 w/c substrate.	232
5.31	Material A with 0.8 w/c substrate.	232
5.32	Material B with 0.4 w/c substrate.	233
5.33	Material B with 0.8 w/c substrate.	233
5.34	Material C with 0.4 w/c substrate.	234
5.35	Material C with 0.8 w/c substrate.	234
5.36	Nyquist plots for repair material B with 0.8w/c substrate.	235

List of Figures

5.37	Resistivity values for repair material A with 0.4 w/c substrate.	244
5.38	R_{SOL} values for repair material A with 0.4 w/c substrate.	244
5.39	Resistivity values for repair material A with 0.8 w/c substrate.	245
5.40	R_{SOL} values for repair material A with 0.8 w/c substrate.	245
5.41	Resistivity values for repair material B with 0.4 w/c substrate.	246
5.42	R_{SOL} values for repair material B with 0.4 w/c substrate.	246
5.43	Resistivity values for repair material B with 0.8 w/c substrate.	247
5.44	R_{SOL} values for repair material B with 0.8 w/c substrate.	247
5.45	Resistivity values for repair material C with 0.4 w/c substrate.	248
5.46	R_{SOL} values for repair material C with 0.4 w/c substrate.	248
5.47	Resistivity values for repair material C with 0.8 w/c substrate.	249
5.48	R_{SOL} values for repair material C with 0.8 w/c substrate.	249
5.49	Distribution of resistivity and solution resistance results.	253
5.50	Relationship between solution resistance and resistivity.	254
5.51	Rest potentials for repair material A with 0.4 w/c substrate.	258
5.52	Rest potentials for repair material A with 0.8 w/c substrate.	258
5.53	Rest potentials for repair material B with 0.4 w/c substrate.	259
5.54	Rest potentials for repair material B with 0.8 w/c substrate.	259
5.55	Rest potentials for repair material C with 0.4 w/c substrate.	260
5.56	Rest potentials for repair material C with 0.8 w/c substrate.	260
5.57	Corrosion currents measured using impedance spectroscopy and LPR for material A with 0.4 w/c substrate.	271
5.58	Corrosion currents measured using impedance spectroscopy and LPR for material A with 0.8 w/c substrate.	271
5.59	Corrosion currents measured using impedance spectroscopy and LPR for material B with 0.4 w/c substrate.	272
5.60	Corrosion currents measured using impedance spectroscopy and LPR for material B with 0.8 w/c substrate.	272
5.61	Corrosion currents measured using impedance spectroscopy and LPR for material C with 0.4 w/c substrate.	273
5.62	Corrosion currents measured using impedance spectroscopy and LPR for material C with 0.8 w/c substrate.	273

List of Figures

5.63	Comparison of corrosion currents obtained using LPR and impedance spectroscopy measurements.	274
5.64	Distribution of ratio of corrosion currents from impedance spectroscopy and LPR measurements.	275
5.65	Corrosion currents for material A with 0.4 w/c substrate.	276
5.66	Corrosion currents for material A with 0.8 w/c substrate.	276
5.67	Corrosion currents for material B with 0.4 w/c substrate.	277
5.68	Corrosion currents for material B with 0.8 w/c substrate.	277
5.69	Corrosion currents for material C with 0.4 w/c substrate.	278
5.70	Corrosion currents for material C with 0.8 w/c substrate.	278

6. Analysis of the Effect of Disparity in Material Properties on Reinforcement Corrosion

6.1	Relationship between Resistivity and Permeability Coefficients.	285
6.2	Relationship between Resistivity and Chloride Concentration at the Steel Surface.	286
6.3	Relationship between Solution Resistance and Permeability.	287
6.4	Relationship between Solution Resistance and Chloride Concentration.	288
6.5	Variation of potentials in repair and substrate materials against log of permeability	298
6.6	Ecorr against chloride concentration	299
6.7	Difference in potentials between substrate material and repair against mismatch in permeability	300
6.8	Graph of potentials against corrosion currents	308
6.9	Variation in corrosion currents in repair and substrate materials against permeability	309
6.10	Difference in corrosion currents between repair and substrate against the ratio of substrate to repair permeability coefficients	310

7. Factors Affecting the Galvanic Cell

7.1	Simple electrical circuit to represent a galvanic cell.	313
7.2	Schematic of repair macro-cell.	315
7.3	Transmission line mode.	317
7.4	Current distribution for material A combined with 0.4 w/c substrate.	319
7.5	Current distribution for material A combined with 0.8 w/c substrate.	320
7.6	Current distribution for material B combined with 0.4 w/c substrate.	321
7.7	Current distribution for material B combined with 0.8 w/c substrate.	322
7.8	Current distribution for material C combined with 0.4 w/c substrate.	323
7.9	Current distribution for material C combined with 0.8 w/c substrate.	324
7.10	Average current densities for the anode and interface of the repair substrate combinations over final 6 months of study.	325
7.11	Effect of repair permeability on galvanic corrosion combined with a high permeability substrate.	326
7.12	Comparison of low permeability and high permeability repair substrate combinations	327
7.13	Effect of changes in resistivity on the distribution of galvanic current.	328

List of Tables

2. Literature Review

2.1	General requirements of patch repair for compatibility	16
2.2	Comparison of the most widely used methods for measuring corrosion.	71
2.3	Half-cell potential measurements ASTM C876.	72
2.4	Corrosion levels in reinforced concrete related to corrosion current measured by linear polarisation resistance.	82
2.5	Relationship between resistivity and corrosion rate.	96

3. Introduction to Experimental Work

3.1	Typical manufacturers data for repair material A	104
3.2	Typical manufacturers data for repair material B	105
3.3	Typical manufacturers data for repair material C	106
3.4	Typical chemical composition of Ketton OPC	108
3.5	Typical chemical composition of Bellmoor sand	109

4. Physical Properties of substrate and repair materials

4.1	Porosity results for substrate concrete and repair materials.	118
4.2	Permeability test specimens.	129
4.3	Repair substrate combinations..	132
4.4	Chloride content in repair materials after 12 months exposure to 3.5% NaCl solution.	149
4.5	Resistivity measurements.	155
4.6	Properties of repair and substrate materials	157

5. Corrosion Testing

5.1	Potentiodynamic polarisation test results.	171
5.2	Tafel constants from averaged polarisation curves	177
5.3	Comparison of I_{CORR} values from intercepts and from use of the Stern Geary equation.	181
5.4	Material Properties	186
5.5	Differences in properties of substrate repair material combinations	189
5.6	Property mismatch of substrate repair material combinations investigated.	191
5.7	Tafel constants used in LPR measurements.	196
5.8	Number of readings used to calculate the average corrosion currents for each specimen at each reading.	197
5.9	Tafel constants used for corrosion current calculations.	230
5.10	Number of readings used to calculate the average charge transfer resistance for each specimen at each reading.	231
5.11	Relationship between resistivity readings and corrosion rates.	240

6. Analysis of the Effect of Disparity in Material Properties on Reinforcement Corrosion

6.1	Average resistivity and solution resistance measurements	284
6.2	Average corrosion potentials of steel embedded in each cementitious material	290
6.3	Average corrosion potentials measured	297
6.4	Average corrosion rates	303

7. Factors Affecting the Galvanic Cell

7.1	Summary of repair and substrate values from experimental work.	318
7.2	Theoretical half-cell potentials and resistivity values for repair materials combined with a high permeability substrate.	334

1.0 Introduction

During the life time of any reinforced concrete structure it is likely to require maintenance and repair. The most usual scenario is to carry out repair to the structure as and when it is needed. Repairs are carried out with a number of set aims in mind:

- Aesthetics - the look of the structure.
- To maintain the structural integrity.
- The durability of the structure. i.e. the prevention of further deterioration of the structure.

The success will obviously be reliant on the repair meeting all these criteria to some extent. Repairs are treated as a “one stop” solution and repair materials are designed to enhance the performance of the structure at the site of repair.

One of the main causes of deterioration of reinforced concrete structures is the corrosion of the reinforcement. Corrosion may be due to carbonation of the concrete or chloride diffusion into the structure, breaking down the passive film on the steel allowing corrosion to initiate. Repair materials are used as a form of “corrosion prevention” on deteriorated areas of a structure. As a result repair materials are typically designed to have the following properties:

- Low permeability to prevent water, chloride and oxygen ingress.
- High alkalinity to preserve the passive oxide film on the steel
- High resistivity to reduce the rate of corrosion reactions.

The properties of the repair material are such that they should offer maximum protection to the steel at the repair, but often no consideration is given to the impact of

the repair to the entire structure or its implications to the long term performance of the repair and the structure.

Problems can occur because the repair material provides a totally different chemical and physical environment to that of the existing concrete. A single reinforcement bar may have more than one repair along its length, therefore, the bar can be subjected to a complex chemical and physical environment. To further complicate the situation, these environments are constantly changing as a result of the interaction of the interior environment with the exterior environment. It is recognised that variations in chemical environment, such as oxygen and chloride concentration, can create galvanic cells on the surface of a section of metal. This results in the separation of the anodic and cathodic reactions involved in corrosion to distinct sites on the metal. The variations in chemical environment can result in high corrosion rates of the anodic site and a corresponding absence of corrosion at the cathodic site.

It is possible, therefore, that by applying a fresh alkaline repair material to a corroded structure with the aim of preventing corrosion, it may actually initiate corrosion and allow the formation of new galvanic cells. Depending on the properties of the materials used, this “incipient corrosion” may occur in the steel embedded in the repair material or may increase the rate of corrosion of the steel embedded in the substrate concrete. Conversely it is also possible that the effect of this “mismatch” in properties on the overall corrosion of the structure is negligible. There is a lack of basic knowledge of the effect of the disparity in properties on the corrosion of the larger structure. This research project is concerned with the durability of repairs and their success at preventing corrosion in a structure.

1.1 SCOPE OF RESEARCH

As there is little or no published data in this specific area, much of the work involved in this project will be novel. The project will concentrate on examining the following key areas:

1. The investigation of the mechanisms of macro-cell corrosion between the reinforcement bar embedded in repair material and that embedded in the normal substrate concrete, with a special emphasis on the interface between the repair material and the existing structure.
2. The parameters required for the initiation of corrosion of the reinforcement bars embedded in the repair material.
3. The long term performance of the repair patches with regards to corrosion.

The main objective of this research is to provide useful information and data to assist in the development of repair materials, to provide durable repair systems capable of increasing the longevity of the structure to which they are applied.

1.2 SCOPE OF CURRENT WORK

The primary aim of this project is to investigate the electrochemical systems developed by the use of repair patches on reinforced concrete structures. This work requires the assessment of the relevant properties of repair and substrate materials which create galvanic cells. This will involve the study of a range of repair systems providing a selection of property combinations with the substrate concrete.

The selected repair and substrate materials will be combined into specimens to allow the study of the electrochemical cells developing from repair systems. The work concentrates on the physical and chemical properties required to initiate corrosion and in generating galvanic cells. The reinforcement at the interface between the repair and substrate materials will be subjected to careful study. The electrochemical, physical and chemical properties of the repair system and their variation with time will be included in the experimental investigation on the electrochemical cells generated in repair patches.

Finally the project will theoretically model the development of incipient corrosion cells initiated through concrete repair and assess the mechanism of corrosion in repaired reinforced concrete structures. This work will fulfil the primary aim of the project to produce strong and durable repair systems to improve the longevity of any structure to which they are applied.

1.3 THESIS STRUCTURE

The thesis is divided into ten chapters. The first chapter is this introduction. Chapter two is a detailed review of current literature on corrosion of reinforced concrete and related subjects. This is split into five subsections covering, repair materials, corrosion of reinforced concrete, mass transport in concrete, modelling corrosion and electrochemical test methods.

Chapter 3 is an introduction to the experimental work undertaken in the study.

Chapter 4 covers the determination of physical properties identified from the literature review as important to corrosion, for a selection of repair and substrate materials used in

the study. Four basic properties were examined; porosity, permeability, chloride diffusion and resistivity.

Chapter 5 covers the measurement of corrosion in specimens made from combinations of different repair and substrate materials over the period of the study. This has involved a variety of experimental techniques and interpretation of the measurements. Five measurement techniques were employed; linear polarisation resistance, impedance spectroscopy, resistivity, corrosion potentials and potentiodynamic polarisation. Also covered in this chapter is a comparison of the corrosion currents obtained by the linear polarisation resistance and impedance spectroscopy techniques.

Chapter 6 examines the effect of the mismatch in properties on the corrosion of the repair-substrate test specimens. This work identifies permeability as the primary property in assessing the effect of a miss-match in properties between the repair and substrate materials on the development of galvanic cells. In chapter 7, the effect of differences in permeability between repair and substrate materials is used to model the galvanic current. Techniques employed in modelling galvanic currents in chloride macro-cells are used and the distribution of current in the cell is attempted. This allows the assessment of the effect of the galvanic cell on the repair patch and at the interface between the repair and substrate materials.

Chapter 8 provides a summary and conclusions. Chapter 9 makes recommendations on further work. Chapter 10 lists the references.

2.0 Literature Review

2.1 REPAIR SYSTEMS

As the stock of older reinforced concrete structures increases it is inevitable that the need for repair will also increase. The aim of repair is based on a number of requirements [1]:

- To restore structural integrity
- To restore the original profile
- To arrest deterioration
- To disguise or seal cracks or other blemishes
- To restore the original appearance

Achieving these aims requires the selection of a repair system comprising the materials and methods appropriate for the repair site on the structure. In order to choose the correct repair system, Allen [2], has proposed that it is necessary to consider the following questions:

1. What caused the damage?
2. Is repair needed?
3. What are the objectives of the repair?

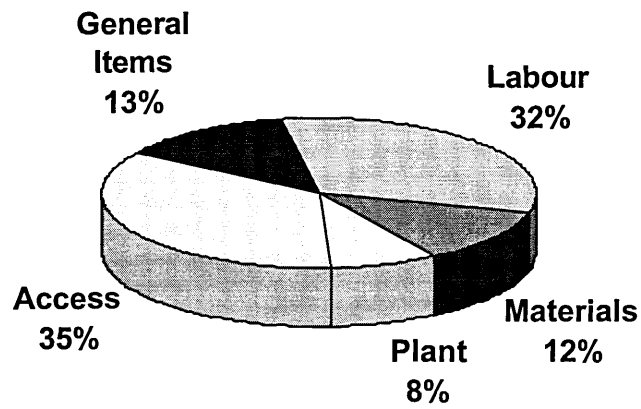
Diagnosing the cause of damage will determine whether it was the result of an isolated or a recurring event. After fire or mechanical damage, it may be possible to return the structure to its original condition. However if the cause is from a recurring problem such as an aggressive environment then the repair considerations may be more complex.

Diagnosis of the cause and need for repair is normally achieved through a series of structural inspections and investigations [3]. Many of the procedures involved have

been standardised in a number of reports such as Concrete Society Technical Report 36. Patch Repair of Reinforced Concrete subject to Reinforcement Corrosion [4]. A new European Standard for concrete repair has been proposed.[5]. The aim of this work is to provide cost effective repair and maintenance strategies for structures [6]. This requires an understanding of the degradation processes occurring to provide an estimation of the optimum durability of any repair system. With the knowledge of the costs, it is possible to consider the cost effective of the repair systems alternatives in comparison to the lifetime of the structure. Robery [6] gives examples of the typical split of repair costs for a building and a bridge (see figure 2.1).

From figure 2.1 it can be shown that for the repair of a bridge access has a much larger share of the costs than for a building. For a building, materials have a larger share of the costs. This type of assessment can have an effect on the repair materials chosen. The assessment of access costs for the bridge is probably an underestimate in that the associated economic costs from traffic delays can be huge. A repair material that produces a durable long lasting repair while potentially more expensive would cut the additional access charges and economic costs caused from repeated repairs to the structure. Robery [6] calls this a “one hit” repair. A building however has lower access but correspondingly higher materials costs. In this set of circumstances it may be more cost effective to allow multiple repairs (figure 2.2) [6]. This view ignores any structural, safety or aesthetic requirements considering only the economic costs of the repair.

Typical repair costs for a bridge.



Typical repair costs for a building.

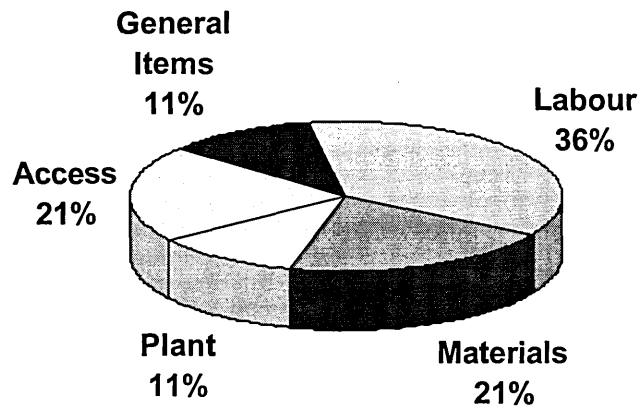


Figure 2.1 Typical repair costs [6].

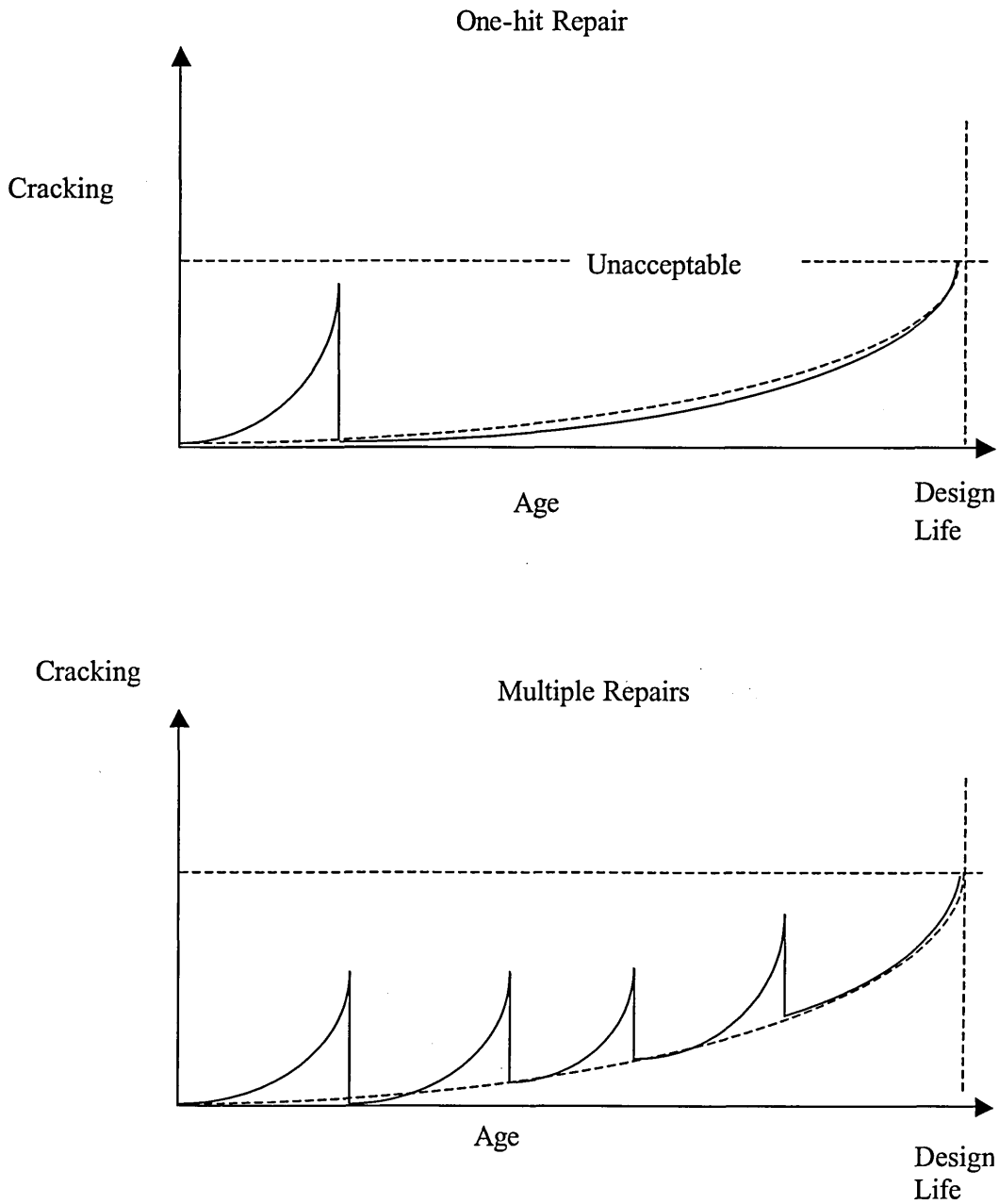


Figure 2.2: Comparison of a one hit repair to multiple repairs on design life.[6]

The term, “repair system” need not be restricted the use of cementitious repairs materials. In the common application of patch repairs, [2] systems can also include the use of epoxy primers or zinc rich primers to provide extra protection for the reinforcing

steel [7, 8]. Crack repair resins and the use of surface coatings to reduce the corrosion risk to reinforced concrete can also be considered part of a repair system [7, 9]. A repair system is the total package of repair, repair technique and protection applied to the structure during the repair process. This definition of a repair system includes any material used in repair of concrete structures. For the remainder of this project a repair material is considered to be the cementitious material used to repair a structure, assumed to be damaged by corrosion.

2.1.1 Nature of Repair Materials

The properties of the repair material will be controlled primarily by the structural performance requirements of the repair:

- Strength in tension, compression and flexure.
- Modulus of elasticity in tension and compression and flexure.
- Coefficient of thermal expansion.
- Adhesion to substrate concrete and reinforcement.
- Shrinkage.
- Creep

The repair material will also need to respond to the techniques of the application method such as [10]:

- Sprayed mortar or concrete.
- Hand applied mortar.
- Poured concrete or mortar with the aid of shuttering.

In addition, the repair needs to be able to stop further deterioration of the structure, by preventing corrosion. This requires knowledge of the corrosion mechanisms involved. McCurrich et al [10] recommend that oxygen and moisture be excluded from the steel and that the repair material maintains the passivity of the reinforcing steel. These recommendations are the outcome of years of research into corrosion in reinforced concrete. Thus the repair material needs the following properties:

Low permeability to oxygen, chlorides and water.

High alkalinity to preserve the passive oxide film.

High resistivity.

On an actual structure the situation is more complex, chlorides may not be evenly distributed across a structure and areas of a structure contaminated with chloride may not show signs of degradation [11]. Corrosion of the reinforcement may only be observed in the section of steel reinforcement in the concrete exposed to highest chloride levels, creating what is called chloride corrosion “macro-cell”. Chloride macro-cell corrosion will be discussed further in Section 2.2.5. The repair of the chloride macro-cell corrosion site with fresh cementitious material may only act to move corrosion to a totally different area of the structure. This phenomenon is known as incipient anode formation and suggests that repairing one area of a structure merely moves corrosion to another area. This can be further complicated by variations in oxygen and moisture availability.

2.1.2 Properties of Repair Materials

Repair materials have been designed to offer improved properties compared to normal concrete [12]. A wide variety of such materials have now been developed. These materials have also been found to offer improved corrosion resistance, in that they are more impervious.

Polymer modified concrete materials were developed mainly for their enhanced properties [13]. Polymer emulsions such as latexes are used to improve the adherence of fresh concrete or mortars to hardened concrete and so are well suited to repairs.

There are three basic types of polymer modified concrete:

Polymer-impregnated concrete. Here conventional OPC concrete is dried then saturated with a liquid monomer such as methylmethacrylate or styrene. Polymerisation is then achieved using gamma radiation or thermo-catalytic methods. This technique is not used for concrete repair.

Polymer concrete, formed by mixing a monomer with the aggregate and using a curing agent or chemical catalyst to achieve polymerisation. This type of material is not cementitious.

Polymer Portland cement concrete. Although most organic polymers are incompatible with mixtures of Portland, cement water and aggregates, some substances such as latices of rubber, acrylics or vinyl acetates can be added either as an aqueous or powdered form of the monomer and polymerised in-situ.

Ohama et al [14] found that polymer modified mortars showed a decrease in pores in the range 240nm or greater and an increase in the pores of 140nm or less compared to ordinary Portland cement. It was concluded that this refinement of the pore structure resulted in the lower oxygen diffusion coefficients of polymer modified mortars. Kobayashi et al [15] found similar results. For polymer modified cements with a polymer/cement ratio of 15%, the oxygen diffusion coefficient was 1/10 that of OPC.

Kobayashi et al [15] also examined the oxygen diffusion coefficients of various cementitious materials. The oxygen diffusion coefficient was found to be dependent on curing conditions i.e. poor curing will give a high oxygen diffusion coefficient. The effect was greater for those cement types with slower rates of hydration. When the water/cement ratio was lowered from 0.8 to 0.4 the oxygen diffusion coefficient increased by about 15 times. Repair materials generally have a lower water/cement ratio. This generally results in a lower oxygen diffusion coefficient of mortar than for concrete. Different cement types give different diffusion coefficients, blast-furnace slag as 60% cement replacement gives a diffusion coefficient 33-50% that of ordinary Portland cement.

Other types of repair materials use mixtures of replacement materials such as PFA and superplasticisers to keep low water/cement ratios. These together with shrinkage compensation compounds produce dense impermeable high strength repair materials. There is relatively little published work available on the properties of commercial repair materials. However some research has been conducted on the corrosion behaviour of different cement blends and types. Parrot [16] found that carbonation was strongly dependent on cement type as opposed to curing conditions. The carbonation front was

found to correlate with the air permeability of the concrete. Nilson et al [17] found that chloride diffusion was linked to porosity and so depended on water/cement ratios, cracks and compaction. However they also stated that pozzolans such as fly ash, blast furnace slag and microsilica had a beneficial effect on chloride diffusion. Pozzolans are widely used in repair materials and contribute to the low chloride diffusion coefficients of the material. (see section 2.3.3 on chloride diffusion).

Additions of fly ash, slag and micro silica have been found to refine the pore structure of concrete mixes after the initial set. This continued refinement of the pore structure during hydration reduces the permeability of the material to chlorides, oxygen and moisture, the main requirements for corrosion. Many repair materials are based on replacements for cement [18] and are assumed to be ideal for the purpose. Research clearly shows that these repair materials slow corrosion initiation by reducing chloride diffusion and carbonation. In addition they lower oxygen diffusion and reduce corrosion rates.

2.1.3 Effect of Property Mismatch

Ping Gu et al [19] examined the effect of combining materials with differing properties such as porosity. This work concentrated on chloride induced corrosion and found that at first the oxygen concentration was similar both in the low porosity cement and the high porosity cement. This led to general corrosion across the entire metal surface.

As the oxygen concentration fell due to consumption by the corrosion process, this was buffered in the high porosity material by the ease of diffusion of air to the steel cement

interface. However the low porosity material rapidly became oxygen deficient. The effect of this depletion of oxygen was to make the low permeability material anodic i.e. a site for the reaction for metal dissolution and the high permeability material cathodic i.e. the site for oxygen reduction.

This indicates that a low porosity repair material used next to high porosity substrate would result in corrosion of the reinforcement in the repair. In fact the repair material reinforcement would corrode in preference to that in the substrate concrete. This argument has been further developed by Ping Gu et al [20] examining the “electrochemical incompatibility of patches in reinforced concrete”.

Cusson et al [21] in considering the durability of repair materials extends the discussion beyond the matching of porosity and resistivity to that of the relationship between the physical and mechanical properties of repair and substrate. Many failures of repairs are linked to the premature cracking of the repair material. This is caused by the low water/cement ratio and high cement content of the repair materials making them susceptible to shrinkage. This generates strains within the repair leading to the premature cracking. This has led in part to the idea that there should be a match between the mechanical properties of the repair and the substrate concrete in order to produce a durable repair system. This has been developed into the system concept for designing and constructing durable repairs by Emmons et al [22, 23]. This suggests a systematic approach to concrete repair by treating the structure as a whole rather than just the repair site. Cusson et al [21] recommend the general property requirements of patch repair materials for compatibility (see table 2.1).

Table 2.1: General requirements of patch repair for compatibility [21]

Property	Relationship of repair material (R) to concrete substrate (C)
Shrinkage Strain	$R < C$
Creep (Compression)	$R < C$
Creep (Tension)	$R > C$
Thermal Expansion Coefficient	$R = C$
Modulus of elasticity	$R = C$
Poisson's ratio	$R = C$
Tensile strength	$R > C$
Fatigue Performance	$R > C$
Adhesion	$R > C$
Porosity & Resistivity	$R = C$
Chemical reactivity	$R < C$

Table 2.1 recommends the matching of properties such as porosity and resistivity to prevent the creation of these macro-corrosion cells. To match properties however means dispensing with the corrosion protection potential which a traditional dense high resistivity repair material was designed to provide. It suggests that repair cannot be considered as a method of corrosion protection and needs to be used in conjunction with other techniques such as inhibitors or cathodic protection. The work implies that repair can initiate macro-cells between the steel embedded in the repair and substrate materials. The theoretical and experimental work to support this is unclear. Fresh highly alkaline repair material will make the steel passive, therefore for corrosion to initiate in

the repair a mechanism for the depassivation of the steel leading to active corrosion is required. Page et al [24] showed that the oxygen level can fall low enough to destroy the passive oxide film in water saturated concrete specimens. However, the resistivity of repair materials can be high, this would hinder the movement of charged ions between anodic and cathodic and prevent the completion of the electrochemical cell. It is not clear from the current work if the theoretical electrochemical mismatch between repair and substrate is possible and there is little experimental work to support it. The work of Ping Gu et al [20] on the analysis of the electrochemical impedance spectra measured failed to be conclusive, relating to porosity mismatch and not specifically to repair material/substrate concrete mismatch.

Other work has been conducted on the performance of repair materials. Wheat et al [25] determined corrosion rates of repaired reinforced concrete specimens, using electrochemical impedance spectroscopy to track corrosion. The results were not fully analysed, but concluded that the quality of concrete and the mixing and placing procedure had a large effect on the corrosion behaviour of the specimen. Other work by Lambe et al [26] has investigated the effect of repair on corrosion. This work concluded that it was important to view the region of repair and surrounding concrete as one electrochemical system. However it also suggested that from diffusion measurements that mortars with low diffusion coefficients for oxygen, chloride and moisture give better protection to the repair.

Schiessl et al [27] and Raupach [28] examined the effects of the repair on galvanic currents flowing between repair and substrate. The tests were performed on typical repair systems in use today. The specimens varied in water/cement ratios and were

subjected to various types of attack e.g. moisture, chloride and carbonation. The corrosion rate was found to be only significantly affected by moisture levels but the presence of carbonated or chloride contaminated concrete at the repair site was found to establish macrocells leading to a high corrosion risk at sites near the repair. This is shown by the results obtained by Raupach [28] in figure 2.3. When an area of concrete subject to corrosion through contamination of chlorides or carbonation is repaired, it will become passive and a cathode. Areas of the steel adjacent to the repair which still contain chloride contamination now become anodic and begin to corrode. This is an example of incipient anode theory, with repair moving the active sites of corrosion around the structure. This work was confirmed by Hollinshead et al [29] using naturally exposed repaired specimens . This work found the interface between repair and substrate to be very vulnerable to carbonation and chloride ingress. This could spread along the reinforcement if voids were present. This effect was minimised with good compaction of the repair and in this situation diffusion of chlorides from the substrate into the repair became more important.

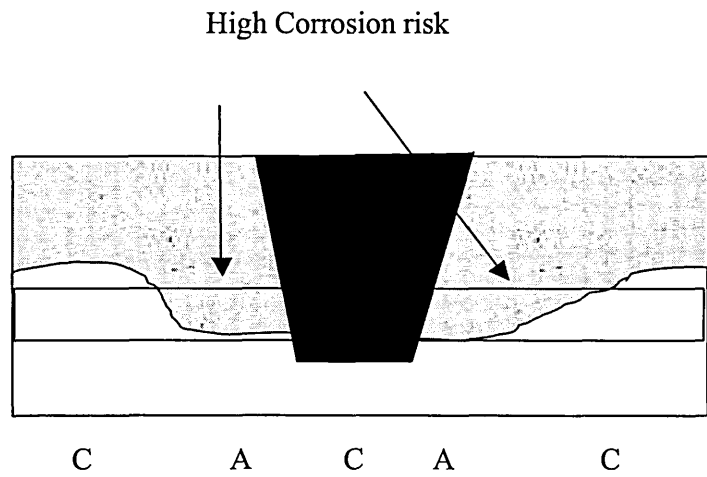
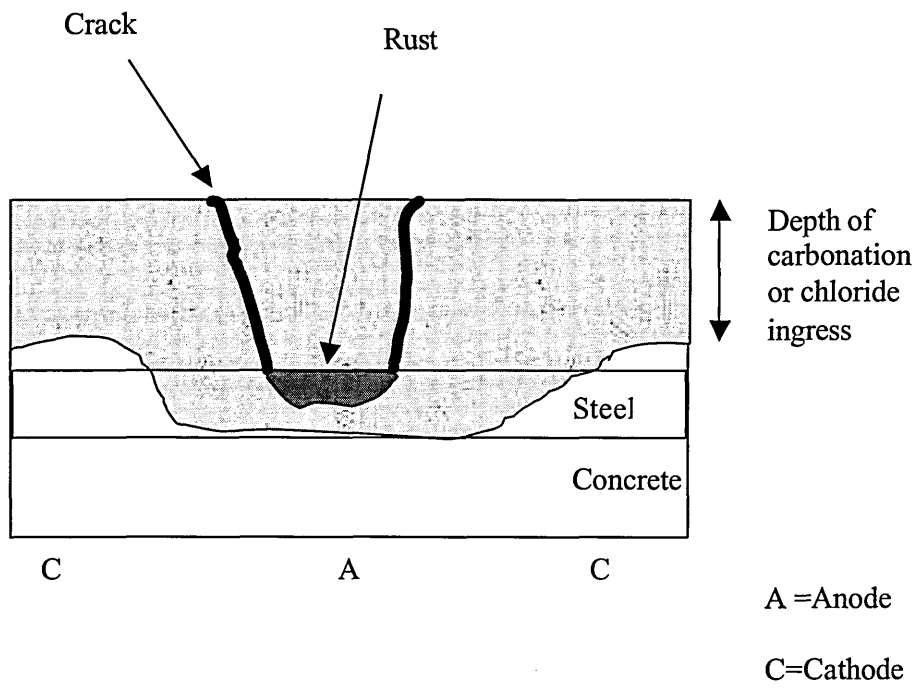


Figure 2.3. Corrosion mechanism due to macrocell action before and after patch repair [28]

2.2 CORROSION OF REINFORCEMENT IN CONCRETE

Reinforcement corrosion in concrete has been well researched and the basic mechanisms of corrosion are well understood. A number of review papers and books exist to cover this area [31-33] and the basic theory of corrosion in concrete is well accepted. The high pH of concrete produces a passive film on the surface of the steel. A significant corrosion rate is only possible if this passive film is removed. The break down in the passive film is achieved in two ways:

- The lowering of pH of the concrete by carbonation to a point when the passive film is no longer stable (pH 9).
- The ingress of Cl⁻ into the concrete causing breakdown of the passive film.

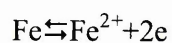
In addition 3 basic factors are required for corrosion [30]:

1. Electrolyte, such as the pore solution in concrete
2. A metal, the steel reinforcement.
3. An oxidant, in this case oxygen, which can be reduced.

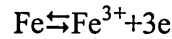
Corrosion of the reinforcement in concrete is a system of electrochemical reactions. This requires mass transport of chlorides and/or carbonation to cause breakdown of the passive film to initiate corrosion and the diffusion of oxygen to maintain the corrosion reaction.

2.2.1 Electrochemistry of Corrosion

Corrosion is an electrochemical redox reaction consisting of separate anodic (oxidation) and cathodic (reduction) half reactions. The principle anodic reactions are:

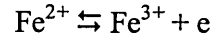


The oxidation of iron to iron²⁺ ions.



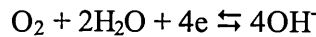
The oxidation of iron to iron³⁺ ions.

A number of different intermediate anodic (oxidation) reactions are also possible:

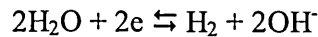


The formation of Fe²⁺ and FeO.OH are the most thermodynamically stable reactions.

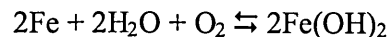
The main cathodic reaction is the reduction of oxygen, which in the alkaline environment of concrete takes the form:



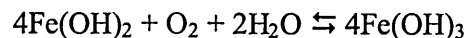
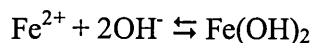
An alternative cathodic reaction also exists in the hydrolysis of water. This involves the evolution of hydrogen and can generate particular corrosion problems such as, hydrogen embrittlement and hydrogen induced cracking.



This is common in acidic solutions, but can occur in highly alkaline environments such as concrete, when the electrochemical potential is unduly low due. For example, in poorly operated cathodic protection systems. However in the normal steel concrete environment the reduction of oxygen is the most thermodynamically stable half reaction. The complete redox corrosion reaction is the combination of the anodic and cathodic half reactions, an example of which is the production of iron hydroxide:



Bazant [215] suggests that the following reactions are also anodic reactions.



The first reaction is not an oxidation half reaction, but an intermediate reaction. The second reaction is the oxidation of Fe^{2+} to Fe^{3+} but is the complete redox reaction not an anodic half reaction. The author stated [215] that these reactions are anodic reactions and used this to argue that a supply of oxygen was required at the anodic site. This is not the case and the cathodic reaction is the site of oxygen consumption.

The value of the electrochemical potential is related to the activity of the reduced and oxidised species in the electrolyte and is given by the Nernst equation [36]:

$$E = E^\theta + \frac{RT}{zF} \ln \frac{[\text{oxid}]}{[\text{red}]} \quad 2.1$$

Where E^θ is the standard electrode potential, T is the temperature, z the number of electrons transferred and R and F are the gas and Faraday's constant. The possible reactions involve the reduction of oxygen and oxidation of iron and will produce hydroxide (OH) and hydrated protons (H^+). The Nernst equation suggests that the cell potential of these reactions will be dependent on pH.

Pourbaix diagrams [34] are used to show the theoretical stability of different oxidation products in terms of electrochemical potential and pH. Pourbaix diagrams are used by a number of authors [31, 37, 38] to explain corrosion processes. Figure 2.4 shows the Pourbaix diagram for the iron water system. It indicates that over the normal pH range expected for concrete, steel is either passive or immune from corrosion. The stability of the oxidation products in the Pourbaix diagram are based on theoretical calculations for the solubility of iron in pure water. This would be different in water with a higher degree of ionic activity, such as, concrete pore solution. A better approximation for the actual situation can be seen in figure 2.5 when chlorides are present in the water. Here a

wider variety of corrosion processes are predicted over a wide range of pH and potentials and passivity is only assured over a limited pH-potential range.

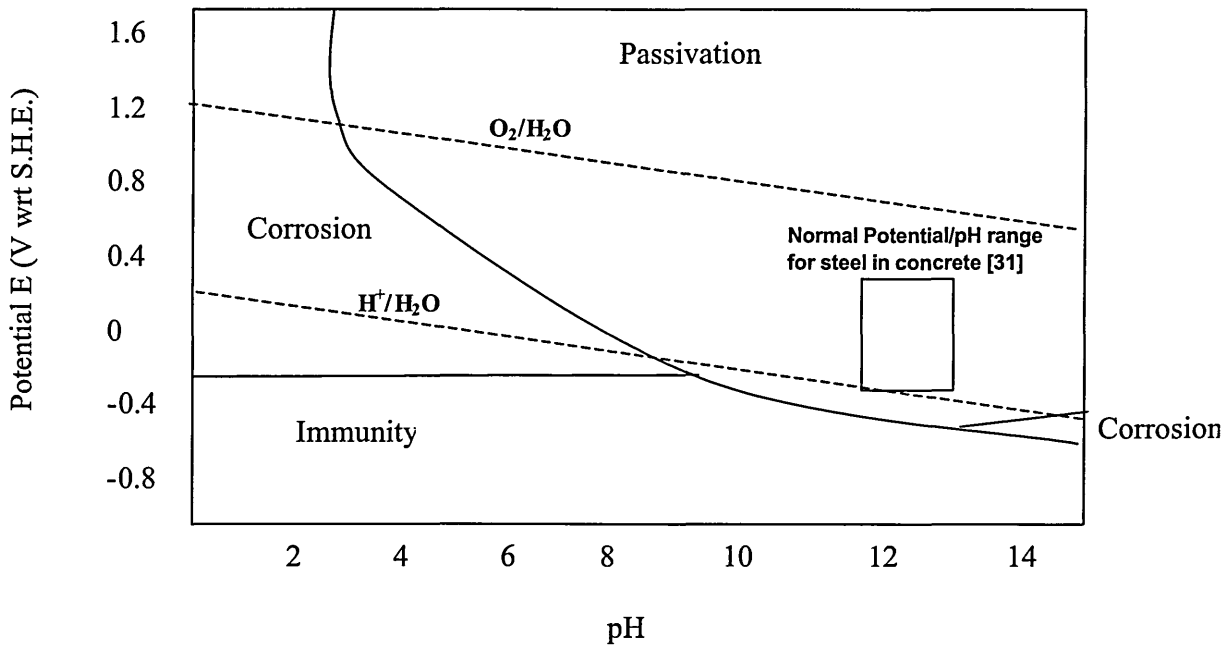


Figure 2.4 Pourbaix Diagram for Fe – H₂O System

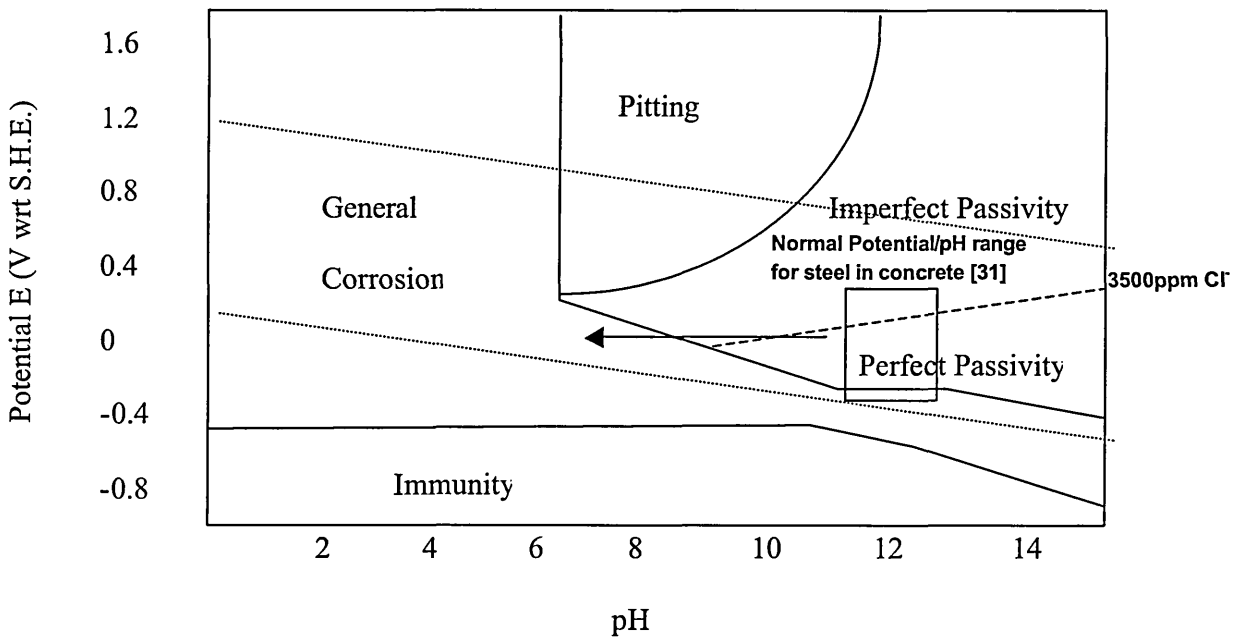


Figure 2.5 Influence of chloride on Fe-H₂O system..

Corrosion can also be described by the use of Evan's diagrams (figure 2.6) [31, 38, 39]

Corrosion under these situations is described as being under anodic control, mixed control or cathodic control.

Anodic control is a condition best demonstrated by the dissolution of passive metals in dilute acid solutions [36]. Here metal ions have to penetrate an oxide film causing a high anodic polarisation. Increase of corrosion with the diffusion of chlorides and or carbonation, produces a situation similar to anodic control in concrete [31], as these agents act to breakdown the passive oxide film on the steel.

Cathodic control (figure 2.6) occurs in water-saturated concrete, where oxygen availability will control the rate of corrosion. The rate of corrosion is limited by oxygen diffusion through the concrete, as oxygen reduction is the most likely cathodic reaction in the corrosion of reinforcement steel in concrete.

Another situation that may occur in concrete corrosion is resistance or ohmic control. This occurs when the concrete is dry the lack of electrolyte, the low conductivity of the concrete prevents corrosion from taking place. Where isolated pockets of electrolyte are available corrosion can occur but is limited. Ohmic control also occurs in corrosion cells when the corrosion products act to shield the corrosion site, preventing further corrosion. Corrosion in these situations could be described as under ohmic control.

The mechanism of control will be dependent on the environmental conditions present on the structure. Dry concrete would be under ohmic control, atmospherically exposed concrete would be predominantly under anodic control and submerged concrete under

cathodic control. Mixed control is normally taken to be a combination of anodic, cathodic and ohmic control [36]. The type of control mechanism affects the corrosion potential, cathodic control gives a more noble corrosion potential, anodic control gives a less noble potential and for mixed control the potential varies according to circumstances.

There are clear similarities between atmospheric corrosion, underground corrosion and corrosion in concrete [39]. Atmospheric corrosion shows the dependence of corrosion on moisture thickness on the surface of the steel. In a dry atmosphere, no corrosion can occur. When the electrolyte is thin (100\AA - $1\mu\text{m}$) the corrosion products shield the anodic site reducing anode efficiency and reducing corrosion rate. However, when the moisture layer is thicker than $1\mu\text{m}$ then availability of oxygen at the cathodic site controls corrosion. This is an example of mixed control.

Underground corrosion or corrosion in soils is very similar to concrete. Soil has a capillary porous structure filled with water or air very similar to concrete. It might be expected that the corrosion problems exhibited in soils will be similar to concrete. Escalante [40] examined the effect of soil resistivity and soil temperature on the corrosion of galvanically coupled metals in soils. This work found that in soils that are well aerated, resistivity has a strong influence on the corrosion rate. In poorly aerated soils oxygen diffusion controls corrosion.

The main difference between corrosion in soils, the atmosphere and concrete, is the passivation of the steel by the high alkalinity of the concrete. The time of wetness [38, 39] is strongly recognised to have an effect on corrosion. i.e. dry concrete exhibits a

high resistivity and therefore low corrosion rate. The highest corrosion occurs in concrete with pore solution at the steel concrete interface. In saturated concrete the corrosion rate falls due to restricted oxygen access.

Arup [41] suggested four states of corrosion in concrete.

1. Passivity, brought about by the high pH and the availability of oxygen. In the absence of chlorides, the passive potential range is very wide +200mV to -700mV vs CCS.
2. Pitting corrosion, brought about by the ingress of chloride ions and the localised breakdown of passivity. The potential range for pitting is -200 mV to -500 mV vs CCS.
3. General corrosion, from the loss of passivity due to carbonation or excessive amounts of chloride. The typical potential range is -450 mV to -600 mV vs CCS. However carbonation would increase this range according to the Pourbaix diagram and depending on the pH.
4. Active low-potential corrosion. This occurs in environments where the oxygen content is very low. If the oxygen level falls below the level that the passivation current density cannot be supported then the passive oxide film will break down and the steel will become active. However the oxygen level will be so low that the rate of corrosion it can support will be very low. The equilibrium potential that this will occur is around -1000 mV vs CSS.

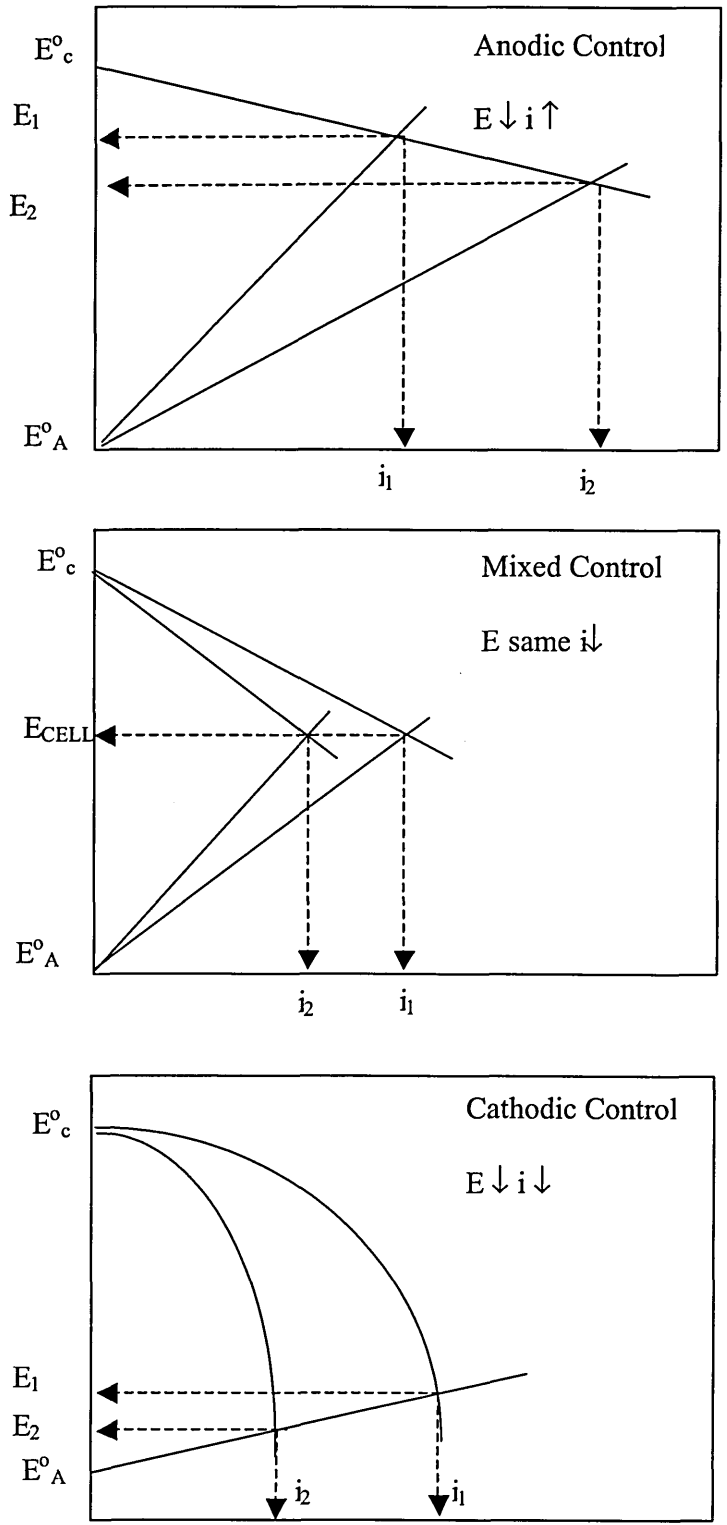


Figure 2.6 Evans diagrams for types of corrosion control.

2.2.2 Passivity of Steel in Concrete

The nature of the passivity provided to the reinforcement by concrete is important in predicting the initiation of corrosion. A number of papers examine passivity. Kruger [42] reviews the general state of understanding of passivity of metals. The paper considers the basic definitions of passive when applied to corrosion science. The definition of passive given in ASTM (G15-83) is “passive – the state of metal surface characterised by low corrosion rates in a potential region that is strongly oxidising for the metal”. This is a definition of passivity in terms of kinetics. Kruger studied the thermodynamics of passivity using the Pourbaix diagram for iron and water system, and the kinetics of film formation using polarisation curves. Kruger also examined the nature of the passive film using a variety of chemical analysis techniques. This showed the passive film on iron to be an oxide film, which has a multi-layered structure of mixed oxides principally Fe_2O_3 and Fe_3O_4 .

The breakdown in passivity results in localised corrosion such as pitting, crevice corrosion and intergranular attack. This causes rapid loss of steel section at very small “localised sites” as opposed to corrosion of the entire surface by general corrosion. The rate of loss from general corrosion can normally be predicted and allows the calculation of service lifetimes for repair and maintenance, this is not the case for localised corrosion. Many theories exist to describe the initiation of localised corrosion, however certain conditions are required to initiate localised corrosion;

1. A critical potential must be exceeded.
2. Damaging species such as halides (Cl^-) are required to initiate corrosion.
3. An initiation period exists to the start of breakdown.
4. Breakdown occurs at highly localised sites.

Three models for initiation are discussed;

1. Adsorbed ion displacement model, where adsorbed Cl^- ions displace the oxygen forming the passive film. After a Cl^- ion is adsorbed on the surface it weakens the bonding of the metal ions in the metal lattice.
2. Ion migration or penetration model. Here the anions move through the passive film and breakdown is complete when an anion reaches the metal/film interface.
3. Breakdown repair model. Here the adsorption of the damaging anion is said to lower the interfacial surface tension at the solution film interface, because of mutual repulsion of adsorbed anions. When these forces are great enough it will cause the film to crack. The exposed metal can now be attacked by anions unless the conditions exist where rapid repair (repassivation) of the film can occur.

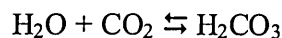
Leek [37] examines passivity in terms of steel in concrete. The formation of the passive film is discussed using Pourbaix diagrams similar to Kruger [42]. However, protection generated from the cement paste is also considered. Concrete provides an interfacial layer between the steel and the concrete matrix. This layer is an aggregate free zone disrupted by inclusions of CSH gel. It acts as a barrier to oxygen diffusion and an alkaline buffer to pH reductions from anodic corrosion reactions. The structure of the concrete matrix covering the steel is recognised as being important in controlling the ingress of aggressive agents such as CO_2 and Cl^- . It is also recognised by Page and Treadaway [30], that the concrete provides a physical barrier to corrosion and increasing the concrete quality or cover increases the time to initiation of corrosion. This means that the initiation of corrosion by carbonation or chloride ions is a function of the concrete cover as well as the nature of the passive film that protects the steel. In addition the concrete also controls the diffusion of oxygen to the steel and therefore in

situations where the corrosion is under cathodic control, concrete quality will control the rate of corrosion.

Martin and Olek [43] also studied the nature of passivity of the reinforcing steel in concrete. This was an experimental study and used electrochemical techniques to examine the effect of chloride ions and corrosion inhibitors on passivity and corrosion rate. This showed that mild steel is able to retain passivity in the presence of significant concentrations of chlorides provided the pH is high. Corrosion inhibitors appear to reduce corrosion rate but can compromise the passive oxide film due to a drop in pH in the pore solution.

2.2.3 Carbonation

In carbonation, carbon dioxide from the atmosphere dissolves in the pore solution of the concrete to produce carbonic acid [37, 30].



This will destroy the alkalinity of the concrete from the acid base reaction between the carbonic acid and calcium hydroxide, which will produce calcium carbonate. When the pH has fallen to around pH 9 then the passive film on the steel will break down and general corrosion may start in the presence of moisture and oxygen. If carbonation occurs in conjunction with chloride ions then the passive film may breakdown at a higher pH than would be expected in the absence of chloride ions.

The concrete quality and cover acts as a barrier to the movement of the carbonation front. A parabolic relationship exists between depth of penetration (x) and time (t) that can be represented by the relationship.

$$x = kt^{\frac{1}{2}}$$

2.2

Here k is a constant dependent on the material properties of the concrete. This is controlled by the tortuosity of the pore structure. The longer the diffusion path for the CO_2 the longer it takes the carbonation front to reach the steel. Once the carbonation front reaches the steel the passive film breaks down.

Parrot [16] found that carbonation was also strongly dependent on cement type. The carbonation front was found to correlate with the air permeability of the concrete. Gonzalez et al [44] studied carbonation with electrochemical techniques such as linear polarisation resistance. They found that carbonation on its own does not create appreciable levels of corrosion. In addition a relative humidity of above 50% is required. This fits the generally accepted requirement for corrosion that an electrolyte is required. This suggests that the relative humidity may need to drop below 50% to stop corrosion. The presence of chlorides within the carbonated mortar also was found to increase corrosion. The use of corrosion inhibitors was found to reduce corrosion. Houst et al [45] examined the diffusion of CO_2 in concrete. Diffusion was found to strongly depend on porosity. The diffusion of CO_2 was found to be lower than O_2 . To model the diffusion of CO_2 it was necessary to use two levels of porosity. In fine capillary pores, diffusion was strongly influenced by water content. In the second level of coarser pores, water content was found not to have such a strong influence. This was said to explain the formation of non-carbonated islets in an otherwise carbonated matrix. Diffusion was found to be based on Knudsen diffusion with pores separated into three domains of cylindrical pores, corresponding to different hydraulic radii where different transport mechanisms take place.

There is little work relating carbonation to repair materials and repair systems. However the work of Parrot [16] linking carbonation to different cement types and Houst et al [45] linking carbonation to porosity are relevant to the study of repair materials. The research suggests that by controlling porosity particularly by using different cement types it is possible to produce a cementitious material with lower rates of carbonation.

2.2.4 Chloride Induced Corrosion

Page and Treadaway [30] reviewed the loss of protection by chloride ions as did Leek [37]. This work indicates that there is a threshold level of chloride above which corrosion will be initiated. There does not appear to be one level for all types of concrete and environment. The value of the chloride threshold has been the subject of considerable research [17, 46] The following threshold values have been recommended by the Building Research Establishment Digests 444 [47], which gives the degree of risk associated with a chloride content;

Low - up to 0.4% by weight of cement or 0.05% by weight of concrete.

Medium – from 0.4% to 1% by weight of cement or 0.05% to 0.15% by weight of concrete.

High – above 1% by weight of cement or 0.15% by weight of concrete.

This is for chlorides added to the concrete during the mix, for chlorides diffusing into the concrete risk is much greater and significant corrosion has been found to occur at levels as low as 0.05 % by weight of concrete.

These values for chloride threshold are not universal and different authors have different threshold values [17, 46]. It was recognised by Leek [37] that pH was related to the

threshold chloride content required to initiate corrosion. Martin and Olek [43] showed that mild steel is able to retain passivity in the presence of significant concentrations of chlorides provided the pH is high. Many authors have attempted to identify a chloride threshold. Wheat et al [11, 48] concluded that it was not a unique value but a function of pH, oxygen content and surface condition. Page et al [49] and Mangat et al [50] studied the effect of pH on the chloride threshold level. Page et al [49] found that the method of applying external chlorides produced different effects in the pore solution chemistry with alternative wetting and drying having the greatest effect on chloride concentration. The chloride threshold concentration was expressed as the Cl^-/OH^- ratio and a critical ratio of 3 was found.

Concretes with different compositions have been found to exhibit different Cl^-/OH^- ratios. Mangat et al [51] stated that for the generally accepted chloride threshold values of 0.15 to 0.4% suggested a Cl^-/OH^- of 0.61. However experimental work suggested much higher values were applicable with values reaching 11 being recorded. Depassivation of rebars was found to occur quicker in cements for higher w/c ratios.

Kayyali and Haque [52] examined the threshold value in terms of Cl^-/OH^- ratio. A variety of different concrete mixes including the use of fly ash and super-plasticisers were used in the experimental study. The study investigated chlorides added with the mix and from external diffusion through the concrete. The pH, chloride content and evaporable water content were measured for each mix and pore fluid was also extracted to measure the pH and chloride content in the pore solution. It was concluded that the critical threshold Cl^-/OH^- ratio varied for different concrete mixes.

Yonezawa et al [53] used a pore solution expression technique to examine the Cl^-/OH^- threshold level. As with other authors they found a much higher threshold ratio than those expressed by Gouda or Hausman [53, 68]. The passivity of the steel was maintained at higher Cl^-/OH^- ratios for steel in mortar than in experiments that used artificial pore solutions. The mortar was said to provide a higher level of protection than pore solutions alone. The dissolution of calcium hydroxide crystals at the steel cement interface act to restrain any pH drop at the steel and act as a protective mechanism. The threshold level was not to be a simple parameter of pore solution but depends on the steel –mortar interface conditions.

Chlorides are introduced into the concrete as part of the original mix materials, either as contaminants or additives. These react with the calcium aluminate minerals in the cement and form solid compounds that are effectively immobile. Hydration slows with time, but in a good quality concrete hydration can occur for many years. This means that concrete has a capacity to absorb chlorides when cast into the concrete and can still be combined, but at a slower rate until hydration is complete. Not all chlorides will be combined whether cast or diffused into concrete and the remainder will remain as free chlorides. Different concrete mixes have different abilities to bind chlorides accounting for the differing threshold levels of Cl^-/OH^- ratios for different concrete's. There are two different types of chlorides present in concrete:

- Bound Chlorides
- Free Chlorides.

Free chlorides, as the name implies, remain in solution and are free to move, usually within the cover zone, by ionic diffusion through the pore solution. Free chlorides

increase the electrical conductivity of the pore water and as a result of their electrochemical properties, increase the rate of dissolution of the metallic ion, so forming corrosion products.

The ability of concrete to bind chlorides is controlled by the tri-calcium aluminate, (C_3A) content of the cement. Low C_3A cements have a lower threshold at which corrosion can start. The binding capacity of fresh concrete is at its maximum but the sheer amount of chloride added at mixing can be so large that significant levels of free chlorides remain. It is unlikely that an absolute threshold chloride level could be found, one reason is that concrete has a finite chloride binding capacity and this will effect the free chloride level in the pore solution.

The chemical binding capacity of concrete has attracted research interest as it would appear to offer a method of producing a concrete more tolerant to chloride induced corrosion. Tang et al [54] examined the binding capacity of OPC pastes and mortars. The chloride binding capacity was found to be strongly dependent on the CSH gel content in the concrete and independent of the w/c ratio and aggregate content. The relationship between bound and free chlorides could be described by binding isotherms, which obey Freundlich equation at high chloride concentrations and Langmuir equation at low concentrations. Some of the bound chlorides are bound irreversibly, while others can unbind as free chloride concentration decreases. Mangat et al [55] found binding capacity to increase with w/c ratio in contrast to Tang et al [54]. Silica fume was found to result in greatly reduced chloride binding capacity, due to the lower alkalinity of the resulting mortar increasing the solubility of C_3A in the pore solution. The chloride level was found to correspond with corrosion rates. Suryavanshi et al [56] found that

chlorides bind by increasing an equivalent amount of hydroxide ions in the pore solution. Two mechanisms of chloride binding due to Friedel salt formation, by adsorption and ion exchange, were identified based on the Afm (aluminato ferrite mono) structure.

There is little research into the effect of the disparities in chloride thresholds and binding capacities on the corrosion of steel embedded in these materials. Many commercially used repair systems have different binding capacities and chloride thresholds when compared to the substrate concrete to which they are applied. It is possible that differences chloride levels, and therefore corrosion macro-cells, could develop between repair and substrate sites.

2.2.5 Chloride Induced Macro-cell Corrosion

There has also been a significant level of research into the corrosion mechanisms that occur after initiation. The work has used a variety of techniques to study corrosion. The theoretical conditions for corrosion can be predicted using the Pourbaix diagram (figures 2.4 and 2.5 modified for the presence of chlorides). These do not fully represent the actual conditions in a structure, but show that the steel may exist in one of three different states: passivity, localised breakdown of passivity (characterised by pitting corrosion) and active corrosion. The mechanisms that will occur are dependent on the environment within the concrete.

Once the chloride level has exceeded the threshold level localised corrosion can begin and this will continue unless environmental factors, such as a limited supply of oxygen

intervene to limit corrosion. Hawkins et al [57] examined environmental effects on corrosion rates and found corrosion rate increased with chloride concentration. However increases in humidity and surface moisture levels and temperature also increased corrosion. Mangat et al [58] found that corrosion rates were higher in different concrete mixes and this appeared to relate to chloride content. However chlorides are not directly consumed in the corrosion reaction. Logic would suggest that once the steel had depassivated then chloride would not continue to increase the rate of corrosion. Gonzalez et al [44] found that a 2% addition of CaCl_2 to carbonated concrete increased the corrosion rate by up to 10 times. According to Arup [41], pitting corrosion is most likely to develop in concrete with a moderate chloride content, with higher levels of chloride general corrosion is the most likely. In carbonated concrete, however, chlorides may play another role besides causing the depassivation of the steel, in depolarising the anodic steel to a more active corrosion potential.

Corrosion damage of steel can be controlled by concrete quality even in the presence of chlorides [59]. Wheat et al [48,11] found that because of the variation in permeability in concrete it could not be assumed that a specimen exposed to a salt solution would have a more negative corrosion potential. Rather than exposure to chloride the corrosion potential was a better indicator of the corrosion state of the steel. Corrosion is, therefore, dependent on other factors besides chloride content such as oxygen levels and moisture content.

In a concrete structure the levels of chloride at the steel will vary from location to location, particularly with different cover depths. The differing chloride concentrations will produce differing anodic polarisation curves for the steel (figure 2.7)[60].

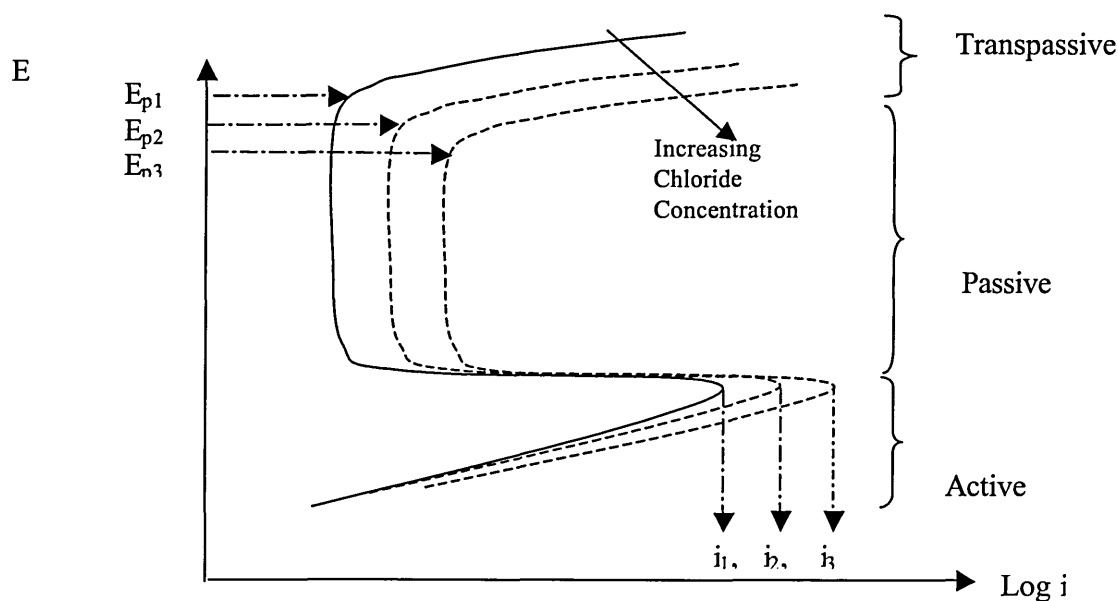


Figure 2.7 Schematic Anodic Polarisation Curves for Chloride Contaminated Concrete

If for example a piece of steel embedded in concrete has three different chloride concentrations along its length, it will also have three different critical pitting potentials. In figure 2.7 E_{p1} represents a situation with no chloride, E_{p2} and E_{p3} representing increased chloride concentrations. A higher chloride concentration has a lower critical pitting potential. The steel at E_{p3} with the higher chloride concentration would pit at a lower potential than the other chloride concentrations. The steel at E_{p3} would pit in preference to the other sites. As all the sites are electrically continuous the concrete at sites E_{p1} and E_{p2} would be cathodic to site E_{p3} even if these sites were above the threshold potential. If site E_{p3} was repaired and the polarisation curve returned to a situation without chloride like E_{p1} , then E_{p2} with the next lowest pitting potential would begin to corrode. The corrosion would be moved from site E_{p3} to E_{p2} , the moving of corrosion from one site to another on a structure is known as incipient anode effect.

Unless the concrete is completely dry corrosion activity can be related to differences in potential. Any areas of the concrete where the chloride is above the threshold level will become active and tend to have a more negative potential when compared to passive areas. If the steel is continuous between the two sites, the difference in potentials could create corrosion macro-cells. The sites with the lower potentials will be the anode areas while the higher potential site will be cathodic. A current will flow from the anodic site to the cathodic site. In dry concrete the size of the cathodic site is often limited by the high resistivity of the concrete reducing the size of the macrocell current. In fully immersed (in water) concrete the resistivity is lower and the cathode to anode size ratio is much larger. This means that even when the oxygen levels are low, as in submerged structures, the cathodic area can be large and carry a very high current to a small anode [61]. Repair of a site damaged by macro-cell corrosion will move the anodic site to the next highest chloride concentration, so moving corrosion around a structure.

One particular example of macrocell corrosion is in cracked concrete. In sound concrete a good quality of concrete cover will prevent the depassivation of the reinforcement. This is not the case in cracked concrete, where carbonation and chlorides can penetrate much more readily. Capillary suction in the crack plays an important role and the distance from steel to crack tip is shorter than the level of cover. This enables differentials of chloride concentration to occur readily around a crack tip and large macrocells can develop [28]. This has been widely recognised and studied [28, 62, 63, 64, 65].

Suzuki et al [65] and Ohno et al [66] measured potential, linear polarisation resistance and macrocell currents of cracked specimens. The test consisted of single cracked or multi-cracked specimens made from concrete mixes of different w/c ratios. Changing the steel stress could also alter crack widths. Corrosion was found to initiate readily at the major crack in the specimens, samples with wider cracks were found to depassivate quicker. The minor cracks also depassivated but the steel at the widest crack started to corrode much earlier. The most important factor influencing the degree of corrosion is the w/c ratio. Macro-cell corrosion increased as the w/c ratio increased. However while these results show that corrosion initiates at cracks, it is not clear that this was caused by macrocell corrosion.

Raupach [28, 62] used a segmented steel bar with zero resistance ammeters to measure the macro-cell current flowing between the segments. This showed that the steel at the crack acted as the anode and steel behind the crack acted as the cathode and a current flowed between them. Steel up to several decimetres from the cracks was found to act as the cathode. Higher w/c ratio also appeared to increase the macrocell corrosion validating the work of Suzuki et al [222] and Ohno et al [224]. Shorter crack distances were found to limit the corrosion rate as it limited the cathode size. However using small bars to reduce crack widths resulted in higher percentage losses of cross-section nullifying the effect of the shorter crack distance. The conclusion was that adequate concrete cover and quality was the only protection from corrosion. Berke et al [63, 64] also looked at corrosion of cracked concrete and found that $\text{Ca}(\text{NO}_2)_2$ inhibitor significantly improved corrosion resistance of embedded steel when cracks were present. Other work on inhibitors in chloride contaminated concrete has been carried by Ping Gu et al [67] and Gouda et al [68] .

Macro-cell corrosion has been studied outside of cracked concrete. Noggerath et al [69] produced an experimental and mathematical model of macro-cell corrosion. Schiessl et al [70] designed a concrete corrosion cell to experimentally examine parameters that influence macro-cell corrosion. Gulikers et al [71,72] also designed a galvanic corrosion probe and completed numerical analysis of galvanic interaction in reinforcement corrosion. In this case modelling is used to study the macro-cells that arise from differences in oxygen supply, chlorides or carbonation. The galvanic current I_{gal} , in the macro-cell was modelled using the following equation;

$$I_{gal} = \frac{E_{corr}^c - E_{corr}^a}{R_p^a + R_{con} + R_p^c} \quad 2.3$$

E_{corr}^a = anodic potential

E_{corr}^c = cathodic potential

R_p^a = anodic polarisation resistance

R_p^c = cathodic polarisation resistance

R_{con} = concrete resistance

The size of the galvanic current is dependent on the cell geometry and the area of the anodic and cathodic sites. Raupach [28] included correction factors for area (A_a – anodic area, A_c – cathodic area) and cell geometry (k);

$$I_{gal} = \frac{E_{corr}^c - E_{corr}^a}{\frac{R_p^a}{A_a} + \frac{R_{con}}{k} + \frac{R_p^c}{A_c}} \quad 2.4$$

The measurement of the area involved in the anodic and cathodic processes is not practical. It is, therefore, not possible to measure corrosion rates by this method. Arya et al [73] studied the effect of the anode to cathode ratio using a segmented bar to measure the current flowing between anode and cathode. The maximum anodic current was found to occur at relatively low anode to cathode ratios. This was not related to different

environments. For example, changes in concrete moisture content would have altered the anode to cathode ratios obtained. Even though a limited size effect was found for cathode to anode ratio, it was found that even when the distance between anode to cathode was over a metre a significant current still flowed.

These effects are important in repair situations where it has been shown that the incipient anode effect moves corrosion around a structure. There is little work that examines the effect of the mismatch in properties between repair and substrate concrete on corrosion

2.2.6 Differential Aeration Corrosion

Differential aeration is macro-cell corrosion caused by differences in oxygen concentration. Its importance has long been recognised in corrosion science by Evans and Pourbaix [34] and it is an important corrosion mechanism in soils [40, 74]. The differential aeration process is similar to that from chloride induced macro-cells. From the Nernst equation (equation 2.1) an area of the steel with a higher oxygen concentration will have a higher (more +ve) potential than an area with a lower oxygen concentration. If these two areas were electrically continuous a galvanic cell would be created. The area with the highest oxygen concentration would be cathodic and the area with the lowest oxygen concentration would be anodic.

This is the opposite of what might be logically expected with the level of oxygen consumption controlling the rate of corrosion. This would suggest an area with low oxygen concentration would have a lower corrosion rate than an area with a higher oxygen concentration. This is the situation in soils if the steel in the two areas is isolated from each other [74]. Steel in soil with a low oxygen concentration would have a lower

corrosion rate. However when the two areas are connected the situation is reversed and the corrosion rate in the low oxygen concentration area is higher.

Escalante [40] found that in well aerated soils, resistivity has a strong influence on the galvanic corrosion current. In poorly aerated soils the oxygen diffusion was found to control the magnitude of the galvanic current. In addition at a depth of 1m, the resistivity of the soil was found to be independent of seasonal moisture and temperature changes. The situation in concrete would be expected to be similar with the resistivity controlling the development of the size of the galvanic cell. However Pourbaix [34] states that differential aeration operates in different manner depending on pH of the solution:

- pH < 7: abnormal operation with a small current flow between the anode and cathode and a small change in corrosion rate.
- pH 7 to 10 : normal operation – passivation of the cathode and a large current and corrosion rate at the anode.
- pH 10 to 13: abnormal operation with passivation of the anode and cathode without current flow.
- pH above 13 normal operation similar to at pH 7 to 10 but less vigorous.

The normal pH of concrete falls in the range 12.5 to 13.5 (i.e steel is passive) this would put it in the border between abnormal behaviour and normal behaviour for differential aeration.

Differential aeration has not been widely investigated in concrete. Chloride ingress or carbonation is normally assumed to control corrosion. Some work has been carried out into the influence of oxygen on corrosion in reinforced concrete. Raupach [75, 76]

carried out work similar to that in chloride induced macro-cell corrosion [28]. The role of oxygen was found to be dependent on environment conditions and it was defined for four cases in which different parameters dominate corrosion rate.

1. Constantly dry concrete, no corrosion due to lack of electrolyte and therefore, oxygen concentration is irrelevant.
2. Short term wetting, here oxygen access is not impeded and corrosion rate is controlled by resistivity.
3. Wetting, the water content restricts oxygen access to the steel which causes corrosion rate and potential to drop when the wetting ends and the corrosion rate and potential rise back to the original level.
4. Constantly water saturated, once any residual oxygen is consumed the corrosion rate and potential falls to a diffusion-limited rate of corrosion.

Gonzalez et al [77, 78] have proposed mechanisms on the role of oxygen diffusion on corrosion in concrete. As with Raupach the degree of pore saturation was found to have an effect on corrosion and in fully saturated concrete oxygen diffusion was found to control corrosion rate. Gonzalez et al [78, 155] also proposed a mechanism for corrosion involving the establishment of crevice corrosion conditions in concrete at interfaces between coarse aggregate and the steel. A crevice forms behind the coarse aggregate and as the residual oxygen is consumed a differential aeration cell is set up between the area of steel at the crevice and the steel in the rest of the concrete. This initiates corrosion in the crevice and leads to the localised acidification of the solution in the crevice. Eventually the situation will be reached when the potential and pH will allow an alternative cathodic reaction of hydrolysis and hydrogen evolution. Once this situation is reached corrosion in the crevice will be autocatalytic and independent of oxygen diffusion.

This is the classic crevice corrosion mechanism, however it relies on the ability to establish a differential aeration cell to initiate crevice corrosion. Pourbaix [34] suggests this will not happen unless the $\text{pH} > 13$ or chlorides are present to depassivate the steel. If chlorides were present they would have to be greater than the threshold concentration at the aggregate rather than in the concrete mortar. This would probably require chloride contamination of the aggregate. In addition the localised fall in pH assumes that the calcium hydroxide at the steel interface will not buffer the pH at a higher value. There may be situations where this does occur, but the mechanism has not been generally accepted in literature.

Ping Gu [19] connected the reinforcement of samples made using different w/c ratio concretes. One sample has a high porosity (easy oxygen access), the other low porosity (poor oxygen access). The specimens are immersed in 10% NaCl solution or with 3% NaCl cast into the samples. The low porosity side of the cell with low oxygen concentration was found to have a higher corrosion rate than the high porosity side. This is said to indicate the establishment of a differential aeration cell. However, the experimental results are obtained using impedance spectroscopy and general changes in impedance and phase angle are taken to indicate an increase in corrosion activity. No Nyquist plots are presented in the data and the analysis of the results is not clear. This work is used as a justification for a differential aeration corrosion mechanism (figure 2.8) used in subsequent work [20, 22].

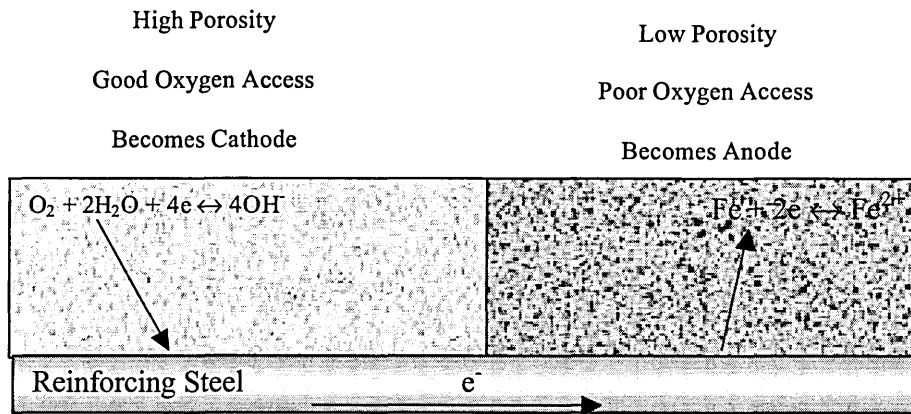


Figure 2.8. Differential Aeration Mechanism (27)

Suzuki et al [80] conducted similar work but with embedded stainless steel plates and mild steel reinforcing bars. The samples were in a 3.1% NaCl solution at 65°C. The stainless steel is nobler than ordinary steel. When the two are connected the mild steel becomes the anode and corrodes at an enhanced rate. However, the stainless steel embedded in the concrete when connected to a mild steel bar in solution shows a reversal and the steel becomes the cathode and the stainless steel the anode. This was found to be irrespective of chloride concentration. This would suggest the establishment of differential aeration, but the mild steel cathode was not embedded in concrete and at the temperature of 65°C used, oxygen concentration would be very low. This is not a normal application as it does not show if differential aeration conditions can be established in concrete.

The work on the role of oxygen diffusion on corrosion in reinforced concrete is not conclusive. The work into differential aeration does not provide any widely accepted mechanisms. However it has been used to justify corrosion models by some authors.

2.3 MASS TRANSPORT IN CONCRETE

The proposed mechanisms of corrosion indicate that the following factors are important in initiating corrosion and controlling the rate of corrosion:

- Moisture content in the pores, i.e. the presence of an electrolyte which controls the resistivity of the concrete
- Chloride ingress or carbonation, which control depassivation of the reinforcing steel in concrete.
- Oxygen level in the concrete, which controls the rate of the cathodic reaction.

Mass transport studies in concrete are normally concerned with diffusion of chlorides, oxygen and moisture. The diffusion properties of concrete are controlled by its microstructure and in particular the pore structure. Modification of the pore structure is an important factor in the durability of concrete repairs and needs to be considered in corrosion studies.

2.3.1 Porosity

Porosity is a volume property and it represents the total pore content of the material [81, 82]. These pores will vary considerably in size and this has a large impact on the mechanical properties of the concrete. Permeability is a measure of the continuity of the pores and the resistance they offer to the passage of a fluid or gas. It is an important indicator of mass transport properties.

Pores are formed during hydration of concrete, the initial porosity being determined by the volume of mixing water, entrained air and accidental voids from incomplete compaction of the concrete. As the cement hydrates new material, composed of mainly calcium silicate hydrate (CSH) gel, will partially occupy the water filled space between

cement grains. Thus the changes in the porosity of the material can be classified as follows:

1. Porosity of the original aggregates
2. Voids filled with water and air after partial hydration of the cement.
3. Voids filled with water and air after consolidation and final set.

The porosity of cement for most practical purposes depends on the water/cement (w/c) ratio and the degree of hydration. The w/c ratio will determine the original porosity and the degree of hydration how much the original pores are filled with new solid products. Two classes of pores can be identified, capillary and gel pores. Gel pores form approximately 28% of the total gel volume and range in size from 1 to 10 nm [83]. Capillary pores range in size from 10 nm to 10 μm . The gel pores are only an order of magnitude greater than the size of water molecules. Capillary pores, particularly the larger pores, generally have the largest influence on the porosity of the cement paste.

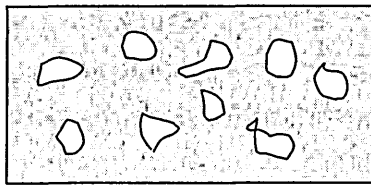
Porosity is typically measured by liquid displacement techniques. A sample is vacuum saturated in liquid and weighed in the saturated surface dry condition (W_s). The buoyed weight (W_b) of the sample is measured by suspending it in a liquid. The liquid is then removed by drying in an oven at 110°C until a constant weight (W_d) is reached. The percentage porosity can then be calculated using:

$$\%Porosity = \frac{W_s - W_d}{W_s - W_b} \times 100 \quad 2.5$$

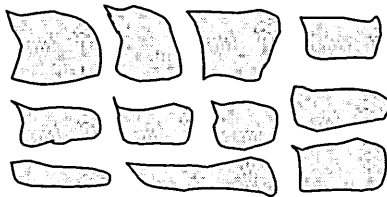
The porosity measured from displacement of water is higher than that measured using displacement of other liquids such as methanol or isopropanol, as water can be absorbed by the cement paste. An alternative method of measuring porosity is mercury intrusion porosimetry [84]. This technique can measure pore sizes ranging from 200 μm to 2 nm.

Other techniques to measure pore sizes involve image analysis of samples typically by scanning electron microscopy [83].

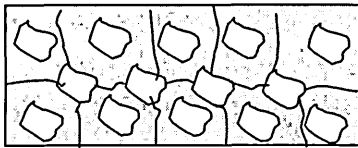
It has been shown that supplementary cementitious or pozzolanic materials such as fly ash or blast furnace slag, hydrate later than ordinary Portland cement [85]. This refines the pore structure of concrete and leads to blockages of capillary pores without reducing the percentage porosity measured. This implies that there is no definitive link between permeability and porosity (figure 2.9) [81, 82].



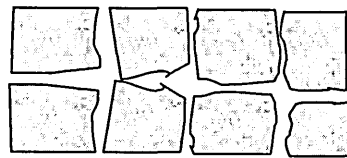
Porous impermeable



Porous, permeable



High porosity, low permeability



Low porosity, high permeability

Figure 2.9 Illustration of permeability and porosity [13, 8]

Garboczi et al [86, 87, 88] have conducted work on modelling the microstructure and transport mechanisms of concrete. The methodology uses the ideas of percolation theory to model the microstructure and physical properties at various scales in the concrete. However the model has not been widely adopted and will not be considered further in this project.

2.3.2 Permeability

Permeability is a measure of the resistance to the flow of water or gasses. As corrosion rates are generally controlled by diffusion rates into concrete, it is assumed the more impermeable the concrete the lower the corrosion rates. A review of techniques and theory of permeability can be found in Concrete Society Technical Report 31 [82]. Permeability is strictly related to the flow that occurs under an applied pressure. However it is frequently used to describe other transport mechanisms such as absorption, adsorption and diffusion.

- Adsorption is the process by which molecules adhere to the surface of the concrete by either Van der Waals forces or chemical bonds.
- Absorption is the process by which the concrete takes in fluid to fill spaces within the concrete.
- Diffusion is the process by which a liquid or gas moves under a concentration gradient and is defined by a diffusion coefficient.

The permeability of a concrete can result from a combination of absorption, flow and diffusion. The measurement techniques employed would be dependent on the moisture content in the sample.

Diffusion studies use Fick's Laws to calculate diffusion coefficients for various concrete mixes. In gas diffusion tests the diffusion coefficient of a gas such as carbon dioxide or oxygen is measured for a concrete sample [89]. Ionic diffusion tests monitor the diffusion of ions such as chlorides from one side of a sample to the other and are analysed using Fick's Law. Water vapour diffusion is a measurement of the weight of

water diffusing into a sample, the concentration gradient being achieved by maintaining the sample at varying relative humidities [90, 91]

Absorption measurements have been characterised and standardised in BS1881:122 [102, 82, 103] and relate to water uptake in concrete. The tests normally involve the intake of fluid into the sample by capillary suction as a result of the surface tension forces. Water absorption capacity tests are carried out to obtain information on the water holding capacity of concrete. The capillary rise has been found to show a linear relationship with the square root of time and the proportionality constant of this relationship is termed sorbtivity [89].

Absorbitivity tests determine either the quantity of water absorbed in a specific direction or the time needed for the absorption of a specific quantity of water. It is not essential that the water is absorbed from one surface as in the sorbtivity tests. The most common absorption test used is the ISAT test [89, 94, 95]. It has shown potential as a measurement of the durability of concrete mixes [94].

Diffusion, absorption and permeability are functions of the pore structure, the constituent materials of the concrete and the environment of exposure. Investigations in the laboratory can be undertaken under controlled moisture conditions but this is not easily achieved on site. There are a number of different methods of measuring permeability, both on site [89, 96, 97] and in the laboratory [81, 82, 98, 99, 100, 101], but comparing the results from different methods can be difficult. Permeability from saturated flow tests will be considered in this study. This test involves subjecting a

saturated specimen to a pressure head. The measurement of the flow through the sample allows the calculation of the permeability coefficient K from Darcy's Law:

$$\frac{dq}{dt} = K \frac{\Delta h A}{L} \quad 2.6$$

$\frac{dq}{dt}$ = the rate of flow of water (m^3 / s)

A = cross sectional area (m^2)

L = sample thickness (m)

Δh = pressure head (m)

K = Darcy coefficient of permeability (m/s)

The saturated flow technique also allows the intrinsic permeability coefficient (k) to be calculated from the Darcy coefficient by;

$$k = \frac{\mu}{\rho g} K \quad 2.7$$

ρ = density of the permeant

μ = viscosity of the permeant

g = acceleration due to gravity

For tests carried out using water at 23°C , this simplifies to:

$$k = 9.75 \times 10^6 K.$$

The intrinsic permeability coefficient enables the estimation of the pore radius as follows:

$$k = \frac{r^2 v \rho g}{8 \eta} \quad 2.8$$

r = pore radius

ρ = density

v = porosity

g = acceleration due to gravity

η = viscosity

The main advantage of adopting the saturated flow test to measure permeability is that only one transport mechanism is involved due to the flow of water through pores. A

further advantage is that the saturation mechanism does not cause any damage to the existing microstructure of the sample [81].

With the progression of the permeability test the flow is found to decrease [81, 101]. This is due to the self-sealing property of concrete under hydrostatic pressure that can interfere with the measurement of the permeability of concrete as it may take several days to reach a steady flow rate. The cause of the self-sealing phenomenon is not clear. The most quoted cause is from physical clogging of pores by loose debris in the sample. According to Hearn et al [101] self-sealing is permanent and irreversible and it is unlikely that physical blocking plays a significant role. Dissolved and re-crystallised material especially silicate hydrates are likely causes as water has been found to interact with the cement matrix under test. This supported by the observation that when samples were tested using propan-2-ol instead of water self-sealing did not occur [101].

Experimental techniques that can be used to define the operating parameters for permeability tests are described in the literature [82, 102]. Concrete Society Technical Report No. 31, Permeability testing of site concrete [82] provides recommendations on good practice for the measurement of permeability by flow. These guidelines have been adopted from the work of Jeffries at King's College London and provide a basis for defining the test parameters.

1. Capillary forces in the material would control the initial flow of water and act until water has passed through the full length of the specimen. Until this happens Darcy's Law does not govern the flow. This means that true permeability can only be measured on saturated specimens.

2. Any leaks in the system can have a large impact on the accuracy of flow rates being measured. Both the inflow and outflow should be monitored to allow compensation to be made for leaks.
3. Water free voids in the sample will disrupt the movement of water through the specimen. Applying a backpressure of 2 bar will dissolve any entrapped air in the specimen or apparatus.
4. Temperature of the apparatus must be kept constant, changes may cause fluctuations in low flow rate measurements.
5. Water flow rate can be expected to vary in a non-Darcian fashion with applied pressure. At low pressure gradients chemical interactions may result in the generation of osmotic pressures between the concrete and the pore water. High pressures can result in the compression of the pore structure resulting in a lower calculated permeability and may damage the specimen. Test pressure should be chosen as near as possible to the practical situation and quoted along with the calculations. A constant test pressure should also be used during the test as changes in pressure could result in movement of the specimen.
6. Leaching of calcium hydroxide etc, from high and medium permeability concretes may affect the permeability of the material. It may be advisable to use calcium hydroxide solution as the permeating fluid. However the effectiveness of this remains unclear from literature and there seems only a small chance of significant leaching from the low permeability materials.

Materials with very low permeabilities can take many days to achieve steady state flow. This makes determining permeability by saturated flow a lengthy procedure. It is also possible to measure permeability by depth of penetration. Khatri et al [102] found

relatively good agreement between penetration measurements and flow measurements of penetration. However according to previous work [101, 102] penetration tests would involve diffusion, absorption, capillary and flow mechanisms and therefore show poor agreement with the saturated flow technique test results .

The measurement of intrinsic permeability allows a comparison of permeability of liquids and gases [103]. Permeability from a gas is normally defined by the equation:

$$k = \frac{Qx2P_2}{A(P_1^2 - P_2^2)} \quad 2.9$$

k = intrinsic permeability
A = area of flow
x = depth of penetration
Q = volume flow rate
P₁ = upstream pressure
P₂ = downstream pressure

Bamforth [103] found significant differences in intrinsic permeability between those determined using a gas and those from a liquid. The differences were considered and a conversion factor proposed based on the gas slippage theory. Gas permeability has been studied by Dinku et al [98], while Hearn et al [99] proposed a permeability cell that could be used for liquids and gases.

2.3.3 Chloride Diffusion

The time taken for the threshold at which a critical Cl⁻/OH⁻ ratio is reached and chloride induced corrosion occurs, is largely dependent on the diffusion of chloride ions through the concrete. The diffusion coefficient for chloride is related to concrete quality and controlled by properties such as porosity and permeability. The diffusion properties of chlorides into concrete have been well researched [17].

The movement of ions in a solution can be described by three properties of the ion in solution, migration, convection and diffusion. Migration is movement under the influence of a potential gradient, convection is movement under the influence of a temperature gradient or mechanical mixing and diffusion is movement under the influence of a concentration gradient. Diffusion is [17 36] expressed in terms of Fick's First Law:

$$J = -D \frac{\partial c}{\partial x} \quad 2.10$$

Where J is the flux of species, dc/dx is the concentration gradient and D is the diffusion coefficient. The diffusion coefficient is the value calculated by most authors when studying chloride diffusion in concrete. This has been used as a material property for comparing different concrete mixes. Fick's First Law has been used to obtain diffusion coefficients for concrete [104 - 107].

The diffusion coefficient (D) normally varies between 10^{-5} and 10^{-6} cm²/s in aqueous solutions. The diffusion coefficients found for concrete are several orders of magnitude lower. Page et al [106] found chloride diffusion coefficients increased with the water/cement ratio. The diffusion coefficients found, were in the order of 10^{-8} cm²/s. Dhir et al [105] also used a similar technique to study chloride diffusion. The coefficient of diffusion for chloride was found to be in the order of 10^{-9} cm²/s, and to vary with the introduction of pfa and different curing techniques. Atkinson et al [102] found the diffusion coefficients to be in the range 10^{-9} to 10^{-6} cm²/s depending on w/c ratio with lower w/c having lower D values.

Short term experiments are used generate chloride diffusion data [104] for different concrete mixes. A potential or concentration gradients can be used to accelerate

diffusion tests to produce measurable data over short time periods [105,110]. These tests are largely used to rank the differences between concretes, rather than to accurately predict long-term performance.

Diffusion under the application of an applied electric field is known as migration [108,109]. The Nernst-Einstein relationship is used to calculate diffusion coefficients from chloride profiles and resistivity measurements.

$$\lambda_i = \frac{z_i^2 F^2 D_i}{RT} \quad 2.11$$

λ_i = ion conductivity

z_i = valency of ion

F = Faradays Constant

R = Ideal Gas Constant

T = Temperature

D_i = Diffusion Coefficient

Alternatively the diffusion coefficient can be calculated from measuring the diffusion limited current I [105 - 107] given by:

$$I = nFAD \left(\frac{\partial c}{\partial x} \right) \quad 2.12$$

n = number of ions

F = Faradays Constant

A = Area of Electrode

$\partial c / \partial x$ = Concentration Gradient

D = Diffusion Coefficient

A test method based on the migration principle has been standardised in the AASHTO T227 test (American Association of State Highway and Transportation Officials) and described by Andrade et al [104]. This method relies on measuring the amount of charge passing through a 100 mm by 50 mm disc in a six hour period under an applied potential of 60V. The test is a qualitative test for ranking purposes.

The corresponding “natural diffusion measurements” test, using a concentration gradient, is a 90 day ponding test covered in AASHTO standard T259. Andrade et al [104] compared both test methods and found that natural diffusion and migration were controlled by the same basic principles and regulated by the diffusivity or mobility of the ions. This meant that similar chloride profiles were achieved comparing the AASHTO T227 and T259 tests. However the 90 day ponding test in AASHTO T259 produced higher apparent diffusion coefficients, this was attributed to the short term nature of the tests. This indicated that while both tests were useful in quantifying differences between materials, the tests would need optimising to be able to predict the long-term performance of concrete structures.

An alternative approach for finding the diffusion coefficient is from the application of Fick’s Second Law;

$$\frac{\partial c}{\partial t} = D \frac{\partial^2 c}{\partial x^2} \quad 2.13$$

A common solution when the diffusion coefficient D is constant with time is:

$$C_{(x,t)} = C_0 \left[1 - \operatorname{erf} \left(\frac{x}{2\sqrt{D_c t}} \right) \right] \quad 2.14$$

Where C_0 is the effective surface chloride concentration and $C_{(x,t)}$ is the concentration at a depth of x at time t . Therefore to calculate the diffusion coefficient requires the measurement of the chloride content of the cementitious material at a variety of depths and times. A typical method of obtaining the chloride level is to measure the acid soluble chloride content [51, 58, 111-113]. Dust samples from a known depth of concrete are added to dilute nitric acid, to dissolve the acid soluble chlorides. The

solution is filtered and a Mohr titration carried out. The chloride concentration is found from the following formula;

$$\%Cl^{-} = \frac{35.453vN}{10w} \quad 2.15$$

N is the concentration of $AgNO_3$, v is the volume of $AgNO_3$ and w is the mass of the powder sample.

This approach allows the calculation of the diffusion coefficient for the concrete. The results can be used to predict long-term chloride concentrations in actual structures [114, 115]. This offers the opportunity to predict time to initiation of chloride-induced corrosion. Many authors have investigated the possibilities of using diffusion data for predicting the long-term corrosion in reinforced concrete structures [105, 116 - 121]. There are differences in the techniques employed for making these predictions. Dhir et al [116] used a series of nomograms calculated from Fick's Second law for various levels of concrete cover, surface chloride concentration levels and water soluble chloride levels. This provided an estimate of the time to reach a certain chloride concentration. This is a practical solution to the problem in that an accurate diffusion coefficient calculation requires a large amount of chloride penetration data and that this is generally unobtainable for site concrete. The nomograms can cope with variations to materials, curing, cover, initial chloride content and surface chloride concentration. However as yet exposure conditions such as temperature and humidity variations have not been considered. These factors are important considerations in chloride penetration of actual structural concrete this provides a limitation to the work.

Berke et al [121] found that while the examination of chloride profiles in field structures provided useful data on the initiation of corrosion, data from existing concrete was not

reliable for predicting chloride diffusion in new concretes. Materials over 70 years old were found to have significantly lower diffusion coefficients than 27 years old concrete due to different mixing techniques. The authors claim good correlation from the use of ASTM Test Method C1202.

Not all authors accept the accuracy of this method of chloride prediction. Bentz et al [122] found that the application of the error function solution to marine exposed concrete samples revealed significant errors. The errors appeared to be more marked for concretes with lower diffusivities. This work did not use a correction factor for changes in diffusion coefficients with time. The diffusion coefficients were calculated over a 2 to 4 year period and did show a reduction with time. Nilson et al [17] also came to the conclusion that the application of Fick's 2nd Law to the estimation of chloride concentrations with time produces gross over estimations of the chloride levels.

Mangat and Molloy [119,120] investigated the use of Fick's Second Law of diffusion to predict long-term chloride concentration in concrete. Good agreement was found between surface concentration values and predicted surface values. It was shown that the diffusion coefficients decreased with time. An empirical relationship between the effective diffusion coefficient (D_c) at time t and the exposure period was proposed:

$$D_c = D_i t^{-m} \quad 2.15$$

D_i is the diffusion coefficient after 1 second and m is an empirical coefficient. This was related to the water/cement ratio as follows;

$$m = 2.5(w/c) - 0.6 \quad 2.16$$

Taking account of the fine variation of the diffusion coefficients produced the following modification to Fick's second law of diffusion:-

$$C = C_o \left\{ 1 - \operatorname{erf} \left[\frac{x}{2 \sqrt{\frac{D_i}{(1-m)} t^{(1-m)}}} \right] \right\} \quad 2.17$$

The solution for Fick's 2nd law assumes diffusion in one dimension in a plane surface of infinite size. This is not the case in real life as most structures are composed of complex shapes. Sagues et al [123] modelled chloride diffusion for corners and round columns. The normal way to solve Fick's 2nd Law is to use a Laplace operator (∇). The solution then becomes;

$$\frac{\partial c}{\partial t} = D \nabla^2 c \quad 2.18$$

The Laplace operators in various coordinate systems are of a standard form. This approach may not find a real solution in every case.

$$\begin{aligned} \text{Cartesian Coordinates} & \quad \frac{\partial}{\partial x} + \frac{\partial}{\partial y} + \frac{\partial}{\partial z} \\ \text{Cylindrical Coordinates} & \quad \frac{\partial}{\partial r} + \frac{1}{r} \frac{\partial}{\partial \phi} + \frac{\partial}{\partial x} \\ \text{Spherical Coordinates} & \quad \frac{\partial}{\partial r} + \frac{1}{r} \frac{\partial}{\partial \theta} + \frac{1}{r \sin \theta} \frac{\partial}{\partial \phi} \end{aligned} \quad 2.19$$

However inaccurate the predictions of chloride concentrations are with time, the method of fitting concentration curves to a solution of Ficks 2nd Law does allow the calculation of a chloride diffusion coefficient. This has been used as a material property to assess the performance of different concrete mixes to chloride ingress. Polder [124] studied five different concrete types in a marine environment, calculating the effective chloride diffusion coefficient and time to depassivation. The estimated service lives were found

to be in the range 10 to 80 years. The addition of blast furnace slag, fly ash and silica fume by improving the resistance to chloride ingress was found to lengthen estimated service life as compared with ordinary Portland cement. Bentz et al [122] also found fly ash to improve resistance to chloride ingress.

Mangat et al [58,111] examined chloride diffusion in blended cements and microsilica concrete. Microsilica was found to produce cement with a higher intruded pore volume but a lower chloride diffusion coefficient and corrosion rate. Fly ash was also found to produce a higher pore volume and a coarser pore size. As with microsilica the chloride diffusion coefficient was lower, but a higher corrosion rate was measured. Slag was also found to improve chloride resistance and lower corrosion rate while increasing pore volume. This suggests that chloride diffusion is not linked to the structure of the paste matrix.

Nilson et al [17] found that chloride diffusion was linked to porosity and so depended on water/cement ratio, cracks and compaction. However they also stated that pozzolans such fly ash, blast furnace slag and microsilica had a beneficial effect on chloride diffusion. Pozzolans are widely used in repair materials and contribute to the low chloride diffusion coefficients of the materials.

The factors effecting chloride diffusion do not act separately but in combination so the following will contribute to the chloride diffusion coefficient of a concrete [17];

- Quality of cement (Composition, Fineness, Alakali content)
- Addition of Pozzolans (PFA, Slag, Microsilica)
- Admixtures (super plasticisers, polymers, air entraining agents)

- Aggregate (Porosity, Transition zone)
- Concrete Composition (w/c, Binder content, Grading Curve)
- Curing (Refines Pore Structure)
- Cracking (Cracks increase chloride access (Mangat et al[119, 120])

The chloride level in the environment, the type of concrete and its microstructure are the important factors in predicting the time for the threshold chloride level to be reached. At this point corrosion would be initiated due to depassivation of steel.

2.3.4 Oxygen Diffusion

A number of authors have investigated the oxygen diffusion rates into concrete [14, 15, 106, 125] by employing a similar approach to the study of chloride diffusion in concrete. An Arrhenius equation has been used to determine diffusion coefficients experimentally (see equation 2.20) [14, 15]. In water, the bulk diffusion characteristics of oxygen and chloride are the same. However, for cement mortars and concrete the diffusion rates for oxygen have been found to be far higher than those measured for chloride. As the concrete/mortar mixes get denser (i.e. lower water/cement ratios, (0.35-0.40) then this difference gets greater. This has been used to suggest [15] that the charge carried by the Cl^- ion has an effect compared to the neutral O_2 molecule.

$$D_{eff} = D_0 \exp\left(\frac{-U}{RT}\right) \quad 2.20$$

D_{eff} = Effective diffusion coefficient
 D_0 = pre-exponential diffusion coefficient
 U = activation energy
 R = ideal gas constant
 T = temperature (K)

Although different authors have used different techniques to investigate the oxygen diffusion characteristics of cements their findings have been very similar:

Oxygen diffusion coefficient is dependent on :-

- Curing conditions. Poor curing will give a high oxygen diffusion coefficient. The effect is greater for cements with slower rates of hydration.
- Moisture content of the concrete. When the water/cement ratio is lowered from 0.80 to 0.4 the oxygen diffusion coefficient is about 15 times higher [15]
- Type of cement and replacement material. Oxygen diffusion coefficient of mortar is lower than that for concrete and different cement types give different diffusion coefficients. Blast-furnace slag as 60% cement replacement gives a diffusion coefficient $\frac{1}{2}$ to $\frac{1}{3}$ that of ordinary Portland cement. Cement with 15% added polymer has an oxygen coefficient $\frac{1}{10}$ that of OPC [15].

Other effects have been noted. Hansson (125) found that the rate of diffusion through water saturated mortars was not dependent on cover thickness and had to be controlled by other factors such as cast surface layer at the steel/mortar interface. The presence of chlorides in the environment will reduce oxygen diffusion by an amount greater than that expected by the decrease of oxygen solubility in the pore solution. A possible explanation for this is the precipitation of chloroaluminates in the pores resulting in reduced porosity. However there seems to be no direct relationship between the diffusion of oxygen and chlorides into concrete.

The results also show a difference in diffusion coefficients of dry and saturated concretes. Kobayasi [15] and Ohama [14] studied the diffusion coefficients of dry concrete specimens and obtained results in the order of 10^{-6} cm²/s. Measurements on wet concrete samples by Yu et al [106] and Page et al [24] using electrochemical measurements of oxygen flux gave results of the order of 10^{-8} cm²/s. In comparison, the

oxygen diffusion coefficients in water are in the range 10^{-4} to 10^{-5} cm²/s. Houst et al [45] also carried out measurements of oxygen diffusion coefficients over a range of relative humidities and water contents of samples and confirm the results of other studies.

Page et al [24] modelled the diffusion coefficients of oxygen in water saturated concrete. They concluded that for water saturated concrete the level of oxygen diffusion is so low as to be unable to maintain the exchange current required for passivity of the steel. This has been taken to indicate that the passivity of the steel could be borderline in water saturated concrete.

The work on oxygen diffusion suggests that materials with longer diffusion paths have lower oxygen diffusion coefficients. This would appear to be linked with pore structure and porosity. The degree of connectivity of the pores would appear to be important. Therefore permeability would be an important indicator of oxygen diffusion. Repair materials tend to have low permeabilities and correspondingly low oxygen diffusion coefficients.

2.4 MODELLING OF CORROSION IN REINFORCED CONCRETE

There have been a number of models of the corrosion of reinforcement in concrete. The approach the models take varies from service life and whole life costing predictions [126] to physical models of the electrochemical corrosion processes [96, 215, 216].

Tuutti [126] developed a basic model in 1983 which has been developed further by other authors such as Andrade et al [132]. This model recognises an initiation period which represents the time taken for aggressive agents (chloride or carbonation) to depassivate the reinforcement. The propagation period is then regarded as a linear relationship controlled by oxygen diffusion, temperature and relative humidity (figure 2.4.1). The service life is then taken as the time when an unacceptable degree of corrosion has taken place or the time before repair is required.

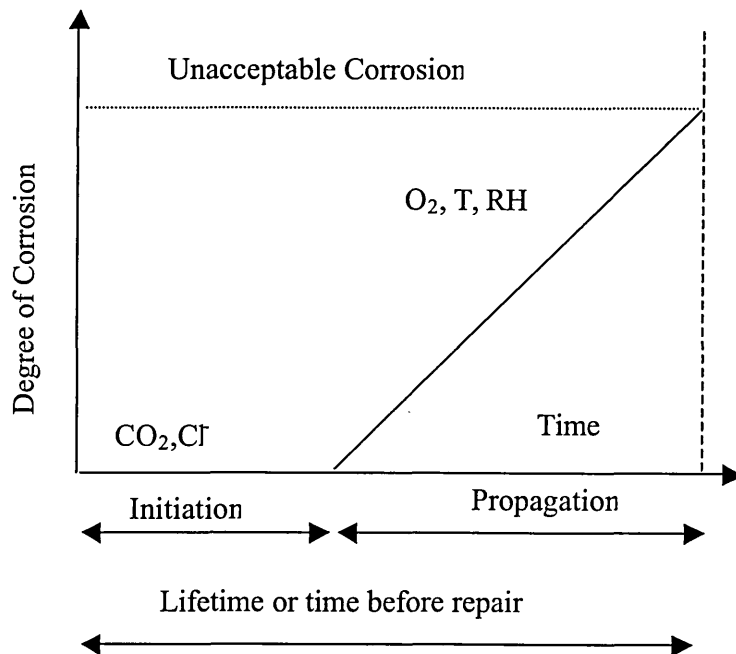


Figure 2.10 Service life model (Tuutti) [126]

The work of Tuutti was extended and refined to identify the following parameters;

- The aggressivity of the environment.
- Definition of service life.
- Consideration and calculation of the propagation parameters.
- Effect of protection methods on service life.

The initiation area has been well quantified by previous work into the diffusion of chlorides and the movement of the carbonation front through concrete. This uses Fick's 2nd Law to predict chloride concentration at the steel (C_x):

$$C_x = C_s \left(1 - \operatorname{erf} \frac{x}{2\sqrt{Dt}}\right) \quad 2.21$$

The prediction of the carbonation front is given by the expression:

$$X = K\sqrt{t} \quad 2.22$$

Where: X= carbonation front

K= proportionality constant

t= exposure period

In addition, knowledge of the relevant Cl⁻/OH⁻ threshold value for the depassivation of steel is required. There is enough research information available to model the initiation period [114]. The assessment of the service life can be proposed in a number of ways. Time to cracking [128] of the concrete is a key parameter and requires information on the extent of corrosion to cause cracks in the cover concrete. A simpler method [132] is to consider the loss of section of the reinforcement bar. Calculations of the load capacity of beams and columns make possible a prediction of service life from known corrosion rates. Recent research, however, has shown that cross-section bears no relationship with loss of strength and serviceability of corroded reinforced concrete structures; the

structural performance is governed by the loss of bond caused by the corrosion products and consequent cracking [133].

Predictions of the propagation period require knowledge of how corrosion develops over time. The suggestion of a linear relationship for this period would appear to be simplistic (figure 2.9). Previous research has shown moisture availability to have a key influence on corrosion. Knowledge of environment changes with time such as seasonal changes in temperature and relative humidity may therefore be needed. In addition the effect of concrete quality and pore structure need to be quantified and related to oxygen diffusion for different concrete types.

Physical models for the corrosion of steel in concrete have been developed by Bazant [35, 38]. These models are technically more advanced than Tuutti service life prediction. The author uses mass transport formulae to predict the concentration of chlorides and oxygen. These values can be used to calculate cell potentials and currents to model the development of corrosion rates with time over a structure. This work is continued by Balabanic et al [127] who use Bazants work as the basis for their own model. However the work has not gained general acceptance from other authors. A further limitation of this model is that it is based on concrete structures saturated with seawater and so is not directly applicable to land based situations.

Other techniques have been employed to model corrosion of steel in concrete. Hausmann [129] uses a probability model using a Monte Carlo simulation of passivation and corrosion. The model can cope with oxygen variation and Cl^-/OH^-

variations. The model has been compared with the work of other authors, but not extensively tested to take into account variations in concrete quality.

Models of cathodic protection systems [130, 131] provide techniques that can be applied to concrete corrosion. The electrochemical reactions are the same in cathodic protection as in corrosion. Koretsky et al [131] developed a two dimensional finite element model of cathodic protection system behaviour. The model uses oxygen flux to predict oxygen concentrations and the Butler-Volmer equation to predict current density resulting from the oxidation reactions. The Butler-Volmer equation is only strictly accurate for processes activated by a single reaction. For reaction sequences of more than one stage it may not be applicable. In addition, if oxygen diffusion is the limiting step of the reaction then a diffusion-limited current will be generated and the Butler-Volmer equation will not be applicable.

2.5 ELECTROCHEMICAL TEST METHODS

A variety of electrochemical tests have been employed by authors to study corrosion of reinforcement in concrete. An understanding of the limitation of these tests is important for the experimental study in the project.

There are a number of sound technical reasons to use electrochemical methods to measure corrosion;

- Corrosion is an electrochemical reaction and electrochemical monitoring techniques provide mechanistic information about the type of corrosion
- By employing Faraday's Law it is possible to calculate corrosion rates. This provides a method for measuring low corrosion that is more sensitive than the alternative gravimetric techniques.
- It is possible to adapt some of the laboratory monitoring techniques as a non-destructive assessment tool for site management [199, 215, 216].

Rodriguez et al [134] assessed the features of many of the most common techniques currently available for assessing the rate and extent of corrosion (see table 2.2). Other similar surveys have also been published, for example, Andrade et al [33].

The comparison between visual observations and electrochemical methods given in table 2.2, indicates that the visual observations provide little quantitative information in the absence of lengthy and destructive investigations. Electrochemical measurements can offer the prospect of quick, quantitative and highly sensitive measurements of corrosion.

Table 2.2 Comparison of the most widely used methods for measuring corrosion Rodriguez et al [134]

Characteristic	Qualitative Visual Obs	Quantitative Visual Obs.	Weight loss Ana.	Potential Mapping	LPR	Coulostatic	Electrochemical Noise	EIS	Harmonics	Galvanic
Speed of Measurements	A	C	C	A	A	A	B	B	B	A
Speed of response	C	C	C	A	A	A	A	A	A	A
Quantitative Information	C	A	A	C	A	A	B	B	A	B
Non-destructive	A	C	C	A	A	A	A	A	A	A
Non-perturbing	A	C	C	C	C	B	A	B	C	A
Measurement Parameter	Appearance Changes	Geometrical Changes	Average Mass	Half-Cell Potential.	LPR	Current Density	Half-Cell Potential	R _{CT}	R _{CT}	Current

Key (A) Optimum

LPR – Linear Polarisation Resistance

(B) Satisfactory

EIS – Electrochemical Impedance Spectroscopy

(C) Unsatisfactory

R_{CT} – Charge Transfer Resistance

2.5.1 Half-Cell Potentials

One of the first widely used electrochemical measurements was the half-cell potential and have been in regular use since the growth in use of cathodic protection for pipelines after World War II. The measurement of a half-cell potential is relatively easy in comparison to other techniques and hence a large amount of research has been conducted. A commonly used standard for half-cell potential measurements is ASTM C876. In the standard potential measurements in certain ranges are related to the probability of corrosion (table 2.3)[48, 135, 136, 137, 138, 145].

Table 2.3 Half-Cell Potential Measurements ASTM C876

Half-Cell Pot. Wrt Cu/CuSO ₄	Probability of Corrosion
< -200mV	< 5%
-200 to -350mV	Uncertain
>-350mV	>95%

The measurements according to ASTM C876 have been widely used on site to assess corrosion damage to structures. However, this relationship of potential to corrosion is an empirical relationship. This relationship has been based on studies of the corrosion of concrete that have not always proved to be accurate. For concrete in carbonated structures, cell potentials higher than -100mV can still indicate high rates of corrosion. Conversely in repaired structures with dense low permeability repair patches half-cells readings lower -500mV can still indicate low corrosion rates.

Many papers relate the use of ASTM C876 for measuring the extent of corrosion on site [18, 60, 95, 139 - 144]. The potentials are usually displayed as a potential contour map

with areas of highest activity related to the ASTM C876 values. The technique does require skilled interpretation, with knowledge of factors such as the IR drop in the concrete to give an accurate representation of the level of corrosion. Other measurements such as resistivity and chloride and carbonation measurements often accompany the on site potential measurements, to provide additional data

The Nernst equation [199] is the justification for half-cell potential and is the relationship between cell potential and the activity of oxidised and reduced species in the corrosion reaction.

$$E = E_o + \frac{RT}{nF} \ln \left(\frac{\alpha[O]}{\alpha[R]} \right) \quad 2.23$$

Where:

E= Cell potential

E_o= Standard Electrochemical potential

α[O]= activity of oxidants

α[R]= activity of reductants

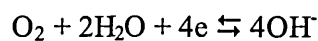
R= ideal gas constant

T= temperature (Kelvin)

F= Faraday's constant

n= number of moles of electrons transferred for a mole of reaction.

This shows that the cell potential measured is dependent on the concentrations (activities) of the oxidised and reduced ions in the chemical reaction. For the cathodic reaction:



Oxygen is the oxidant and the hydroxide ions are the reduced species. If the activity of oxygen falls then the value of ln([O]/[R]) will be negative and the cell potential will be lower. Therefore, sites with lower oxygen concentrations such as in dense repair patches [37] tend to have lower half-cell potentials. The Nernst equation only gives an

indication of the cell potential, not the cell current and so does not measure the corrosion rate. The Butler – Volmer equation can relate potential to current density [41,76].

$$i = i_0 e^{\left[\frac{2.3(E^\ominus - E^{eq})}{b} \right]}$$

i = current density

i_0 = exchange current density

2.24

b = Tafel constant

E^\ominus = Std. Cell Potential

E^{eq} = equilibrium potential

This procedure is only truly valid for charge transfer controlled processes and not strictly for diffusion controlled processes as may apply in concrete. Therefore this process is not commonly applied in practice and the empirical relationship of ASTM C786 is preferred.

Half -cell potential measurement is a common technique used in experimental studies of reinforced concrete mainly due to the ease of taking measurements [11, 50, 58, 63, 64, 68, 148 - 152]. Most of these studies do not carry out rigorous interpretation of cell potentials, but use them as evidence of corrosion activity in conjunction with other techniques such as LPR or galvanic currents. In these situations changes in potential with time are the important criteria. Therefore, a potential that becomes more negative with time is taken to show increased corrosion activity. Alternative assessments look at the development of distinct difference in potential between an anode and cathode to indicate macro-cell corrosion.

Electrochemical noise measurement involves a more detailed assessment of potentials. A large number of rapid and accurate potential measurements are taken and statistically examined. This is a highly specialised technique with a limited amount of work available in reinforced concrete [153, 60, 144]. Noise measurements give mechanistic information on the type of corrosion and are particularly useful in measuring localised corrosion phenomenon such as pitting. It is also possible to relate the standard deviation of the noise to changes in E_{corr} and I_{corr} .

2.5.2 Potentiodynamic and Potentiostatic Polarisation Curves

Potentiodynamic and potentiostatic polarisation curves are commonly used for assessing the kinetics of a corroding system and standardised in ASTM G5 and G61. The experimental procedure is to sweep through a range of potentials either side of the corrosion potential. Measurements of the electrochemical potential between the reference electrode and the working electrode are taken, and the current flowing between the counter electrode and the working electrode. The results are then plotted as potential versus log current density curves (figure 2.11). The curves are used to study mechanisms of corrosion and measure corrosion rates.

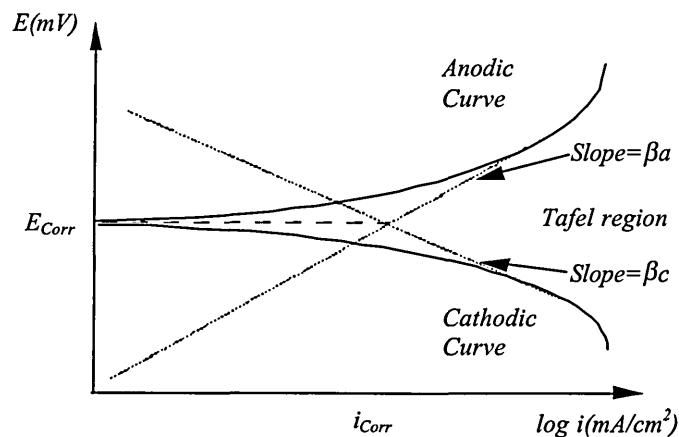


Figure 2.11 Polarisation curves showing Tafel extrapolation

Although polarisation curves provide mechanistic information for the measurement of the corrosion rate [143, 152, 155], to generate these curves you are required to sweep through a large voltage range. Polarisation tests are destructive and require a new test specimen for each measurement. The accuracy of measurement of Tafel slopes may also be a problem. Under ideal conditions these are as accurate as weight loss measurements. However, in most cases the Tafel regions do not extend over a reasonable range for accurate measurement. Knowledge of the Tafel constants is also used in the calculation of the corrosion current from linear polarisation resistance (LPR) measurements [50, 58, 63, 137, 138, 149, 152, 156 – 162].

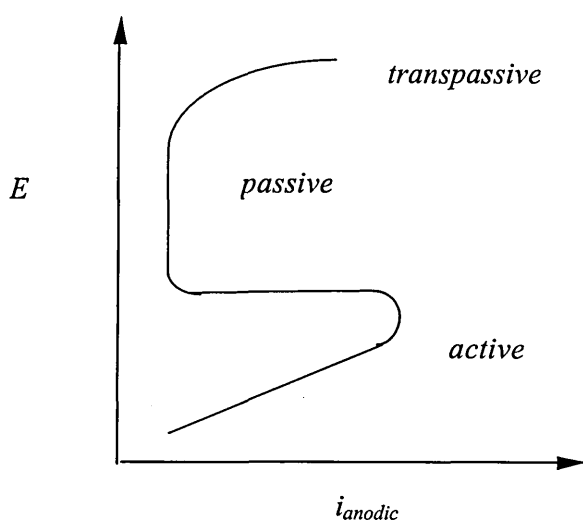


Figure 2.12 Anodic Polarisation Curve Showing Active-Passive Transition

The use of schematic polarisation curves is common in explaining corrosion theory [31, 204]. Figure 2.12 shows the predicted behaviour for steel exposed in an alkaline environment such as concrete. The curve is divided into three sections. The active zone covers the potential range over which the steel is actively corroding, with an increase in current with potential measured. In the passive zone the steel is protected by an oxide film, which acts to prevent corrosion hence a low constant current is measured. The

transpassive zone covers the range of potentials over which the passive film is no longer stable and localised corrosion such as pitting can occur.

However this stylised curve differs from what is actually measured. The behaviour of the metal in a particular environment is also dependent on the relative positions of the anodic and cathodic curves. The measured polarisation curve is dependent on whether the working electrode (steel in this case) is anodic or cathodic at any given point. Therefore a piece of steel embedded in concrete will produce a polarisation curve dependent on the position of the cathodic curve (oxygen reduction).

Examples of measured curves in different environments for a piece of steel exhibiting active, passive and transpassive behaviour can be seen in figure 2.13 [163]. Case 1 shows a situation where the cathodic curve (oxygen reduction) crosses the anodic curve (metal loss) in the active zone of the theoretical polarisation curve. This would indicate general corrosion giving a wide range of possible corrosion rates. Case 2 the cathodic curve intersects the anodic curve at three potentials, one active two passive. If the middle active passive zone is not stable very high corrosion rates are possible at these upper and lower intersections. In case 3 the cathodic curve crosses in the passive region. This indicates a metal which has formed a passive oxide film and therefore low corrosion rates, in many cases the desired situation.

There is little actual published experimental data of polarisation curves for steel embedded in concrete [143, 155]. Cigna et al [155] studied the effect of different concrete mixes on the polarisation curves, with very low corrosion rates being measured in the test samples. The effect of oxygen saturation was also examined and samples

tested in nitrogen purged solutions exhibited very low limiting corrosion currents. The corrosion rates determined from polarisation curves were found to be similar to those obtained from linear polarisation resistance test. However no attempt to calculate Tafel constants was made.

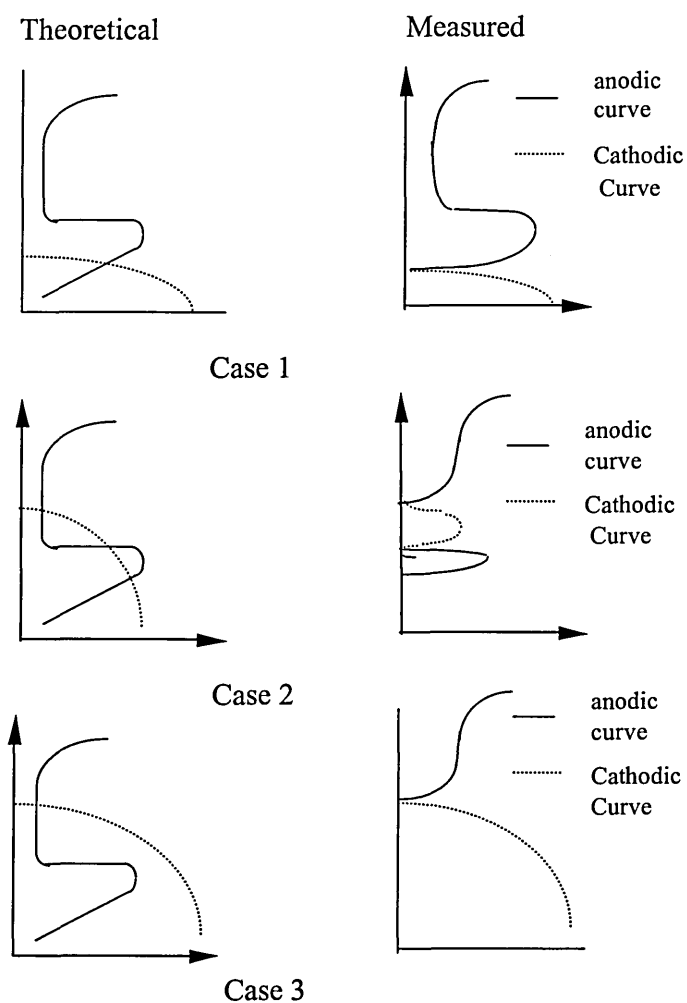


Figure 2.13 Theoretical & Measured Polarisation Curves [163]

2.5.3 Linear Polarisation Resistance (LPR)

This has become one of the most common electrochemical techniques employed in the corrosion monitoring of reinforced concrete and a large body of literature exists. The basis of the LPR test is that the relationship between potential and current in a polarisation curve approximates to a linear relationship as it passes through the origin [31, 33, 164] figure 2.14.

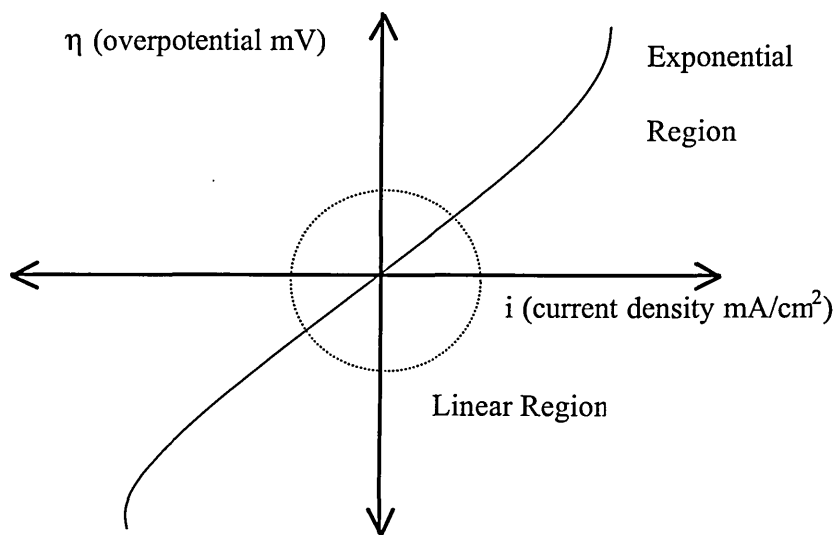


Figure 2.14. Linearity of polarisation curves.

The linear region extends over an area of +/- 20mV about the corrosion potential (E_{corr}). The exact extent is dependent on the system under test. In this region the polarisation resistance (R_p) is the slope of the linear region (figure 2.14) in accordance with Stern's relationship [33, 162].

$$R_p = \frac{\Delta E}{\Delta I} \quad 2.25$$

The polarisation resistance can be related to the corrosion current i_{corr} from the Stern Geary relationship;

$$i_{corr} = \frac{\beta_a \beta_c}{2.3(\beta_a + \beta_c)} \frac{1}{R_p} \quad 2.26$$

Where β_a and β_c are the anodic and cathodic Tafel constants, derived from the Tafel curve. It is clear that a full polarisation curve would be required to determine the Tafel constant. However i_{corr} is relatively insensitive to changes in the Tafel constants allowing them to be equated into a single constant B;

$$B = \frac{\beta_a \beta_c}{2.3(\beta_a + \beta_c)} \quad 2.27$$

Then the relationship between i_{corr} and R_p will simply be as follows:

$$i_{corr} = \frac{B}{R_p} \quad 2.28$$

For many different corroding systems approximate values of B of 26mV for actively corroding systems and 52mV for passive systems have been found. This is the technique that has been investigated by large number of authors to study corrosion in concrete [30, 33, 156, 164]. LPR has been compared to other techniques and the advantages of the technique have found to be:

- The non-destructive nature of the test .
- The ability to measure a quantifiable corrosion rate.
- Speed of making corrosion rate measurements.
- Very high resolution of corrosion rate can be made using Faraday's Law as follows:

$$P = \frac{Mi_{corr}t}{\rho zF}$$

P = penetration (cm)

t = time (s)

ρ = density (g/cm³)

2.28

F = Faradays constant (96500 C/mol)

M = molecular weight (g)

z = number of electrons transfered per atom

Gonzalez et al [164] has examined errors inherent in the measurement, this work recognises the disadvantages of the measurement technique, but considers them acceptable in the light of the advantages. The main problem of the technique is that it is an approximation of corrosion rate rather than an accurate measurement. A corrosion rate from LPR measurements may be in error by as much as a factor of 3. This is recognised by some authors [33, 134, 164 - 166] but many however ignore the question of the inherent inaccuracies. [38, 50, 58, 63, 138, 149 - 152, 157 - 162]. The approximation for the constant B used in the Stern Geary equation has been developed over a long period of time from use in measuring corrosion rate in the process industries. There is little published data available on the applicability of this approach to reinforced concrete measurements. Some authors point to work suggesting that this approach is applicable [43, 167].

Weight loss measurements to confirm LPR measurements are difficult to achieve for reinforced concrete due to the low rates of corrosion and the difficulty in removing the concrete from the test coupons. There is a lack of published Tafel constants from polarisation curves to show the accuracy of the approximation, Sagues and Kranc [166] detail some values for B which suggest a value of 16-19 is more appropriate than 26mV used for actively corroding systems. Sagues and Kranc also suggest that the B value of

52mV for passive systems is a method of adjusting the underestimation of corrosion rate during the transition from passive to active behaviour.

A number of authors have investigated the use of LPR as a commercial structural assessment technique [33, 95, 158, 165, 168]. Flis et al [165] found that the commercial LPR units had several problems;

- The area of steel polarised is undefined. This produces an unquantifiable error in the i_{corr} measurements made.
- Localised corrosion such as pitting is underestimated using LPR.

The commercial LPR units use “guard ring” electrodes to identify the area of rebar polarised in the test. The different units produce a wide range of corrosion rates, higher than those produced using a potentiostat polarising the entire rebar under test. Flis et al [165] suggest that the units all overestimate the corrosion rate. The measurements do produce similar levels of reproducibility, showing that they can detect changes in corrosion (table 2.4)

Table 2.4 Corrosion levels in reinforced concrete related to the corrosion current measured by LPR

I_{corr} ($\mu\text{A}/\text{cm}^2$)	Condition
0.1 to 0.2	Passive
0.2 to 0.5	Low to moderate corrosion
0.5 to 1.0	Moderate to high corrosion
>1.0	High corrosion rate

The values quoted in table 2.4 would seem to be low in comparison to those from other surveys [165]. The approximation used in the calculation of corrosion current means they are not absolute values. However as relative measurements to show changes in corrosion rate with time the evidence suggests that they have value.

Berke et al [167] has compared LPR measurements to macrocell corrosion current measurements. This work suggests that macro-cell corrosion currents underestimate corrosion rate. They are also difficult to quantify as corrosion rates as the relative cathodic and anodic areas are difficult to estimate. Sagues and Kranc [166] suggest that polarisation measurements significantly underestimate corrosion rates especially from localised corrosion. The conclusion from the published data is that LPR is the simplest method for measuring corrosion rate and for detecting relative changes in corrosion. This is despite the inherent errors from the Stern Geary approximation.

2.5.4 Impedance Spectroscopy

Impedance spectroscopy is a relatively new technique for studying the electrochemical behaviour of reinforcing steel in concrete. The technique has been used to study corrosion for a number of years and has been particularly useful in the study of coatings. Rodriguez et al [134] and Andrade [33] review the major techniques for studying corrosion in reinforced concrete and cover the use of impedance spectroscopy. The technique is similar to LPR except that an AC signal of 10- 20mV about the corrosion potential (E_{corr}) is applied to the working electrode. The signal is applied over an extensive frequency range.

$$V = V_0 \sin \omega t \quad 2.29$$

Where V_0 is the maximum amplitude and ω is the frequency (rad s^{-1}). The response is a current, which is phase shifted relative to the input signal.

$$I = I_0 \sin(\omega t + \phi) \quad 2.30$$

Where ϕ is the phase shift between the perturbation and the response. The ratio between V/I is a impedance (Z), according to Ohms law. Impedance can be represented as a combination of reactances on real or imaginary planes. The magnitude of Z can be represented by the magnitude of $|Z|$ and angle ϕ . Alternative it can be specified by real (Z') and imaginary (Z'') components.

$$Z' = Z \cos \phi \quad 2.31$$

$$Z'' = Z \sin \phi \quad 2.32$$

In complex notation;

$$Z = Z' + jZ'' \quad 2.33$$

The real and imaginary components can be plotted on a Nyquist chart (figure 2.15).

The Nyquist chart will show a pattern of semicircles or straight lines at 45° . These patterns have the characteristics of electric components and can be modelled by using equivalent circuits. This is the strength of the impedance spectroscopy technique. Information on the use of impedance spectroscopy is available from textbooks such as Bret et al [36] and J. R. Macdonald [74]. Many general papers on the use of the technique are available [169 - 172]. These are not written specifically for use with concrete but contain basic ideas on the modelling and interpretation of data. Figure 2.15 shows Nyquist plots and the equivalent circuits that produce them. These allow the modelling of the electrode processes and the characterisation of the system. In the case of a basic corrosion process the Randles circuit (figure 2.15) models a semicircle in the Nyquist plot. The diameter of the semicircle is the charge transfer resistance (R_{CT}) and

is equivalent to R_p from LPR measurements. In this situation the corrosion rate can be readily calculated from [171, 172];

$$I_{corr} (A/cm^2) = \frac{0.026}{R_{ct} (Ohms/cm^2)} \quad 2.34$$

Measuring the size of R_{CT} from the Nyquist curve allows the corrosion rate to be calculated. The position of the semicircle is shifted by an amount equivalent to the solution resistance without affecting the size of the semicircle. This is unlike the effect solution resistance has on IR drop in LPR measurements. The Randles circuit (figure 2.15) is not universally applicable. In situations controlled partly or entirely by diffusion results in a line at 45° to the real axis at low frequencies. This can obscure the R_{CT} semi circle as it will no longer intercept the real axis at low frequencies. It may not be possible to resolve a value of R_{CT} from the Nyquist plot. A mathematical model of a suitable equivalent circuit will be required to analyse the results from the measurement. In concrete this normally requires the use of a Warburg parameter to represent the diffusion process in the measurement.

The elements of the circuits such as impedance, capacitance and Warburg impedance can be combined according to electrical theory. Impedances in series are summed and for impedances in parallel the reciprocals are summed. This allows a mathematical model for the equivalent circuit to be generated. However, producing an equivalent circuit from the experimental data and fitting that model to the system under tests is a process prone to error. It requires a considerable amount of knowledge about the system under test and the experimental method. The same experimental data derived from different equivalent circuits will produce different results. (see figure 2.16).

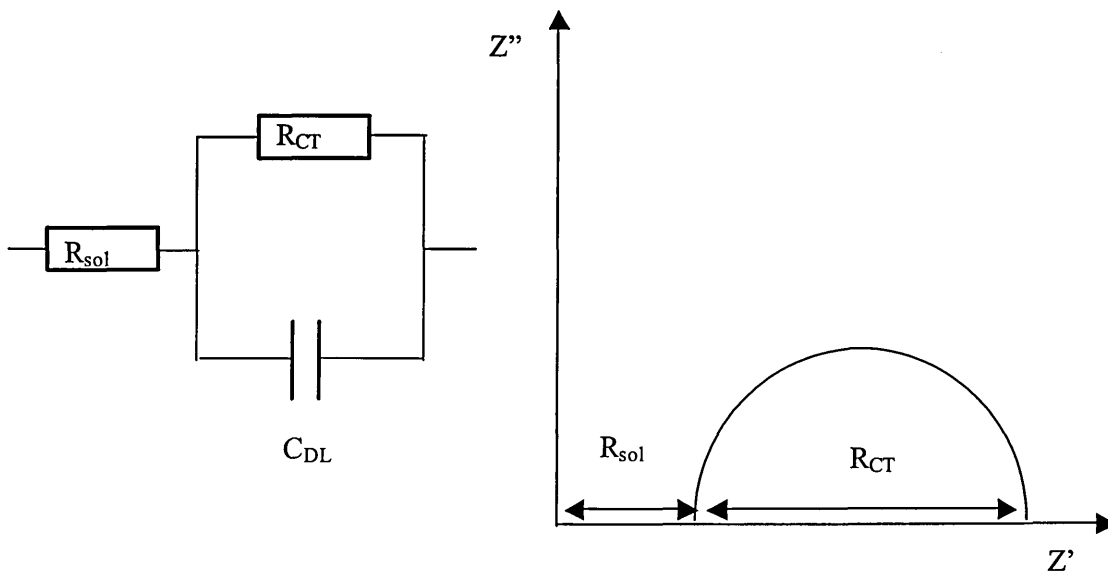


Figure a. Randles Circuit

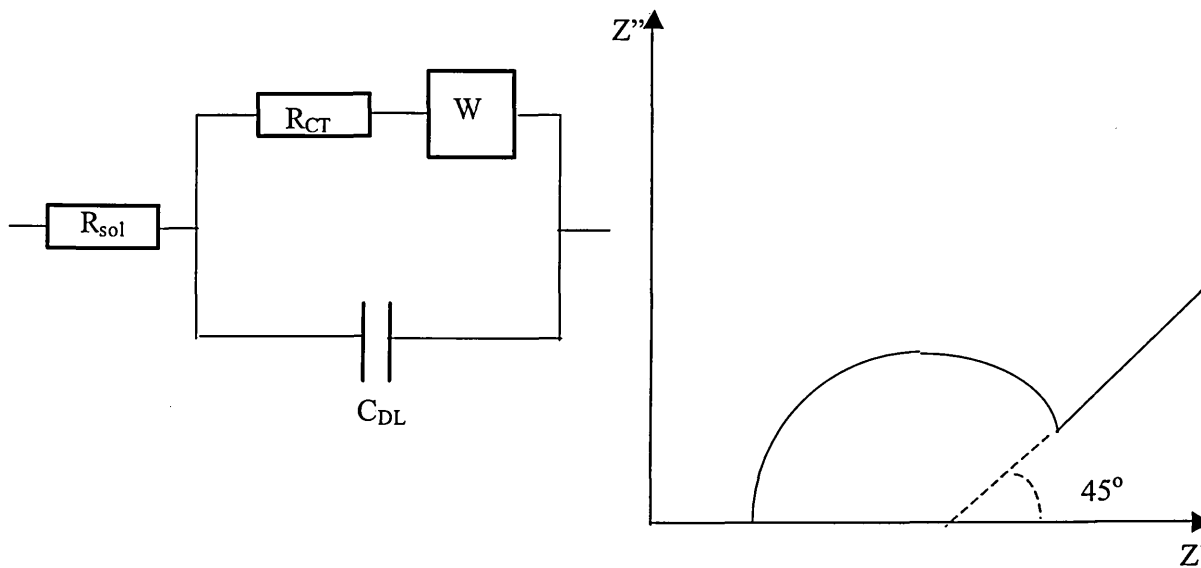


Figure b. Warburg Diffusion Impedance

R_{sol} = Solution Resistance

R_{CT} = Charge Transfer Resistance

C_{DL} = Double Layer Capacitance

W = Warburg Impedance

Figure 2.15 Equivalent Circuits and Resulting Nyquist Diagrams [36, 171]

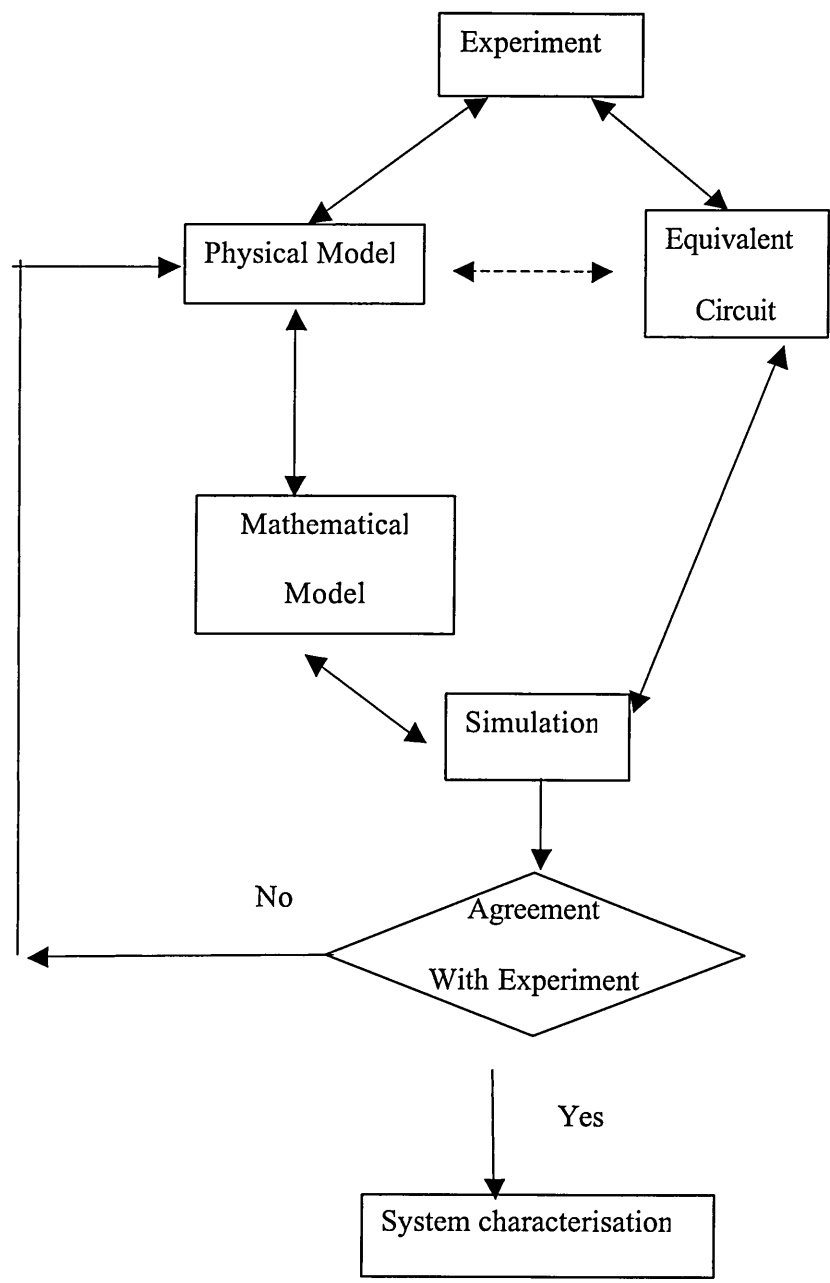


Figure 2.16 Flow Diagram for evaluating experimental impedance results [36, 74]

The extent to which different authors analyse their results varies considerably. Wheat [25] used impedance spectroscopy in the examination of corrosion rates in repaired reinforced concrete specimens. He postulated the equivalent circuit seen in figure 2.17. However, the author conducted a limited analysis of the results based on a mathematical model and did not determine corrosion rates from impedance spectroscopy. Lemoine et al [173] used a more complex equivalent circuit, but did not include a Warburg diffusion term. Lemoine et al went somewhat towards a mathematical analysis but did not apply the model to experimental data. Hatchani et al [174] (figure 2.17) used a simpler model without a Warburg diffusion. Sagoe-Crentsil et al [21] used another equivalent circuit model (figure 2.17) and partially analysed the experimental data from the model. All the experimental data presented by these authors are similar in form and magnitude, yet the equivalent circuits produced are different. Many authors do not fully analyse their data with models. It may be that the data does not fit the proposed model. Complex models are awkward and difficult to analyse while simpler models do not provide good fit to the data.

The complexity of data analysis overlooks the strength of impedance spectroscopy as a technique. From the measurement of impedance over a range of frequencies in the order of 10^7 to 10^{-4} Hz, it is possible fully to characterise a cementitious material. The high frequency end of the spectrum produces information on the bulk material properties such as the properties of bulk cement paste. This can be determined from the appearance of an arc in the high frequency part of the spectrum [19, 176 -179]. The high frequency arc is modelled using a capacitor and resistor in series and accounts for the appearance of C_{mortar} , or C_m Capacitor in many of the equivalent circuits used by authors [21, 25 173, 174]. The size of the arc will be related to the conductivity and dielectric

response of the cement. It is likely that this is related to the pore structure and the constituent materials of the cement. Some work has been done in this area [19, 176, 177]. Coverdale et al [176, 177] used impedance spectroscopy in the study of early hydration and were able to use the high frequency arc to part model the early hydration of cement paste. Ping Gu et al [19] also examined the high frequency arc and concluded that it was mainly reflected the liquid phase and the microstructure of the solid phase. They proposed that there was a relationship between porosity and impedance while the conductivity of the pore solution was constant. From this work impedance spectroscopy has shown potential for the study of early hydration of cements and the study of time dependent changes in the porosity in the materials [201, 214, 236].

The low frequency behaviour from around 10 KHz to 10^{-4} Hz is the region largely effected by the electrochemistry of the system. This is the region of the spectrum, which gives a measure of corrosion rates. The spectra produced from this area by different authors do show a lot of similarity. In the 10 KHz to 10 Hz range many authors find a spur or partially formed arc [202, 30, 21, 171, 174]. This is represented by the capacitor and resistor in parallel. This can be seen in many of the equivalent circuits in figure 2.17 such as that of Sagoe-Crentsil et al [21]. The arc is represented as C_F and R_F produced by an interfacial film linking the steel to the concrete matrix.. A similar feature is found by Lemoine et al [30] but who proposed that it was related to the Ca(OH)_2 layer.

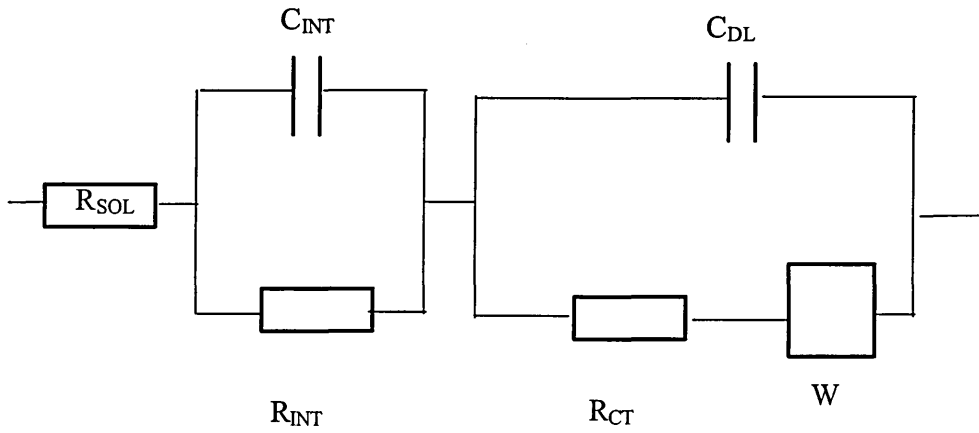


Figure a. Equivalent Circuit from Wheat [25]

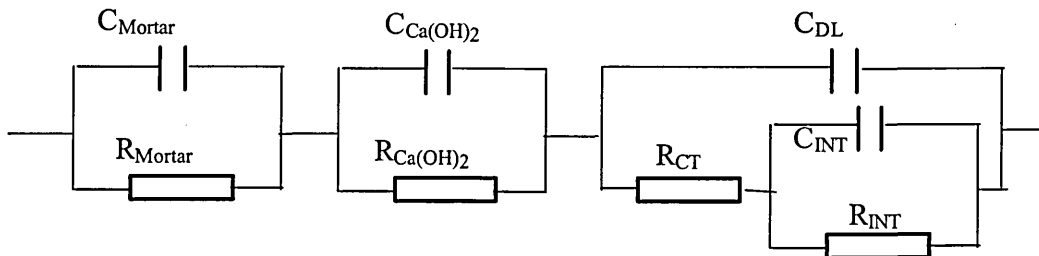


Figure b. Equivalent Circuit Lemoine et al [173]

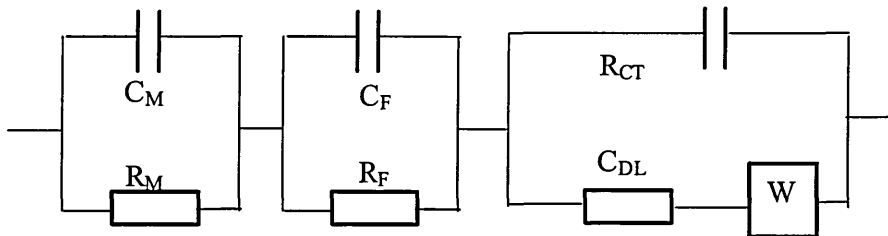


Figure c. Equivalent Circuit Sagoe-Crentsil et al [21]

Hachani et al [174]

Figure 2.17 Equivalent Circuits Used to Represent Corrosion in Reinforced Concrete

Beyond the interfacial arc the classic electrochemical arc is found. This contains the Helmholtz double layer capacitance at the surface of the electrode represented by C_{DL} and the charge transfer resistance R_{CT} . As with the Randles equivalent circuit R_{CT} is the value, which is equivalent to R_p in LPR tests. However even at low frequencies (10^{-4} Hz) the arc does not appear to be fully resolved [173, 178, 180]. It is not possible in this situation to accurately measure R_{CT} from the Nyquist chart. The appearance of the arc approaches a straight line at 45° at low frequencies. This has led many authors to include a Warburg diffusion impedance in series with R_{CT} in the equivalent circuit. [144, 173, 178, 180, 181]. The assumption is that the reaction here is under diffusion control. The slope of line is usually lower than unity [180] and the line appears to reach a limit at low frequencies. This is more consistent with a time limited diffusion impedance. In many measurements the arcs are depressed below the origin. This would make the fitting of data to the equivalent circuits difficult. Most of the work done with this type of equivalent circuits is not fully analysed [19, 144, 173, 181], R_{CT} values and corrosion rates are not calculated. Other authors take a simpler approach and remove the Warburg impedance [174, 178]. This makes analysis simpler and values for R_{CT} can be considered. However R_{CT} is treated in the same way as R_p in LPR tests and has the same inaccuracies of the Stern-Geary equation.

Impedance spectroscopy is being used to study the corrosion in reinforced concrete in a variety of situations. Ping Gu et al [90] has used impedance spectroscopy to study the effect of inhibitors on corrosion. Lee et al [182] study Epoxy-Coated reinforcement steel. Coatings are routinely studied by impedance spectroscopy and a lot of general work exists in this area [171]. Kazumi et al [183] used impedance spectroscopy in a surface mounted corrosion probe as opposed to embedded electrodes. The influence of

the counter electrode position was studied by Pech-Canul et al [175], who found that surface position was important for achieving a stable contact required for reproducible spectra. Ping Gu [19] used the technique to examine the effect on corrosion of uneven porosity in cement paste. The spectra were not fully analysed, but changes in impedance and phase angles were used to show evidence of increased corrosion. A similar approach was used by Wheat [25] in examining corrosion of repaired concrete specimens, as did Aguilar [184] in studying the effect of oxygen access on corrosion in partially submerged concrete slabs.

It is clear that impedance spectroscopy has achieved widespread use in a variety of areas. The ability of impedance spectroscopy to characterise cementitious materials for properties such as porosity and for the examination of corrosion shows the technique to be potentially very powerful. Impedance spectroscopy can give mechanistic information on corrosion not available for other techniques. However analysis is complex and many authors have failed to produce detailed analysis of their results. Even if R_{CT} values are measured any corrosion rates calculated will be as potentially inaccurate as LPR measurements.

2.5.5 Galvanic Corrosion Currents

This is a common method of monitoring corrosion of the reinforcement in concrete in the laboratory. It requires a corrosion cell to be set up with distinct anodic and cathodic sites. The current that flows between the anode and cathode is measured with time. The technique has also been described as macro-cell current [27, 28, 69, 80, 143] or corrosion current measurements [57, 59, 75, 185]. In all cases a galvanic cell is created and therefore galvanic current would appear to be the correct description for the technique.

The distinction between anode and cathode can be achieved in different ways. Some authors use a different metal normally stainless steel for the cathode [38, 73, 80, 143]. Stainless steel is nobler and therefore more cathodic than the mild steel reinforcing bar, which will be anodic. An alternative method is to separate the environment of the anodic bar and the cathodic bar. This is achieved by adding chlorides to the concrete around one bar thus making it corrode and by leaving the other bar in uncontaminated concrete. The actively corroding bar in the chloride contaminated concrete will be at a lower potential than the uncontaminated concrete and this will create a galvanic cell. The steel within chloride contaminated concrete will form the anode and the steel in the uncontaminated concrete will be the cathode.

The major problem with the measurement of galvanic currents is that the current measured is not the corrosion current and so cannot be directly related to the rate of corrosion. What is being measured is the net current flow between the anodic site and the cathodic. The magnitude of this current will be affected to some degree by the cathode to anode area ratio [27]. It is difficult to convert this value to corrosion rate as it ignores the possibility that the anodic and cathodic sites may contain complete macrocells independent of the measuring circuit. Under ideal conditions it may be possible to relate the galvanic currents to a corrosion rate [28, 71, 72]. However other authors report that galvanic currents underestimate corrosion rate in comparison with other techniques such as LPR [27]. A key advantage of the technique is the ability to record changes in galvanic current with time, without complex instrumentation. Changes in galvanic current yield a lot of information about the effect of different experimental conditions on the corrosion of the reinforcement bars.

Gulikers et al [71, 72] prepared test specimens from steel rebars in carbonated concrete to act as the anode and steel in repair mortar to act as a cathode. This created a “galvanic corrosion probe”. The galvanic currents were modelled and related to the polarisation resistance. With this form of numerical analysis it was argued that the corrosion rate could be calculated and from monitoring the galvanic current as follows:

$$I_{gal} = \frac{E_{corr}^c - E_{corr}^a}{R_p^a + R_p^c + R_{con}} \quad 2.35$$

I_{gal} = galvanic current

R_p = Polarisation Resistance

R_{con} = Concrete Resistance

E_{corr} = Corrosion potential

^a = anode

^c = cathode

Guliker et al designed a probe based on embedding active steel and some passive steel in a repair mortar. This however, would suggest that the current that flowed between the anode and cathode would be proportional to the conductivity of the concrete between them, rather than a measure of the state of corrosion in the steel in the structure.

Raupach [28] developed a similar theory to Guliker and related his model to the corrosion of cracked concrete and to corrosion between concrete repair and substrate concrete. Raupach uses the changes in galvanic current to show the establishment of a macrocell in the test environment. Similar work was done by Schiessl et al [27].

Raupach [75, 76] and Cao et al [59] apply a potential between the anode and cathode and measure the current that flows to show the influence of oxygen on corrosion.

The work carried out with galvanic corrosion cells suggests that they are extremely efficient at detailing the conditions by which a macrocell may be established in concrete. However they cannot accurately represent corrosion rate and are generally unsuitable for work outside the laboratory. The technique assumes by its definition that the anodic site must be entirely anodic and the cathodic site must be completely cathodic. If this is not the case the ratio between the area of the anode and the area of the cathode could cause an error in the modelling of the galvanic current. In the laboratory it may be possible to contrive a situation where this is so. In most cases the galvanic current is likely to be strongly influenced by the conductivity of the concrete making the areas of anode and cathode impossible to calculate. This possible error in the modelling and interpretation of galvanic currents is not taken into account by most authors. Raupach [28] includes the factors in the published model, but not how to estimate the anodic and cathodic areas.

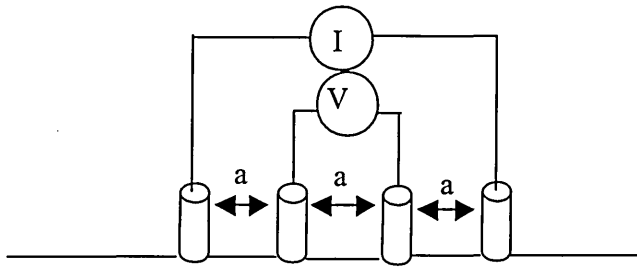
2.5.6 Resistivity

Resistivity has been recognised as a diagnostic technique for measuring the tendency of the reinforcement in concrete to corrode. The technique is often used in conjunction with corrosion potentials to give an actual indication of corrosion rate [186]. Values of resistivity that correlate to corrosion rates have been drawn up from practical experience as shown in table 2.5 [186].

Table 2.5 Relationship between resistivity and corrosion rates.

Resistivity (kΩcm)	Corrosion Rate
< 5	Very High
5 - 10	High
10 – 20	Low/Moderate
> 20	Low

Resistivity is measured by the Wenner technique. This uses four equally placed electrodes in contact with the concrete surface [160, 186, 187]. Figure 2.18 shows the arrangement of the four electrodes. [186].

**Figure 2.18** Resistivity Electrode Arrangement [186]

A known alternating current I is passed between the outer electrodes and a potential difference V is measured between the two inner electrodes. The spacing between all four electrodes is constant at a . The resistivity is then given by:

$$\rho = 2\pi a \frac{V}{I} \quad 2.36$$

Resistivity varies with water content, temperature and with conductivity changes in the pore solution of concrete. While a change in resistivity indicates a change in the

concrete it does not follow that this is representative of the corrosion rate. A strong link exists between water content in the concrete and the initiation of corrosion when under resistance control. Also the ingress of Cl^- would lower resistivity and indicate the initiation of corrosion. However the resistivity of the concrete at the surface does not indicate the state of the steel or the corrosion rate of the steel. Another problem is that resistivity is a function of the materials of the concrete and the structure of the concrete [186, 188]. Corrosion is largely a function of the electrolyte and the ability for diffusion through the concrete. A concrete mix made up high resistivity materials would still have a high resistivity irrespective of the resistivity of the pore solution. Conversely a material with a high porosity could still exhibit a low resistivity even though the pore structure is discontinuous and diffusivity in the material is low. These problems are not successfully addressed by authors researching the area.

Fiore et al [189] shows that resistivity is a function of relative humidity and cement type. Resistivity was found to fall with increasing relative humidity Carassiti et al [160] found the relationship between corrosion rate and resistivity required further work to clarify the position. Other authors suggest that the relationship is a valid method of detecting the change between passive state and active corrosion [187]. The technique has also been used for a considerable period of time in soils. Escaltante [40] found that soil resistivity had a strong impact on the magnitude of galvanic current in well aerated soils. However in poorly aerated soils, oxygen controlled the magnitude of galvanic current rather than resistivity. At a depth of 1m the resistivity of soils was strongly influenced by soil temperature and was only slightly affected by seasonal moisture changes. This was also likely to be the case for concrete. As the mechanism of

corrosion changed from resistance to diffusion control the ability of resistivity measurements to detect corrosion rates would fall.

Other authors have used resistivity measurements in different ways. McCarter [190] used resistivity measurements to evaluate the properties of the concrete cover zone. The measurements were successfully used to monitor the ingress of water into the cover zone and showed considerable promise as a method of assessing the effectiveness of concrete surface treatments. Hunkler [191] examined the resistivity of the pore solution as a parameter of rebar corrosion. The author found a lack of fundamental research on the effect of resistivity and a lack of systematic studies in the subject. Resistivity of concrete was found to have a strong relationship to pore volume and relative humidity. The resistivity of the pore solution was highly effected by ionic concentration such as Cl^- concentration. It was also shown that not all water in the cement mortar was conducting, some water being retained in the gel pores. There was no satisfactory model available to describe the formation factor between the resistivity of the concrete/mortar and the resistivity of the pore solution. Other authors have used impedance spectroscopy [72] to measure the solution resistance of the corrosion cell. This measured the resistance of the path from reinforcing steel through the concrete/mortar and included the effect of pore solution and concrete structure. As this covered the actual diffusion path for oxygen or aggressive ions involved in corrosion it should provide scope for further measurements.

Resistivity has a long history of use for the measurement of corrosion in concrete and in soils. However research indicates that the relationship is not as simple as suggested by initial research.

2.5.7 Other Techniques

Galvanostatic or coulometric electrochemical techniques have been used by relatively few authors [30, 33, 150, 192, 193]. Rodriguez et al [134] indicate that these tests are quick, non-destructive and provide quantitative information in terms of an I_{corr} measurement. The technique involves applying a potential step $\pm 10\text{mV}$ and measuring the current response. From the response, the solution resistance the polarisation resistance and double layer capacitance can be calculated. The technique does require the use of an equivalent circuit as with impedance spectroscopy. This makes the technique difficult to interpret.

Harmonic analysis has also been applied to concrete by Gonzalez et al [199]. The technique is similar to impedance spectroscopy in applying a small amplitude AC signal to an electrode and measuring the first three harmonics from the response signal. It is faster than impedance spectroscopy and can be used to calculate I_{corr} and the anodic and cathodic Tafel constants [194, 195, 197].

Corrosion monitoring techniques are required to investigate incipient corrosion in concrete repair. A wide variety of techniques are available for this purpose and amongst these, electrochemical tests have been seen as one of the best solutions. Most of the tests are based on polarisation techniques largely developed by Stern in the late 1950s. All the authors have applied these techniques for studying the corrosion of steel reinforcement in concrete and a significant history of use for these tests has been built up. Gonzalez et al [164, 196] have studied the limitations in accuracy for all the major tests.

3.0 Introduction to Experimental Work

3.1 INTRODUCTION

The primary aim of this project is to investigate the corrosion of the steel reinforcement in repair patches on reinforced concrete structures and to provide an insight into the influence of concrete repair on the corrosion of the structure.

The corrosion arising from the use of repair materials on a reinforced concrete structure can be the result of factors such as:

- Repair methods and placement techniques. This would include the workmanship employed in making the repair to the structure.
- Incompatibility in mechanical properties between the repair material and substrate concrete. This has been identified as a prime cause of the failure of repair on a structure [21 - 23]. This can lead to cracking of the repair due to shrinkage and the redistribution of load in the structure due to creep. The cracks offer sites for corrosion macrocells to develop and as a consequence have been extensively studied [28, 62 – 66, 197].
- Incompatibility in physical properties of the repair material and the substrate concrete. The low permeabilities of repair materials to aggressive species provides a potential mismatch in physical properties between the repair and the substrate concrete. An hypothesis has been proposed that this allows macro corrosion cells to develop between the repair and the substrate [20 – 23, 169].

It is not possible to investigate all three areas in the present study. The effect of repair methods and workmanship is highly subjective and difficult to study experimentally and the effect of cracking on corrosion has been extensively studied. Therefore, the current

work will study the effects of the mismatch in physical properties between the repair and substrate on the development of corrosion within the repair patch. Previous work in this area [20 – 23, 169] shows a lack of experimental results and understanding of possible mechanisms involved. This area, therefore, offers the greatest scope for original work and contribution to knowledge.

A greater understanding of the effects of mismatch in the properties of repair material and substrate concrete would allow the production of more durable repair systems. This should improve the longevity of the structure to which they are applied.

3.2 AIMS AND OBJECTIVES OF THE EXPERIMENTAL PROGRAMME

The aim of the current study is to investigate the effect of the mismatch in physical properties between a repair material and the substrate concrete on the corrosion that develops in both materials. The study will involve test specimens made from commercially available repair materials and representative substrate concrete mixes. The specimens will combine a repair material and a substrate concrete, both representing a wide range of property mismatch and will also incorporate continuous reinforcement bars through the two materials. Standard corrosion monitoring techniques will be used to measure the development of corrosion in the specimens.

The experimental work will examine the following key areas:

1. The investigation of the long-term performance of the repair patches in resisting corrosion. This will involve
 - Study of the variations in the electro-chemical, physical and chemical properties of the repair system over time.

- Investigation of the possibility of an equilibrium between the corrosion of the parts of reinforcement bars passing through the repair material and those parts embedded in substrate concrete.
 - Determination of the requirements for initiating corrosion in the repair patch.
2. An investigation of the mechanisms and the relationship between the macro-cell corrosion of the reinforcement bars embedded in the repair material with those embedded in the substrate concrete, with special attention to the interface between repair and substrate materials.
 3. The effect of the repair patch on corrosion within the substrate concrete.

3.3 EXPERIMENTAL PROGRAMME

Test specimens that combined both a repair material and a substrate concrete in a single specimen were prepared. The samples were then exposed to an environment designed to accelerate the corrosion of reinforcement in the specimens. The corrosion rates were monitored over a period of time. The relevant physical properties of the repair and substrate materials used were measured in order to quantify the level of property mismatch between the two materials.

The experimental programme falls into two distinct sections:

1. Measurement of the relevant physical properties of the materials used and the identification of the mismatch in properties between substrate and repair. The literature review has identified that the physical properties important for initiation and continuation of corrosion are those which govern mass transport processes in the materials. In addition, it has been recognised that the physical properties can change with time as hydration continues within the cementitious materials. The following properties were identified as important for the corrosion processes and

were measured over a period of time to establish the level of property mismatch: porosity, permeability, resistivity and chloride diffusion.

2. The monitoring of corrosion within the specimens over a period of time to assess the corrosion rate of the steel embedded in the repair, at the interface and within the substrate material. The literature review identified a number of suitable techniques for corrosion monitoring. It was decided to use more than one technique to prevent over reliance on a single set of measurements and consequently provide more reliable data. The following techniques have been employed to monitor and identify the corrosion processes involved: Linear polarisation resistance, impedance spectroscopy, potential measurements, resistivity and polarisation curves.

The experimental investigations reported in the thesis have, therefore, been split into two distinct sections:

- Physical properties of the test materials.
- Corrosion testing

3.4 TEST MATERIALS

Three commercially available repair materials were selected based on manufacturer's information to provide a wide range of properties and to represent the typical range of repair materials currently available in the market. In addition, two substrate concrete mixes were used to represent a high and low grade substrate material. These allowed a range of combinations of repair and substrate materials to be studied.

3.4.1 Repair Materials

3.4.1.1 Repair Material A

Material A was a blend of low alkali Portland cements with microsilica and fly ash (PFA) admixtures combined with high purity limestone aggregate graded to a 5mm

average size. The material was shrinkage compensated in the both the plastic and hardened state using an ettringite forming binder system. The equivalent sodium oxide content of the material was less than 3.0 kg/m^3 and the aggregates were deemed by the manufacturer to be unreactive to alkali silica reactions or any form of alkali aggregate reactions. The mix was specified as containing no chlorides or carbon particle dispersions. The material was supplied as a complete mix in the form of a powder blend. According to the manufacturer's literature, the powder when mixed with water produced a non-shrink, homogeneous microconcrete that is non-slumping and has excellent adhesion and low permeability. The material was mixed according to the manufacturer's directions using a 12% water to powder ratio. Table 3.1 shows the expected properties of material A from the manufacturer's literature.

Table 3.1 Typical Manufacturers Data for Repair Material A

Property	Value
Density	2210 kg/m^3
28 day Compressive Strength	60 MPa (min)
Modulus of Elasticity	24 GPa
Bond Strength	2.4 MPa
Shrinkage (28 days)	>0.01%
Coefficient of Thermal Expansion	$11.1 \times 10^{-6} \text{ }^\circ\text{C}$
Water Permeability	$2.4 \times 10^{-15} \text{ m/s}$
Coefficient of Chloride ion Diffusion	$2.3 \times 10^{-13} \text{ m}^2/\text{s}$
Resistivity	9.4 k Ω cm
Working life	30 minutes at 20°C

3.4.1.2 Repair Material B

Repair Material B was a low density, high strength, shrinkage compensated mortar suitable for structural repair rendering and profiling of both vertical and horizontal surfaces. The material was supplied as a blended powder based on a styrene acrylic polymer modified cement with microsilica, fibre reinforcement and a graded aggregate of 2.5 mm maximum size. The material was mixed according to the manufacturer's directions with fresh water using a 16% water to powder ratio. This produces a rapid hardening, low density mortar. Table 3.2 shows the expected properties for material B from the manufacturer's literature.

Table 3.2 Typical Manufacturer's Data for Repair Material B

Property	Value
Density	1700 - 1750 kg/m ³
28 day Compressive Strength	48 MPa (min)
Modulus of Elasticity	19.6 GPa
Bond Strength	4.3 MPa
Flexural Strength	8.1 MPa
Water Permeability	9.65×10^{-15} m/s
Coefficient of Oxygen Diffusion	2.72×10^{-4} cm ² /s
Working life	60 minutes at 20°C

3.4.1.3 Repair Material C

Repair material C was an acrylic polymer modified cementitious mortar mix with lightweight fillers. The material was supplied as a blended powder and only required the addition of fresh water to produce a lightweight mortar suitable for application to both horizontal and vertical surfaces. The powder was mixed with fresh water in accordance

with the manufacturers directions, using a 12.5% water to powder ratio. Table 3.3 shows the expected properties for material C from the manufacturer's literature.

Table 3.3 Typical Manufacturer's Data for Repair Material C

Property	Value
Density	1420 kg/m ³
28 day Compressive Strength	30 MPa (min)
Tensile Strength	2.5 MPa
Flexural Strength	5.5 MPa
Water Permeability	1.21 x 10 ⁻¹⁴ m/s
Shrinkage	0.005% cured above water at 20°C
Working life	30 -40 minutes at 20°C

3.4.2 Substrate Concrete Materials

Two substrate concrete mixes to represent a high and low quality substrate were used. The easiest method of achieving this and still have a chemically similar mix was to vary the water cement ratio of a standard concrete mix. Two concrete mixes used to represent the substrate concrete were:-

- Substrate Concrete mix 1: Mix proportions (by weight) of 1:2:4 (cement: fine aggregate; coarse aggregate) with a water/cement ratio of 0.4. This resulted in a concrete with a typical cube compressive strength of 40 MPa
- Substrate Concrete mix 2: Mix proportions (by weight) of 1:2:4 (cement: fine aggregate; coarse aggregate) with a water/cement ratio of 0.8. This resulted in a concrete with a typical cube compressive strength of 28 MPa.

No attempt was made to keep the placement properties (such as workability) of the materials constant. It was decided to determine the properties of the materials (substrate and repair) in the laboratory. This ensured the use of a common set of test procedures for all materials, instead of different techniques adopted by different manufactures of repair materials. Details of the constituent materials used to make the substrate concretes are given in the following sections.

3.4.2.1 Ordinary Portland Cement

Ordinary Portland Cement, from Ketton, was used for the substrate concrete mixes. The cement complied with BS EN 197-1:2000, CEM I 42,5N (1) and had an average fineness of 400 m²/kg. The particle size distribution of the cement is given in Figure 3.1 and the typical chemical composition is given in table 3.4

Figure 3.1 Particle size distribution for Ketton OPC.

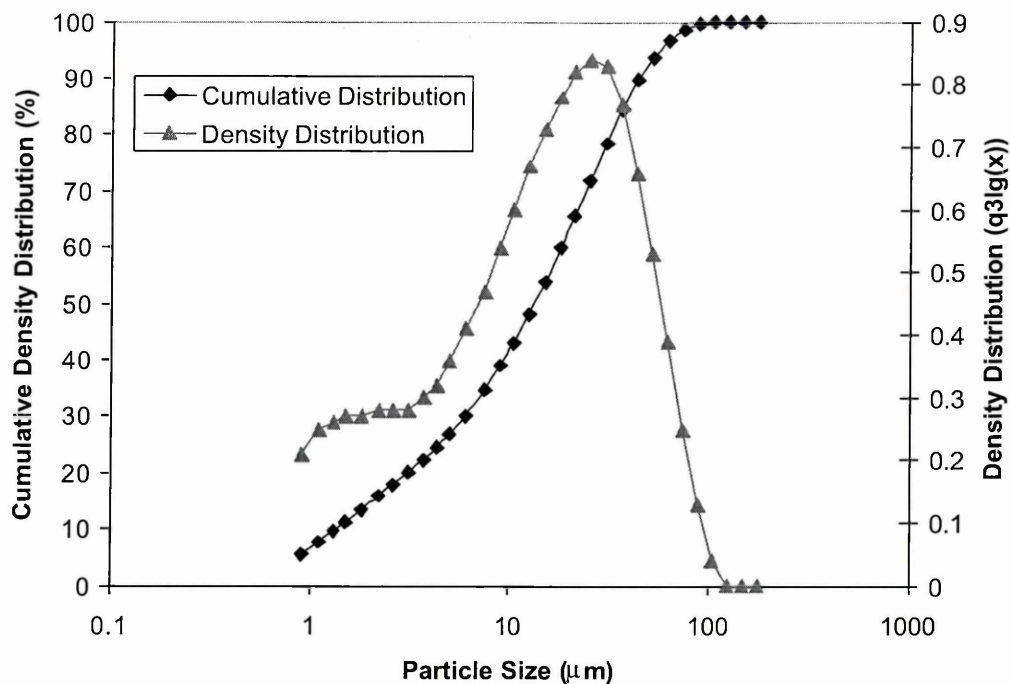


Table 3.4 Typical chemical composition of Ketton Ordinary Portland Cement

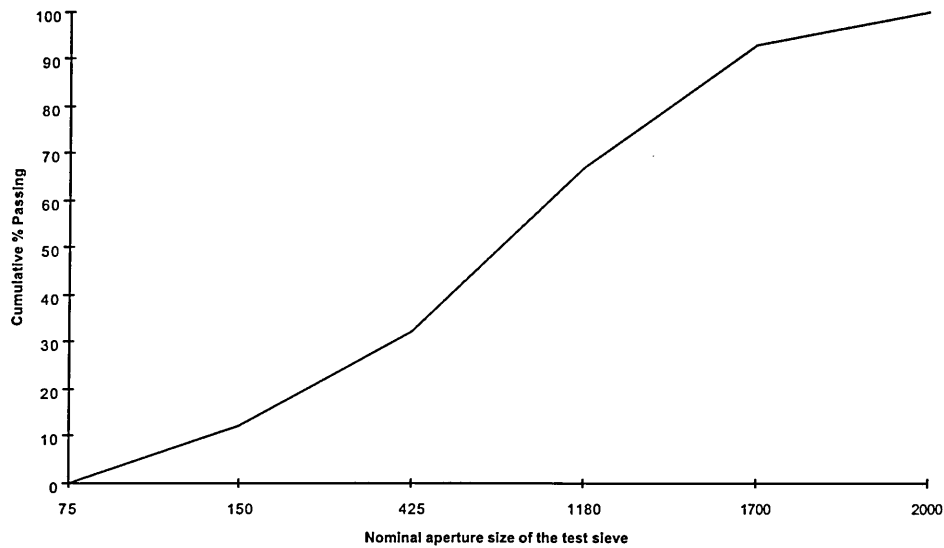
Compound	%
SiO ₂	20.95
Al ₂ O ₃	4.51
Fe ₂ O ₃	2.77
CaO	63.92
MgO	1.1
SO ₃	3.17
K ₂ O	0.68
Na ₂ O	0.17
Cl	0.02
Loss on Ignition	1.17
Not Detected	1.54
Total	100

	%
Insoluble Residue	0.38
Free CaO	1.5
Total Alkali Na ₂ O (Equiv)	0.62
LSF (x 100)	93.7

Cement compounds by calculation	
C ₃ S	52.5
C ₂ S	20.1
C ₃ A	7.2
C ₄ AF	8.4
CaCO ₃	Rem

3.4.2.2 Sand

A medium grain sand from Belmoor quarry was used. The grading curve is presented in Figure 3.2. Tarmac Quarry Products Ltd supplied the sand. Its chemical composition is presented in Table 3.5.

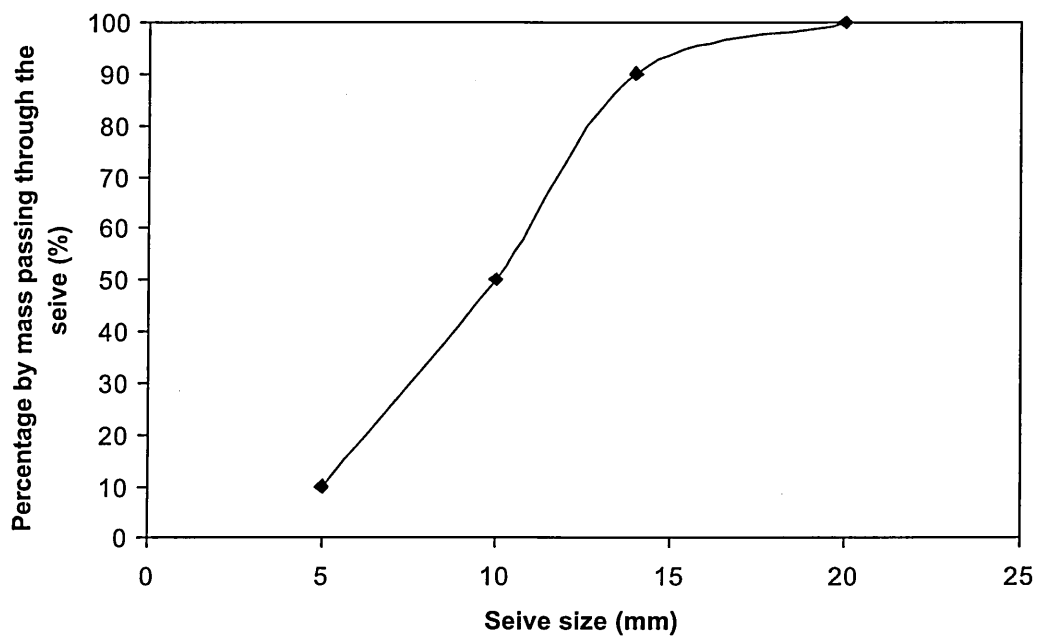
Figure 3.2 Grading curve for Belmoor sand**Table 3.5** Chemical composition of Belmoor sand

ELEMENTS	Content [%]
Silicon dioxide (SiO_2)	93.6
Aluminium oxide (Al_2O_3)	3.2
Iron oxide (Fe_2O_3)	0.9
Magnesium oxide (MgO)	0.2
Calcium oxide (CaO)	0.3
Sulphate (SO_3)	0.01
Potassium oxide (K_2O)	1.0
Sodium oxide (Na_2O)	0.1
$\text{Na}_2\text{O}_e = 0.658 \cdot \text{K}_2\text{O} + \text{Na}_2\text{O}$	0.76
Chlorite(Cl)	<0.01
Loss of Ignition	0.7
Bulk Density (kg/m^3)	1765 to 1620
<u>$\text{CaO} + \text{MgO} + \text{Al}_2\text{O}_3$</u> SiO_2	0.04

3.4.2.3 Coarse Aggregate

The coarse aggregate used was a non-reactive crushed graded gravel between 5 and 14 mm maximum size in accordance with BS 882. The grading curve for the aggregate is given in figure 3.3. The aggregate was washed before use to make it free from clay, silt, organic impurities and chlorides.

Figure 3.3 Grading curve for coarse aggregate



4.0 The Physical Properties of Substrate and Repair Materials

4.1 INTRODUCTION

The initial stage of the experimental programme was the measurement of the corrosion related physical properties identified in Chapter 3 for the repair and substrate materials. The following properties were identified as important to corrosion processes: porosity, permeability, resistivity and chloride diffusion. These properties are used to define the level of mismatch between the repair and substrate materials, which will then be related to the reinforcement corrosion measured in test specimens produced with different combinations of repair and substrate materials.

4.2 POROSITY

4.2.1 Introduction

Pores or voids in concrete consist of pores in the hardened cement paste, entrained or entrapped air voids and voids in the aggregate. These are created during mixing and initial hydration of the cement and are further refined by the setting and continued hydration of the cement paste with time. Other void spaces can be created as a result of effects such as bleeding, honeycombing and air pockets.

Most of the important properties of hardened concrete can be related to the volume and size distribution characteristics of the various types of pores in it. The mechanical properties such as strength and elastic modulus are primarily affected by the total pore volume, not their size or continuity. The durability properties of concrete involve mass transport phenomenon of deleterious substances and are concerned with the permeability and ionic movement in the

concrete. The volume, size and continuity of the pores have been found to influence these types of properties.

4.2.2 Experimental Procedure

4.2.2.1 Test Materials

Three commercially available repair materials were selected to provide a wide range of properties and to reflect the typical variety of repair materials currently available in the market. Details of the materials, A, B and C, used are given in section 3.4 The two concrete mixes, of 0.4 and 0.8 w/c ratios, represented the substrate concrete. The repair materials and substrate concrete mixes represent a wide range of permeability and porosity values.

4.2.2.2 Test Specimens

The materials were cast into cylindrical steel moulds 100mm diameter X 200mm high. The cylinders were filled in three layers, each layer was compacted on a vibrating table. The moulded cylinders were covered with polythene and cured overnight in a mist curing room. The specimens were demoulded 24 hours after casting and then cured in a water tank for 28 days at 20°C. Two cylinders were cast for each test material.

After 28 days curing, one of the two cylinders of each test material was sectioned across the 100mm diameter cross-section using a masonry saw. Two discs 25mm thick and 100 mm diameter were cut from the top and bottom of each cylinder and discarded. The remaining 150 mm length of the cylinder was cut into three discs of 100mm diameter X 50mm (+/-5mm) thick. These disc specimens were used to measure the porosity. Following cutting and prior to testing all disc specimens were stored in a water tank at 20°C for approximately 3 to 7 days.

The second cylinder of each material was cured in a water tank at 20°C for 12 months, following which it was also cut into discs as described above.

4.2.2.3 Experimental Technique

Porosity was determined by measuring the evaporable water from the disc specimens. The experimental technique of BS3921 (1985), for the determination of porosity of bricks, was used. The disc specimens were dried at 105°C until a constant mass was achieved and were then cooled down to 20°C in a dessicator and weighed to give the dry mass (m_d). The samples were then vacuum saturated according to BS3921. The mass of the water-saturated sample (m_s) was taken, followed by the buoyed mass of the sample suspended in water (m_b). The buoyed and water saturated mass measurements were taken in water at a constant temperature of 20°C (+/- 2°C). This minimized errors in the calculations from changes in water density with temperature. A value of 998.21 kg/m³ was taken as the density of water, ρ_w , for the calculations. Standard methods allow the calculation of porosity, bulk density, percentage water absorbed and apparent solid mass from the experimental data as shown in the next section. Each calculation represents the average of the three disc specimens tested for each material at each age.

4.2.2.4 Calculations

Total Volume

Total volume of solids and voids, V_T , is equal to the buoyed mass of the test specimen suspended in water, m_B , after correction for the true density of water (ρ_w).

$$V_T = \frac{m_B}{\rho_w} \quad [\text{cm}^3] \quad 4.1$$

Volume of Voids

Total volume of voids in the specimen, V_V , is calculated by subtracting the dry mass of the sample, m_D , (solids plus voids filled with air) from the saturated mass, m_S , (solids plus voids filled with water).

$$m_v = m_S - m_D \quad [\text{kg}]$$

Where m_v = mass of water in the saturated voids.

$$V_V = \frac{m_v}{\rho_w} \quad 4.2$$

$$\therefore V_V = \frac{m_S - m_D}{\rho_w} \quad [\text{cm}^3]$$

Volume of solids

Volume of solids in the specimen, V_S , is calculated by subtracting the volume of voids, V_V , from the total volume, V_T .

$$V_S = V_T - V_V \quad [\text{cm}^3] \quad 4.3$$

Bulk Density

Bulk density, ρ_{Bulk} , is the mass of the whole material per unit volume, reflecting the density of the mineralogical content of the material and the amount of pore spaces. It is usually specified as mass per unit volume e.g. g/cm^3 or kg/m^3 .

$$\rho_{Bulk} = \frac{m_D}{V_T}$$

Substituting for V_T from equation 4.1 gives: 4.4

$$\rho_{Bulk} = \frac{m_D}{m_B / \rho_w} \quad [\text{g/cm}^3]$$

Apparent Solid Density

Apparent solid density, $\rho_{\text{Apparent Solid}}$, is the density of the solids in a material, which is due purely to the mineralogical components of the material. It is usually specified as mass per unit volume e.g. g/cm^3 or kg/m^3 . However, using the vacuum saturation method, the measurement of the volume of the sealed pores is impossible. Picnometry is the only method which can calculate the true solid density of the material. Therefore, the solid density determined in this investigation is not the true solid density of the material but the apparent solid density.

$$\rho_{\text{Apparent Solid}} = \frac{m_D}{V_S}$$

Substituting for V_S from equation 4.3 gives:

4.5

$$\rho_{\text{Apparent Solid}} = \frac{m_D}{V_T - V_V} \quad [\text{g/cm}^3]$$

Apparent Porosity

Apparent porosity, p [%], is the amount of voids expressed as a percentage of the total volume V_T and is given by the expression.

$$p \text{ [%]} = \frac{V_V}{V_T} \cdot 100$$

4.6

Water Absorption

Water absorption (w_A) is the amount of water taken in by the material under normal temperature and pressure. Water absorption of each specimen was calculated as the increase in mass resulting from submersion, expressed as a percentage of the mass of the dry specimen.

$$w_A = \frac{(m_s - m_D)}{m_D} \times 100 \text{ [%]} \quad 4.7$$

4.2.3 Results and Discussion

Table 4.1 presents the values for bulk density, solid density, water absorption and porosity of the test materials after 28 days and 12 months of curing. The results are consistent with under 2% variation in calculated values for the three disc specimens of each material. All the materials showed a slight increase in porosity between 28 days and 12 months. The reason for this is unclear, but the variation for most materials was under 1% (Figure 4.1).

The technique was sensitive enough to detect differences in the mix proportions of the materials. The 0.4 w/c and 0.8 w/c substrates have similar solid densities, reflecting the fact that they have the same solid constituents, but different bulk densities reflecting the different water content. Repair material A also has a similar solid density to the substrate materials. This would be consistent with repair material A, containing PFA as a cement replacement material, but otherwise containing similar solid constituents. Repair materials B and C are both polymer modified materials and this is reflected in lower solid densities.

The 0.4 w/c substrate had the lowest porosity of 10.79%. The 0.8w/c substrate and repair materials A and B all had porosities in the range 20-25%. Repair material C had the highest porosity 34 - 37%. The higher porosities of the repair materials result from the different constituent materials used. The repair materials contain finer aggregates, which makes them similar to cement mortars. These have higher porosities than concrete mixes due to the absence of the low porosity coarse aggregate [81,82].

The experimental techniques adopted are sensitive to changes in the absorption properties of the materials, but do not provide evidence of the relative continuity of the pore structure in the different materials. The results, therefore, offer little to allow comparison of mass transport properties in the materials, which govern the potential durability of the repair materials and their protection against reinforcement corrosion. It is judged that water permeability measurements would provide a better assessment and correlation with the durability potential, therefore, this property will be determined in the next section.

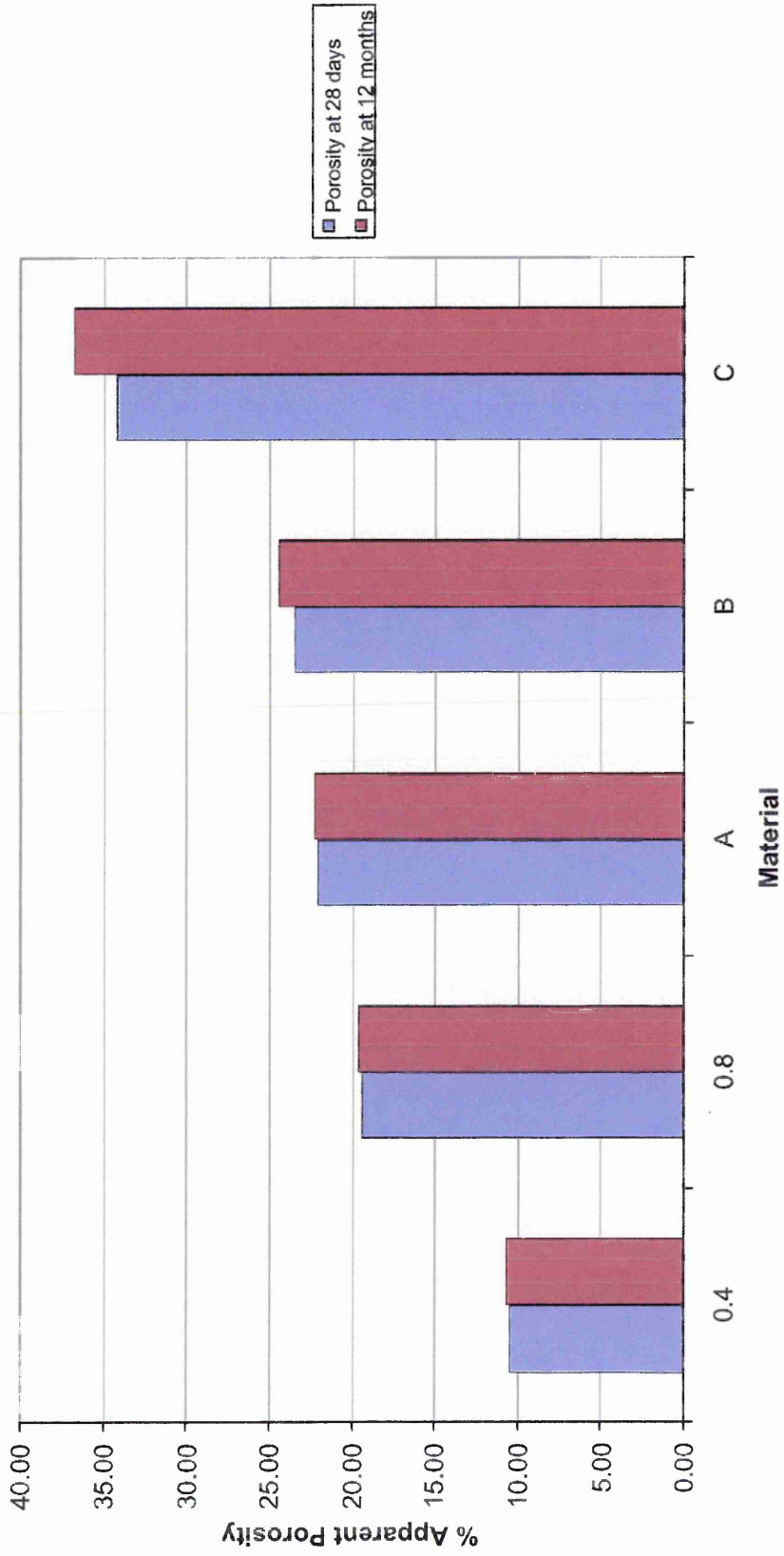
4.2.4 Conclusions

The repair and substrate materials selected for the investigation provided a wide range of porosity values. The experimental technique proved to be sensitive enough to detect these differences. The 0.4w/c concrete had the lowest porosity of 10.4%. The 0.8w/c substrate and repair materials A and B all had porosities in the range 20-25%. Repair material C had the highest porosity 34-37%. A likely cause for the higher porosity of the repair materials was their lack of coarse aggregate.

Table 4.1 Porosity results for Substrate concrete mixes and Repair materials.
 * = Manufacturers supplied minimum compressive strengths.

Material	Compressive Strength (MPa)	28 Days					12 Months				
		Bulk Density [Kg/m ³]	Solid Density [Kg/m ³]	Water Absorption [%]	Apparent Porosity [%]	Bulk Density [Kg/m ³]	Solid Density [Kg/m ³]	Water Absorption [%]	Apparent Porosity [%]		
0.4 w/c Substrate	40	2351	2626	4.47	10.50	2428	2721	4.44	10.79		
0.8 w/c Substrate	28	2109	2619	9.23	19.47	2097	2607	9.45	19.64		
Repair Material A	40*	1977	2537	11.17	22.09	2120	2733	10.58	22.42		
Repair Material B	48*	1051	1374	22.37	23.51	1245	1660	20.08	25.00		
Repair Material C	30*	1255	1909	27.26	34.22	1402	2244	26.67	37.52		

Figure 4.1 Change in Porosity between 28 days and 12 months



4.3 PERMEABILITY

4.3.1 Introduction

Permeability is a measure of the resistance to flow of water or gasses. It represents the mass transport properties of the material. This is an important parameter when considering the durability of concrete repairs as corrosion rates of reinforcement will be under mass transport control. Permeability can, therefore, provide a method of distinguishing the relative performance of different repair materials and also give a measure of the mismatch between a repair material and the substrate to which it has been applied.

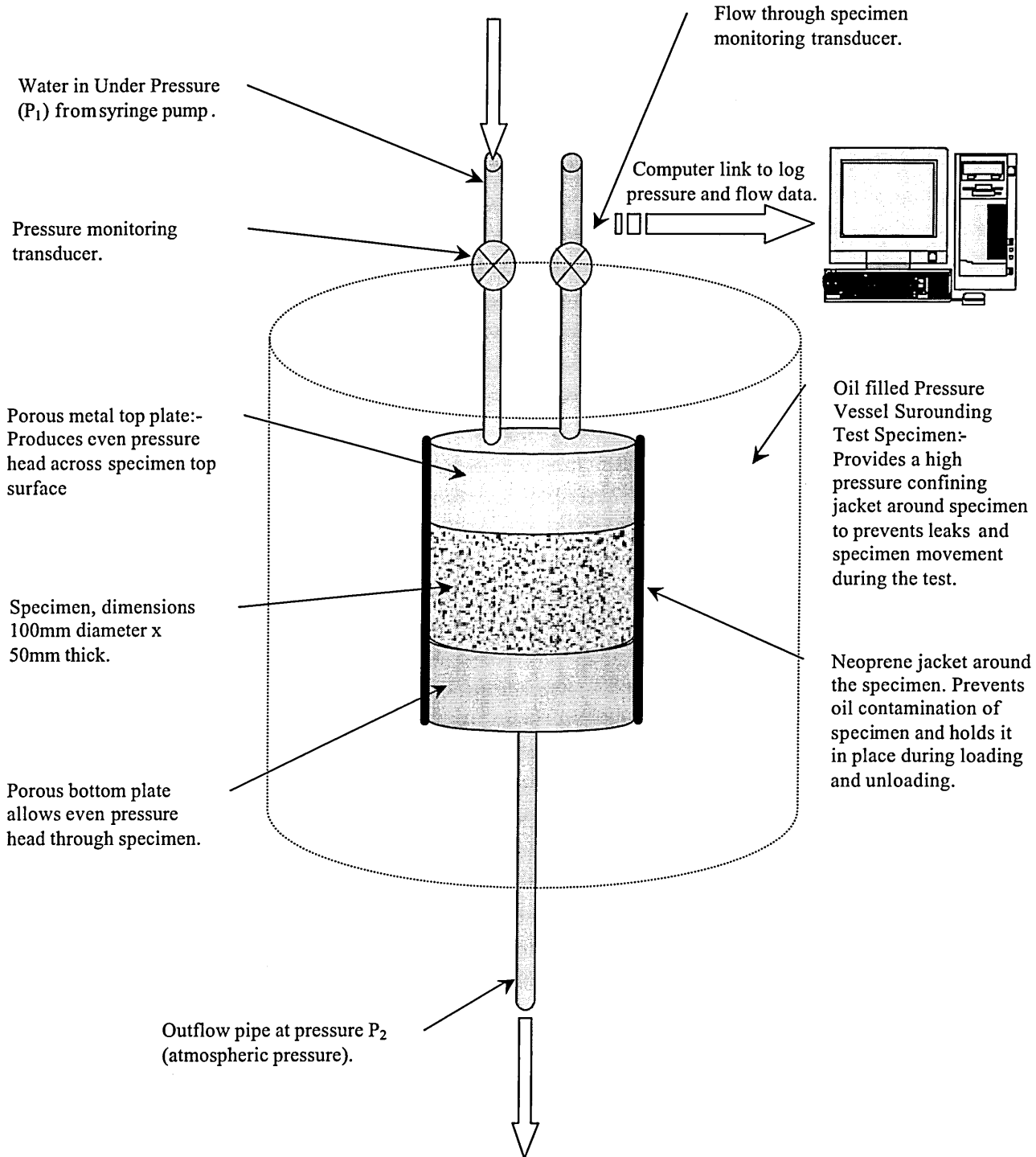
In this study a purpose built permeater has been used to measure the Darcian coefficient of permeability for the materials under test. This involves applying a constant “head” pressure of water to one surface of a specimen and measuring the flow of water through the specimen. There are currently no standards governing measurements made with this type of apparatus. This means information on the operating parameters used has to be taken from literature and adapted for the current study.

4.3.2 Permeater Apparatus

The permeater used in the current study is a SP2 permeability apparatus manufactured by SPT. A schematic diagram of the permeater is given in figure 4.2. This equipment uses a high precision syringe pump to push water through a cylindrical specimen of the test material. Two highly accurate transducers measure the pressure and the flow rate through the sample. These values are logged and stored by computer to provide a record of pressure, flow and time when the readings were taken.

A feature of this permeater is the oil-confining jacket around the specimen. The sample and sample holder are surrounded by a reservoir of oil, kept at a higher pressure than the water being pumped through the specimen. This prevents leaks in the system and, therefore, allows a higher accuracy in flow measurements. The oil confining pressure also allows higher head pressure to be applied allowing faster measurements for low permeability materials.

Figure 4.2. Schematic diagram of Permeater



4.3.3 Operating Parameters

A number of review documents [82, 102] provide information on experimental techniques, which can be used to define the operating parameters for permeability tests. Concrete Society Technical Report No. 31 [82] provides recommendations on good practice for the measurement of permeability by flow. These guidelines have been adopted from the work of Jefferies at King's College, London and provide a basis for defining the test parameters. Relevant guidelines are as follows:-

- i. Specimen Saturation: The flow of water into the specimen is controlled initially by capillary forces in the material. These forces continue to act until water has passed through the full length of the specimen and wetted the under surface. Until this happens flow is not governed by Darcian flow. This means that true permeability can only be measured on fully saturated specimens. All the specimens used in this study were kept in a saturated condition in a water bath at 20°C until testing. Vacuum saturation was also tried but did not produce substantially different results from the saturated specimens.
- ii. Leak Compensation: as the permeabilities of the repair materials used are likely to be below 10^{-13} m/s, any leaks in the system can have a large impact on the accuracy of flow rates being measured. It is recommended that both the inflow and outflow should be monitored to allow compensation to be made for leaks in the system.
- iii. The presence of air in the sample will act as water free voids in the sample that will disrupt the movement of water through the specimen. Applying a backpressure of 2 bar will dissolve any entrapped air in the specimen or apparatus.
- iv. Temperature changes in the apparatus may effect the low flow rate measurements; therefore temperature of the apparatus must be kept constant.

- v. Water flow rate can be expected to vary in a non-Darcian fashion with applied pressure. At low pressure gradients, chemical interactions may result in the generation of osmotic pressures between the concrete and the pore water. High pressures can result in the compression of the pore structure resulting in a lower calculated permeability and may damage the specimen. Test pressure should be chosen as near as possible to the practical situation and quoted along with the calculations. A constant test pressure should also be used during the test; changes in pressure could result in movement of the specimen which may be recorded as apparent flow.
- vi. There is a possibility of leaching of calcium hydroxide etc, from high and medium permeability concrete during the test. This may effect the permeability of the material and so it may be advisable to use calcium hydroxide solution as the permeating fluid. However, the effectiveness of this remains unclear from literature and the chance of significant leaching from the low permeability materials used in this study is small due to the low velocity movement of water through the specimens.

4.3.4 Experimental Conditions.

It is clear from examining these recommendations that care needs to be taken in defining the experimental parameters of the permeability test, in order to be able to produce reproducible results. The test apparatus used in this study keeps the specimen under pressure in an oil filled jacket. This will minimise the risk of interference from entrapped air. Saturated specimens were used in the study to speed up measurements of Darcian flow. The apparatus was also kept in a temperature-controlled environment to minimise the effect of temperature changes on flow measurement. Distilled water was

used as the permeating fluid and the effect of leaching on the low permeability specimens used in this study was considered negligible.

The risk of leaks of water in the permeator used in this study was considered negligible due to the high-pressure oil jacket surrounding the specimen. This confining pressure was always kept at 10 bar above the pressure head. However, there was still a risk of contamination of the specimen from the confining oil and water leaks if the head pressure exceeded the confining pressure. The permeameter used in this study only measured the inflow. Collecting the water passing through the specimen made the only check on the outflow. However, measurements could not be made to the level of accuracy of the inflow measurements and, therefore, the measurements were used as a check for leaks and oil contamination. At regular intervals, a test was made on an impermeable calibration specimen to check for leaks in the system. These tests did not detect the presence of leaks during this study.

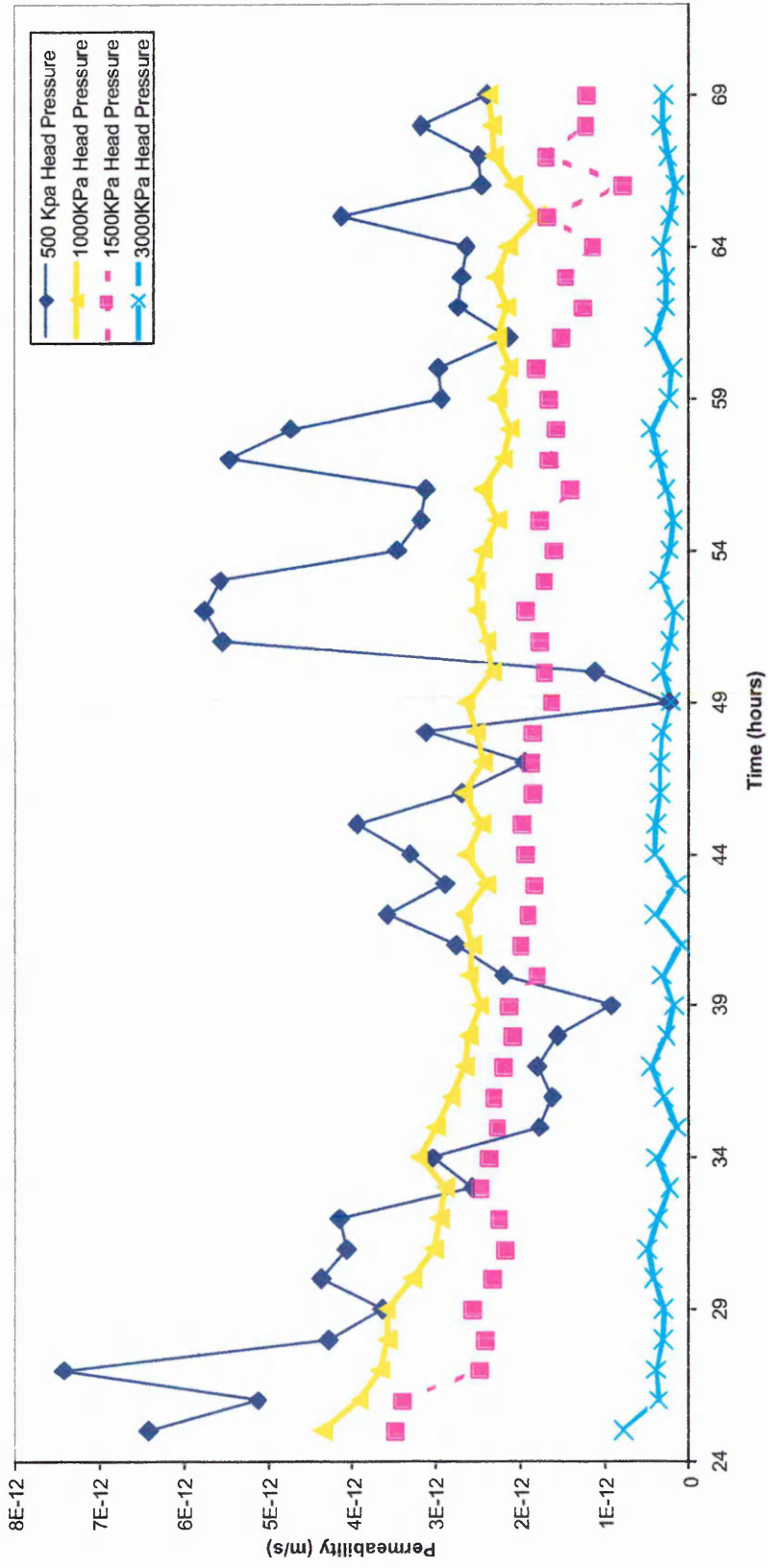
The two major experimental parameters for this study were the inflow head pressure and the time over which the measurements were conducted.

- i. Head Pressure: The head pressure effectively controls the confining oil pressure used during the test. As the head pressure increases so will the confining pressure used leading to the compression of the pore structure and lower calculated permeabilities. This can be seen in the calibration runs shown in figure 4.3. As the head pressure increases, the calculated average permeability falls. However, figure 4.3 also reveals that the lower the head pressure the greater the scatter in the inflow values measured. This lowers the confidence in the permeability value calculated. This implies that with this permeameter there is a trade off between the lower measured permeabilities, but less scatter in the measured flow as head pressure

increases. Higher head pressures also produce more measurable flow rates in low permeability materials and reduces the time taken to produce steady state flow, so reducing the time required for each test. In this study it is important to be able to compare the permeability values for the different materials used. It was decided to use a constant head pressure of 1000 KPa with a confining pressure of 2000 KPa. This compromise gives results with reasonable scatter and measurable flows for the low permeability materials, while providing a head pressure relevant to practical situations.

- ii. The second important experimental parameter is the duration of the test. It has been found in literature [81, 82, 101, 102] that flow varies with time during a permeability test. Constant flow is only achieved under special conditions. It is normally observed that flow rate reduces with time. The self-sealing property of concrete means that the time over which permeability measurements are taken will influence the calculated value of permeability. The self-sealing phenomenon usually occurs between the first 20-40 hours of the test; after this a constant value is generally reached. In this study, it was decided that all the tests should be run over the same time period and results used to calculate the permeability should cover the same period. The permeability tests were run for a period of 3 days (72 hours) and the readings used for permeability calculations covered the last 48 hours of the test. These test durations were shorter than some of those used in literature of 4-7 days, so direct comparison of the values calculated in this study with those in literature may not be accurate.

Figure 4.3: Effect of Head Pressure on Permeability Coefficient.



4.3.5 Darcy Coefficient of Permeability

A summary of the experimental parameters used in the study is as follows:- Saturated specimens were used and leaks in the system were prevented. The permeameter operated at a head pressure of 1000KPa with a confining pressure of 2000KPa. The tests were conducted over a period of 72hours with only the readings from the last 48 hours used to calculate the permeability coefficient.

The permeability of the specimens was measured using a saturated flow technique. Here one side of the water-saturated specimen was subjected to a pressure head and the rate of flow through the sample measured. Darcy's law can then be used to determine the permeability coefficient (k) from the following equation:-

$$k = \frac{dq}{dt} \frac{L}{\Delta h A} \quad 4.8$$

$\frac{dq}{dt}$ = rate of flow (m^3 / s)

A = cross sectional area (m^2)

Δh = pressure head accross the sample (m)

L = thickness of sample (m)

k = coefficient of permeability (m/s)

4.3.6 Materials and Test Specimens

The three repair materials A,B and C and two substrate concrete mixes (04. and 0.8 w/c ratios) were used for the tests. Details of these materials are given in Chapter 3 (Section 3.4).

The materials were cast into cylindrical steel moulds 100mm diameter X 200mm long, covered with polythene sheets and left to cure in a mist room at 20°C overnight.

The cylinders were filled in three layers, each layer was compacted on a vibrating table and using a tamping rod. Four cylinders were cast for each test material. The specimens were demoulded 24 hours after casting and then cured in a water tank for 28 days at 20°C.

After 28 days curing, two cylinders for each test material were sectioned using a masonry saw. The top and bottom 25 mm thick discs were removed from each cylinder and remainder was cut into discs of 100mm diameter x 50mm +/-5mm high. These disc specimens provided the test specimens for the permeameter. Specimens with large voids on the side surface, which might cause sealing problems in the permeameter, were discarded. Smaller surface voids were filled with Plaster of Paris prior to testing to ensure a good seal in the test cell. Following cutting and prior to testing all specimens were stored in a water tank at 20°C for a period of up to 2 weeks. . This procedure was repeated after 12 months for the second pair of cylinders of each material (repair and substrate). The total number of disc specimens of each material used for the permeability tests are given in table 4.2.

Table 4.2 Permeability Test Specimens.

Material	28 days	12 months
A	4	4
B	5	4
C	5	5
0.4w/c Substrate	4	4
0.8w/c Substrate	4	4
Total	22	21

4.3.7 Results and Discussion

4.3.7.1 Permeability of Test Materials.

Figure 4.4 shows the Darcy permeability coefficient measured for each test material at 28 days and 12 months. The results show a high and a low value from the standard deviation and an average permeability for each test material. This gives an indication of the permeability and the variation in permeability for each material.

The results indicate that at 28 days all the test materials suffered from a similar large scatter in permeabilities. Material C and the 0.4w/c substrate exhibited the lowest variation and the 0.8w/c substrate the highest. However, the degree of scatter in the results appeared to be random. This is not unusual in permeability studies - figure 4.5 shows a comparison of water permeability data for concrete from literature together with results from the present study. The high level of scatter is an indication of how permeability can fluctuate with variations in materials and test methods. A comparison of the results of this study with those in figure 4.5 show that the present results are totally consistent with those of previous studies, indeed the level of scatter is lower in the present study. The level of scatter is important for the interpretation of the results.

It is clear from figure 4.4 that after 28 days curing, material A had the lowest permeability, followed by material B and material C had the highest permeability of the repair materials used. All the materials have significant differences in permeability. The substrate materials also showed significant differences in permeability with the 0.4w/c concrete having a lower permeability than the 0.8w/c concrete.

Figure 4.4 shows that after 12 months curing the test materials showed a drop in permeability. The difference in permeability between 28 days and 12 months was less marked for the lower permeability materials A and the 0.4w/c substrate. The higher permeability repair materials B, C and 0.8w/c substrate showed much larger drops in permeability. The drop in permeability is caused by the refinement of pore structure with continuing hydration over time [101, 102]. The level of scatter in the results masks the changes in permeability with time but the change is clearly more significant for the more permeable repair materials B and C.

The results of the permeability tests allow the characterisation of the test materials in accordance to the concrete society technical report 31 [82]. Repair material A and the 0.4w/c substrate are low permeability materials ($<10^{-12}$ m/s). Repair material B and the 0.8 w/c substrate are of average permeability (10^{-12} - 10^{-10} m/s) and repair material C is a high permeability material ($>10^{-10}$ m/s).

4.3.7.2 Level of Mismatch in Materials

The level of mismatch in the pore structure between the substrate concrete and any repair material used in conjunction with it, may affect the durability of a repair. The difference in the permeability of the repair material and substrate concrete can provide a measure of the mismatch of pore structure in the materials.

Figure 4.4 shows that the 0.4w/c substrate concrete has a similar permeability to repair material A. However, it is significantly less permeable than repair materials B or C. The 0.8 w/c substrate is similar in permeability to B, but is less than C and more

permeable than A. When different repair materials are applied to the same substrate then the mismatch in permeability will differ for each combination.

The repair and substrate materials used in this study provide six different repair-substrate combinations as shown in table 4.3.

Table 4.3 Repair Substrate Combinations

Specimen Identification	Repair Material	Substrate Material	Repair Permeability	Substrate Permeability
A04	A	0.4w/c	Low	Low
A08	A	0.8w/c	Low	Average
B04	B	0.4w/c	Average	Low
B08	B	0.8w/c	Average	Average
C04	C	0.4w/c	High	Low
C08	C	0.8w/c	High	Average

Figure 4.4 also shows that the level of mismatch in permeability between substrate and repair material can change with time. Repair material B gets significantly less permeable over 12 months, while the 0.4w/c and the 0.8w/c substrates change only marginally over 12 months. Therefore the match between material B and the 0.4w/c substrate improves with time, while its match with the 0.8w/c substrate worsens with time.

A method of expressing the level of mismatch between repair and substrate would be to use the ratio of substrate permeability to repair permeability. A value of 1 indicates that the repair and substrate have the same permeability. A value less than one indicates the repair is more permeable than the substrate. A value greater than 1

indicates that the substrate is more permeable than the repair. The scatter in results suggests that there may be significant variation in permeability within a material. It may not be correct to use an absolute mismatch between a substrate and a repair material based on the average permeabilities of repair and substrate. Therefore, by incorporating the deviation in results about the mean it would be possible to produce a range of mismatch between substrate and repair.

Figure 4.6 shows the change in ratio of the permeability of the substrate material to the permeability of the repair material (mismatch ratio). The results show the possible variation in mismatch with a low, high as well as an average value of mismatch ratio. This gives an indication of the mismatch in permeability of the combinations of repair and substrate.

The best match (match ratio closest to 1) is for material B with the 0.8w/c substrate at 28days. The match gets worse over 12 months, but still remains the best match range of the materials tested. Repair material A with the 0.4w/c substrate has the next closest match, which improves slightly over 12months. The specimens with the closest match cover two different situations. Material B with the 0.8w/c substrate represents the case of both average permeability repair and substrate materials. Material A combined with the 0.4w/c substrate represents the case of both low permeability repair and substrate materials.

The combination of material A with the 0.8w/c substrate represents a low permeability repair and an average permeability substrate. It has the poorest match index greater than 1. Material C with the 0.4w/c substrate had the poorest match index

less than 1 (high permeability repair and low permeability substrate). The other specimens had match indices less than 1, which represent higher permeability repair than the substrate. This was for combinations of material B with the 0.4w/c substrate and material C with 0.8w/c substrate.

Figure 4.5 shows the results of this study with those from literature [82]. It confirms materials A, B and C having a low, medium and high permeability respectively. The concept of matching the permeability of repair materials with those of the substrate concrete may be difficult to achieve in practical repairs. The changes of permeability with time would indicate that any match in permeabilities achieved could be lost as the repair and substrate concrete continue to age. The changes will be greater in the newly applied repair materials, whereas the aged substrate concretes will have stabilised during their service life.

The test materials provided a range of permeabilities from low to high permeability. This provided a range of combinations of materials (table 4.3) and different matches in permeability between repair and substrate. These combinations of materials and their different permeability matches will be used to study the corrosion behaviour of the specimens in this investigation.

4.3.8 Conclusions

- Material A was less permeable than material B, which was less permeable than material C. The 0.4w/c substrate is less permeable than the 0.8w/c substrate.
- Material A and the 0.4w/c substrate were low permeability materials, material B and the 0.8w/c substrate were average permeability materials and material C was a high permeability repair material.

- The permeability range of the materials allows different repair and substrate combinations to be investigated.
- The ratio of the permeability of the substrate to the permeability of the repair (match ratio), defines the difference in permeability between repair and substrate.
- The permeability of the test materials decreases with aging, between 28 days to 12 months, therefore, the match ratio between the repair and substrate also changes with time.

Figure 4.4: Change in Permeability of Test Materials Between 28 Days And 12 Months.

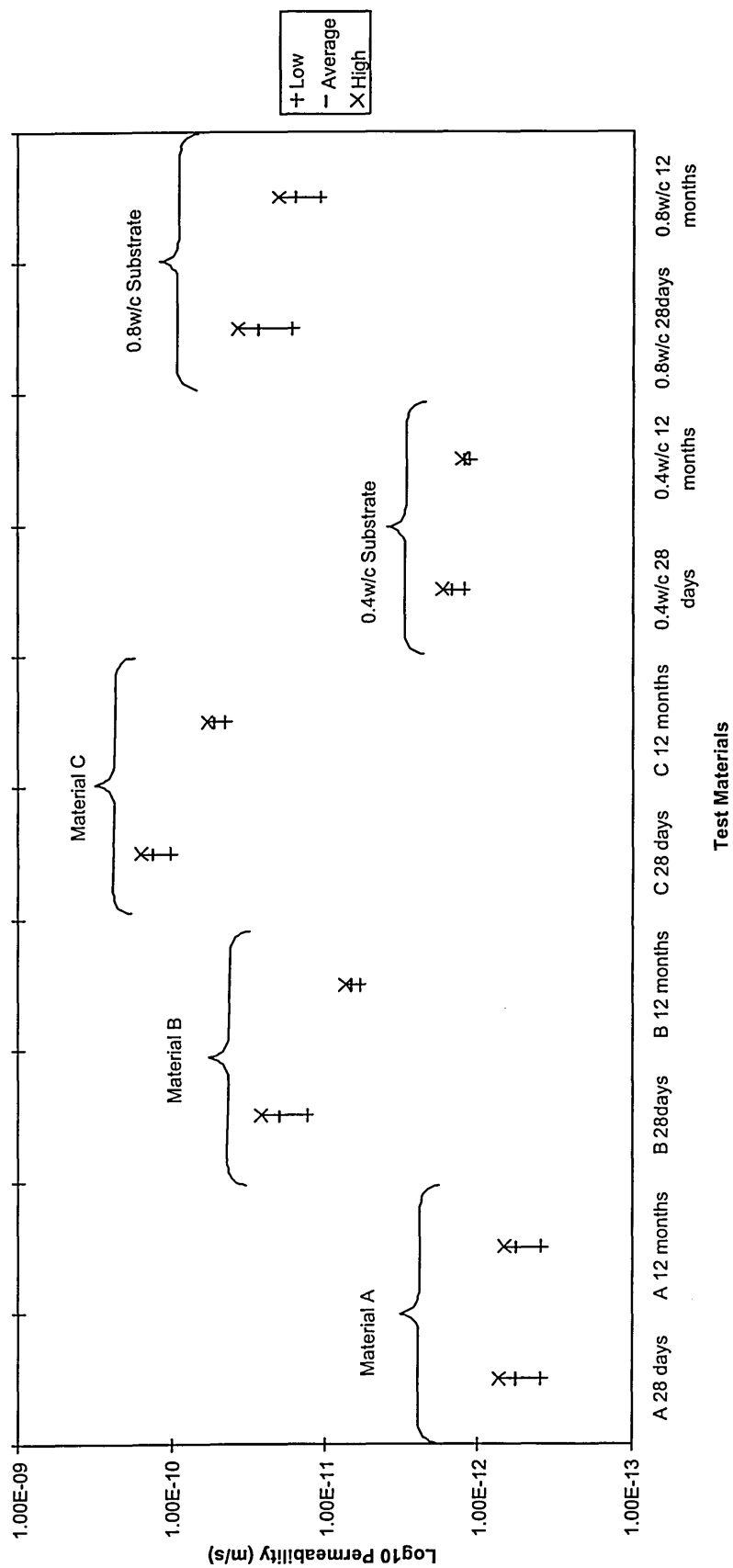


Figure 4.5 Comparison of Water Permeability Data for Concretes and Repair Materials [82].

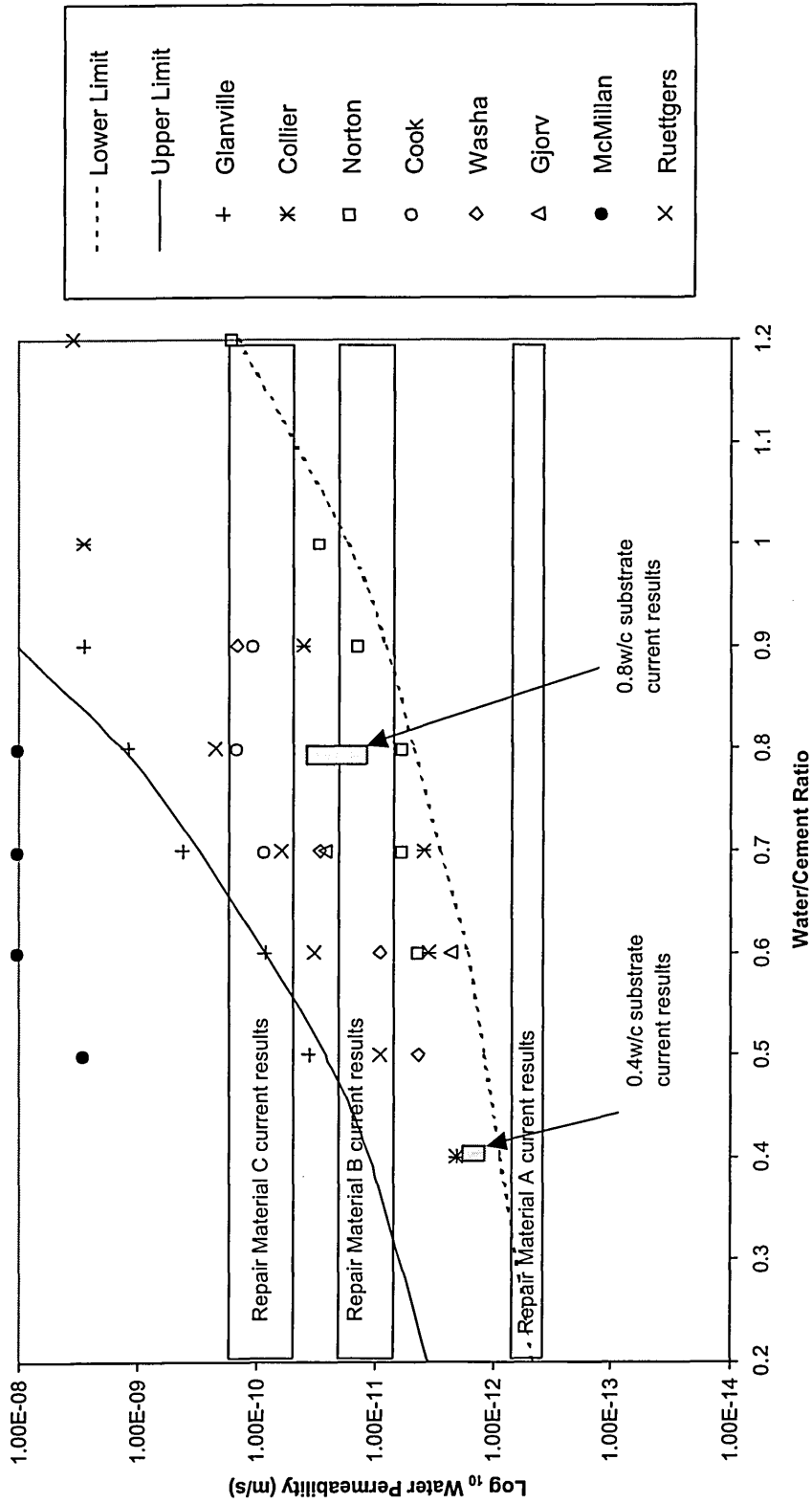
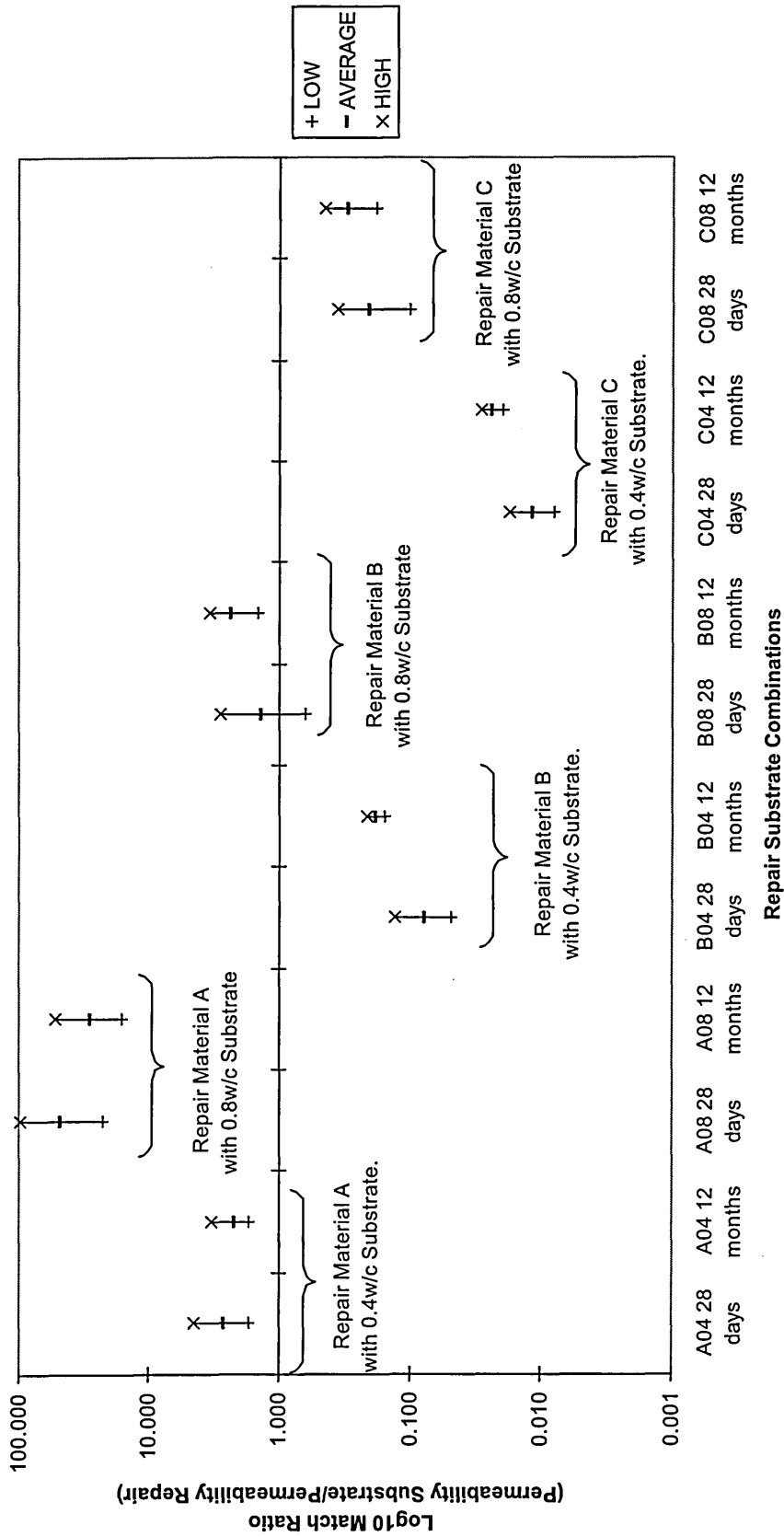


Figure 4.6: Permeability Match between Repair and Substrate



4.4 CHLORIDE DIFFUSION COEFFICIENTS

4.4.1 Test Materials

The chloride diffusion characteristics of the three commercially available repair materials A, B and C and two concrete substrate mixes (0.4 and 0.8 w/c) were determined. Details of the materials are given in section 3.4.1 Mix proportions of the substrate mixes are given in section 3.4.2

The repair materials and substrate concrete mixes represent a wide range of permeability and porosity values. Both the substrate concrete mixes contained 3.5% NaCl (by weight of cement). This was to simulate the substrate mixes used in Chapter 5 on Corrosion Testing, where chloride was added to depassivate the steel reinforcement in the test specimens. No NaCl was introduced in the repair material.

4.4.2 Test Specimen Preparation

The test specimens used for the determination of chloride diffusion coefficients were a combination of a repair material with a substrate concrete. This was to simulate the effect of using different combinations of repair and substrate materials on chloride diffusion. The test cylinders were unreinforced Two cylinders were cast for each of the following repair-substrate combinations:

Repair Material A with 0.4 w/c Substrate.

Repair Material A with 0.8 w/c Substrate.

Repair Material B with 0.4 w/c Substrate.

Repair Material B with 0.8 w/c Substrate.

Repair Material C with 0.4 w/c Substrate.

Repair Material C with 0.8 w/c Substrate.

Cylindrical moulds 100mm in diameter and 400 mm long were used to cast the test specimens. The substrate concrete was first cast into the lower half of the moulds, in three layers and vibrated to achieve optimum compaction. The half-cast moulds were covered with polythene and left in a mist curing room overnight. The repair material was then mixed and cast into the unfilled half of the mould in accordance with the manufacturer instructions. The specimens were demoulded 24 hours after casting and then cured in a water tank for 28 days at 20°C. Following the 28 day curing, the specimens were transferred to a second water tank containing 3.5% NaCl, where they were stored for the remainder of the study (12 months).

4.4.3 Test Methods for Chloride Contamination and pH

After 12 months exposure to the 3.5% NaCl solution, each cylindrical specimen of a repair/substrate combination was prepared for chloride analysis. The specimen was cut in half along the repair/substrate interface. Three slices, each 20mm thick, were cut on either side of the interface (see figure 4.7). These provided three discs for chloride analysis from the substrate concrete and three discs from the repair material. The remaining 40mm thickness at the top and bottom of the specimen was discarded. Powder samples were taken from each disc using a 6mm drill. The samples were taken at two depths from the surface (circumference) of the cylinder, 10mm from the surface and at 40mm from the surface (see figure 4.7). The 40mm depth represented the approximate cover to the reinforcement bar used in later studies on Corrosion Testing (Chapter 5). Different locations at 40mm and 10mm from the surface, shown in Figure 4.7, were drilled to provide a powder sample of 2.5g per disc for chloride analysis. Each powder sample was weighed and then added to 25ml of 0.1 molar nitric acid. The mixture was boiled for approximately 5 minutes. On cooling the mixture was

neutralised with calcium carbonate and then filtered. The resulting solution was then titrated against standardised 0.1 molar silver nitrate solution. The percentage chloride by weight of concrete or repair material was calculated using the following expression (14):

$$\%Cl^- = \frac{35.45VM}{10w}$$

where;

V = volume of silver nitrate solution. 4.9

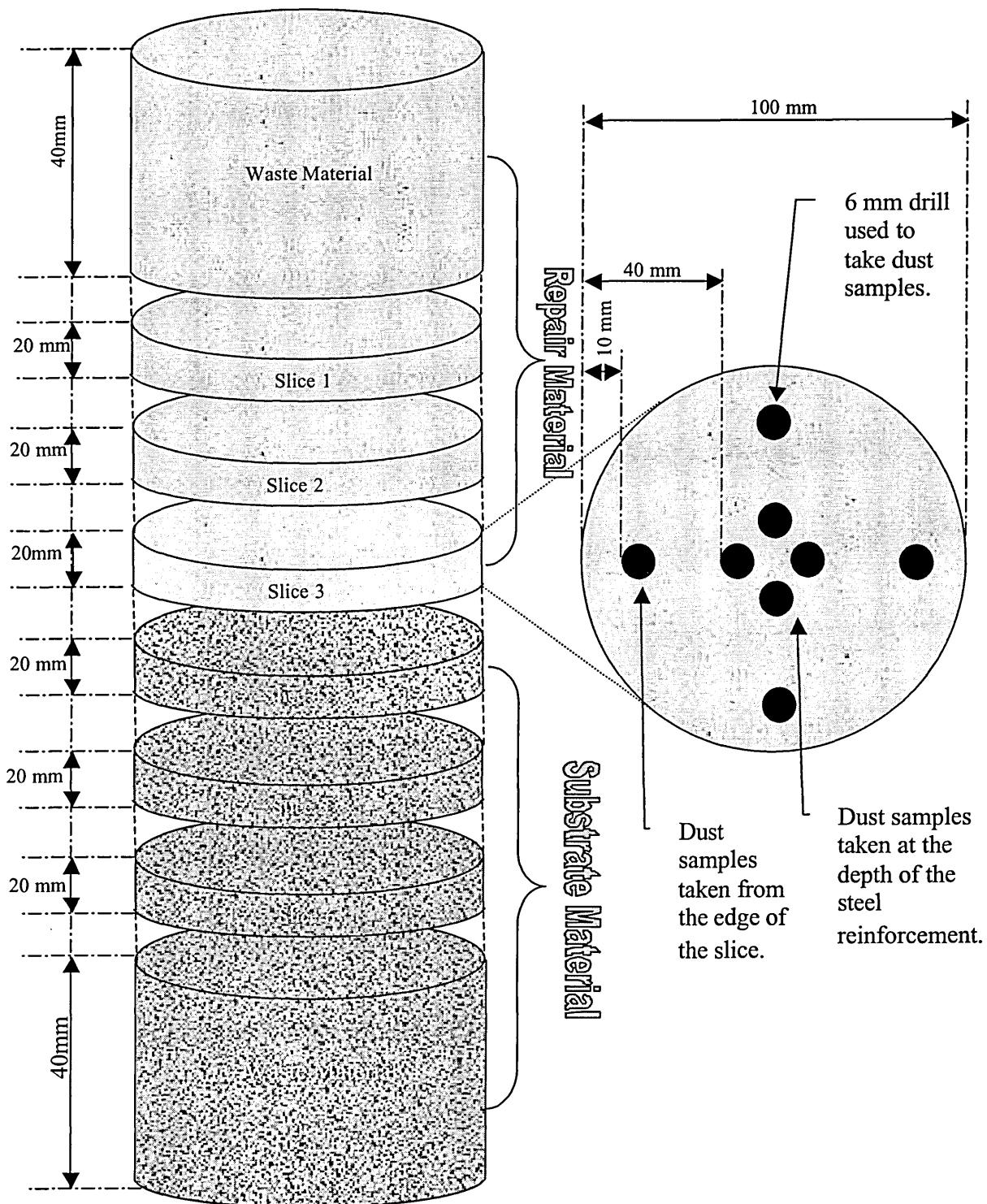
M = molarity of the silver nitrate solution.

w = mass of the powder sample (g)

The pH of the test specimens was also measured using a universal pH indicator solution.

It was found to be in the range 12-13 pH for all materials.

Figure 4.7. Schematic diagram of the Specimen Used for Chloride Analysis.



4.4.4 Chloride Diffusion Coefficients

The chloride diffusion tests provide chloride concentrations at two depths, C_1 1cm depth and C_4 4 cm depth. Using Fick's second law:

$$\frac{\partial C}{\partial t} = D_c \frac{\partial^2 C}{\partial x^2} \quad 4.10$$

It is possible to determine D_c (diffusion coefficient) for each material from this data. This can be used to compare the diffusion rates of chlorides in the different materials used in this study. In addition, as later experiments reported in the thesis expose steel reinforced specimens to chloride contaminated solutions and measure the corrosion rates against time, a pre-determined value of D_c allows the estimation of chloride concentration profiles at the steel surface with time. This allows an evaluation of the relationship between corrosion and chloride concentration at the steel surface. The chloride diffusion coefficient D_c is calculated by using a standard solution for Fick's 2nd Law for a semi-infinite slab:

$$C = C_s \left[1 - \operatorname{erf} \frac{x}{2\sqrt{D_c t}} \right] \quad 4.11$$

Where

x = the distance from the concrete surface (cm).

t = the exposure time to the chloride source in seconds.

D_c = the diffusion coefficient of the concrete in cm^2s^{-1} .

C_s = the equilibrium chloride concentration on the concrete surface

C = the chloride concentration at any position x and time t .

Now let:
$$z = \left(\frac{1}{2\sqrt{D_c t}}\right) \quad 4.12$$

Substituting z from equation 4.12 into equation 4.11 for chloride concentrations at $x = 1\text{cm}$ and at 4 cm gives:

$$C_1 = C_s(1 - \text{erf}(z)) \quad 4.13$$

and
$$C_4 = C_s(1 - \text{erf}(4z)) \quad 4.14$$

As C_s is common to equations (4.13) and (4.14), re-arranging gives:

$$\frac{C_1}{(1 - \text{erf}(z))} = \frac{C_4}{(1 - \text{erf}(4z))} \quad 4.15$$

An accurate approximation for the error function [238] is given by:

$$\text{erf}(z) = 1 - ae^{-b(z+c)^2} \quad 4.16$$

and also,

$$\text{erf}(4z) = 1 - ae^{-b(4z+c)^2} \quad 4.17$$

Where a , b and c are constants and e is the exponential function:

Substituting into equation (4.15) gives:

$$\frac{C_1}{ae^{-b(z+c)^2}} = \frac{C_4}{ae^{-b(4z+c)^2}} \quad 4.18$$

Rearranging equation 4.18 gives:

$$\frac{C_1}{C_4} = e^{-b(z+c)^2 + b(4z+c)^2} \quad 4.19$$

Multiplying out the bracket in (4.19) gives;

$$\begin{aligned} & -b(z+c)^2 + b(4z+c)^2 \\ & = -b(z^2 + 2zc + c^2) + b(16z^2 + 8zc + c^2) \\ & = -bz^2 - 2bzc - bc^2 + 16bz^2 + 8bzc + bc^2 \\ & = 15bz^2 + 6bzc \end{aligned}$$

Therefore,
$$\frac{C_1}{C_4} = e^{15z^2b + 6zbc} \quad 4.20$$

Taking logs of equation 4.20:

$$\ln \frac{C_1}{C_4} = 15z^2b + 6zbc \quad 4.21$$

Rearranging equation 4.21 gives a standard quadratic equation;

$$15z^2b + 6zbc - \ln \frac{C_1}{C_4} = 0 \quad 4.22$$

For the error function approximation [238]:

$$b=0.7182$$

$$c=0.7856$$

Therefore, the quadratic equation becomes;

$$10.773z^2 + 3.385z - \ln \frac{C_1}{C_4} = 0 \quad 4.23$$

The standard solution for the quadratic equation is;

$$z = \frac{-3.385 \pm \sqrt{11.458225 + 43.092 \ln \frac{C_1}{C_4}}}{21.546} \quad 4.24$$

Hence, by knowing the chloride concentration in a sample at two depths (C_1 and C_4) it is possible to solve the quadratic equation and calculate the value for z . Substituting this value of z into equation 4.12, a value for D_c can be calculated for the material. Substituting z into equation 4.13 or 4.14 a value for C_s can be found.

An alternative approach uses the following polynomial as the approximation for the error function [239].

$$\text{erf}(z) = 1 - (1 + az + bz^2 + cz^3 + dz^4)^{-4} \quad 4.25$$

where:

$$a = 0.278393$$

$$b = 0.230389$$

$$c = 0.000972$$

$$d = 0.078108$$

Substituting equation 4.25 into equations 4.13 and 4.14 gives.

$$C_1 = C_s (1 + az + bz^2 + cz^3 + dz^4)^{-4} \quad 4.26$$

$$C_4 = C_s (1 + a(4z) + b(4z)^2 + c(4z)^3 + d(4z)^4)^{-4} \quad 4.27$$

As C_s is common to equations 4.26 and 4.27, re-arranging gives:

$$\frac{C_1}{C_4} = \left(\frac{(1 + az + bz^2 + cz^3 + dz^4)}{(1 + a(4z) + b(4z)^2 + c(4z)^3 + d(4z)^4)} \right)^{-4} \quad 4.28$$

Re-arranging equation 4.28 gives:

$$\frac{C_1}{C_4} = \left(\frac{(1 + a(4z) + b(4z)^2 + c(4z)^3 + d(4z)^4)}{(1 + az + bz^2 + cz^3 + dz^4)} \right)^4 \quad 4.29$$

Raising both sides of the equation 4.29 to the power $1/4$ gives:

$$\sqrt[4]{\frac{C_1}{C_4}} = \left(\frac{(1 + a(4z) + b(4z)^2 + c(4z)^3 + d(4z)^4)}{(1 + az + bz^2 + cz^3 + dz^4)} \right) \quad 4.30$$

$$\text{Let } \sqrt[4]{\frac{C_1}{C_4}} = q \quad 4.31$$

Therefore:

$$q = \frac{(1 + a(4z) + b(4z)^2 + c(4z)^3 + d(4z)^4)}{(1 + az + bz^2 + cz^3 + dz^4)} \quad 4.32$$

Re-arranging equation 4.32 gives:

$$q + qaz + qbz^2 + qcz^3 + qdz^4 = 1 + 4az + 16bz^2 + 64cz^3 + 256dz^4 \quad 4.33$$

Rearranging the equation 4.33 gives

$$z^4 d(256 - q) + z^3 c(64 - q) + z^2 b(16 - q) + za(4 - q) + 1 - q = 0 \quad 4.34$$

Equation 4.34 can be solved by iteration using a spreadsheet program such as Microsoft Excel. The two different error function approximations used in equations 4.24 and 4.34 respectively produce values for the diffusion coefficients of each material within 10% of each other. The accuracy of the diffusion coefficients calculated is dependent on the accuracy of the error function approximation at the particular values of z required. In this situation z was in the range 0.020 to 0.195 and the error function approximations were accurate to at least 5 decimal places. For larger or smaller values of z the accuracy of the approximations would need to be confirmed.

4.4.4 Results and Discussion

Table 4.4 gives the chloride concentrations (molar concentration) at 1 cm and at 4 cm depth from the edge (circumference) of the disc specimen. In addition the calculated values for C_s (chloride concentration at the surface) and D_c (chloride diffusion coefficient), using the method detailed in section 4.4.4, are given in table 4.4. The method used for the calculation of the diffusion coefficients is based on a standard solution for Ficks 2nd law based on a semi-infinite slab. The test specimens used for the study were cylindrical (see Figure 4.7). The method employed would not be capable of predicting accurate chloride concentrations, but should be suitable for comparing different repair and substrate materials. There were no discernable trends between the values calculated for different repair substrate combinations and different sample locations within the test specimen (see figure 4.7). Table 4.4 represents the average values for each repair and substrate material from the measurements taken from all the test specimens. The value for each repair material represents the average of measurements from 4 specimens and each substrate the average from 6 specimens. Permeability has also been included in table 4.4 for comparison with D_c values. The D_c values predicted for the repair materials appear to follow the trends in permeability. This confirms that it is the size and degree of connectivity of the pores that controls mass transport phenomenon in concrete and repair materials.

Material A has a lower D_c value (a lower value represents a lower rate of chloride diffusion) than for material B and material C has the highest value. The general trend in D_c values is as would have been predicted from literature. However, the values are higher than those found in previous studies [50 – 58] and the values quoted by the manufacturers of the repair materials. The surface concentration values (C_s) do not give

a single value even though the exposure conditions are constant. This is probably due to experimental limitation from calculations based on only two measurements at C_1 and C_4 . This is partly due to large percentage errors possible from the titration results carried through the calculation. For instance material A was found to have a small chloride concentration after exposure. This means the amount of 0.1M $AgNO_3$ solution was low, in the order of 1 to 1.5 cm^3 . As the end point for the reaction was measurable to the order of 0.5 cm^3 , the average error produced in the chloride calculation for material A was in the order of 60%. The error was considerably less for the other repair and substrate materials, but represents the limit for the experimental technique used.

The situation for the substrate materials is more complex as chlorides were added during mixing. This makes it difficult to distinguish between the chlorides added and the chlorides that have diffused into the test specimens. It is also possible that the presence of chlorides in high concentrations may have affected the activity of the chloride ions and so reducing any measured chloride diffusion coefficient.

Table 4.4: Chloride content in repair materials and substrate concrete after 12 months exposure to 3.5% NaCl solution.

Material	% Error	$C_s(M)$	$C_1(M)$	$C_4(M)$	$D_c(cm^2/s)$	Permeability k (m/s)
A	60.500	0.054	0.042	0.020	2.139E-07	3.59×10^{-13}
B	20.400	0.121	0.104	0.069	6.294E-07	7.48×10^{-11}
C	15.100	0.163	0.158	0.146	1.827E-05	1.53×10^{-10}
0.4w/c Sub	3.800	0.234	0.231	0.184	1.982E-06	1.46×10^{-12}
0.8w/c Sub	4.800	0.204	0.202	0.161	1.340E-05	7.76×10^{-11}

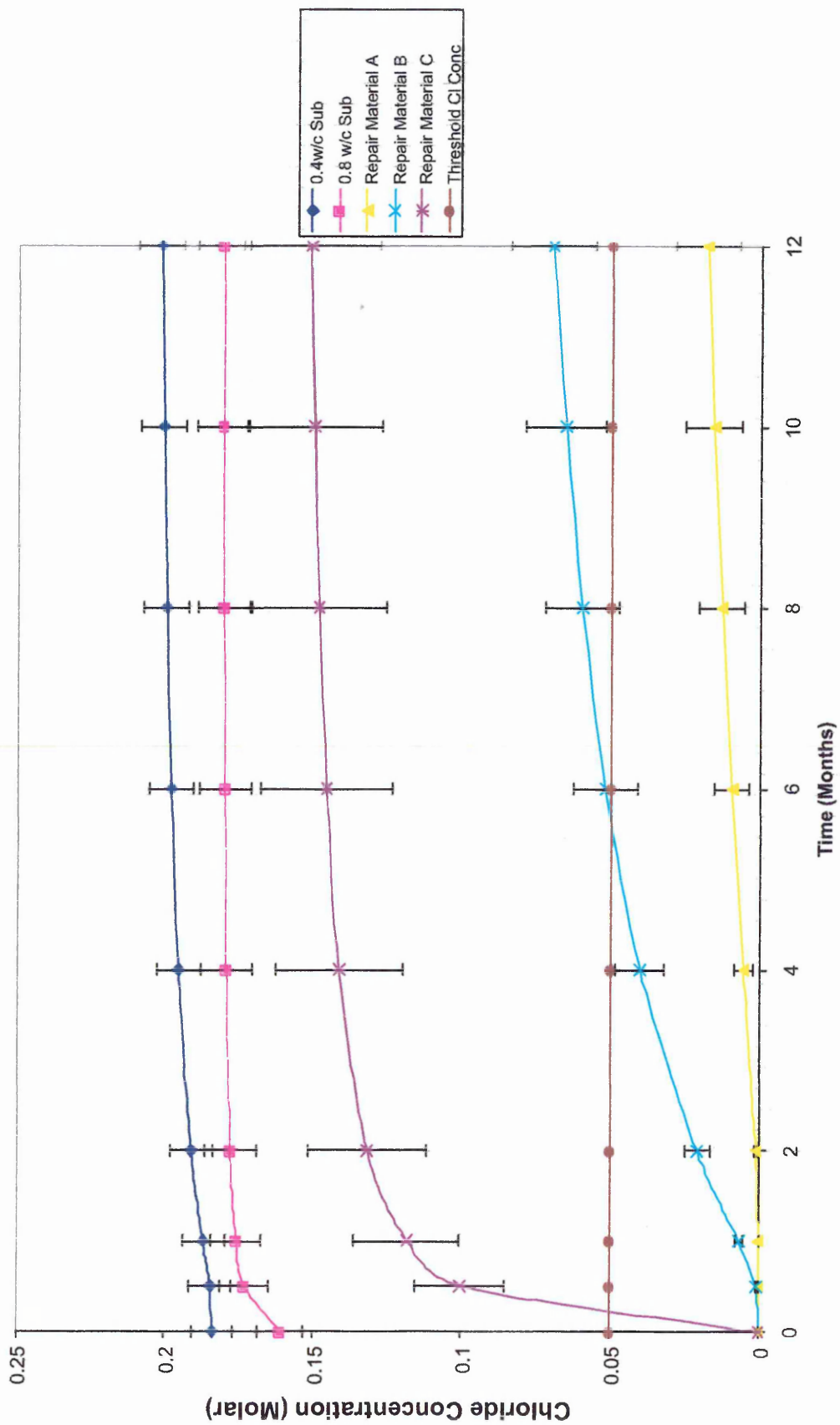
Taking into account the errors present in the results, the trends predicted for the chloride concentration at the steel surface (cover = 4cm) are useful for the investigations reported in Chapter 5 and Chapter 6. Figure 4.8 shows the predicted change in chloride concentrations over 12 months for the repair and substrate materials. A critical chloride concentration for corrosion initiation from literature was taken to be 0.05 M [29], above this value it is likely that corrosion of the steel will occur. From this it can be seen that for material A the chloride concentration is unlikely to have exceeded the critical value of 0.05M during this study. For material B it can be seen that the chloride concentration would only have exceeded the critical value in the last few months of the study. It is, however, probable that for material C the chloride concentration would have exceeded the critical value for the entire study.

4.4.6 Conclusions

The chloride diffusion coefficients for the repair materials increase with increasing permeability coefficients of the materials (see table 4.4). This indicates that the pore structure plays a critical role in mass transport properties. Material A has the lowest D_c value followed by material B and material C the highest value.

Prediction of chloride concentration at the steel surface (cover = 4cm) with time for these materials, suggests that for material A it never rose above a critical value to initiate corrosion. For material B it did exceed the critical value towards the end of the study, whereas for material C it had probably exceeded the critical value for most of the study. The findings of this work can be used to assess the effect of chloride concentration on future corrosion results later in the study (chapter 5).

Figure 4.8 Chloride Concentration at the Steel Over 12 Months Exposure



4.5 RESISTIVITY

4.5.1 Introduction

Resistivity measures the resistance of a material to the flow of an electric current. This is a measure of the ease of movement of ions through the cementitious material [36]. The movement of ions through the material is required in a corrosion reaction, therefore, resistivity is an important parameter in assessing the viability of corrosion cells. Resistivity as a technique is often used in conjunction with rest potentials to give an indication of the corrosion rate [186] of steel embedded in cementitious materials. A low resistivity material indicates easy movement of ions and ,therefore, a possible high rate of corrosion. This depends on the environment within the concrete being suitable to support the corrosion reactions. Resistivity is linked to the mass transport properties of the material such as porosity, permeability and diffusion. It is also likely that the resistivity of the constituent materials used in the repair and substrate mixes will have an effect on the resistivity of the material. The degree of saturation has a critical influence on resistivity and is also governed by the mass transport properties.

4.5.2 Experimental Procedure

4.5.2.1 Test Materials

The materials used in this section were the same as described in Section 3.4 on Test Materials. Three commercially available repair materials A, B and C were selected to provide a wide range of properties and to reflect the typical variety of repair materials currently available in the market.

Two concrete mixes, which represented the substrate concrete, were used, to which a repair material was applied. These are Substrate Concrete mix 1: Mix proportions (by weight) of, 1:2:4 (cement: fine aggregate; coarse aggregate) with w/c of 0.4. Substrate Concrete mix 2: Mix proportions (by weight) of, 1:2:4 (cement: fine aggregate; coarse aggregate) with w/c of 0.8. Both the substrate concrete mixes contained 3.5% NaCl (by weight of cement) to be consistent with the substrate mixes used in the corrosion testing work (Chapter 5). No NaCl was introduced in the repair material.

4.5.2.2 Test Specimens

The materials were cast into cylindrical steel moulds 100mm diameter X 200mm long, in three layers and vibrated to achieve optimum compaction. After casting the cylinders were placed in a mist room to cure overnight. The specimens were demoulded 24 hours after casting and then cured in a water tank for 28 days at 20°C. Two cylinders were cast for each test material.

After 28 days curing one cylinder for each test material was sectioned using a masonry saw. The specimens were cut to remove 25mm thick discs from the top and bottom of each cylinder. The cylinder was then cut into discs of 100mm diameter X 50mm +/- 5mm thickness. Following cutting and prior to testing all specimens were stored water tank at 20°C until all the measurements were completed, approximately 2 to 3 days. The second cylinder of each material was cured in a water tank at 20°C for 12 months, following which it was also cut into discs as described above.

4.5.2.3 Experimental Technique

A hand held resistivity meter was used to measure the resistivity of each test material. The meter had 2 probes with a spacing of 5 cm between them. Two holes of 5mm depth and 5cm apart were drilled into the cut face of each cylindrical disc specimen. This allowed the resistivity to be taken across the diameter of each disc. This technique avoided any high resistance surface films on the as cast cylinder circumference, that could have interfered with the results. The probe was then reversed in the holes and a second reading taken for each specimen. This allowed two readings for each specimen and two specimens for each material provided a total of four readings for each material. The resistivity results were averaged over both specimens.

4.5.3 Results and discussion

The resistivity measurements are given in table 4.5; the porosity values for each material have also been included for comparison. All the resistivity measurements are below 5 k Ω cm, this would indicate the potential for a high corrosion rate of steel embedded in these materials [186].

These measurements were much lower than expected from available literature on the materials [186]. The measurements were made on the cut surface of the specimen, this removed the influence of the fine, high resistance cast surface layer from the measurements. In addition, all the specimens were saturated with water, to ensure that all the measurements were conducted under the same conditions. As a consequence of this, the materials would be expected to have a lower resistivity. A comparison of the resistivity measurements with the porosity measurements (section 4.2) showed a close correlation between the resistivity and the percentage porosity of the material (see table

4.5 and figure 4.9). This suggests that the water contained in the pores of the specimens was the main controlling factor of the material resistivity.

It would be expected that the chloride contamination would have lowered the resistivity of the 0.4 w/c and 0.8 w/c substrate materials. However the trend between porosity and resistivity did not appear to be effected by the chloride addition to the substrate mixes (see Figure 4.9 and 4.10). This suggests that the degree of water saturation was the controlling factor for the values of resistivity measured.

Table 4.5 Resistivity Measurements

Material	Resistivity (kΩ cm)					Porosity (%)
	1	2	3	4	Average	
0.4	4.0	4.0	4.2	4.2	4.1	10
0.8	2.1	2.1	2.5	2.5	2.3	19
A	1.7	1.7	1.7	1.7	1.7	22
B	2.4	2.4	1.8	1.8	2.1	23
C	0.8	0.8	0.8	0.8	0.8	34

4.5.5 Conclusions

The resistivity values were lower than expected at below 5 kΩ cm. This was considered to be due to the water saturation of the specimens and the use of the cut face to take the readings, avoiding the high resistance cast surface layer. There was a close correlation between resistivity and porosity, indicating that the water content in the pores controlled the resistivity reading (see figure 4.9 and 4.10).

Figure 4.9 Trends in porosity and resistivity properties.

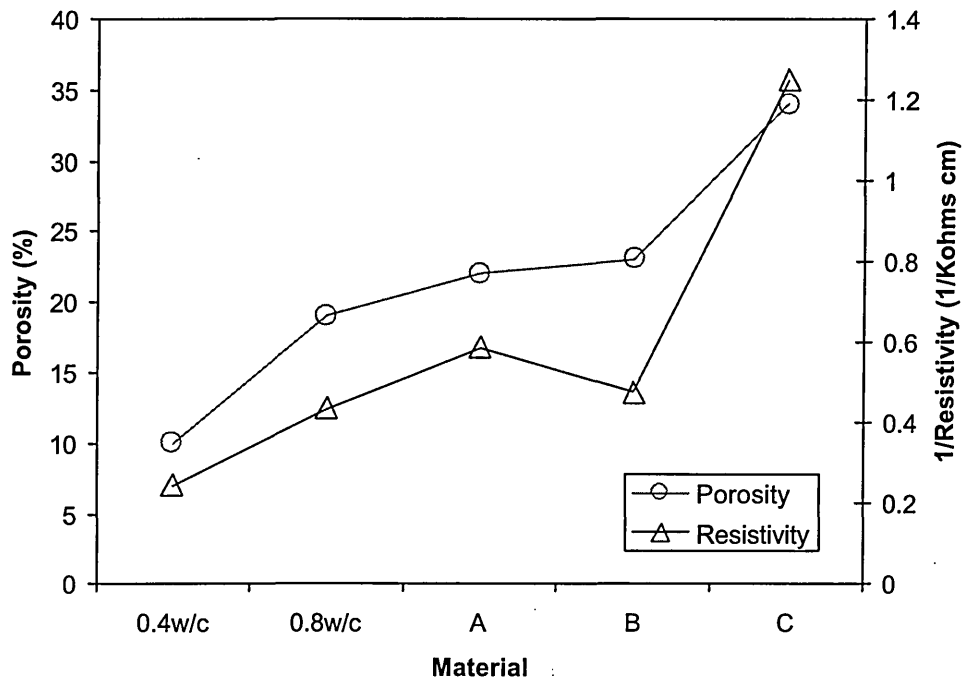
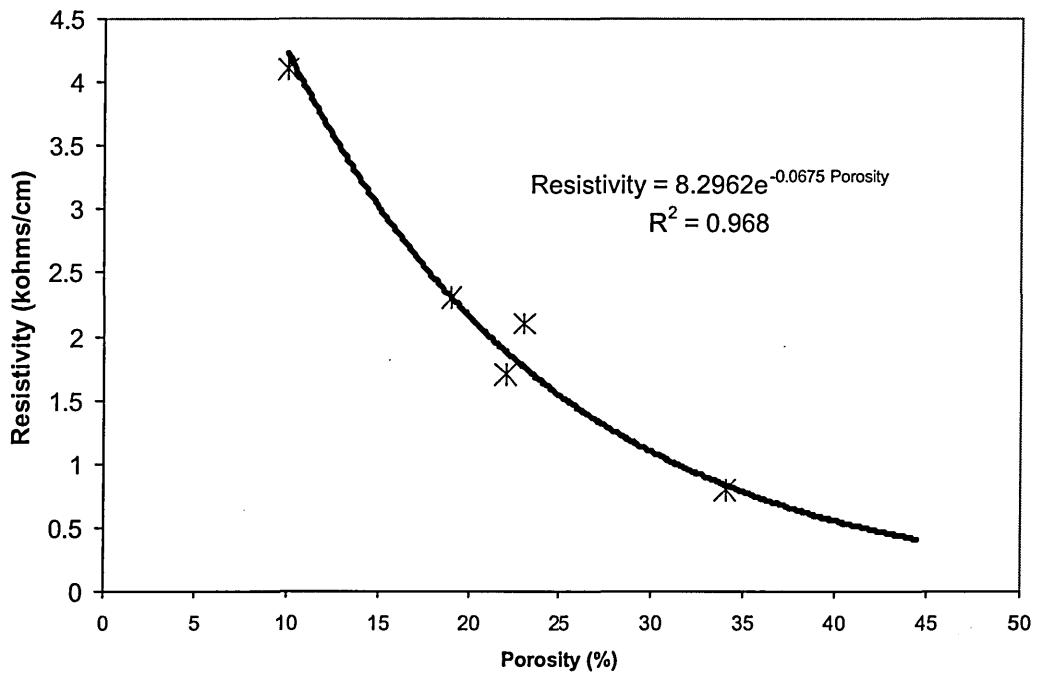


Figure 4.10 Relationship between porosity and resistivity measurements



4.6 DISPARITY IN PROPERTIES BETWEEN REPAIR AND SUBSTRATE

MATERIALS

4.6.1 Introduction

The physical properties have been determined for the five materials used in the study (three repair materials and two substrate materials). Four different properties, porosity, permeability, resistivity and chloride diffusion were determined, which were identified as being important in the development of reinforcement corrosion within cementitious materials. The aim of this was to characterise the differences in properties between the repair and substrate materials (mismatch). The materials investigated here will be joined in different repair –substrate combinations in later chapters in order to study the initiation and propagation of corrosion of reinforcement embedded in these materials. The development of corrosion in the specimens will be related to the disparity in the properties between the repair and substrate material combinations. Table 4.6 summarises the results on the physical properties of the substrate and repair materials.

Table 4.6. Properties of repair and substrate materials

Material	Density (Kg/m ³)	Porosity (%)	Permeability (m/s)	Resistivity (Kohms/cm ²)	Chloride Diffusion Coef. D _c (cm ² /s)
Concrete w/c 0.4	2350	10	1.46x10 ⁻¹²	4.1	1.98 x 10 ⁻⁰⁶
Concrete w/c 0.8	2110	19	7.76 x10 ⁻¹¹	2.3	1.34 x 10 ⁻⁰⁵
A	1980	22	3.59x10 ⁻¹³	1.7	2.14 x 10 ⁻⁰⁷
B	1050	23	7.48x10 ⁻¹¹	2.1	6.29 x 10 ⁻⁰⁷
C	1250	34	1.53x10 ⁻¹⁰	0.8	1.83 x 10 ⁻⁰⁵

4.6.2 Porosity and Resistivity

Table 4.6 shows that the resistivity and porosity measurements appear to be related. This suggests that the measurements obtained are affected by the pore structure of the materials. Figure 4.9 shows the trend between porosity and the resistivity data for each material and Figure 4.10 shows the resistivity and porosity of each material. The graphs show a clear empirical relationship between porosity and resistivity.

The substrate materials (of $w/c=0.4$ and 0.8) have a lower porosity than the commercial repair materials used in this study. Repair materials tend to use smaller proportions of coarse aggregates than present in the substrate materials. Porosity of the aggregates is generally lower than the mortar and is unlikely to contribute to mass transport in the cementitious material, as the pore structure in the aggregate will not be homogenous with the mortar. If a material has a greater proportion of coarse aggregates (e.g. the substrate concrete in this study) it will appear to have a lower porosity although the porosity of the mortar surrounding the aggregates could be higher. This makes comparisons of porosities between materials containing different aggregate proportions and sizes difficult.

The best matches in porosity are achieved for repair materials A and B with the $0.8w/c$ substrate. The size and proportions of aggregates used is different for all the repair materials and it is not possible from these measurements to differentiate porosity of the coarse aggregates from the porosity of the mortar. For the substrate materials, an identical proportion of fine and coarse aggregates were used. Therefore in comparing the $0.4w/c$ to $0.8w/c$ the effect of the aggregate can be ignored to conclude that increasing the water cement ratio changes porosity from 10% to 19%. All the repair

materials have different coarse aggregate sizes and proportions, material A has a 5mm, material B 2.5mm and material C no coarse aggregate (see Chapter 3 for further details).

The effects of differences in porosity of aggregates and mortars could mask the differences in pore structure between repair and substrate materials. This could make porosity an insensitive measure of properties affecting reinforcement corrosion. The porosity measurements, therefore, cannot be used to assess the effect of disparities in the structure of repair and substrate materials as suggested by Cusson et al [21].

A similar problem to porosity exists for the resistivity measurements. Resistivity will be largely controlled by water content and presence of any salts in the pore solution (which may reduce conductivity of the solution). Any remaining differences in resistivity will be caused by differences in the pore structure of the bulk solid material (sand, aggregates and polymers etc). In this study, the substrate materials had chlorides added during mixing, but in the same proportion for each water cement ratio (see Chapter 3). The tests were conducted on saturated samples to ensure that all the specimens were in the same condition. The results found that resistivity showed similar trends to the porosity results for the substrate and repair materials. Figures 4.9 and 4.10 confirm that porosity and resistivity are strongly related.

The substrate materials have higher resistivity values than the repair materials and the best matches are for repair materials A and B with the 0.8w/c substrate (Table 4.6). Cusson et al [21] recommend a match in resistivity, however it is unclear how this could be achieved in practice. The resistivity of substrate concrete in a structure would be a function of the water and salt level in the material, absorbed from the service environment. It would not be possible to measure the resistivity of repair materials in a

matching service environment over time. If such measurements are to be made in a laboratory, a standard condition for the specimens would need to be defined. Cussons et al [21] do not explain how the match in resistivity would be a measure of the electrochemical compatibility of the repair and substrate environments.

The porosity and resistivity measurements conducted in this study indicate that neither property adequately defines the structure of the materials for the purposes of defining the mismatch between repair and substrate materials in practical repair situations. These measurements would appear to be a poor representation of the disparity in properties between the repair and substrate materials in practical situations and in for the corrosion testing investigations detailed in Chapter 5.

4.6.3 Permeability and Chloride Diffusion Coefficient

The Darcian permeability coefficient K and the chloride diffusion coefficient D_c show similar trends for all the materials tested (Figures 4.11 and 4.12) and provide an empirical relationship between the chloride diffusion coefficient and permeability coefficient. Permeability is a measure of the flow of water through the specimen. Permeability is linked to the structure and connectivity of pores in the material and should not be affected by differences in aggregate size and content, or the degree of saturation as in the case of porosity and resistivity. This makes permeability a useful measurement to define the effect of disparity in properties of repair and substrate materials in the present study and in practical situations.

Figure 4.11 Trends in permeability and chloride diffusion coefficients.

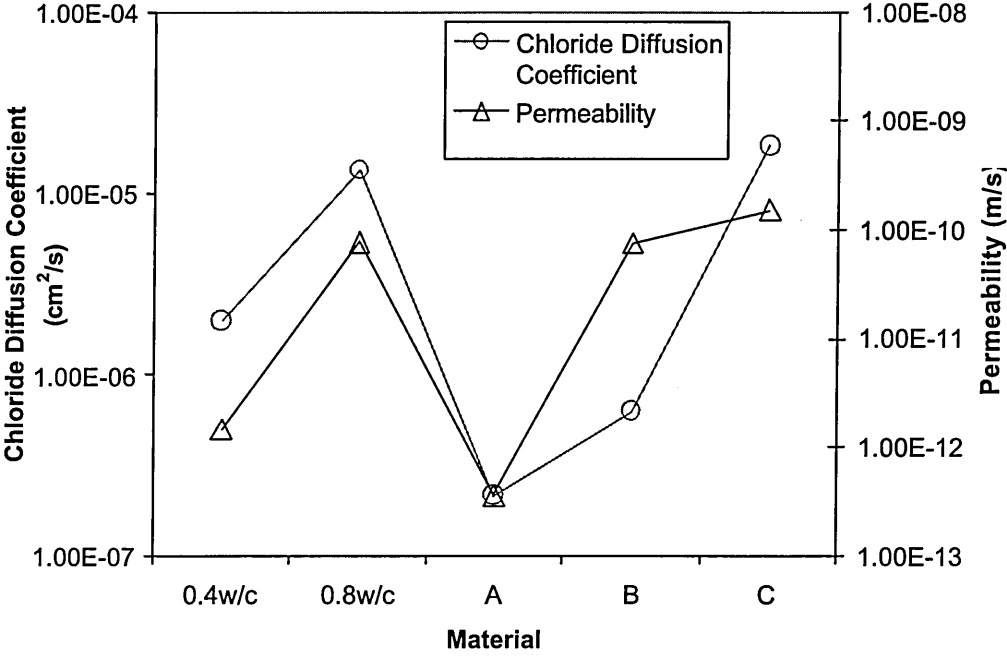
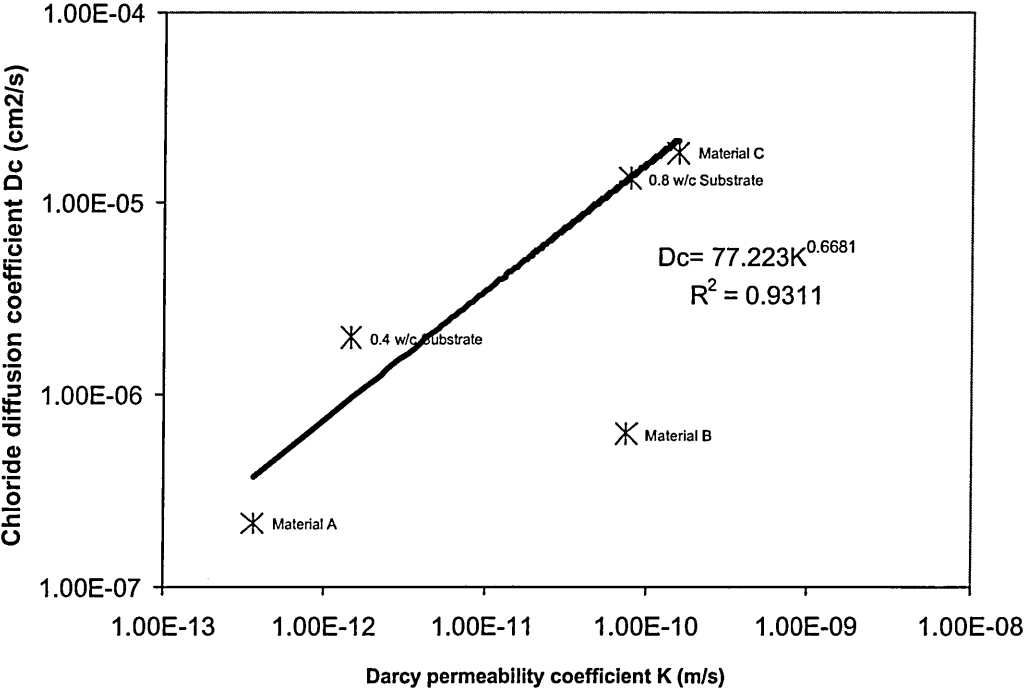


Figure 4.12 Chloride Diffusion Coefficient against permeability



The water permeability of a material should also provides a measure of the permeability of the material to chloride, oxygen and water, all of which are required for the development of corrosion in concrete. This would explain the relationship between permeability and chloride diffusion in Figures 4.11 and 4.12.

Repair Material A had the lowest measured permeability and Repair Material C the highest (Table 4.6). The closest match in permeability between the repair and substrate materials was Repair Material B and the 0.8 w/c substrate. Repair materials A and B have lower chloride diffusion coefficients than either the 0.4w/c or the 0.8w/c substrates. Repair material C has a higher chloride diffusion coefficient than the two substrates. The closest matches (see Table 4.6) were for the 0.8w/c substrate and material C and for material B with the 0.4 w/c substrate. This would suggest that these two combinations would be the least likely to develop corrosion macro-cells, on the basis of good match between repair and substrate.

However, both the substrate mixes had chloride added above the likely threshold level to initiate corrosion. Therefore the chloride level in the substrate is higher than the repair. It is the chloride levels within the repair and substrate materials that determine the development of chloride macro-cell corrosion. The repair materials represent three basic situations;

- Repair material A: The chloride level at the steel level (cover 4 cm) remains below the chloride threshold value for the full period (12 months) of the study.
- Repair material B: The chloride level at the steel level (cover 4 cm)exceeds the threshold level to initiate corrosion after approximately six months, but remains below the chloride level in the substrate concrete for the full period of the study.

- Repair material C: The chloride level at the steel level (cover 4 cm) exceeds the threshold level required to initiate corrosion after approximately one month and approaches that of the substrate material after six months.

Permeability and chloride diffusion coefficients are suitable to define the disparity in properties between repair and substrate materials.

4.6.4 Conclusions

Resistivity and porosity measurements show a clear relationship for the materials used in the present study. The constituent materials, such as, the aggregate and chlorides used in the different materials were found to affect both measurements. As a result, neither technique provides an adequate measure of the disparity in properties between the repair and substrate materials suitable for defining mismatch of materials. The effect of disparity in resistivity and porosity on the development of corrosion in different repair substrate combinations is limited.

There is a clear relationship between permeability and chloride diffusion coefficient measurements made during the study. The constituents used in the different substrate and repair materials did not affect permeability and chloride diffusion measurements. Permeability and chloride diffusion coefficients were selected as the main parameters for measuring the disparity in properties between repair and substrate materials.

5.0 Corrosion Testing

5.1 CORROSION TESTING (DESTRUCTIVE) - POTENTIODYNAMIC

POLARISATION CURVES

5.1.1 Introduction

Cyclic voltametry techniques are a common experimental method for studying the kinetics of electrochemical reactions. In corrosion studies the use of polarisation curves or Tafel curves has become well accepted and this has led to the production of national standards such as ASTM G5 and G61. As it is a destructive test and requires a new specimen for each test, this precludes it from being used on site and so has not been widely employed to study corrosion in concrete. However, in laboratory studies it does offer a powerful investigative tool for studying the corrosion process.

5.1.2 Test Specimens

The repair and substrate materials used for the measurement of the potentiodynamic polarisation curves are as described in Chapter 3. Each test specimen was made from a single repair or substrate material and contained a single steel reinforcement bar. The materials were cast into cylindrical steel moulds, 100mm diameter X 200mm, in three layers and vibrated to achieve optimum compaction. Each specimen contained a single 8 mm. diameter reinforcement bar of high yield 460 grade steel located longitudinally along the centre of the cylinder (see Figure 5.1). A steel wire was connected to the end of each reinforcement bar and sealed with an epoxy-based sealant. The bottom end of the reinforcement embedded in the concrete was sealed with a silicone sealant. This left a reinforcement surface area of approximately 50 cm² exposed to the

environment of the repair or substrate materials. Each of the substrate materials (0.4 w/c and 0.8 w/c) also had 3.5% NaCl added during mixing to depassivate the steel reinforcement embedded in the specimens.

After casting the specimens were left in a mist curing room overnight. They were demoulded 24 hours after casting and then cured in a water tank for 28 days at 20°C. At least three cylinders were cast for each repair material and for concretes of 0.4 and 0.8 water cement ratios.

5.1.3 Test Method

The polarisation test has been standardised in ASTM G61 and G5. However, these standards relate to measurements of a metal in a solution, not to steel embedded in concrete. Polarisation studies normally use nitrogen-purged solutions to remove dissolved oxygen from the test solution. This is done to give a degree of control in isolating the cathodic reaction and in limiting the effects of the reduction of dissolved oxygen from solution. This practice is essential for measuring the full polarisation behaviour of a metal in an oxidising environment.

This is not always practical in concrete as the test cells tend to be larger. It is also not a realistic representation of the service environment of concrete, as the reduction of oxygen is the main cathodic reaction. It has also been suggested that removal of oxygen from the concrete could lead to changes in the concrete structure and so could affect the system under test. Therefore, polarisation studies of concrete generally do not purge with nitrogen. Cigna et al [155] studied the effect of different concrete mixes on the polarisation curves and the effect of oxygen saturation was also examined. Samples tested in nitrogen purged solutions exhibited very low limiting corrosion currents.

The test apparatus used in the current study can be seen in Figure 5.2. Following the initial 28-day curing all the specimens were transferred into a water tank containing 3.5% NaCl solution for the remainder of the study. The specimens were left in the tank for approximately 28 days then tested one by one by placing the specimen in the test apparatus (see Figure 5.2). Each test took approximately 6 hours to complete and approximately 3 weeks to test all the specimens.

A computer-controlled potentiostat supplied by ACM Ltd was used to measure the polarisation curves. The potentiostat was configured to sweep from -1000mV below the rest potential to +1000mV above the rest potential. Prior to commencing the sweep, the cell was held at -1000mV for sixty seconds to use up any dissolved oxygen contained in the concrete test sample. A sweep rate of 6 mV/min was used for the tests, therefore, each sweep took approximately six hours from start to finish. On completion of the sweep the computer automatically completed a reverse sweep from +1000mV to -1000mV about the rest potential using the same sweep rate. The potentiostat monitored the current flowing between the working electrode and the auxiliary electrode and the potential between the reference electrode and the working electrode. Approximately 200 measurements of potential and current were taken at equally spaced intervals during the test.

The results from the tests were used to plot polarisation curves. These are plots of potential against current density. Current density is the current measured per unit area of the working electrode. From the polarisation curve it is possible to measure the corrosion rate from

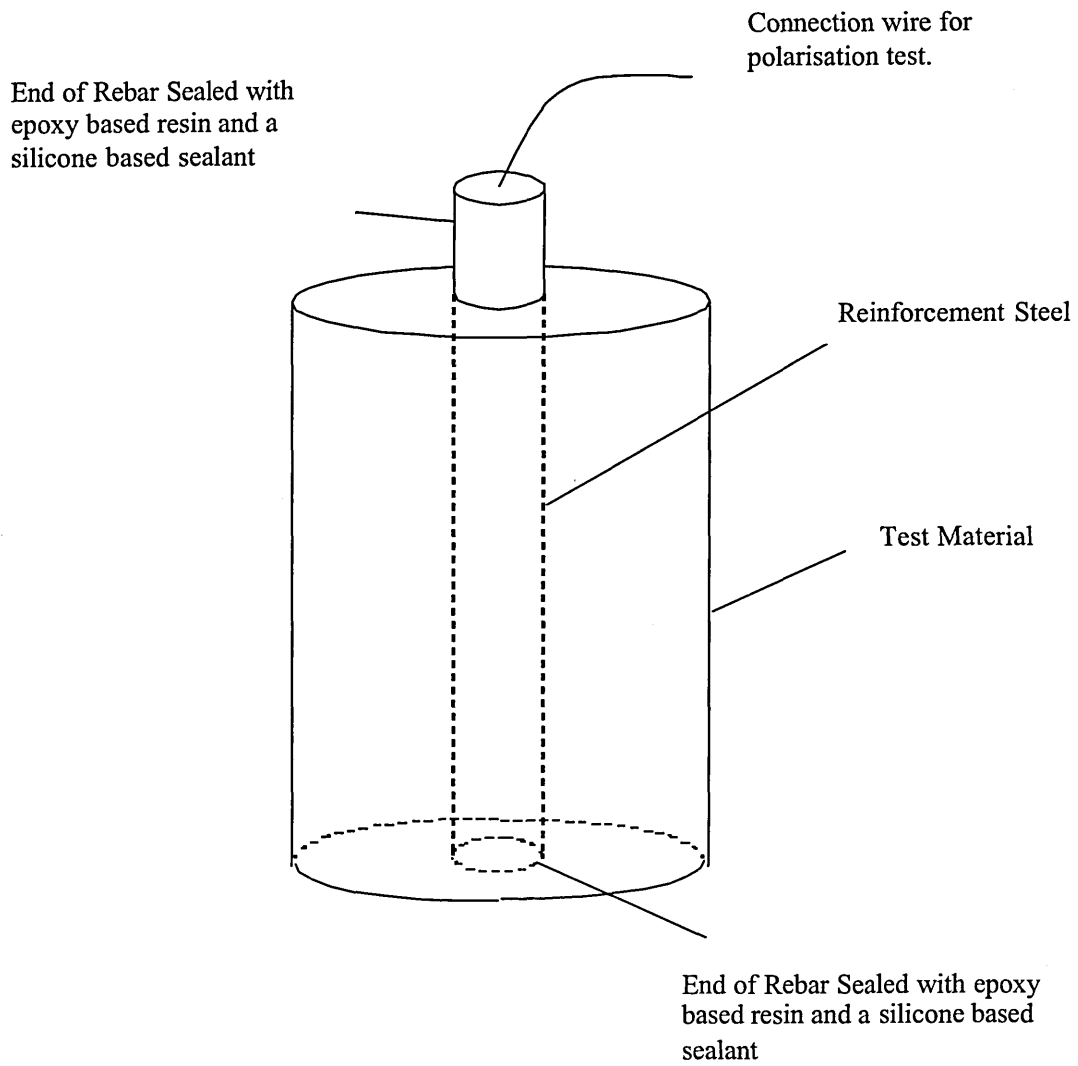


Figure 5.1 Test Specimen

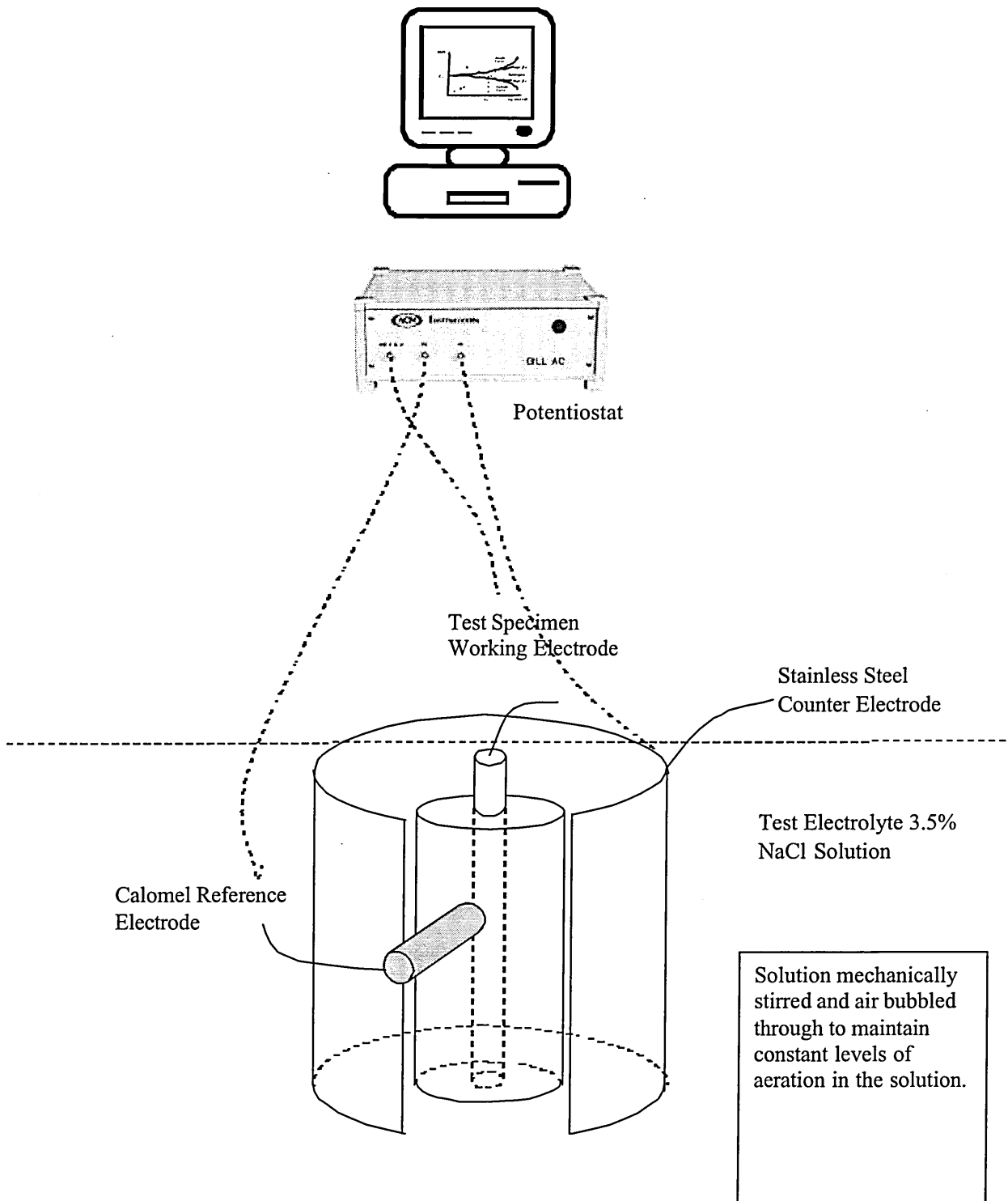


Figure 5.2: Schematic Diagram of Test Equipment.

measurements of the Tafel slopes (see Section 2.5.2 Potentiostatic and Potentiodynamic Polarisation Curves).

The interpretation of the morphology of the polarisation curve can provide information on the mechanism of corrosion [143, 152, 155]. This is dependent on the electrode kinetics for the cell under investigation. Previous research has shown that a passive oxide film forms on the surface of the steel in concrete, if the concrete can maintain a pH of approximately 12.5. The action of Cl⁻ ions or changes in pH will cause breakdown of the passive film. The polarisation curve for a metal - electrolyte combination that shows an active-passive transition can be seen in Figure 5.3 [31, 204].

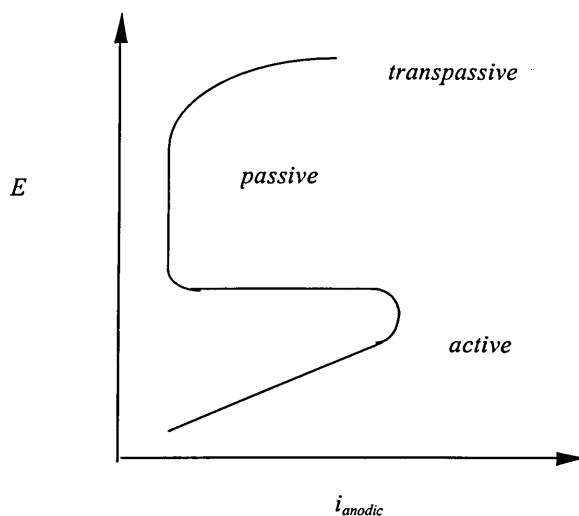


Figure 5.3 Anodic Polarisation Curve Showing Active-Passive Transition

However, this stylised curve differs from what was actually measured in the experiments. The measured anodic curves are dependent on where the cathodic and anodic curves cross. This is the point where the working electrode, in this case the rebar, switches from being a cathode to an anode. The cathodic curve implies oxygen reduction is occurring on the rebar surface at that point

in the sweep and the anodic curve implies that metal loss is occurring at that point. Examples of measured curves can be seen in Figure 5.4. In Figure 5.4 [163], case 1 shows a situation where the cathodic curve (oxygen reduction) crosses the anodic curve (metal loss) in the active zone of the theoretical polarisation curve. This would indicate general corrosion giving a wide range of possible corrosion rates. In Case 2 the cathodic curve intersects the anodic curve at three potentials, one active two passive. If the middle active passive zone is not stable, very high corrosion rates are possible at these upper and lower intersections. In case 3 the cathodic curve crosses in the passive region. This indicates a metal which has formed a passive oxide film and, therefore, has low corrosion rates, usually the desired situation.

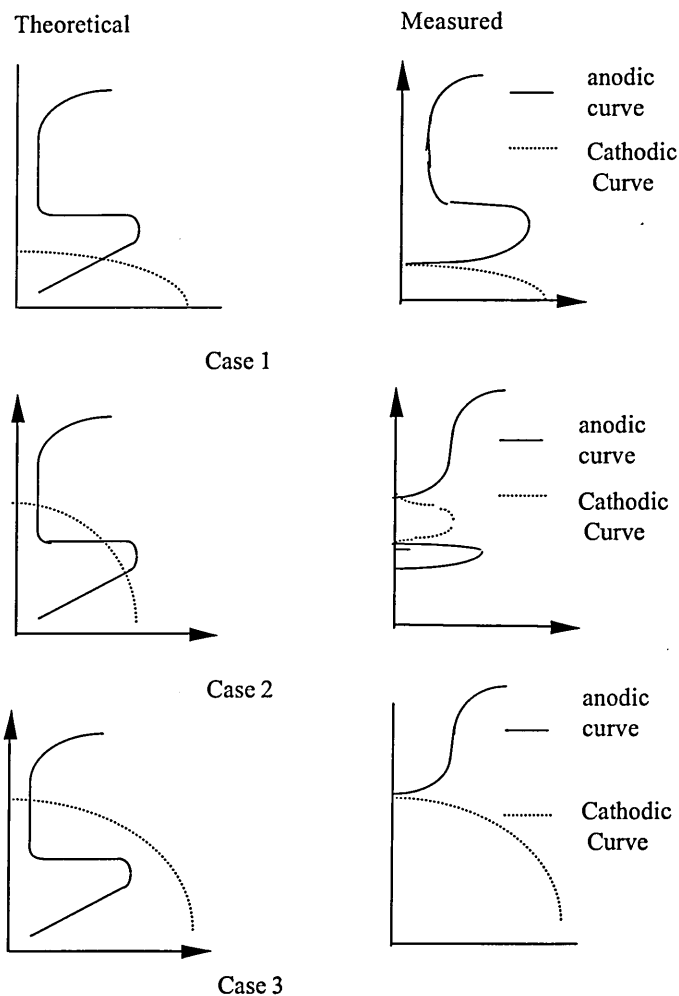


Figure 5.4 Theoretical & Measured Polarisation Curves

5.1.4 Results

Up to 5 polarisation curves for each material were generated (see Table 5.1). The curves for each material were combined to produce an averaged curve. The averaged curve for each material was constructed using the results that were within +/-5mV of each other. In practice this meant that the averaged curve was constructed from between 2 and 4 of the 5 curves generated for each material (see table 5.1).

Table 5.1 Potentiodynamic Polarisation Test Results

Material	Number of specimens tested	Percentage deviation in results	Number of specimens generating average curve
A	4	5	4
B	4	7	3
C	3	8	2
0.4w/c	5	12	3
0.8w/c	5	10	3

Figure 5.5 shows typical polarisation curves measured for a repair material during the test programme. The curves show both the initial forward sweep and the reverse sweep. Figure 5.6 shows the average curves for all the materials tested. The averaged curves show just the initial forward sweep, the reverse sweep has been omitted for clarity. From the average curves the anodic (β_a) and cathodic (β_c) Tafel constants were measured by calculating the slopes from the

Figure 5.5 Typical polarisation curves for a repair material

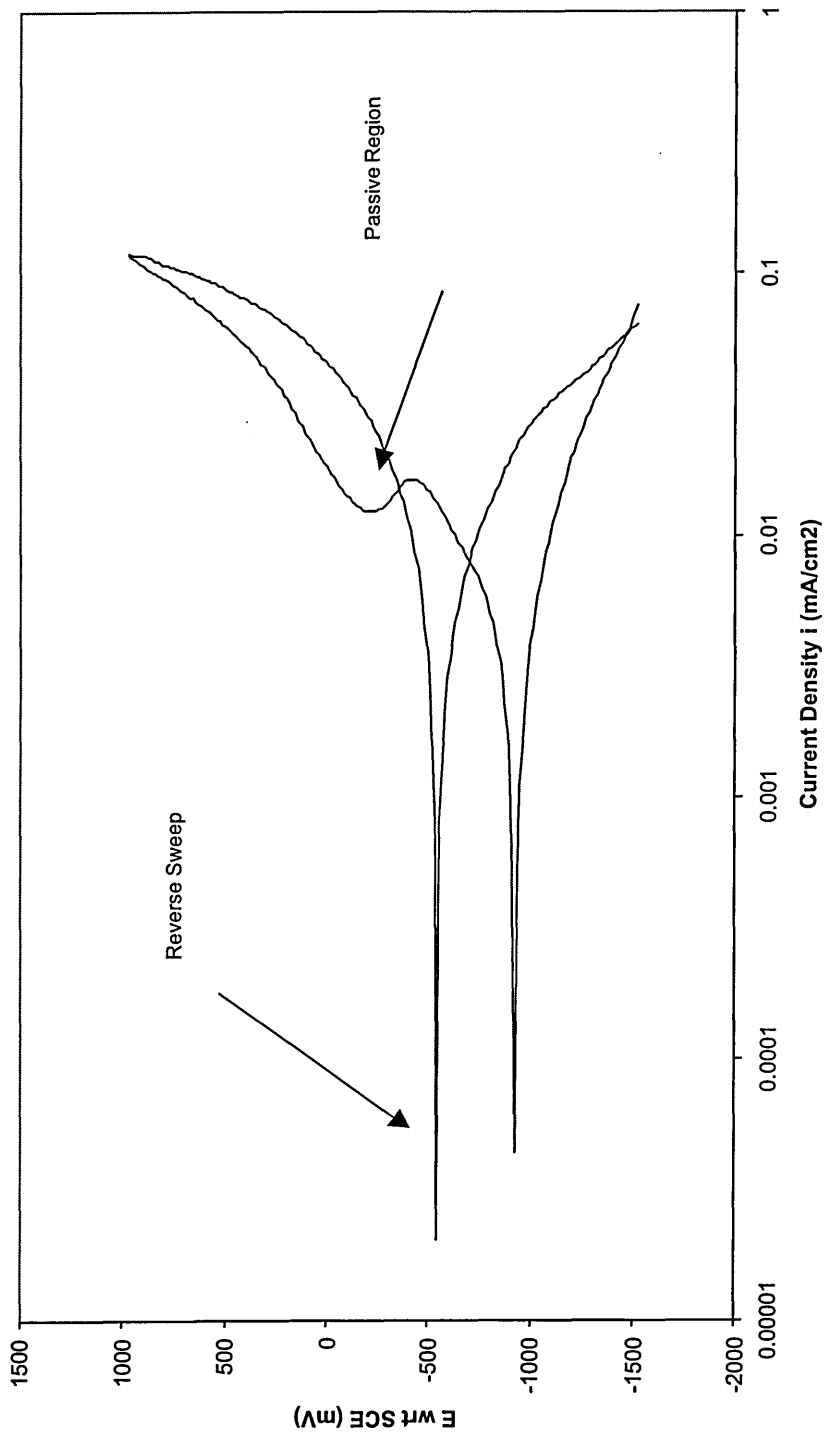


Figure 5.6 Average Polarisation Curves

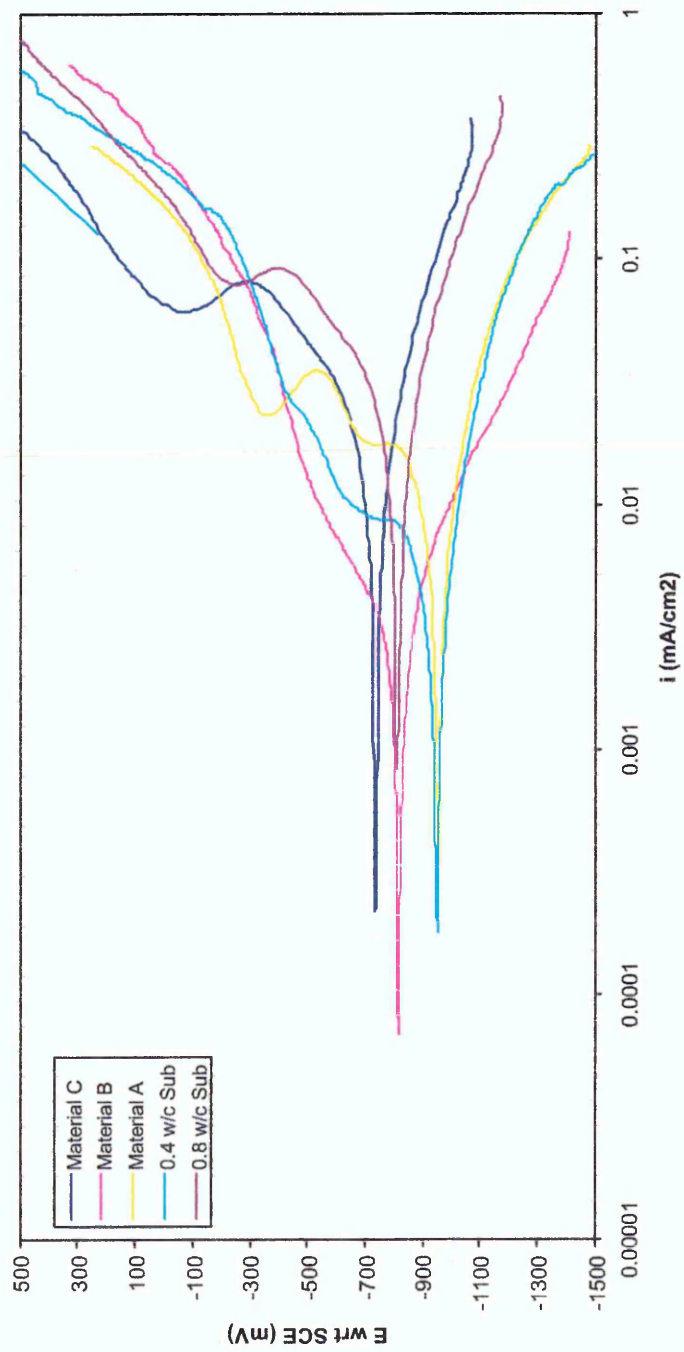


Figure 5.7 The Relationship between E_{corr} and Permeability

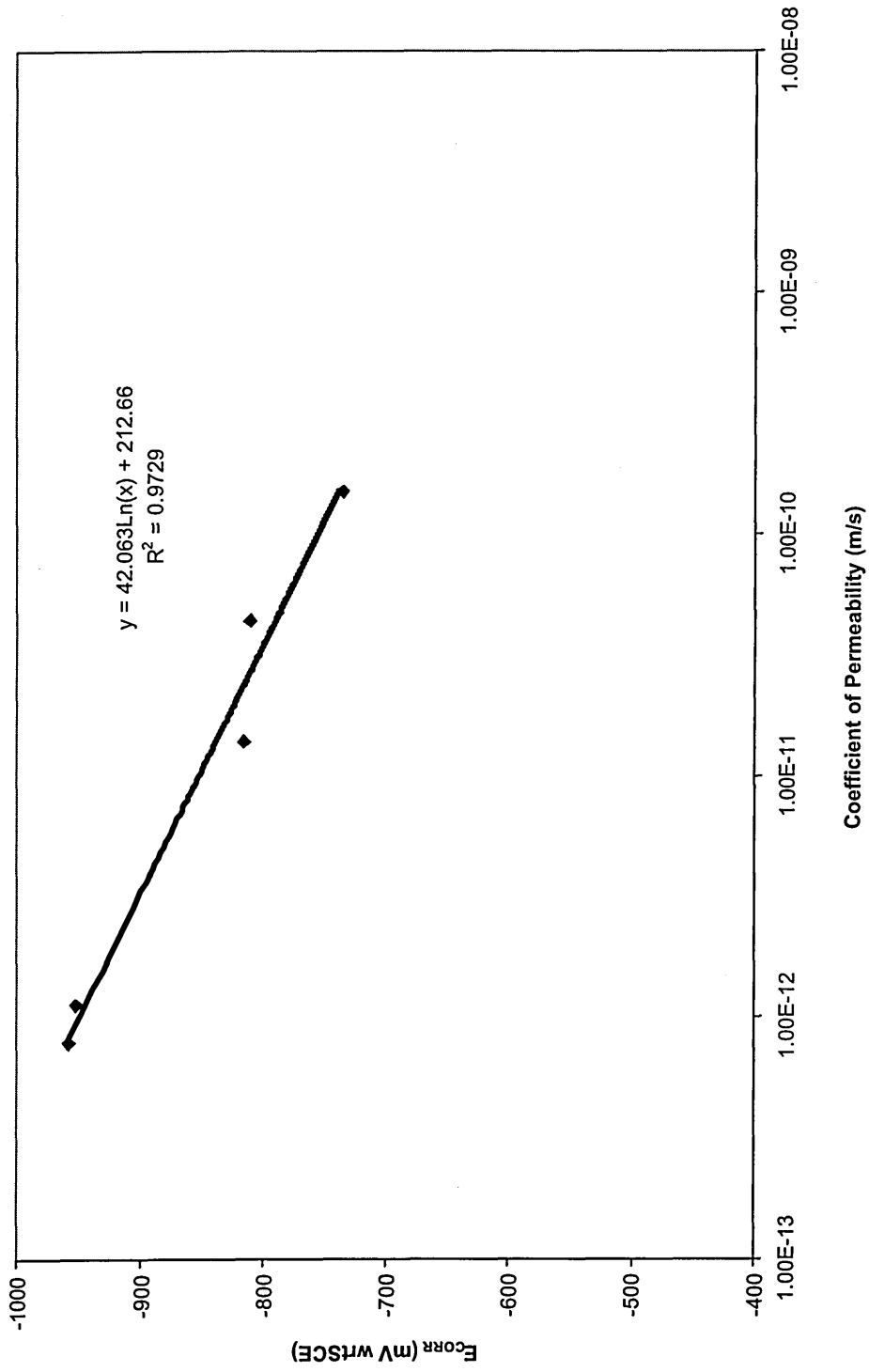


Figure 5.8 Repeated Cathodic Sweep on Material A

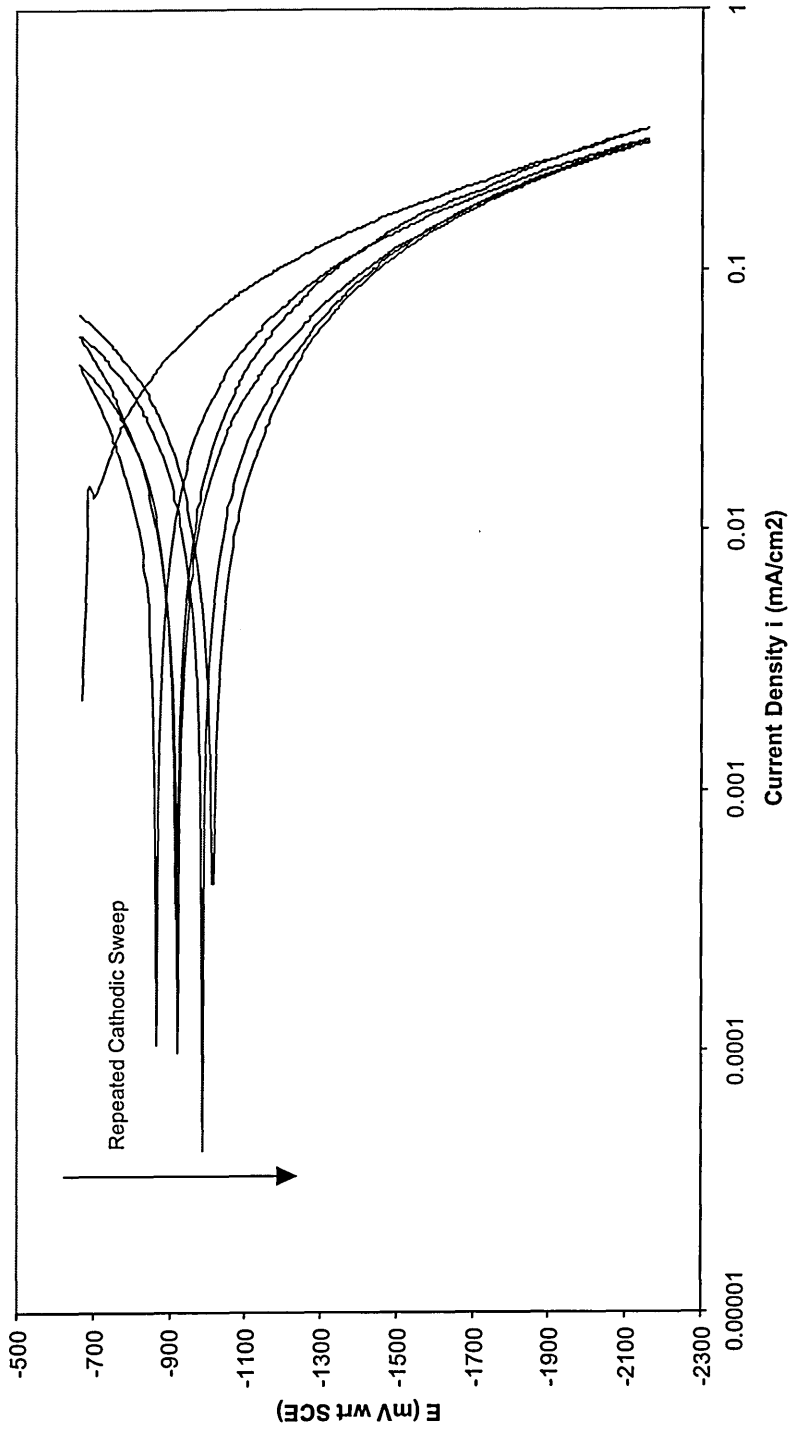
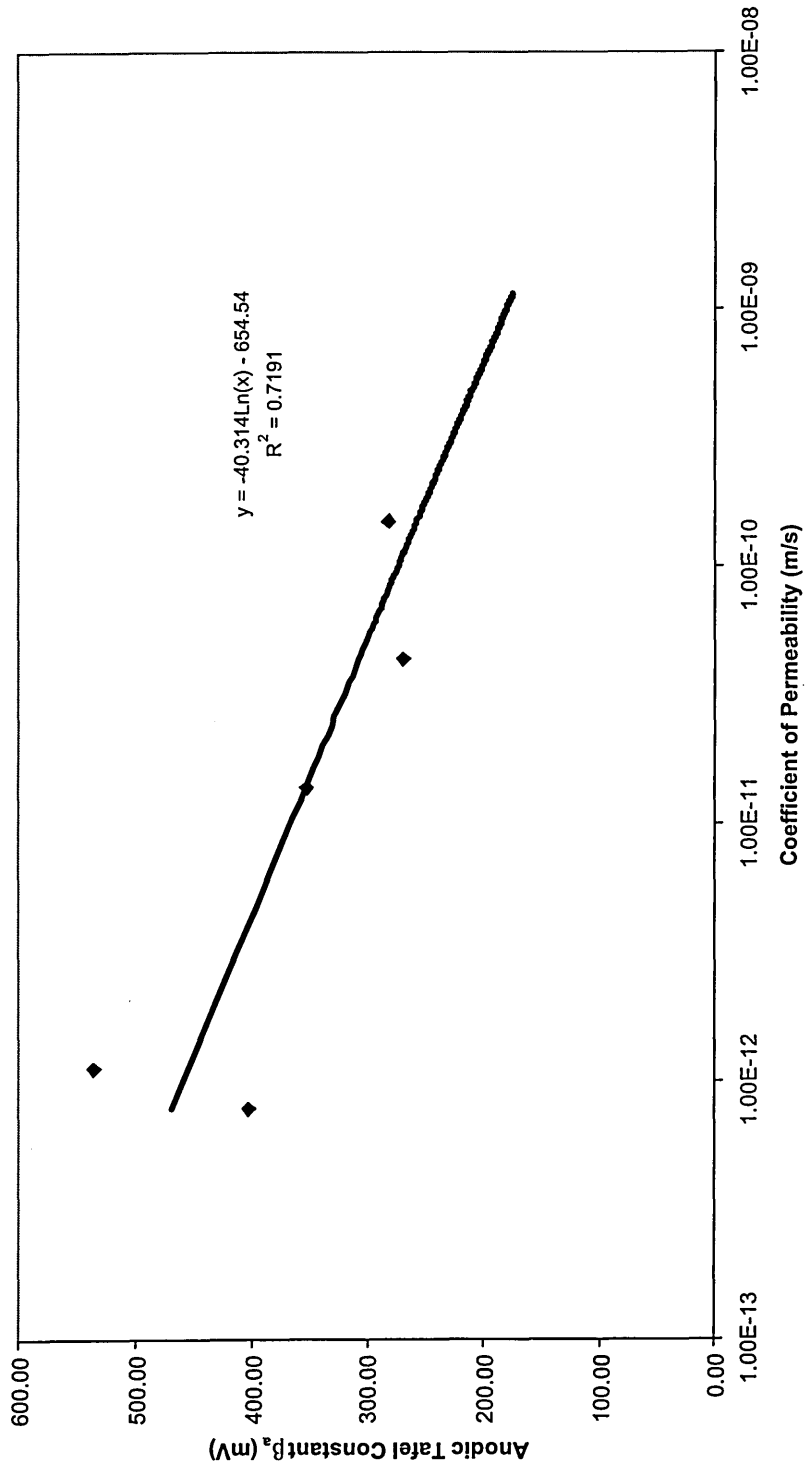


Figure 5.9 Relationship between anodic Tafel constants and permeability



anodic and cathodic sections of the curve. These have been tabulated in Table 5.2, together with constant B which is a function of β_a and β_c (see section 5.2.5).

Table 5.2 Tafel Constants from Average Polarisation Curves.

Material	Permeability Coefficients (m/s)	E _{corr} (mV)	β_a (mV)	β_c (mV)	B (mV)
0.4w/c	1.46×10^{-12}	-952	536.24	137.79	47.66
0.8w/c	7.76×10^{-11}	-811	268.80	149.78	41.82
A	3.59×10^{-13}	-958	402.03	138.34	44.75
B	7.48×10^{-11}	-816	352.47	177.01	51.23
C	1.53×10^{-10}	-735	281.25	122.22	37.04
Average			368.16	145.03	45.24

5.1.5 Discussion

5.1.5.1 Interpretation of Measured Polarisation Curves

The anodic polarisation curve for concrete Figure 5.6 indicates case 1 or 3 behaviour (see figure 5.4) [163]. The reinforcing steel shows the behaviour of a metal with an active passive transition. This was found to be typical for all the materials tested. In comparison to the idealised curve in Figure 5.4, the size of the passive area is small. This would suggest that case 3, from Figure 5.4, is the most likely behaviour. Here, the rebar working electrode switches from cathodic to anodic behaviour in the passive region of the metal. The size of the passive region will be controlled by the point at which the change over occurs, which is the E_{CORR} value. The E_{corr} value is given by the Nernst equation;

$$E = E_o + \frac{RT}{nF} \ln \left(\frac{\alpha[O]}{\alpha[R]} \right) \quad 5.1$$

where: E= Cell potential

E_o = Standard Electrochemical potential

$\alpha[O]$ = activity of oxidants

$\alpha[R]$ = activity of reductants

As the reductant in the corrosion reaction is oxygen, the measured E_{CORR} value will be related to oxygen concentration in the concrete and the rate of diffusion of oxygen through the concrete. The measured E_{CORR} values are low which suggests that oxygen concentration in the electrolyte is low. The size of the passive region is approximately 500 mV, the Pourbaix diagram for the iron water system would suggest a much larger passive region of up to 1500 mV at pH 12 in concrete. However, the size of the passive region is also dependent on chloride ions. An increase in the chloride ion concentration will reduce the breakdown potential, this is the point at which the behaviour changes from passive to transpassive and signals the start of pitting corrosion. The results measured do appear to be consistent with the Pourbaix diagram allowing for the presence of chlorides. As the results are consistent for all the specimens it indicates that chlorides, from the 3.5% NaCl solution used in the experiments and added to the substrate materials during mixing, have affected the polarisation curves.

The work of Cigna et al [155] would appear to confirm this, whose results show a very similar behaviour to that presented here. However, Cigna et al [155] also carried out measurements in a lime solution and produced much larger passive regions.

During the reverse sweep the passive area disappears and the curve resembles that for an actively corroding metal. The return E_{CORR} value is higher than the initial E_{CORR} value. This would indicate that the passive oxide film on the metal surface is not stable. It is likely that a metal producing

these sorts of curves would show a tendency towards pitting or crevice corrosion in the electrolyte. This corrosion will be localised i.e. it will be located on a very small section of the steel. Whilst this will produce very high rates of corrosion at the pit, measured rates of corrosion over the metal surface will be low.

Figure 5.6 shows the average curves for all materials used in the study. Only the forward curves have been shown for clarity. The shape of all the curves is similar, however, the E_{CORR} values and the Tafel constants (Table 5.2) are different. This indicates that the corrosion activity of each material is different. The Nernst equation (equation 5.1) shows that E_{CORR} and the oxygen concentration are related. It also would appear to be the case that the rate of oxygen diffusion and the microstructure of the concrete are related. It would, therefore, be logical to expect that E_{CORR} would be related to a property of the microstructure such as permeability. As predicted by the Nernst equation, figure 5.7 shows a linear relationship between the E_{CORR} values measured and the log of the Darcian coefficient of permeability for each material.

The shape of the cathodic curve (Figure 5.8) shows the cathodic reaction (oxygen reduction). In the test results plotted in Figure 5.8 the cathodic section of the polarisation sweep has been repeated a number of times for the low permeability repair material A. The cathodic reaction is diffusion controlled, so the controlling step of any corrosion reaction would be the rate at which oxygen diffused to the metal surface. The repeated tests show that the E_{CORR} value falls with each sweep. This could indicate oxygen is being consumed faster than it can be replaced by diffusion, which leads to the depletion of oxygen in the concrete sample and produces lower E_{CORR} values. The repeated polarisation may reduce the oxygen level below the point where the passive oxide

film cannot be maintained. In chloride contaminated concrete this could initiate corrosion of the steel in the specimen.

5.1.5.2 Corrosion Rate Calculations from the Polarisation Curves

Table 5.2 shows the Tafel constants calculated for each material from the relevant average curve. The cathodic Tafel constant β_c appears to show no clear dependency on material properties such as permeability. The average value for β_c is 145mV which is close to the value of 120mV expected for a diffusion controlled process such as oxygen diffusion. The anodic Tafel constant β_a shows a clear relationship with permeability (Figure 5.9). The anodic and cathodic Tafel constants can be combined to give one constant B using the following equation [50, 58, 63, 137, 138, 149, 156 – 162]:

$$B = \frac{\beta_a \beta_c}{2.3(\beta_a + \beta_c)} \quad 5.2$$

And this can be related to the rate of corrosion i_{corr} as follows:

$$i_{corr} = \frac{B}{R_p} \quad 5.3$$

R_p is the polarisation resistance. The value for B is normally taken to be 26mV for a corroding system and 52mV for a passive system [36]. The former is typically used for linear polarisation resistance measurements of corrosion rates. However, these values have been measured in aqueous systems and may not be accurate for reinforcement embedded in concrete. The Tafel values measured in this study can be used in further work to replace the value of 26 mV for the various cementitious materials. From the results presented in Table 5.2 it can be seen that for the

corroding systems of the cementitious materials used in this study, the values of constant B are considerably higher than 26mV and provide an average value of 45.24 mV. This would indicate that a B value higher than 26mV should be used to calculate i_{corr} from polarisation resistance measurements (equation 5.3) taken from these specimens. The percentage error from using a B value of 52 or 26 is large (approximately 50%). However, as R_p is normally of the order of 1×10^3 ohms the i_{corr} values calculated will always be of the same order of magnitude [50, 58, 63, 137, 138, 149, 156 – 162].

The use of Tafel extrapolation to measure corrosion rates has also been explored and Table 5.3 shows a comparison of rates achieved using Tafel extrapolation and from the Stearn Geary Equation (equation 5.3). Figure 5.10 shows a schematic diagram of a polarisation curve showing the extrapolation to obtain an I_{corr} value from the intercepts between the anodic curve and the cathodic curve.

Table 5.3 Comparison of I_{corr} values from intercepts and from the Stearn Geary Equation.

Material	B constant (mV)	R_p (ohms/cm ²)	Icorr Stearn Geary (B =26mV) (mA/cm ²)	Icorr Stearn Geary (B Calc) (mA/cm ²)	Icorr Intercepts (mA/cm ²)
0.4w/c	47.66	11136	0.0023	0.0045	0.0063
0.8w/c	41.82	2732.5	0.0009	0.0149	0.026
A	44.75	5935.3	0.0048	0.0078	0.0099
B	51.23	15347	0.0017	0.0029	0.0026
C	37.04	3600.6	0.0072	0.0115	0.019

The corrosion rates measured from the intercepts are within a factor of 3 of Stearn Geary calculation using a B value of 26 mV and within a factor of 2 when using the B values calculated by this study. The Tafel extrapolation is dependent on being able to find a linear Tafel region, this is difficult for cells that do not involve pure electrolytes. This results in an error in the Tafel constants calculated and an estimated constant B, such as 26mV can be of similar accuracy to the use of Tafel constants.

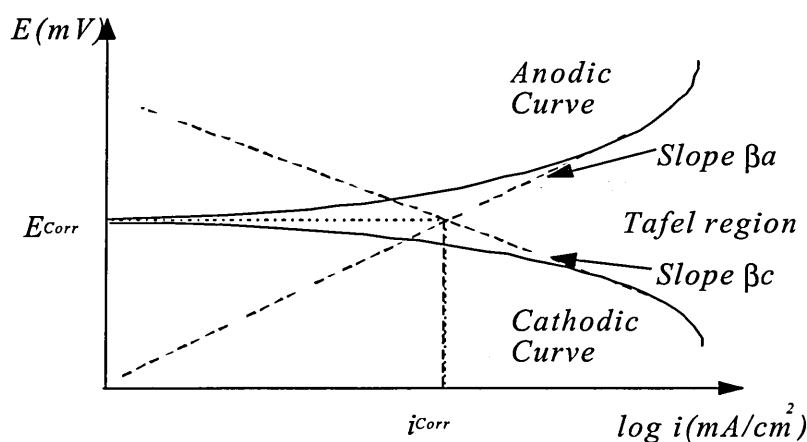


Figure 5.10 Polarisation curves showing Tafel extrapolation

It was also seen that β_a increased with decreasing permeability. This suggests that materials of lower permeability tended towards passivity compared to higher permeability materials. This contradicts the results in figure 5.7 where E_{CORR} decreases with decreasing permeability, suggesting that oxygen concentration is low in low permeability materials. This would mean higher passivation currents and less stable passive films in low permeability materials. This contradiction is probably the result of a trade off between the easier access of chlorides to the electrolyte in the high permeability materials and the low oxygen supply in the low permeability materials. The electrolyte used in the study was a 3.5% NaCl solution. Chlorides in the form of NaCl were also

added to the two (0.4 w/c and 0.8 w/c) substrate materials during mixing. However, there was no apparent trend between chloride concentration calculated from the chloride diffusion measurements (Chapter 4.4) and the β_a constant measured for the material.

The low permeability materials have lower oxygen contents and correspondingly lower E_{CORR} values. This, however, means that a higher passivation current is required to maintain the passive film, which results in a less stable passive film. By comparison, the high permeability materials allow easier access to chlorides, which in turn results in a less stable passive film and lower anodic Tafel constants. This suggests that both low and high permeability materials would have a tendency to initiate corrosion, but for different reasons. It would still suggest that corrosion would occur at a lower rate in a low permeability material since oxygen diffusion appears to be the rate-determining factor. The lower oxygen diffusion rates into the low permeability materials would mean lower corrosion rates.

5.1.6 Conclusions

All the materials produced similar polarisation curves indicating that the steel was in a similar chemical environment in all the materials. The reverse sweep of the polarisation curve did not show the presence of a passive region.

The E_{CORR} values measured from the polarisation curves are related to the coefficient permeability and follow the form predicted by the Nernst equation. This suggested that the lower permeability materials had lower oxygen levels, resulting in the lower potentials.

There was also a relationship between the log of the permeability coefficient, the anodic Tafel constant. This showed that the higher the permeability coefficient the lower the anodic Tafel constant, suggesting that the materials with higher permeability coefficients were more active. The experimental values of the Tafel constants were found to be greater than the assumed values used in the Stearn Geary Equation of 120 mV.

No corresponding relationship was found with the cathodic Tafel constant, which was similar for all the materials examined in this study.

5.2 CORROSION TESTING (NON-DESTRUCTIVE)

5.2.1 Introduction

Most laboratory studies on macro-cell corrosion in concrete have concentrated on the formation of macro-corrosion cells by either differential aeration from varying oxygen concentrations or by differential concentration cells due to differing chloride concentration [176, 180, 184, 194, 197]. Corrosion in these cells is usually measured by monitoring galvanic currents flowing through the cell [19, 169, 180]. In this study the aim has been to study the effect of mismatch in properties between a repair material and the substrate concrete on corrosion reinitiation and propagation in the repair. The test specimens used were designed to simulate the effect of using different repair and substrate material combinations in repair patches. The specimens were capable of exhibiting differential chloride concentration cells due to the addition of chlorides to the substrate mix and differential aeration from the mismatch in permeability between repair and substrate. Linear polarisation resistance, impedance spectroscopy, rest potentials and resistivity measurements have been used to monitor the change in corrosion rate with time.

5.2.2 Materials

The materials used for this part of the study have been described in section 3.4. Three commercially available repair materials A, B and C were selected, to provide a wide range of properties and to reflect the typical variety of repair materials currently available in the market. Two concrete substrate mixes were used (0.4w/c and 0.8 w/c), to which a repair material was applied. Both the substrate concrete mixes contained 3.5% NaCl (by weight of cement) in order to depassivate the steel reinforcement. No NaCl was introduced in the repair material. High yield 460 grade steel reinforcement

bar, 8mm in diameter, was embedded in the test specimens. The physical properties of the repair materials and substrate concrete mixes were determined (see Chapter 4) and have been summarised in table 5.4.

Table 5.4. Properties of materials.

Material	Density (Kg/m³)	Porosity (%)	Permeability (m/s)	Resistivity (Kohms/cm²)	Chloride Diffusion Coef. Dc (cm²/s)
Concrete w/c 0.4	2350	10	1.46x10 ⁻¹²	4.1	1.982E-06
Concrete w/c 0.8	2110	19	7.76 x10 ⁻¹¹	2.3	1.340E-05
A	1980	22	3.59x10 ⁻¹³	1.7	2.139E-07
B	1050	23	7.48x10 ⁻¹¹	2.1	6.294E-07
C	1250	34	1.53x10 ⁻¹⁰	0.8	1.827E-05

5.2.3 DETAILS OF TEST SPECIMEN

Figure 5.11 shows the test specimen and the experimental arrangement used for linear polarisation resistance, impedance spectroscopy, rest potentials and resistivity measurements. The cylindrical test specimens had a diameter of 100mm and a height of 200mm. Half the cylinder was made up of a repair material and the other half by one of the substrate concrete mixes. Three reinforcement bars of 8mm diameter were embedded longitudinally into the cylinder. Each bar was masked off with a silicone rubber based sealant leaving an 8cm² exposed surface area (see inset, Figure 5.1). The first bar was positioned such that the exposed area was located at mid-height within the repair material. The exposed area in the second bar was at the interface of the substrate and repair material and the exposed area of the third bar was located at mid-height of the substrate concrete. A steel wire was connected to each reinforcement bar and sealed

with an epoxy-based sealant. The wires were joined together at a junction box (see Figure 5.11), in order to provide electrical continuity between reinforcement bars. This meant that the corrosion cells could develop in the specimens as though the repair, interface and substrate were common to a single reinforcement bar, while allowing a part of the reinforcement of known surface area (8cm^2) to be used for the corrosion monitoring in each zone (substrate, interface and repair).

Standard cast iron cylindrical moulds were used for the manufacture of the 100mm x 200mm specimens. The bars were accurately positioned in the cylinders by means of plastic spacers so that each bar had a concrete cover of 40mm from the cylinder surface (circumference). The substrate concrete materials were mixed in a forced action pan type mixer. The NaCl was dissolved in the mix water and then added during mixing. The substrate concrete was cast into the lower half of the moulds containing the prepared reinforcement bars. The concrete was added until it reached the middle of the exposed area of reinforcement located at the interface. The half-cast moulds were left in a mist curing room overnight. The repair material was then mixed and cast into the unfilled half of the mould in accordance with the manufacturer instructions and left in a mist curing room overnight. The specimens were demoulded 24 hours after casting and then cured in a water tank for 28 days at 20°C .

Following the initial 28 days curing, the specimens were transferred to a second water tank containing 3.5% NaCl solution, where they were stored for the remainder of the study. The 3.5% chloride-contaminated water was kept at a constant temperature of 30°C in order to accelerate the rate of the corrosion reaction. Air was bubbled in to continuously aerate the water and keep the dissolved oxygen levels constant throughout the storage period.

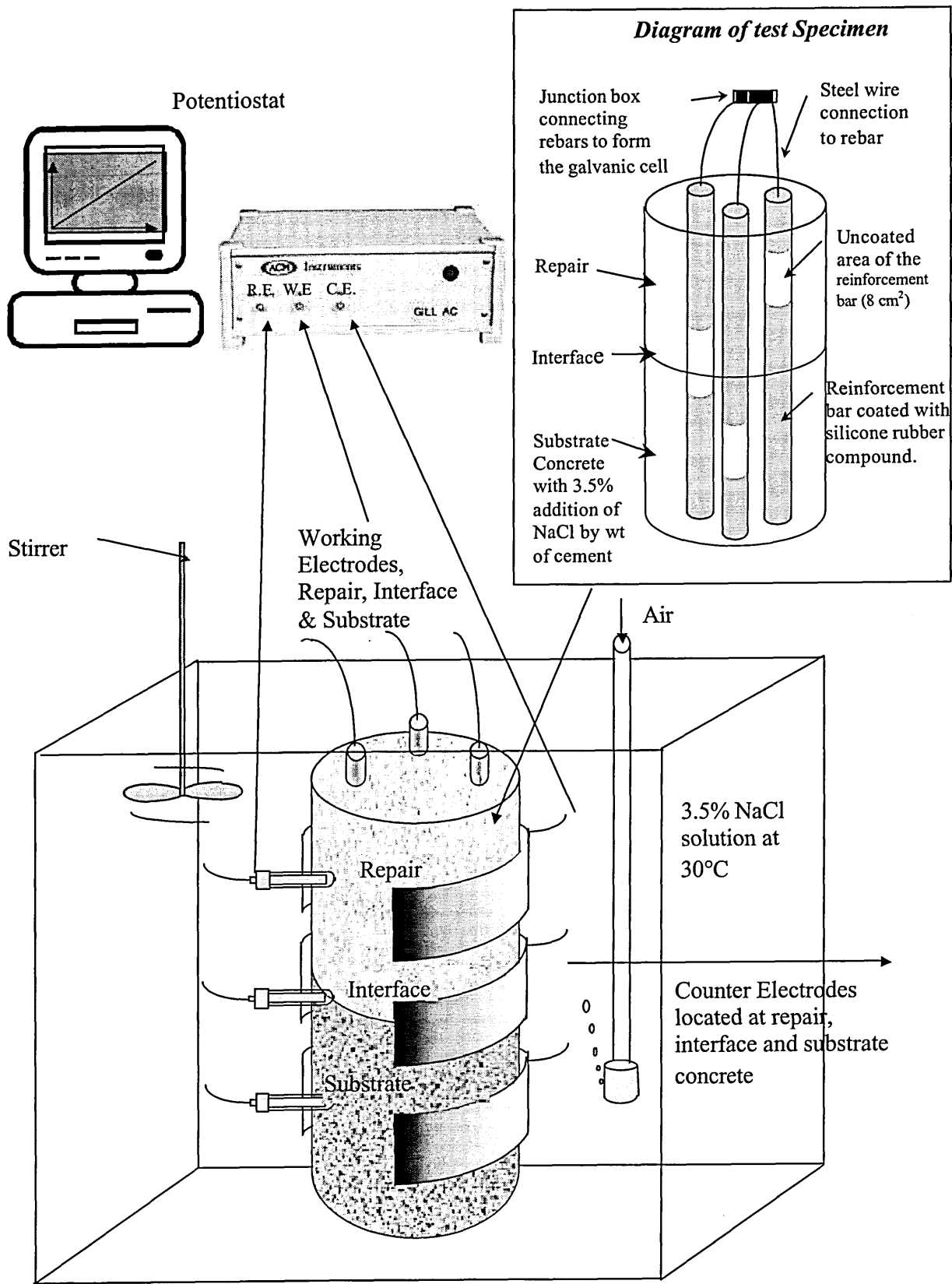


Figure 5.11 Experimental Arrangement

5.2.4 Test Specimen, Repair – Substrate Combinations

Test specimens made with different combinations of repair and substrate materials were produced. The wide range of differences in physical properties shown in Table 5.1 (permeability, porosity, resistivity and chloride diffusion) between the repair materials and substrate concretes allowed a number of property combinations to be investigated. The disparity in properties examined in Chapter 4 indicated that the difference in permeability coefficients and chloride diffusion coefficients between the repair and substrate materials were the most useful parameters to study. Details of the repair material and substrate concrete combinations used in the corrosion investigation are summarised in Table 5.5, together with the differences in properties (permeability and chloride concentration). Two cylindrical specimens for each of the repair/substrate combinations listed in Table 5.5 were prepared as previously described.

Table 5.5 Difference in properties of repair/substrate material combinations.

Combination		Ratio of Repair to Substrate Property at 12 months	
Substrate (w/c)	Repair	Permeability Coefficients	Chloride Concentration.
0.4	A	0.005	0.039
0.8	A	0.246	0.036
0.4	B	51.233	0.181
0.8	B	0.964	0.199
0.4	C	104.795	0.624
0.8	C	1.972	0.685

Note: A value of >1 represents a higher value for repair than substrate.

A value of 1 represents a repair and substrate match

A value of <1 represents a higher value for substrate

There was a wide range of mismatch in the permeability coefficients of the repair/substrate combinations used for the test specimens. This varied from ratio of repair/substrate permeability coefficients greater than one (repair more permeable than the substrate) to value less than one (repair less permeable than substrate). The 0.8w/c substrate combined with repair material B has an approximate match in permeability coefficients. Permeability mismatch appears to be the most meaningful property to which corrosion behaviour can be related. Four different combinations of permeability mismatch are evident in the repair/substrate combinations given in table 5.5 (material properties are given in table 5.4):

- i. Low permeability repair and substrate (combination A-0.4 substrate)
- ii. Low permeability repair and high permeability substrate (combination A-0.8 substrate)
- iii. High permeability repair and low permeability substrate (combinations B-0.4 substrate and C-0.4 substrate)
- iv. High permeability repair and substrate (combinations B-0.8 substrate and C-0.8 substrate).

As chloride is added to the substrate concrete at the time of mixing, the repair always has a lower chloride concentration than the substrate (see Table 5.5). However, there is a wide range of chloride concentrations in the repair materials at the end of the 12 month exposure period and these represent three basic situations for chloride concentration.

- Repair material A: The chloride level at the steel surface (0.025M max) remains below the chloride threshold value (0.05M) for the full period of the study.
- Repair material B: The chloride level at the steel exceeds the threshold level (0.05M) to initiate corrosion after approximately six months, but remains below

the chloride level in the substrate concrete (0.18M) for the full period of the study (12 months).

- Repair material C: The chloride level at the steel surface exceeds the threshold level to initiate corrosion (0.05M) after approximately one month and approaches that of the substrate materials after six months (0.15M).

Table 5.6 shows the property mismatch between the different repair substrate combinations, grouping them as either a poor, fair or good match. The order of the match for the 6 combinations is given in brackets. From Table 5.6 the combinations of repair and substrate provide a wide range of property relations, which can influence the corrosion measured in the test specimens. Material B combined with the 0.8 w/c substrate has a good match in permeability, but a poor match in chloride concentration. Material C when combined with the 0.8 w/c substrate has a poor match in permeability, but a relatively good match in chloride concentration. Therefore, specimen B/0.8 should produce a stronger chloride corrosion macro-cell than C/0.8, which will have a stronger differential aeration cell.

Table 5.6 Property mismatch of substrate/repair material combinations.

Substrate	Repair	Permeability match	Chloride Concentration match (at 12 months)
0.8	A	P(6)	P(6)
0.4	A	P(3)	P(5)
0.8	B	G(1)	P(4)
0.8	C	F(2)	F(3)
0.4	B	P(4)	F(2)
0.4	C	P(5)	G(1)

Match in Property: P = poor, F= fair and G=good

5.2.5 CORROSION TESTS

The aim of corrosion testing was to measure the effect of the different types of repair materials/substrate combinations on the incipient corrosion within a repair patch. A number of tests were conducted on the test specimens. All the tests were non-destructive so that measurements were made on the same specimens over a period of 12 months. Measurements were taken every two months with the first datum readings taken at 28 days after casting the specimens. The specimens were kept in 3.5% chloride solution in a tank as detailed in Section 5.2.3 and were removed temporarily to take the corrosion readings. For each specimen, the corrosion measurements were made in the repair material, substrate concrete and at the interface between the repair and the substrate. The following non-destructive tests were conducted on the test specimens:

- LPR-Linear Polarisation Resistance to measure corrosion rates.
- Impedance spectroscopy to measure corrosion rates.
- Measurements of the electrochemical potential.
- Resistivity measurements.

5.3 LINEAR POLARISATION RESISTANCE MEASUREMENTS

5.3.1 Introduction

Linear polarisation resistance (LPR) is a widely used technique for monitoring corrosion rate in many process plant applications. This has resulted in a large amount of published data on the use of the technique. There are a number of features of the LPR technique that make it attractive for the monitoring of corrosion rates;

- The non-destructive nature of the test.
- The ability to measure a quantifiable corrosion rate.
- Speed of making corrosion rate measurements.
- Very high resolution of corrosion rate measurements using Faraday's law.

These same features have made the LPR technique popular in studying the corrosion of reinforced concrete. A large amount of published data exists on the use of LPR in reinforced concrete [30, 31, 33, 156, 162, 164]. The technique has become important because of the difficulties in carrying out weight loss measurements of steel in concrete due to the low corrosion rates normally found.

There are a number of problems inherent in using the LPR method. The measurements are based on the use of the Stern-Geary approximation to calculate corrosion rates [166]. The main problem is that the corrosion rate measurement is only approximate and can vary by as much as a factor of three [33, 134, 164 - 166]. The LPR technique is now being used commercially in reinforced concrete structures [33, 95, 158, 165, 168]. The ease in use of the technique has meant that the advantages greatly outweigh the disadvantages.

5.3.2 Test Method

The set up for making the linear polarisation measurements is shown in Figure 5.1 of Section 5.1.3 on corrosion testing. Similarly, the test materials and test specimens are as described in Sections 5.1.2 on corrosion testing.

Linear polarisation resistance (LPR) measurements were taken on each of the three reinforcing bars (see Figure 5.1) of each specimen at two monthly intervals. These LPR measurements gave corrosion rates in the repair, substrate and at the interface respectively. The first datum readings were taken at 28 days age when the specimens were transferred from the initial curing conditions (in water) into the chloride contaminated water tank. An ACM instruments AutoLPR potentiostat was used to take the measurements over a range of +/- 10 mV about the rest potential at a 3mV/min sweep rate. All measurements were carried out with respect to a saturated calomel electrode. The potentiostat measures the potential of the steel, then imposes a potential of 10mV lower and measures the current flowing between the counter electrode and the steel. This is repeated through the measurement range producing a series of values of potential and current. The slope of the graph of the overpotential (η) against current density (i) is the polarisation resistance (R_p).

$$R_p = \frac{\eta}{i} \quad 5.4$$

However, the potential is affected by the resistance of the concrete and part of it is lost because of this IR drop. This effectively means that the measured R_p is higher than the actual R_p and needs to be corrected for IR drop.

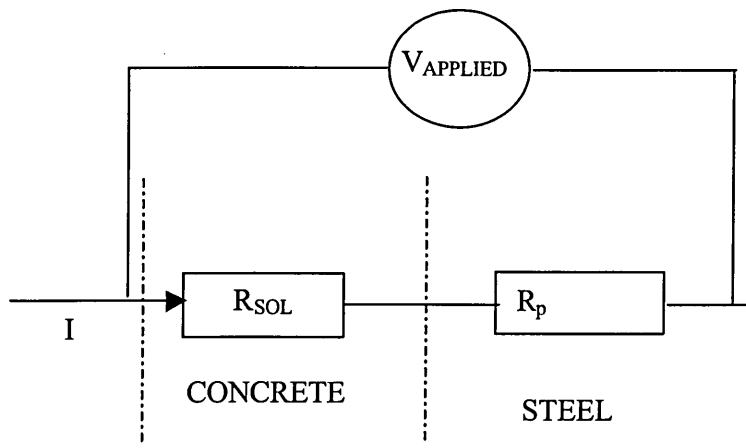


Figure 5.12 Schematic diagram representing the IR drop.

Figure 5.12 shows a schematic diagram of the situation. R_{SOL} , the solution resistance, is in series with the actual R_p . Therefore, using Kirchof's law the resistances can be added to give the total resistance, which is the measured polarisation resistance (R_m) from the experiment.

$$R_m = R_p + R_{SOL}$$

$$\therefore R_p = R_m - R_{SOL} \quad 5.5$$

The IR drop through the concrete was compensated for by subtracting the solution resistance from the measured polarisation resistance. The solution resistance was obtained from the impedance measurements detailed in Chapter 5.4 using the same measurement circuit as described here. An R_{SOL} value was available for each measured polarisation resistance value and was subtracted from it to give the actual polarisation resistance. Figure 5.13 shows the effect of IR compensation on the corrosion currents calculated from the polarisation resistance. The trends in the results remain the same with or without IR compensation. However, the magnitude of the actual calculated currents increased with IR correction.

The corrosion currents were then calculated using the constant B determined for each material from the polarisation curves measured in the Chapter 5.2. The B constants were calculated using the average cathodic Tafel constant measured ($\beta_c=145.03$), as no trends were detected in the cathodic Tafel constants in Chapter 5.1. The anodic Tafel constant was found to vary with the permeability of the test material. To allow for this difference between the test materials the actual value determined from the polarisation curves (Chapter 5.1) was used to calculate the B value. The Tafel constants were used to calculate the constant B as follows:

$$B = \frac{\beta_a \beta_c}{2.3(\beta_a + \beta_c)} \quad 5.6$$

Table 5.7 shows the cathodic, anodic Tafel constants used and the resulting constants B for each material.

Table 5.7 Tafel constants used in LPR measurements.

Material	Anodic Tafel Constant β_a (mV)	Cathodic Tafel Constant β_c (mV)	Constant B (mV)
0.4	536.25	145.03	49.63
0.8	268.80	145.03	40.96
A	402.04	145.03	46.34
B	352.48	145.03	44.68
C	281.26	145.03	41.60

The Stern-Geary relationship was used to calculate the corrosion current i_{corr} ;

$$i_{corr} = \frac{B}{R_{LPR}} \quad 5.7$$

where i_{corr} = corrosion current density (mA/cm²)

R_{LPR} = Linear Polarisation Resistance (ohm/cm²)

The results are an average of 4 readings from two different test specimens for each material, with two measurements being made per test specimen. The average taken was a selective average of the results. i.e. any value that was not within a factor of 2 of the other readings, as expected from the Stearn Geary Equation, was discarded and the average calculated from the remaining results. Table 5.8 shows the number of readings taken to calculate the average corrosion rate at each location.

Table 5.8 Number of readings (from a maximum of 4) used to calculate the average corrosion currents for each location at each age.

Material	Location	Exposure period at time the readings taken (months)						
		0	2	4	6	8	10	12
A04	Repair	4	4	3	3	4	3	3
	Interface	4	3	3	3	4	3	3
	Substrate	3	3	3	2	3	3	3
A08	Repair	2	4	4	4	4	4	4
	Interface	3	3	2	4	4	3	3
	Substrate	3	3	4	4	4	4	3
B04	Repair	3	4	4	4	3	3	4
	Interface	3	3	4	4	3	4	3
	Substrate	3	3	3	4	4	3	3
B08	Repair	2	3	4	3	3	4	3
	Interface	3	3	4	4	4	4	4
	Substrate	2	3	4	3	3	4	3
C04	Repair	3	3	4	3	3	3	3
	Interface	2	2	3	3	3	2	2
	Substrate	3	4	2	4	4	3	3
C08	Repair	2	2	3	4	3	3	2
	Interface	3	2	3	3	4	2	2
	Substrate	2	3	3	3	3	2	3

Figure 5.13 Effect of IR compensation on corrosion current: 0.4w/c Substrate with Repair Material A

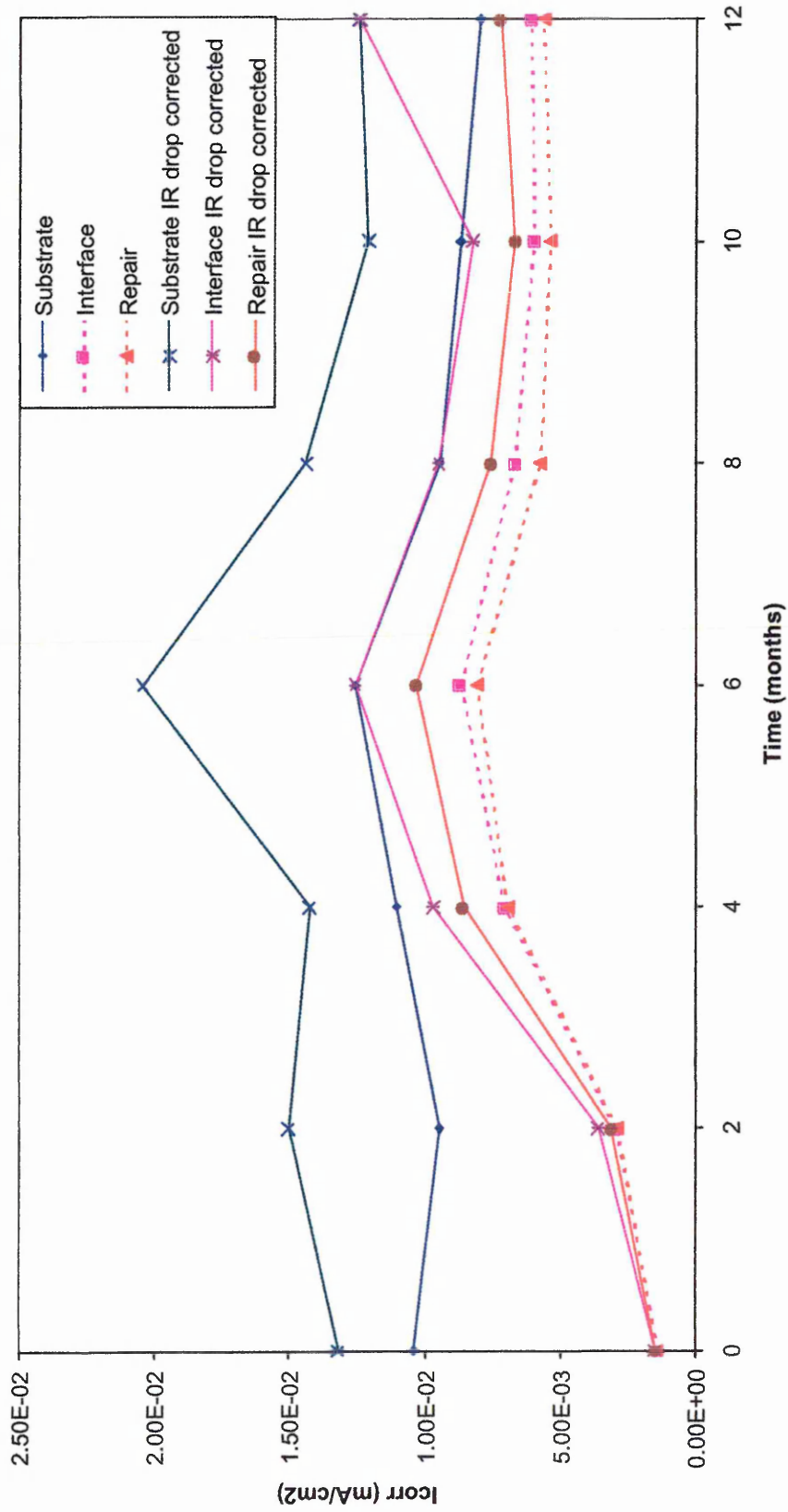


Figure 5.14 Corrosion current with time relationships of 0.8 w/c Substrate with Repair Material A

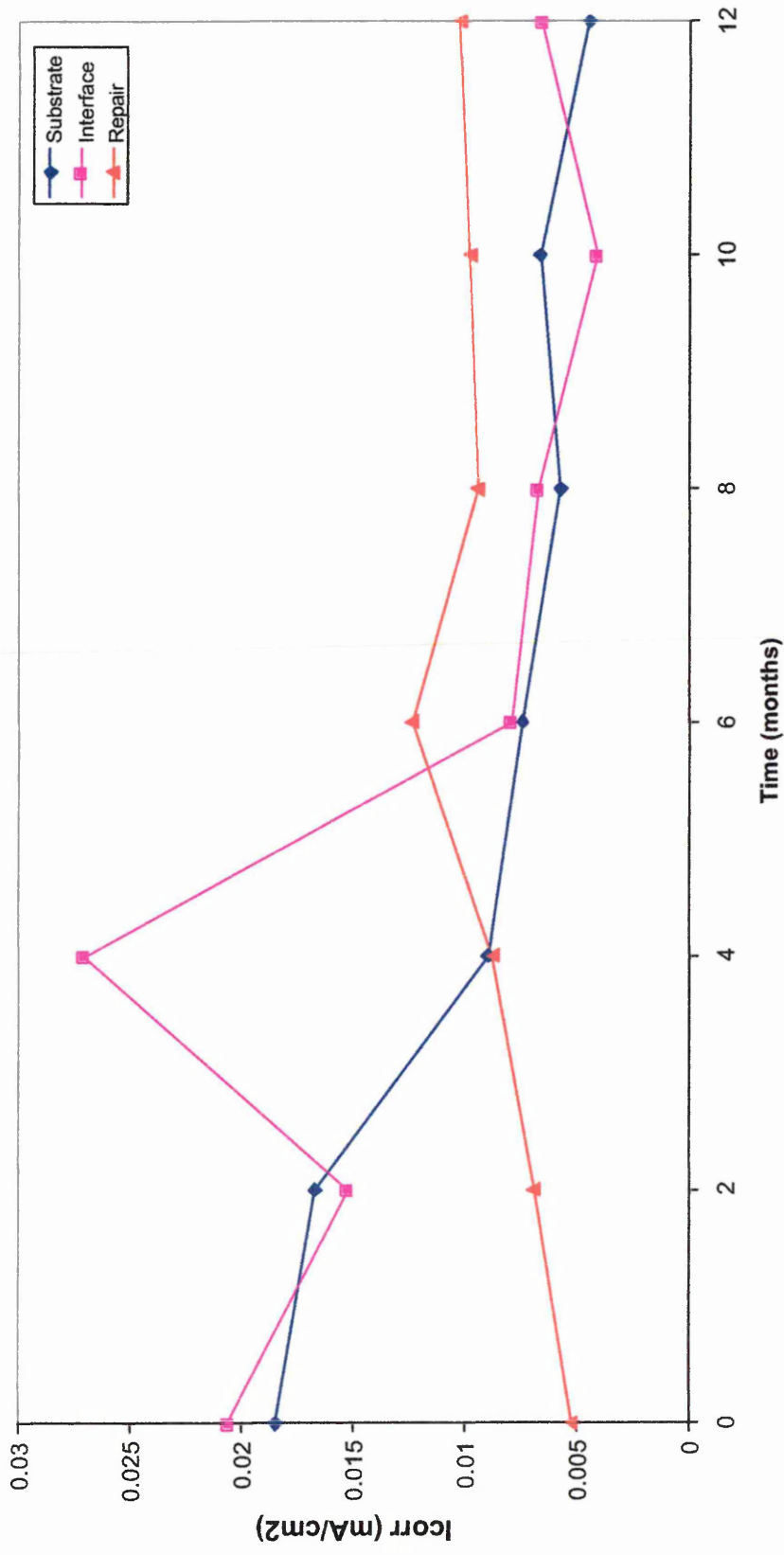


Figure 5.15 Corrosion current with time relationships of 0.4w/c Substrate with Repair Material B

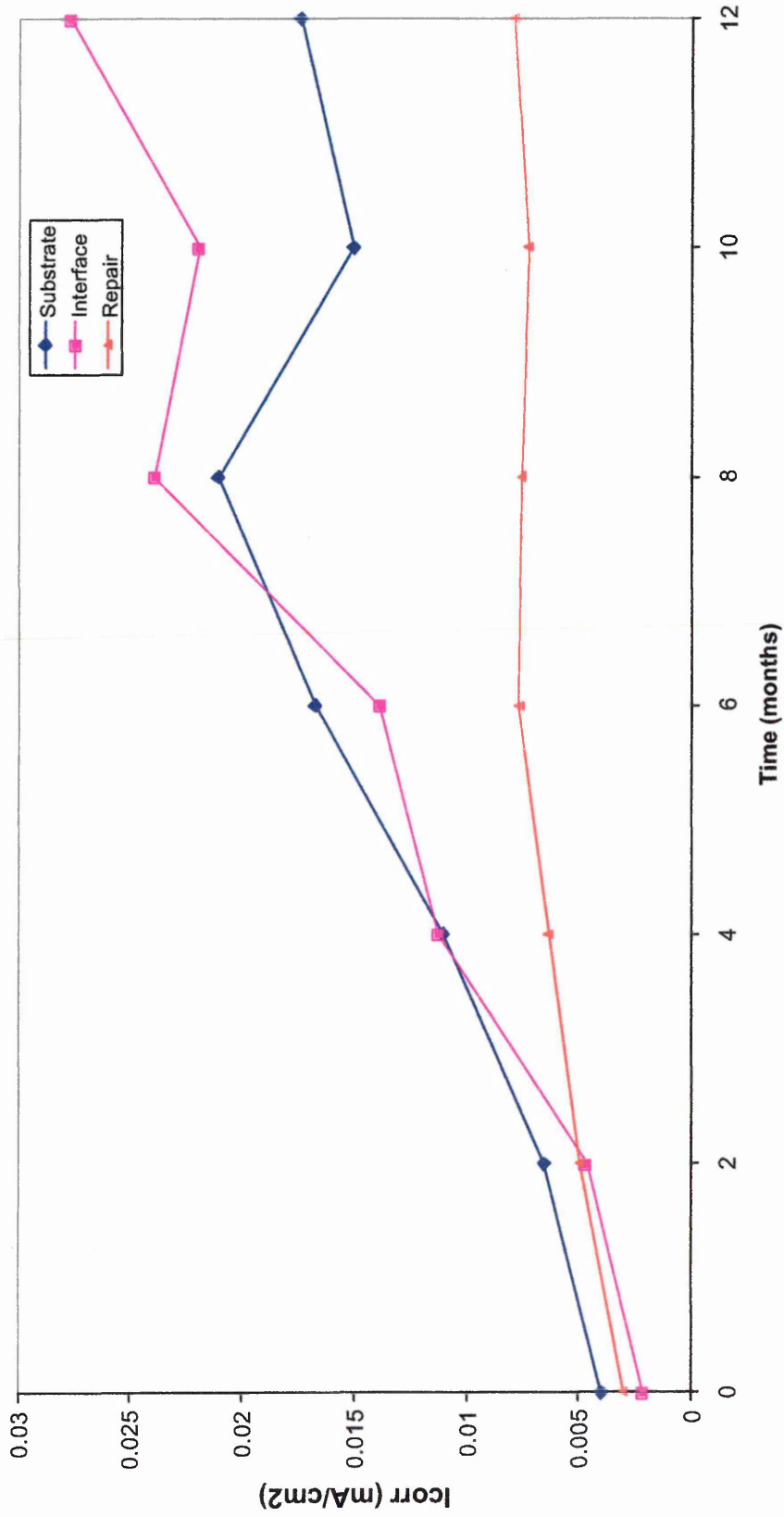


Figure 5.16 Corrosion current with time relationships of 0.4w/c Substrate with Repair Material C

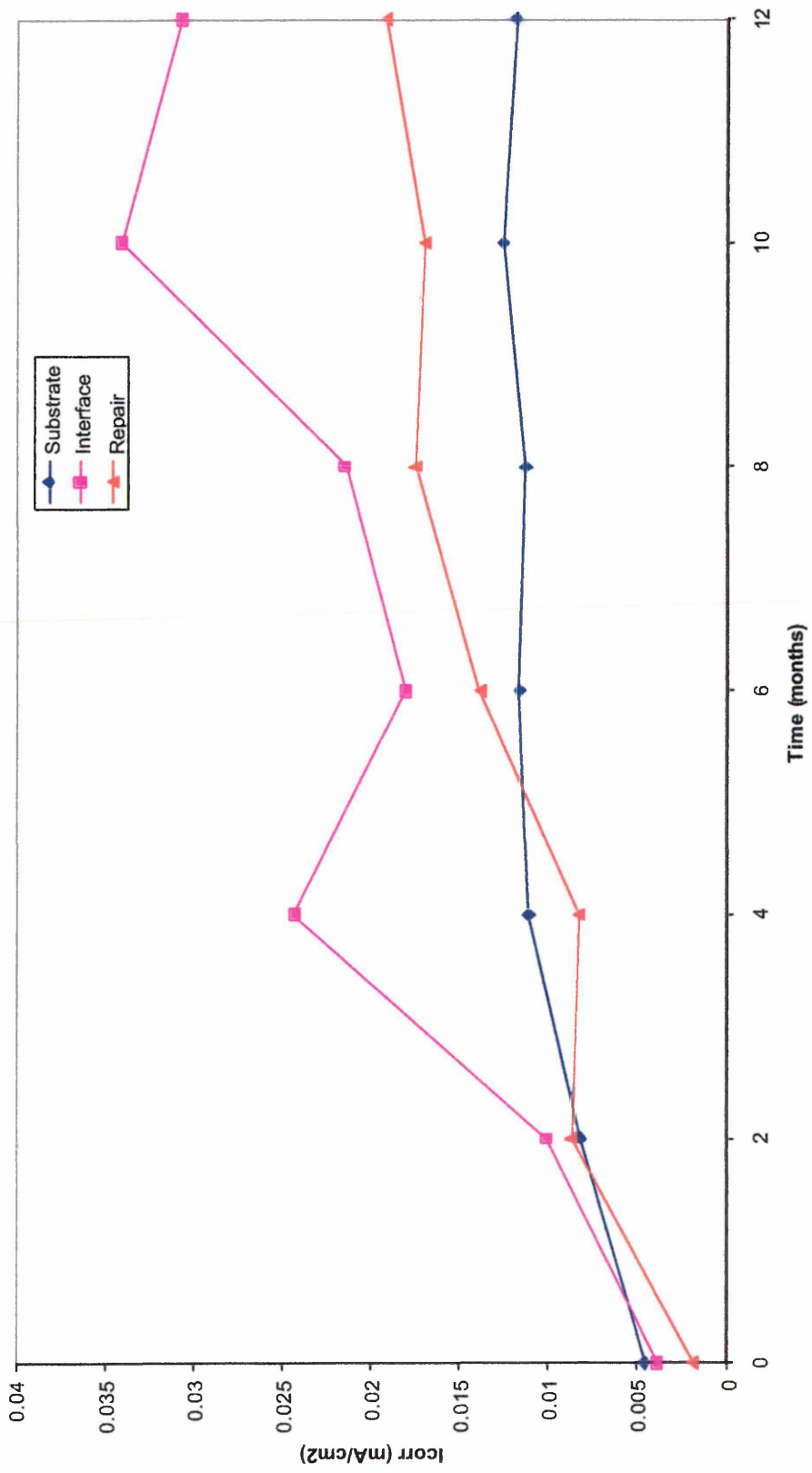


Figure 5.17 Corrosion current with time relationships of 0.8w/c Substrate with Repair Material B

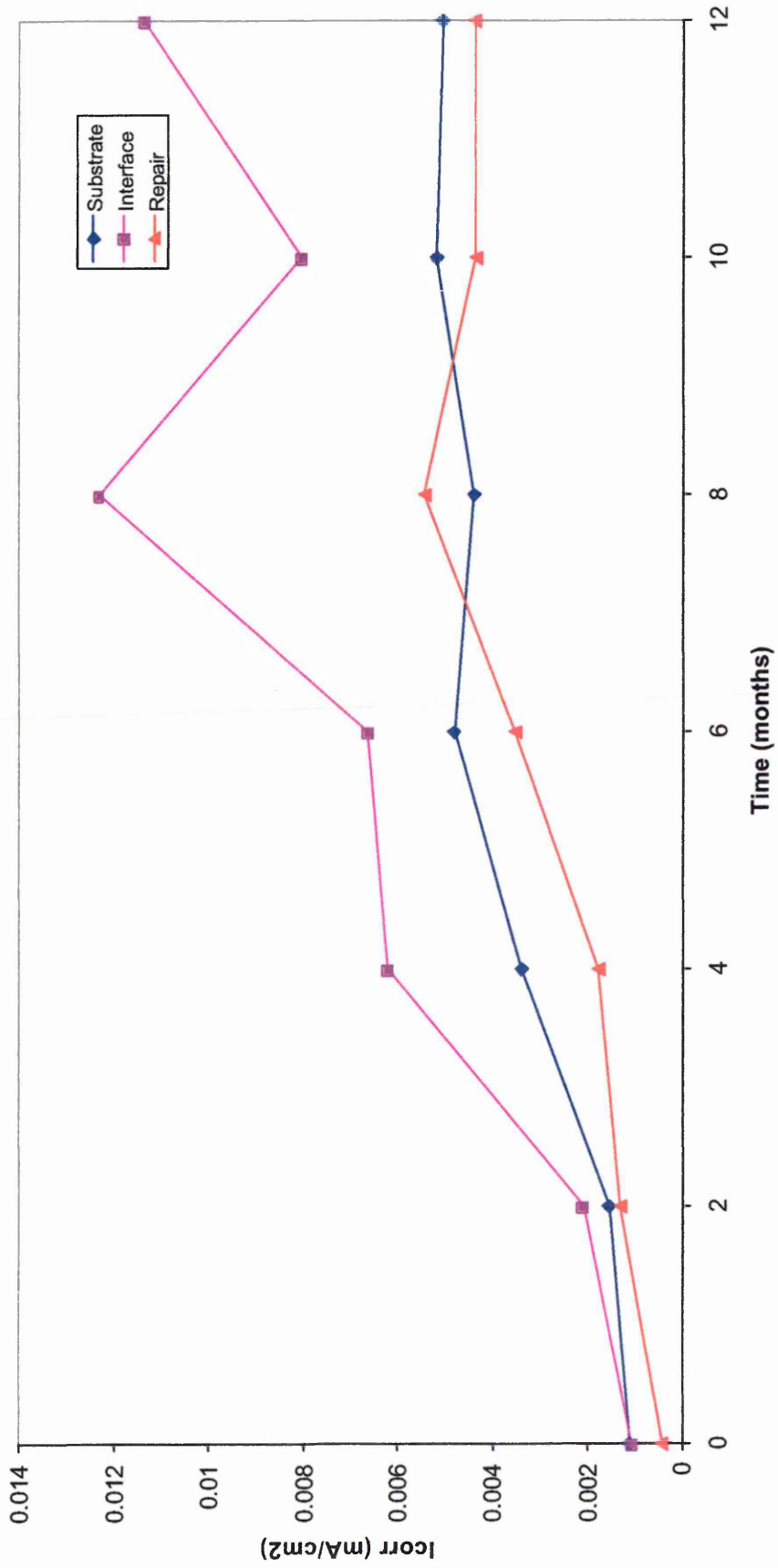
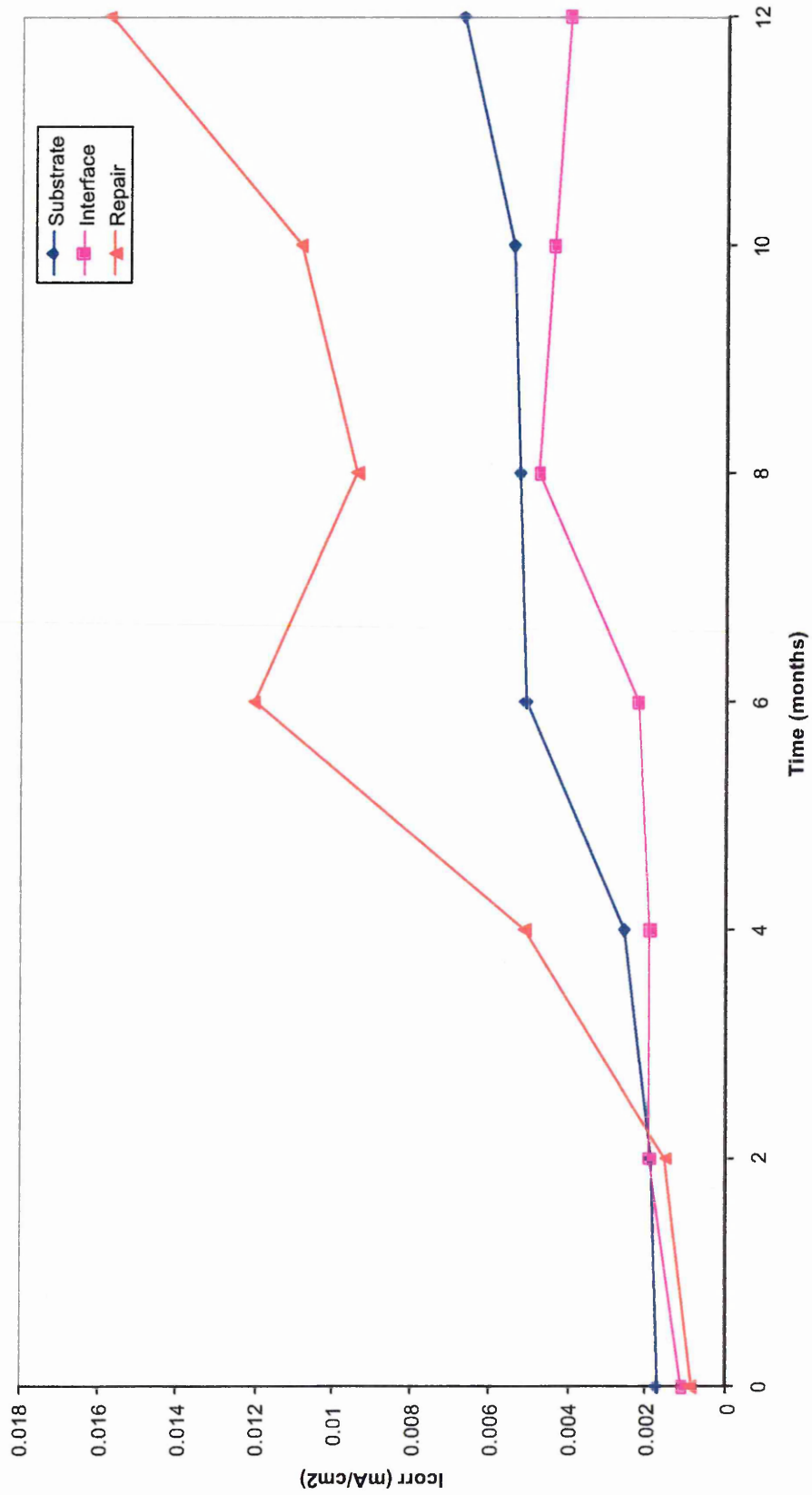


Figure 5.18 Corrosion current with time relationships of 0.8w/c Substrate with Repair Material C



5.3.3 Analysis of Results

The polarisation resistance measurements allowed the calculation of corrosion currents for each test specimen. The polarisation resistance measurements were compensated for IR drop by subtracting the solution resistance. The data was averaged to observe trends in corrosion current with time within each repair material and substrate combination examined. In parallel with this work, Impedance Spectroscopy (Section 5.4) was also used to determine the corrosion currents. The corrosion currents obtained using the two techniques are compared and analysed further in Section 5.7 – Comparison of Corrosion Currents.

The permeability coefficients listed in Table 5.1 of Chapter 5.1 show that four different combinations of permeability mismatch between repair and substrate exist in the test specimens produced for the study:

- Both repair and substrate of low permeability produced by the combination of repair material A with the 0.4w/c substrate.
- Low permeability repair and high permeability substrate produced by the combination of repair material A with the 0.8w/c substrate.
- High permeability repair and low permeability substrate produced by the combinations of repair materials B or C with the 0.4w/c substrate.
- Both repair and substrate of high permeability produced by the combinations of repair materials B or C with the 0.8w/c substrate.

5.3.3.1 Case 1 Both Repair and Substrate of Low Permeability

In the low permeability repair and substrate combination, material A has a permeability of 3.59×10^{-13} m/s and the 0.4 w/c substrate a permeability of 1.46×10^{-12} m/s. These are the two lowest permeability materials used in this study. The substrate had chloride added at the mixing stage, whereas the chloride level in repair material A never exceeded the threshold level of 0.05M for corrosion during the twelve month exposure (Section 4.4, Figure 4.8).

Figure 5.13 shows at time zero the corrosion rate in the substrate steel is relatively high at 0.0125 mA/cm² and the value remains fairly constant with time. The corrosion rate of the steel in the repair material is low at early exposure periods, but increases steadily attaining a value approximately half that of the steel in the substrate after 6 months. The higher corrosion rate of the steel embedded in the substrate is probably attributable to the high Cl⁻ concentration in the substrate. However, the steady increase in the corrosion rate of the steel in the repair is surprising as the repair material is highly impermeable and has insignificant chloride contamination. The rate of oxygen diffusion would be expected to be low in both materials, although it will be relatively higher in the substrate material due to its greater permeability. This would be expected to limit the value of the corrosion currents and probably explains the peak after twelve months.

5.3.3.2 Case 2 Low Permeability Repair and High Permeability Substrate

When repair material A is combined with the 0.8 w/c substrate with a permeability 7.76×10^{-11} m/s, this combination produces a specimen where the repair material is of low permeability and the substrate of high permeability. In terms of mismatch the difference in permeability is 99%, porosity is -7.3% and resistivity 15% (Table 2). In comparison with

the materials used in Case 1 (repair material A and 0.4 w/c substrate) the difference in permeability is much greater in Case 2 as the permeability of the 0.8 w/c substrate is much higher than the 0.4 w/c substrate. The 0.8w/c substrate was contaminated with chloride at mixing and the chloride level in repair material A never exceeded the proposed threshold level for corrosion (0.05M) during the twelve month exposure (Section 4.4, Figure 4.8).

Figure 5.14 shows the relationship between I_{corr} and time of exposure in the salt solution. The initial corrosion rates show a large difference between repair and substrate. The substrate steel has an initial corrosion rate of 0.02 mA/cm^2 , which falls with time to a value of about 0.005 mA/cm^2 after 4 months. The steel in the repair material, at time zero has a corrosion current of about 0.005 mA/cm^2 indicating that it was actively corroding. This was confirmed by examining the corrosion potentials (Section 5.6). The corrosion current in the repair gradually increases with time and attains a value of 0.01 mA/cm^2 at 4 months. This rate is maintained by both repair and substrate steel after 4 months. The steel at the repair/substrate interface shows a rate of corrosion similar to the substrate, in the first 2 months of exposure. Hence repair material A has developed a significant corrosion current over the 12 months exposure period in spite of its low permeability and insignificant chloride concentration. The corrosion current of the substrate is lower for the 0.8w/c substrate compared to the 0.4 w/c substrate in Case 1, when combined with repair material A. In addition repair material A has a higher corrosion current when combined with the 0.8w/c substrate than in Case 1 when combined with the 0.4w/c substrate.

5.3.3.3 Case 3 and 4 High Permeability Repair and Low Permeability Substrate

Two different repair and substrate combinations represent the Case of a high permeability repair with a low permeability substrate. These are repair materials B and C combined with

the 0.4 w/c substrate. Material C has a significantly higher permeability than material B (Table 5.1). The chloride concentration at the exposed steel interface in material C was greatly in excess of the critical value at 12 months exposure (Section 4.4, Figure 4.8), while the corresponding value in material B was close to the critical limit.

Figure 5.15 shows the change in corrosion current with time for material B with 0.4 w/c substrate. The steel in the substrate has a higher corrosion rate than the repair during the 12 months exposure period. The repair material steel has developed a significant corrosion rate (0.005 mA/cm²) although the chloride concentration in the repair is borderline relative to the critical value, at 12 months (Figure 4.8), and would have been much less than the critical value at earlier ages.

The situation of repair material C combined with the 0.4 w/c substrate falls in the same category as material B with the 0.4 w/c substrate, since they both represent high permeability repair applied to a low permeability substrate. A comparison of figures 5.15 and 5.16, shows that while the steel in repair material C corrodes at a higher rate than the substrate steel; this is contrary to the findings of repair material B. This may be due to the very high permeability of material C relative to material B. The chloride concentration in material C exceeds the critical value (0.05M) after approximately 7 days.

5.3.3.4 Case 5 and 6 Both Repair and Substrate of High Permeability

Two different combinations of repair and substrate materials represent the Case of a high permeability repair with high permeability substrate. Repair material B with a permeability of 7.48×10^{-11} m/s combined with the 0.8 w/c substrate with a permeability of 7.76×10^{-11} m/s gave the lowest mismatch in permeability of all the combinations investigated (1.8%,

Table 5.3). Repair material C combined with the 0.8 w/c substrate gave a larger mismatch in permeability. Both repair materials had Cl^- in excess of the critical value at 12 months exposure.

The corrosion currents in Figure 5.17 show that there is no high corrosion current at time zero in the chloride contaminated substrate as in the previous situations. The steel within the 0.8 w/c substrate and in the repair material shows very similar corrosion currents throughout the exposure period. The corrosion currents in Figure 5.17 are lower than those measured in Figures 5.14, 5.15 and 5.18 where repair material B or the 0.8w/c substrate had been used in specimens. This could be due to the very small mismatch in permeability between repair material B and the 0.8 w/c substrate. The corrosion currents measured for this repair/substrate combination were the lowest measured in the study. The corrosion currents measured at the interface were significantly higher than in the repair and substrate, this may indicate that corrosion at the interface is cathodically protecting the substrate and repair materials.

Figure 5.18 for repair material C combined with the 0.8w/c substrate, shows that the repair, substrate and interface initially have similar corrosion rates. Beyond 2 months the steel in the repair goes on to develop a much higher corrosion rate. This is similar to the behaviour of material C combined with the 0.4 w/c substrate in figure 5.16. This is probably due to the high chloride concentration in the substrate (0.52% at 12 months) and in the repair material (0.53% at 12 months), the steel is in an active state and, therefore, can support both anodic and cathodic reactions in both the repair and substrate materials. What is interesting is that the overall corrosion rates in the repair and substrate are much lower for material C combined with a more permeable substrate (0.8 w/c) in Figure 5.18 than

material C combined with a less permeable 0.4 w/c substrate (Figure 5.16). This suggests that improving the match in permeability for material C with the substrate has reduced the corrosion rates in the repair and substrate.

5.3.4 Conclusions

The linear polarisation technique provided a simple but highly sensitive method of measuring the corrosion rate of the specimens. The IR drop error was compensated for by subtracting the solution resistance from each measurement.

Minimising the permeability difference between the repair and substrate reduced the corrosion currents measured in both the repair and substrate. However, figure 5.17 shows a high corrosion rate at the interface.

5.4 IMPEDANCE SPECTROSCOPY

5.4.1 Introduction

A second technique to measure corrosion currents was used to confirm the trends indicated by the linear polarisation resistance measurements and to prevent over reliance on one single set of data. Impedance spectroscopy is a similar electrochemical test to linear polarisation resistance. The linear polarisation resistance produces a resistance value in ohms/cm², which is then converted to a corrosion current using the Stern-Geary equation and a corrosion rate using Faraday's law. This is analogous to the charge transfer resistance value produced by impedance spectroscopy, which has the same units as LPR and is converted to a corrosion current and rate by the same method.

In the impedance spectroscopy measurement, the test electrode is subjected to a small applied potential of 10-20 mV similar to LPR measurements. However, this perturbation is sinusoidal and of variable frequency. The response of the cell to this signal is then measured in terms of impedance magnitude and phase difference from the original signal. The results are then analysed using AC electric circuit theory, in terms of capacitances and resistances (impedances). These impedances, such as the solution resistance, charge transfer resistance and Warburg mass transfer impedances are representative of physical and chemical processes occurring in the cell. As the perturbation applied is small enough not to affect the equilibrium of the cell, the measurements are considered a non-destructive technique. Therefore, the technique provides mechanistic and kinetic information about a system as opposed to the kinetic only measurements of LPR and without the requirement for new specimens for each measurement as is the case for potentiodynamic polarisation curves.

5.4.2 Impedance spectroscopy test method

The materials and test specimens used are as described in section 5.1 “Introduction to Corrosion Testing”. The experimental set up for the impedance spectroscopy measurements is shown in Figure 5.1 and is identical to the test set up used for the linear polarisation measurements. Measurements were taken on each reinforcing bar of each specimen at two monthly intervals. The first datum readings were taken at 28 days when the specimens were transferred from the initial curing (in water) tank into the chloride contaminated water tank. An ACM instruments Auto AC potentiostat was used to take the measurements. The perturbation potential difference applied was +/- 20 mV about the rest potential. The measurements were conducted over a range of frequencies between 30 kHz to 0.001Hz. During the application of the signal, the impedance of the circuit and the phase difference between the applied signal and the response were recorded. All measurements were carried out with respect to a saturated calomel electrode. Measurements were taken on each reinforcement bar to represent the corrosion rates in the repair material, substrate and at the interface respectively.

The measurements were used to produce graphs of impedance against frequency and phase difference against frequency (see Figures 5.19 and 5.20). The two diagrams were then combined into a Nyquist plot of the real and imaginary components (Figure 5.21). The analysis of the resulting Nyquist plot is a fundamental part of the interpretation of the experimental data. Two methods based on the use of equivalent circuits are proposed here. The aim of the analysis is to obtain a value for the charge transfer resistance (R_{CT}), which can then be converted to a corrosion rate. The solution resistance (R_{SOL}) was also obtained to compare to the resistivity measurements in Section 5.5 and was also used to provide IR drop correction to the LPR measurements.

Figure 5.19 Impedance against frequency plot for substrate 0.4 w/c

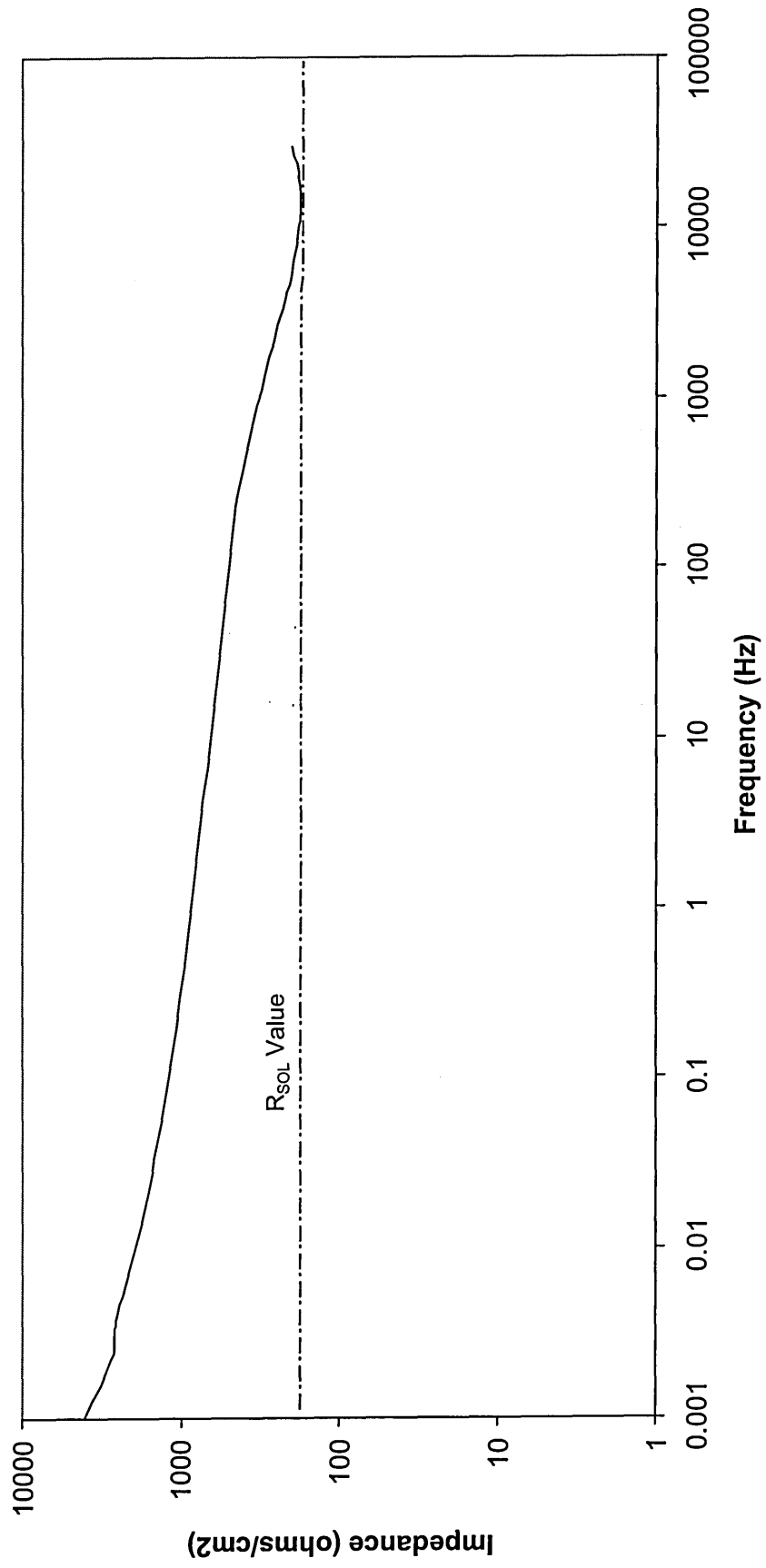


Figure 5.20 Frequency against phase angle theta for 0.4w/c substrate

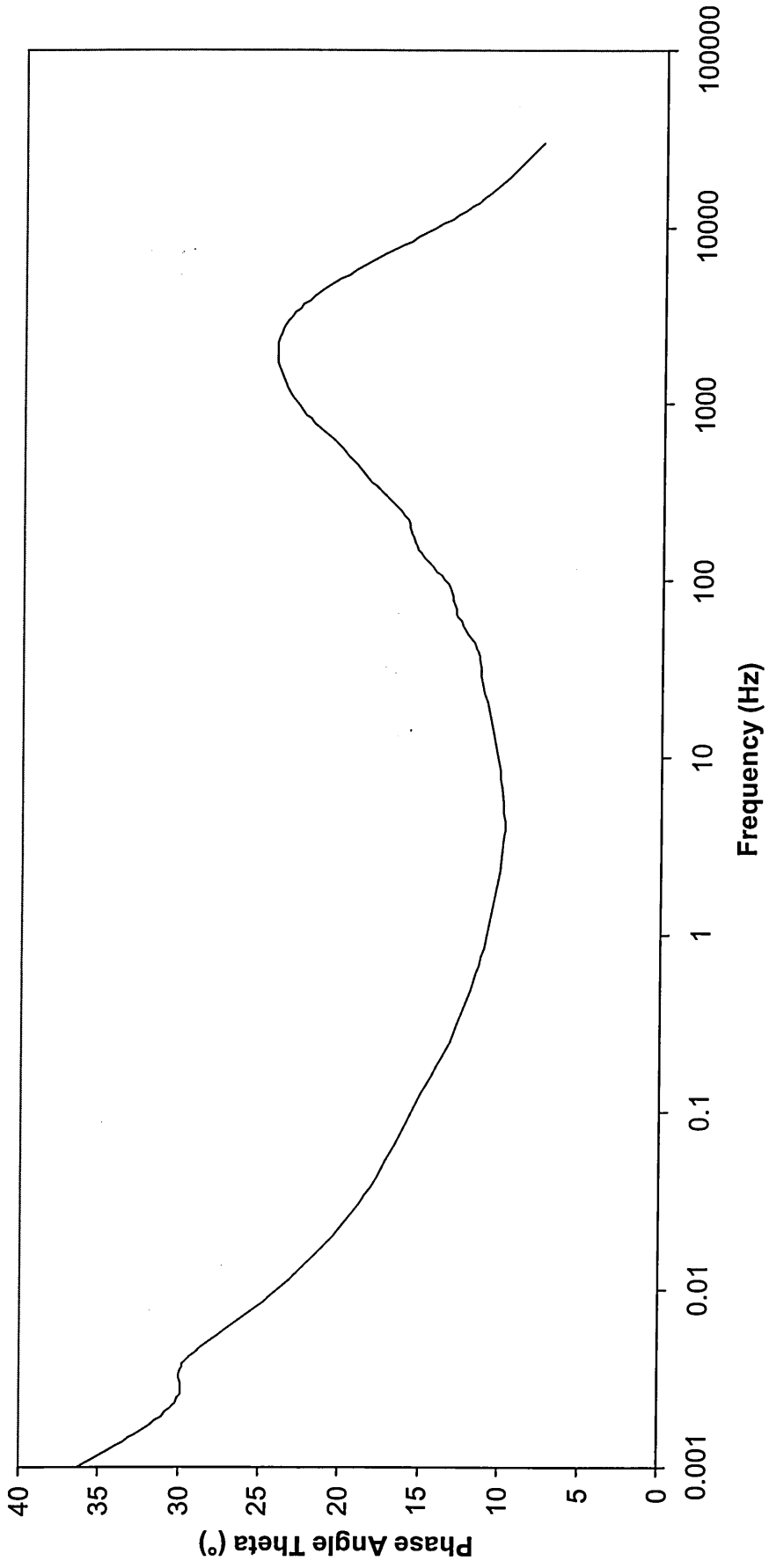
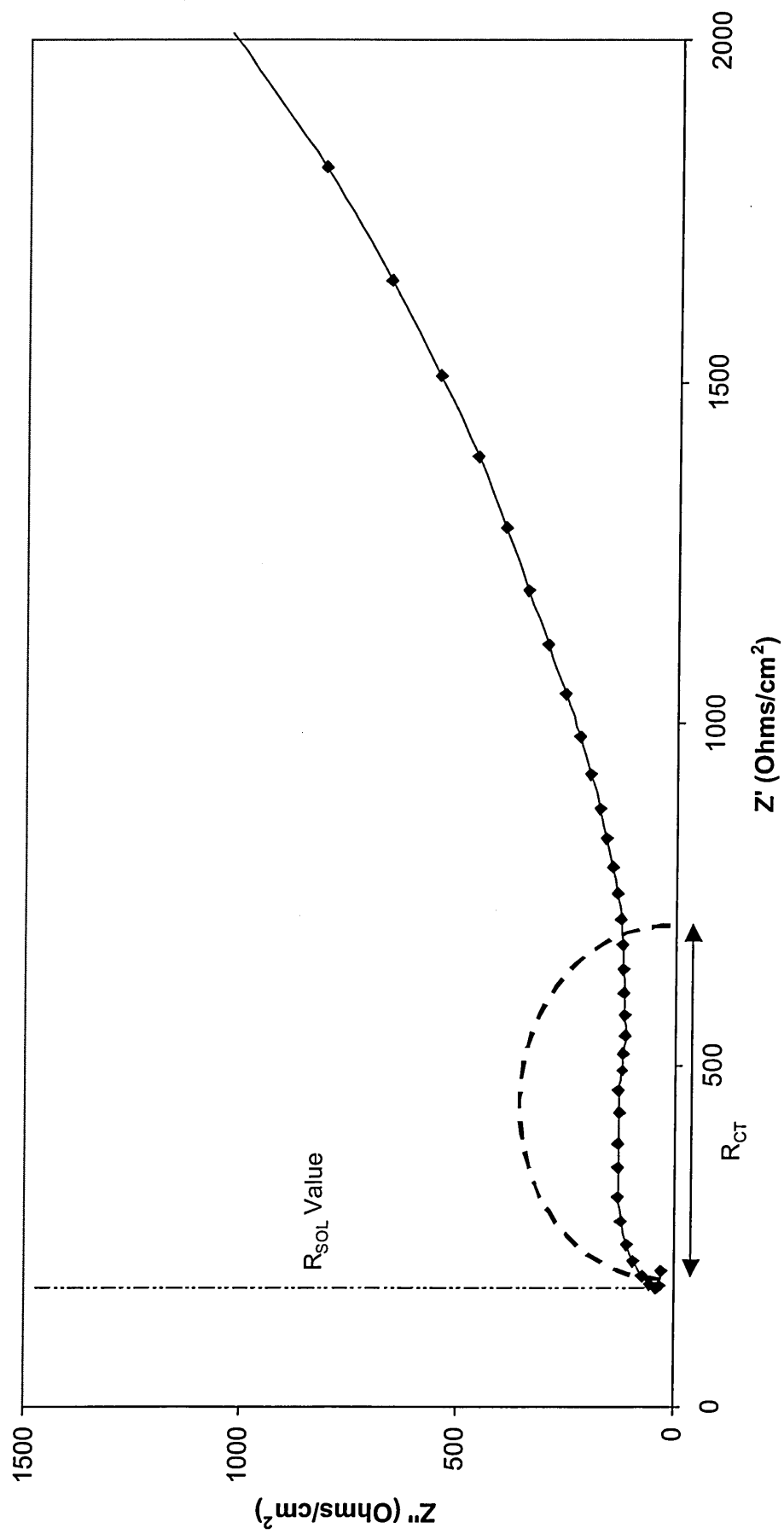


Figure 5.21 Nyquist plot for 0.4 w/c substrate



5.4.3 Analysis of impedance spectroscopy data

The test specimen will respond in different ways to different frequency ranges within the signal. Each of these responses effectively represents a different physical process within the measurement cell. At the higher frequencies ≈ 10 kHz, only the electrolyte resistance is observed, this is the solution resistance and is effectively the conductance of the solution. For frequency ranges 100 Hz \sim 1Hz the signal perturbs the molecules and ions forming the interfacial double layer between the metal and the electrolyte. This allows the measurement of electron transfer processes within the cell, such as the charge transfer resistance. At the lower measurement frequencies, the slower processes involving diffusion of electro-active species are involved. Therefore, by studying different frequency ranges different physical and chemical processes within the cell can be studied.

Analysis of the Nyquist plots can be conducted by a variety of methods. The main method is by the use of equivalent circuits. A corroding interface can be considered as a combination of resistances, capacitances and inductances. The application of an alternating voltage will for example result in a lag for a capacitance and a lead for an inductance. At a particular angular frequency the impedance of the circuit at that point has a magnitude $|Z|$ and the angle ϕ that its vector makes with the real axis of the Nyquist plot. Impedance is, therefore, a resistance in an AC circuit with a direction as well as a magnitude. An electrical circuit with the same response to the AC signal as the cell under study can be defined and a mathematical relationship to describe the circuit derived. By fitting the experimental data into this relationship, values for R_{CT} , R_{SOL} and C_{DL} can be found. Two methods have been employed in this study, a mathematical analysis of the equivalent circuit and the fitting of semi circles to the data.

5.4.3.1 Equivalent Circuits

The process for the characterisation of an electrochemical cell using impedance spectroscopy measurements has become widely accepted [176]. The process has been summarised in the flow diagram in Figure 5.22. The first stage is to produce an equivalent circuit, which fits both the data and the physics of the system under test. A mathematical analysis of the equivalent circuit allows the creation of a mathematical model of the circuit. This is then used to simulate the variation in impedance of the circuit over the frequency range used in the experimental work. A comparison of the simulation to the actual experimental data shows the applicability of the circuit to the system under test. At any stage the equivalent circuit can be altered to achieve better agreement with the experimental data. Once a circuit and model that fits the experimental data has been developed, the system is characterised and the formula derived used to study the on going processes in the cell.

The selection of the equivalent circuit for the experimental system requires knowledge of AC theory and how the circuit elements relate to different physical and chemical processes occurring in the cell. It is possible for two different equivalent circuits to produce the same response from the system over a range of frequencies. By adding more elements to an equivalent circuit it is possible to achieve a better fit to experimental data. However, it may not be possible to justify this from an interpretation of the physical processes occurring in the system under examination. The method is a compromise between the fit to the experimental data and the understanding of the electrochemical cell under study. It is usually considered appropriate to select the simplest equivalent circuit available to model the system under investigation. This also has the advantage of simplifying the mathematical modelling of the system.

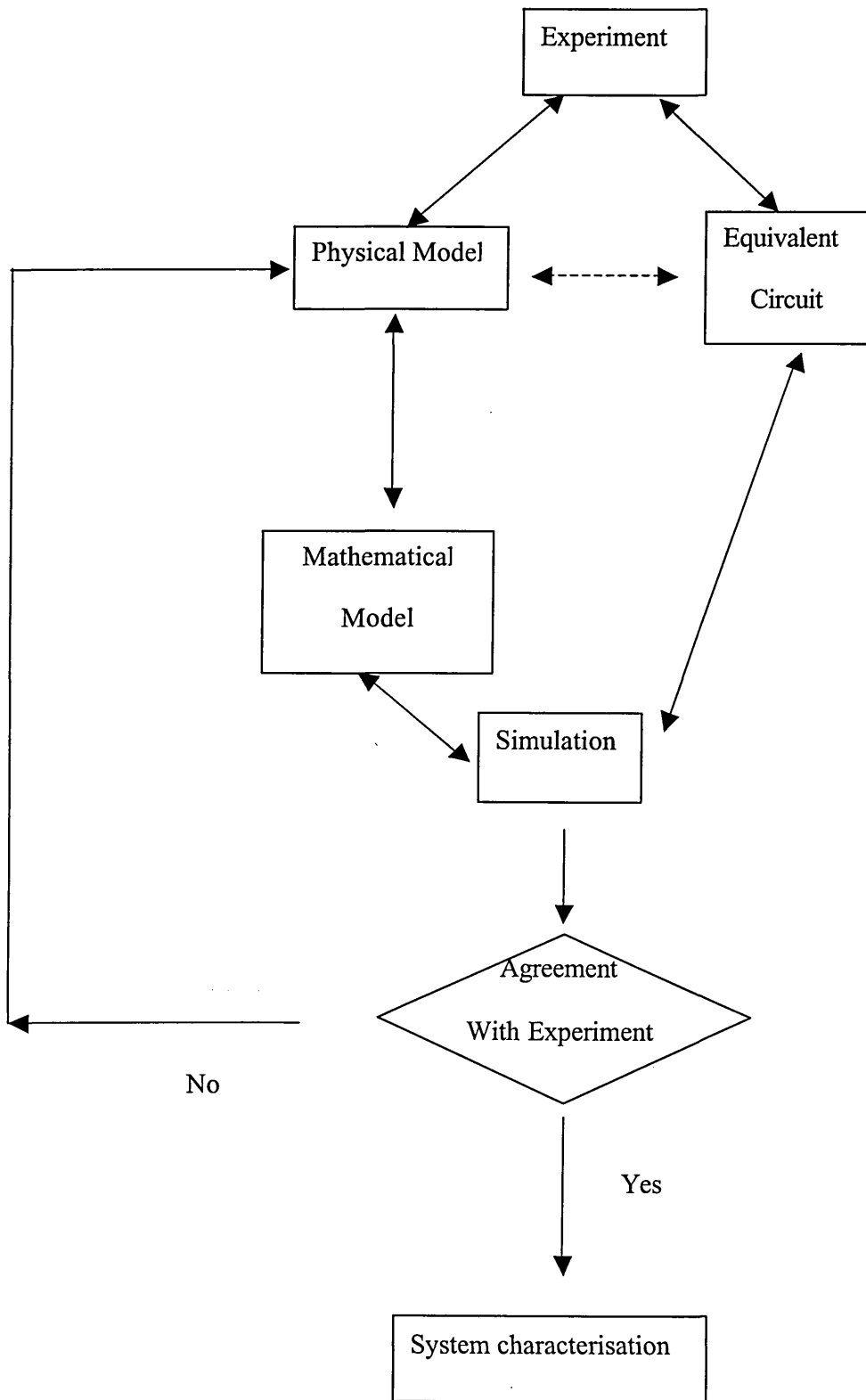


Figure 5.22 Flow Diagram for evaluating experimental impedance results [36, 74]

5.4.3.2 Selection of appropriate equivalent circuit.

Authors studying the corrosion of steel reinforcement in concrete have proposed a number of equivalent circuits, such as Wheat [25] (Figure 5.23) and Sagoe-Crentsil et al [180] (Figure 5.24). The models have a number of elements in common such as R_{CT} (charge transfer resistance) and C_{DL} (double layer capacitance). The presence of a Warburg impedance (W) represents diffusion process in the model. In concrete the diffusion of oxygen and other aggressive species through the electrolyte have been identified as controlling processes in corrosion of reinforcement and the use of the Warburg impedance, therefore, fits with the understanding of the corrosion process. The models also contain elements representing the effect of concrete on the impedance circuits. Wheat and Sagoe-Crentsil et al [25, 48, 180] have circuit elements with an interfacial capacitance and resistance. This is intended to represent the dielectric properties of the band of material between the steel and the concrete matrix. Sagoe-Crentsil et al [180] also include a circuit element composed of C_M and R_M to represent the dielectric properties of the concrete itself. These circuit elements are all justifiable from the physics of the system under test and it is the intention to use a similar model for the interpretation of the impedance data from the experimental study.

The influence of the concrete matrix, from the work of Sagoe-Crentsil et al [180], appears in the high frequency range of the spectrum (in excess of 100kHz). The present experimental work concentrates on medium to low frequencies 30kHz to 0.001Hz. It would appear reasonable to ignore the concrete matrix circuit elements from the equivalent circuit for the analysis of the current data and use an equivalent circuit similar to the one employed by Wheat [25, 48].

A schematic representation of a Nyquist plot that would result from the equivalent circuit put forward by Wheat is shown in Figure 5.23. Comparing this to an example of the data from the current study in Figure 5.21 shows a number of differences. The Warburg impedance is lower than 45° to the x-axis and peaks at low frequencies.

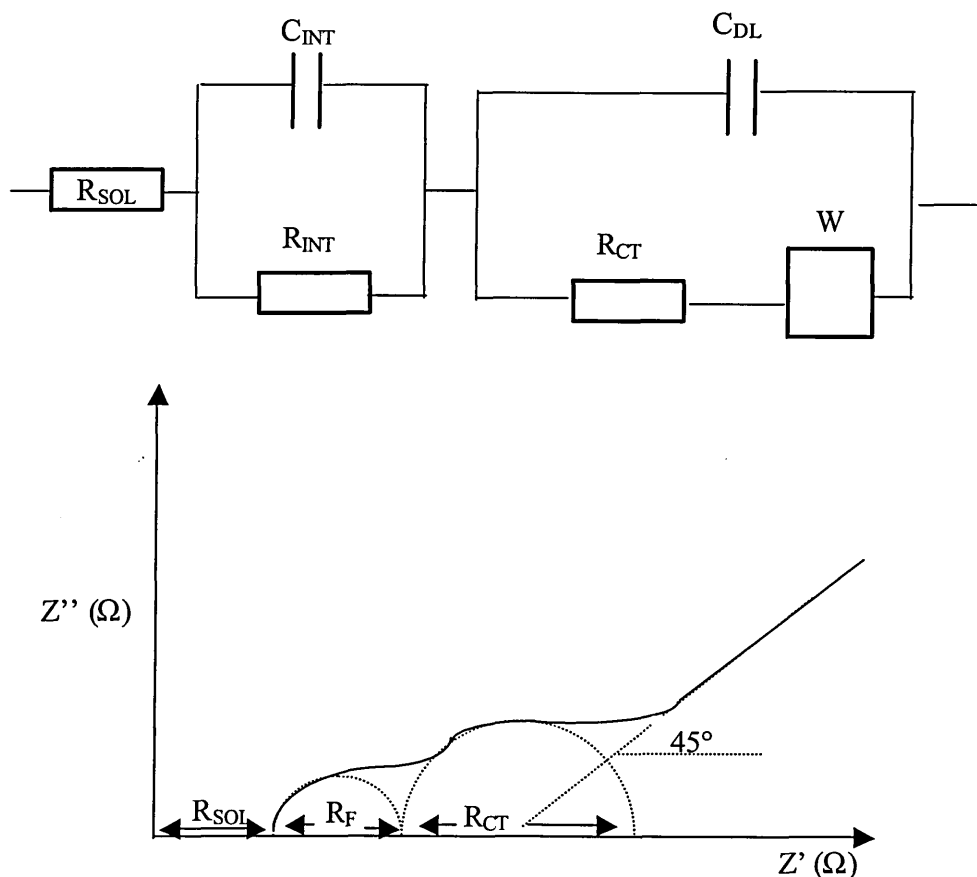


Figure 5.23 Equivalent circuit from Wheat [25]

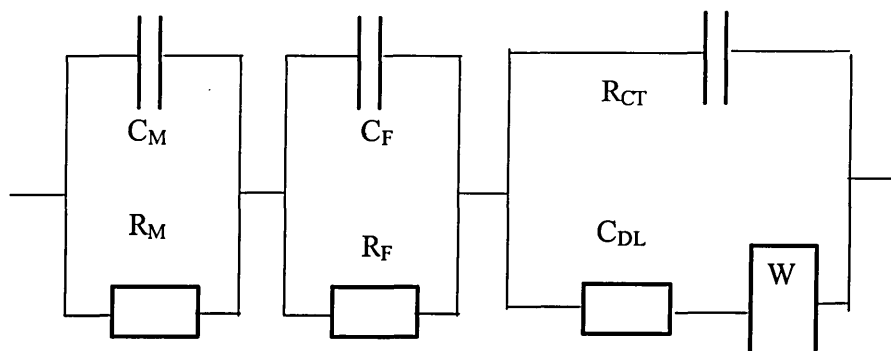


Figure 5.24 Equivalent Circuit Sagoe-Crentsil et al [180]

This is typical of impedance plots in concrete [25] and the diffusion layer is of finite thickness and not infinite as expected from a pure Warburg impedance. This occurs where the interface is blocked by a highly resistive surface or membrane, such as the total coverage of the surface of the metal with an oxide film. It also fits the situation of the metal covered in a layer of concrete. In this situation the Warburg impedance is modified and a finite Warburg impedance (Z_w) parameter is used to describe this phenomenon.

The second difference is that the semi circles of the other circuit elements are not well developed above the x -axis. Again this is a typical feature of Nyquist plots from tests on concrete specimens [25, 175]. This has also been recognised in other situations (De Levie [202]) where porous or rough electrodes have been used. This is also a feature of Nyquist plots where the diffusive part has an angle of less than 45° . It is known that the capacitors in the impedance spectroscopy experiments do not always behave ideally and instead act as constant phase elements (CPE). This element can be described by;

$$Y_{CPE} = b(i\omega C)^\alpha \quad 5.8$$

Where b is a proportionality constant and α has a value of 0.5 for porous electrodes and 1 for smooth electrodes. As most electrodes are rough it is recognised that they will have a value of α of between 0.5 and 1.

The equivalent circuit for the present study is shown in Figure 5.25 and is similar to the circuit used by Wheat [25] (Figure 5.23). However, in this circuit a finite Warburg impedance (Z_w) is used in series with the charge transfer resistance (R_{CT}) and this combined element is in parallel to the double layer constant phase elements (CPE_{DL}). An element of CPE_F and R_F in parallel is used to represent the steel concrete interface and R_S is the solution resistance from the concrete.

5.4.3.3 Analysis of the Equivalent Circuit used in the Present Study.

The equivalent circuit in Figure 5.25 can be analysed using the techniques of AC circuit analysis and a mathematical model of the circuit can be derived. The model can then be used to determine the relative values of capacitors and resistors which fit the model to the experimental data. By this process the suitability of the equivalent circuit to characterise the experimental data can be determined. The ability to determine the size of the R_{CT} (charge transfer resistance) by fitting the model to the data also allows the determination of the corrosion currents and corrosion rate.

The analysis of the circuit is based on Kirchof's laws. The impedance for resistances and capacitances in series is given by:

$$\text{Impedance} = \sum \text{Impedances in the element}$$

For resistances and capacitances in parallel:

$$\frac{1}{\text{Impedance}} = \sum \frac{1}{\text{Impedances in the element}}$$

Therefore, by splitting the equivalent circuit into a series of elements with impedances in series and parallel, the impedance of the circuit can be determined [36, 74].

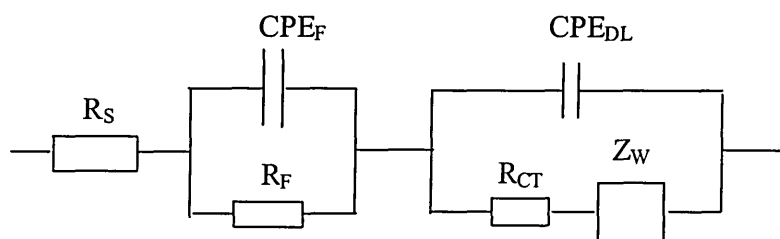


Figure 5.25 Equivalent circuit used in the present study.

$$Z = R_S + \left(\frac{1}{\frac{1}{CPE_F} + \frac{1}{R_F}} \right) + \left(\frac{1}{\frac{1}{CPE_{DL}} + \frac{1}{R_{CT} + Z_W}} \right) \quad 5.9$$

Where:

$$CPE_F = \frac{1}{b_1 (i\omega C_F)^{\alpha_1}} \quad 5.10$$

$$\therefore \frac{1}{CPE_F} = b_1 (i\omega C_F)^{\alpha_1} = B \quad 5.11$$

$$CPE_{CDL} = \frac{1}{b_2 (i\omega C_{DL})^{\alpha_2}} \quad 5.12$$

$$\therefore \frac{1}{CPE_{CDL}} = b_2 (i\omega C_{DL})^{\alpha_2} = C \quad 5.13$$

Substituting into 5.9 for B and C

$$Z = R_S + \left(\frac{1}{B + \frac{1}{R_F}} \right) + \left(\frac{1}{C + \frac{1}{R_{CT} + Z_W}} \right)$$

$$\therefore Z = R_S + \left(\frac{R_F}{BR_F + 1} \right) + \left(\frac{R_{CT} + Z_W}{C(R_{CT} + Z_W) + 1} \right) \quad 5.14$$

Z_W is the Warburg diffusion impedance adjusted for a diffusion layer of finite size.

This takes the form [36, 74, 171, 202, 235]:

$$Z_W = \sigma \omega^{-1/2} (1-i) \tanh \left(\delta \left(\frac{i\omega}{D} \right)^{1/2} \right) \quad 5.15$$

In which, σ is the Warburg Coefficient and is defined as:

$$\sigma = \frac{RT}{n^2 F^2 A \sqrt{2}} \left(\frac{1}{C_O \sqrt{D_O}} + \frac{1}{C_R \sqrt{D_R}} \right) \quad 5.16$$

Where:

ω = radial frequency

D_O = Diffusion Coefficient of the oxidant

D_R = Diffusion coefficient of the reductant.

A = Surface area of the electrode.

n = Number of electrons transferred.

C_O = Concentration of oxidant species.

C_R = Concentration of reductant species.

R = Ideal gas constant

T = Temperature

F = Faraday constant

δ = Nerst diffusion layer thickness

D = an average value of diffusion coefficients of the diffusing species.

Substituting into 5.14 from 5.11, 5.13 and 5.15 gives:

$$Z = R_{SOL} + \frac{R_F}{b_1(i\omega C_F)^{\alpha_1} R_F + 1} + \frac{R_{CT} + \sigma\omega^{-1/2}(1-i)\tanh\left(\delta\left(\frac{i\omega}{D}\right)^{1/2}\right)}{b_2(i\omega C_{DL})^{\alpha_2} \left\{ R_{CT} + \sigma\omega^{-1/2}(1-i)\tanh\left(\delta\left(\frac{i\omega}{D}\right)^{1/2}\right) \right\}} \quad 5.17$$

Equation 5.17 shows the relationship between the total impedance Z and the elements from the equivalent circuit R_{CT} , C_{DL} and the diffusion coefficient from the Warburg impedance Z_w . These represent the elements modelling the corrosion processes. In addition the elements R_{SOL} , C_F and R_F represent the effects of the cementitious material. By introducing values for these factors into equation 5.17, it is possible to model the response of the circuit to changes in frequency ($i\omega$) [36, 74, 171, 202, 235]:.

During the impedance spectroscopy measurements, the frequency of the applied signal, the impedance of the circuit, and the phase difference between the applied signal and the response were all recorded. The measurements were used to produce graphs of impedance against frequency and phase difference against frequency. The two diagrams were combined into a Nyquist plot of the real and imaginary components. As the

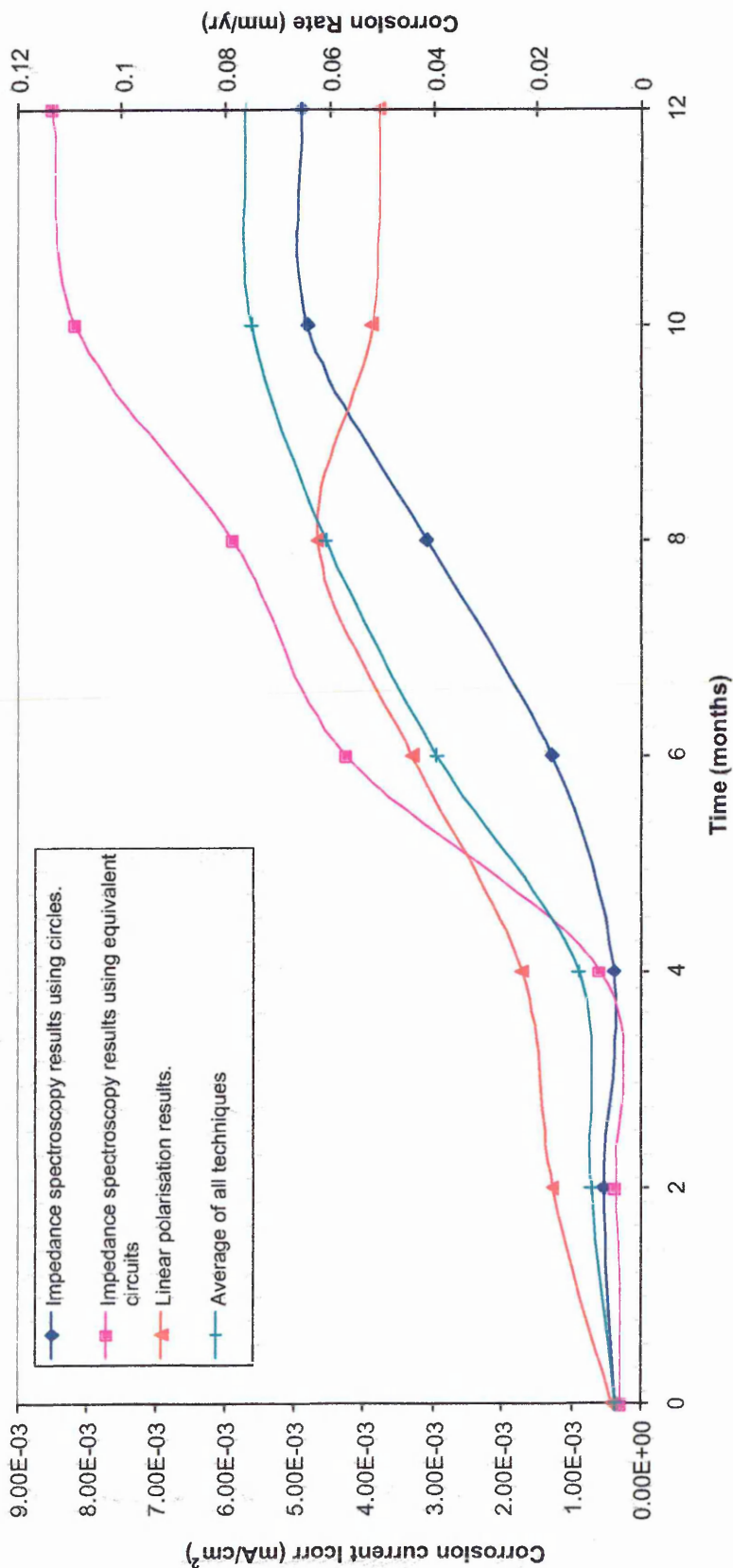
impedance Z represents the vector quantity of the real and imaginary components and the phase difference θ is the angle of the vector, the real and imaginary components can be resolved simply by using trigonometry [36, 74, 171, 202, 235].

Equation 5.17 can also be resolved into the real and imaginary components required to produce the Nyquist diagram for the equivalent circuit. The equations produced by this process can then be solved to produce a value for R_{CT} . The use of complex number non-linear least squares curve fitting computer programs makes this process achievable without the direct determination of the formula for the equivalent circuit [36, 74, 171, 202, 235]. An iterative process is used to estimate for unknowns in the equations. The predicted output from the equivalent circuit can be compared to the experimental results. In this research a software package called Z simpWin was used to fit the equivalent circuit data. The complex equivalent circuits proposed here resulted in a large number of parameters to fit the data, and the software was always able to achieve a fit to the data by varying these parameters. It is, therefore, important to use known values for some of the parameters to prevent a false fit to the data. Figure 5.26 shows an example of the fit achieved using the equivalent circuit described and the present experimental data.

The end result of the process is to obtain a value for R_{CT} from the equivalent circuit. This value is analogous to R_p , the polarisation resistance, from the LPR measurements and can be converted to corrosion currents by the Stearn Geary Equation:

$$I_{CORR} = \frac{B}{R_{CT}} \quad 5.18$$

Figure 5.27 Comparison of corrosion Rates Calculated using different measurement techniques for material B with 0.8w/c Substrate



where B is the Tafel constant. Figure 5.27 shows the values of I_{CORR} obtained by fitting the equivalent circuit shown to the experimental data obtained for material B combined with the 0.8 w/c substrate.

5.4.3.4 Data Analysis by the fitting of Semi Circles

It is possible to find R_{CT} by another method using equivalent circuits. This uses the simpler Randles circuit which describes the interaction of charge transfer resistance and diffusion (see Figure 5.28) [36, 74, 171, 202, 235].

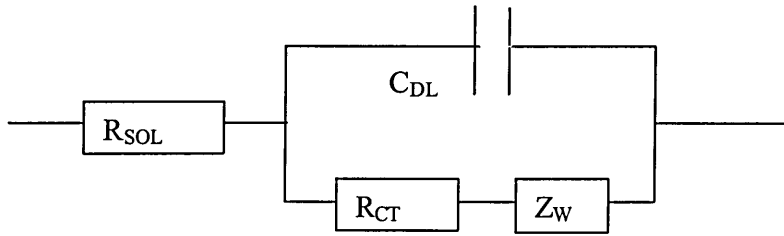


Figure 5.28 Randles Equivalent Circuit

The equation for this circuit is [36];

$$Z = R_{SOL} + \frac{R_{CT} + \sigma\omega^{-\frac{1}{2}}}{C_{DL}(R_{CT} + \sigma\omega^{-\frac{1}{2}})} \quad 5.19$$

This is split into the real and imaginary components:

$$Z' = R_{SOL} + \frac{R_{CT} + \sigma\omega^{-\frac{1}{2}}}{(\sigma\omega^{-\frac{1}{2}}C_{DL} + 1)^2 + \omega^2 C_{DL}^2 (R_{CT} + \sigma\omega^{-\frac{1}{2}})^2} \quad 5.20$$

$$-Z'' = \frac{\omega C_{DL} (R_{CT} + \sigma\omega^{-\frac{1}{2}})^2 + \sigma^2 C_{DL} + \sigma\omega^{-\frac{1}{2}}}{(\sigma\omega^{-\frac{1}{2}}C_{DL} + 1)^2 + \omega^2 C_{DL}^2 (R_{CT} + \sigma\omega^{-\frac{1}{2}})^2} \quad 5.21$$

At low frequency, the limit of the equations produces a straight line of unit slope of 45°, this is indicative of the mass transfer processes due to diffusion, and is represented as the Warburg impedance. At high frequencies the control is kinetic and $R_{CT} \gg Z_W$ and the real and imaginary components become;

$$Z' = R_{SOL} + \frac{R_{CT}}{1 + \omega^2 C_{DL}^2 R_{CT}^2} \quad 5.22$$

$$Z'' = -\frac{\omega C_{DL} R_{CT}^2}{1 + \omega^2 C_{DL}^2 R_{CT}^2} \quad 5.23$$

This simplifies to;

$$(Z' - R_{SOL} - \frac{R_{CT}}{2})^2 + (Z'')^2 = (\frac{R_{CT}}{2})^2 \quad 5.24$$

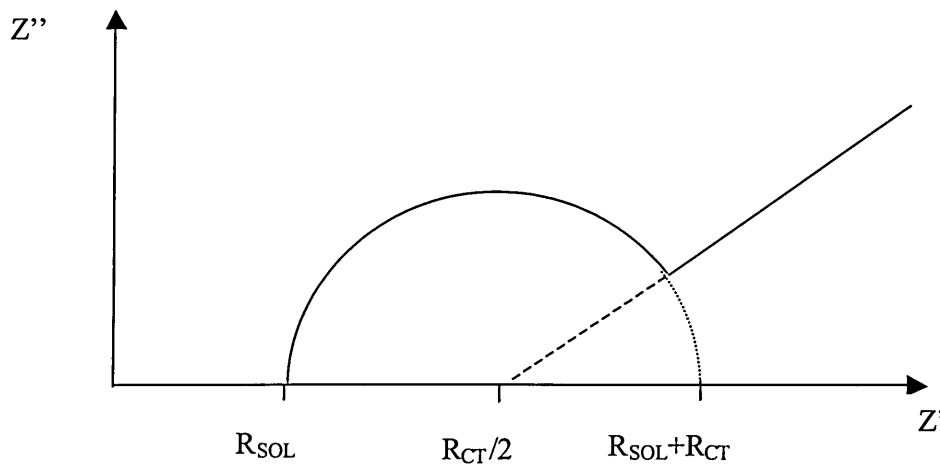


Figure 5.29 Nyquist plot from the Randles equivalent circuit.

Equation 5.24 is the formula for a semi circle with the radius of $R_{CT}/2$ and intercepts on the Z' axis of R_{SOL} and $R_{SOL} + R_{CT}$ (see Figure 5.29) [36, 74, 171, 202, 235]. It is possible to fit a semi circle to the impedance data in the Nyquist diagram (see Figure 5.21). As the kinetic process involved covers a region from approximately 100 Hz to 1 Hz, the semicircle is fitted to this portion of the data. The diameter of the semi circle will provide R_{CT} . As this kinetic process is present in all corrosion processes, then so

will the semicircle for measuring R_{CT} . Providing that care is taken in estimating the size of the semi circle, the values obtained for R_{CT} should be proportional to the actual value for R_{CT} . This is a simpler method of estimating R_{CT} than fitting an equivalent circuit to the data. However, this is potentially a less accurate method of obtaining R_{CT} , as the data does not intercept the real axis at low frequencies and makes estimating the size of the semi circle difficult.

A comparison of the results from equivalent circuits and from fitting a semi circle to the data can be seen in Figure 5.27. This shows that both methods produce the similar trends in data. However the equivalent circuit overestimates the corrosion current in comparison to LPR values and the semi-circle method underestimates the value. All the values were within the factor of three of each other, which is suggested as a limit to the accuracy of currents determined using the Stern-Geary approximation. This is improved by using the B values obtained from the polarisation curves in Chapter 5.1, but is still unlikely to be more accurate than a factor of two irrespective of the method used to fit the data. The closeness of the values obtained provides extra confidence in the trends obtained from the work of this research irrespective of the method used to determine them. To limit the complexity of the data analysis it was decided to use the semi-circle method for the determination of currents from the impedance data.

5.4.4 Results

Once the charge transfer resistance (R_{CT}) has been determined, the corrosion currents can be calculated using the B constant for each material obtained from the polarisation curves (see Chapter 5.1). The Stern-Geary relationship [30, 33, 156, 162, 164] was used to calculate the corrosion current, i_{CORR} ;

$$i_{CORR} = \frac{B}{R_{CT}} \quad 5.25$$

where i_{CORR} = corrosion current density (mA/cm²)

R_{CT} = Charge Transfer Resistance (ohm/cm²)

The B constants were calculated using an average cathodic Tafel constant for all materials. The anodic Tafel constant was the actual value calculated from the relevant polarisation curves. Table 5.7 shows the cathodic, anodic Tafel constants used and the resulting B constants for each material. B was calculated as follows:

$$B = \frac{\beta_a \beta_c}{2.3(\beta_a + \beta_c)} \quad 5.26$$

Table 5.9 Tafel constants used for corrosion current calculations.

Material	Anodic Tafel Constant β_a (mV)	Cathodic Tafel Constant β_c (mV)	B Constant (mV)
0.4 w/c	536.25	145.03	49.63
0.8 w/c	268.80	145.03	40.96
A	402.04	145.03	46.34
B	352.48	145.03	44.68
C	281.26	145.03	41.60

All the results presented are an average of 4 readings from two different test specimens, with two measurements being made per test specimen. The average was a selective average, in that any value not within a factor of 2 of the other readings was discarded and the average calculated from the remaining results. A test matrix is presented in Table 5.10 showing the number of readings used to calculate the average corrosion current. The solution resistance (R_{SOL}) and the corrosion potentials were also taken as part of the impedance measurements. The R_{SOL} values have been presented and discussed in Chapter 5.5 on Resistivity and the corrosion potentials in Chapter 5.6.

Table 5.10 Number of readings used to calculate the average corrosion current

Material Combination	Location	Exposure period at time the readings taken (months)						
		0	2	4	6	8	10	12
A04	Repair	3	4	4	4	4	4	4
	Interface	3	4	4	4	4	4	4
	Substrate	3	4	4	4	4	4	4
A08	Repair	4	4	4	4	4	4	4
	Interface	4	4	3	4	4	3	3
	Substrate	4	4	4	4	4	4	3
B04	Repair	4	4	4	4	3	3	4
	Interface	4	4	4	4	3	4	3
	Substrate	4	4	3	4	4	3	3
B08	Repair	4	4	4	3	3	4	3
	Interface	4	4	4	4	4	4	4
	Substrate	4	4	4	3	3	4	3
C04	Repair	4	4	4	3	3	3	3
	Interface	4	4	3	3	3	2	2
	Substrate	4	4	2	4	4	3	3
C08	Repair	4	4	3	4	3	3	3
	Interface	4	4	3	3	4	3	3
	Substrate	4	4	3	3	3	3	3

Figure 5.29 Material A with 0.4w/c substrate

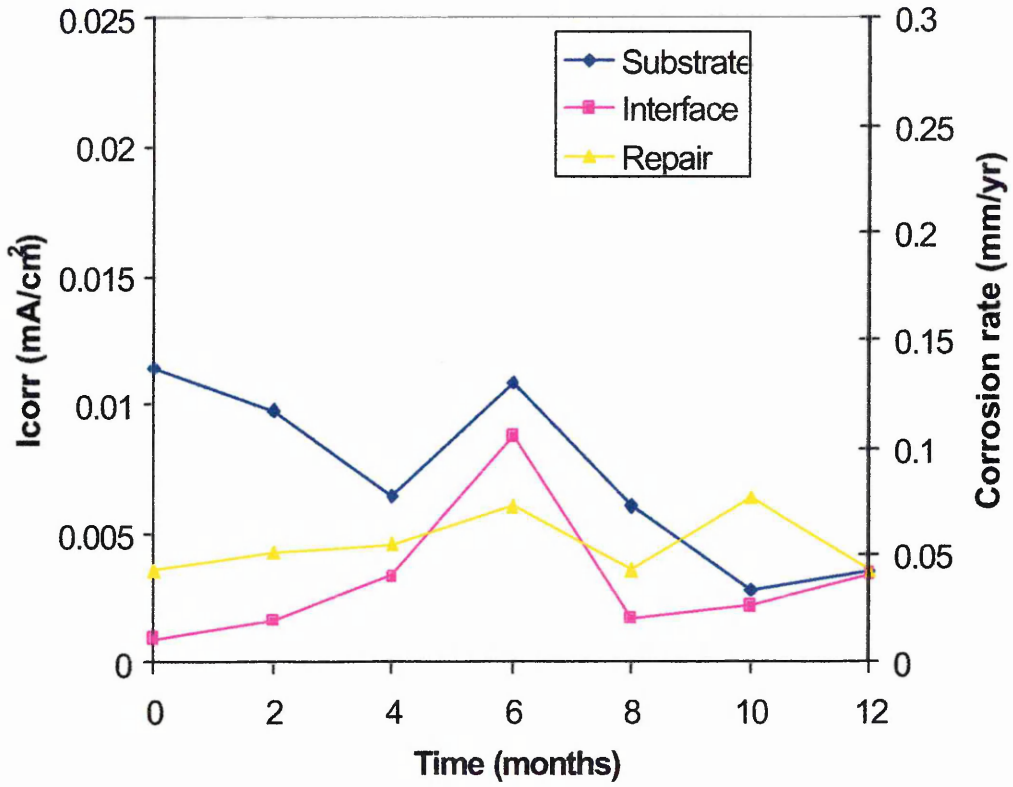


Figure 5.30 Material A with 0.8w/c substrate

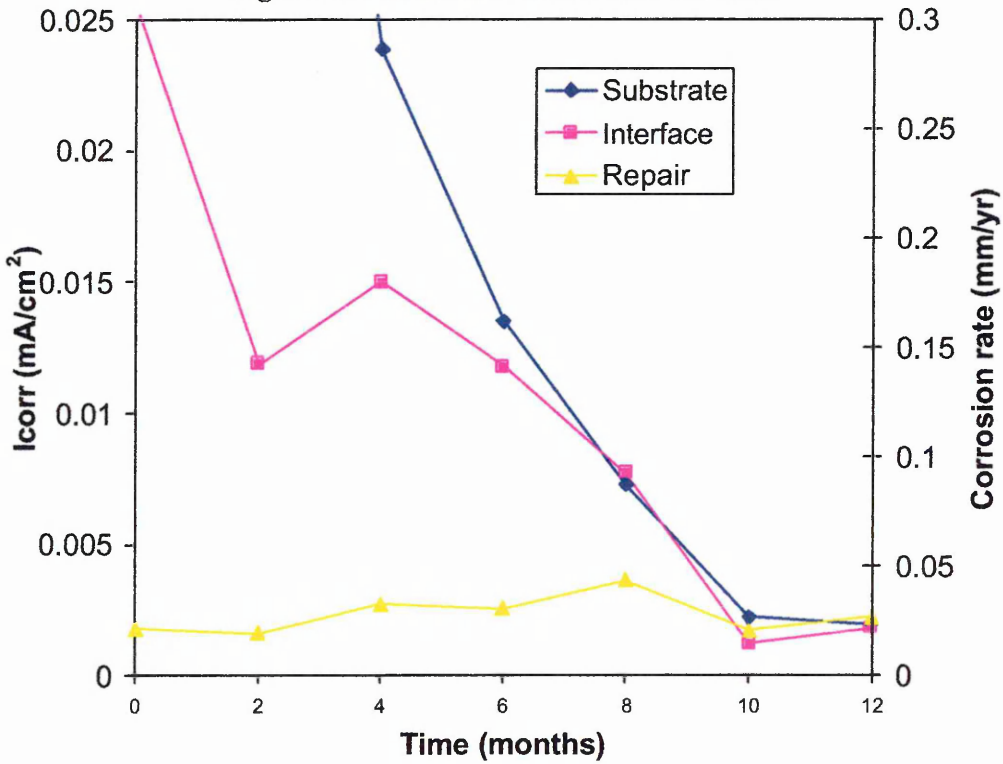


Figure 5.31 Material B with 0.4w/c substrate.

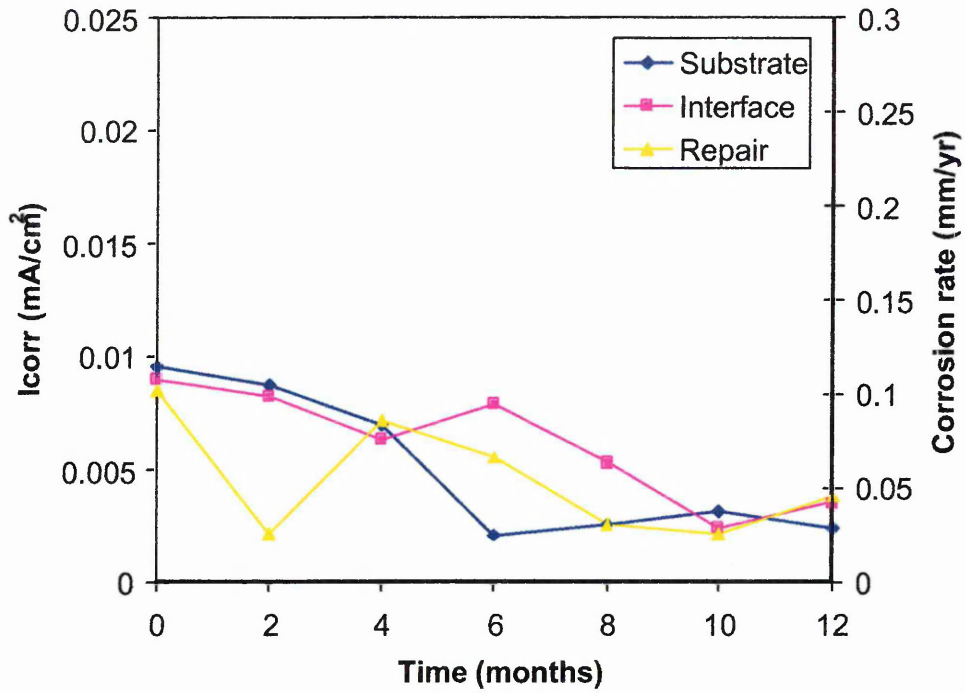


Figure 5.32 Material B with 0.8w/c substrate.

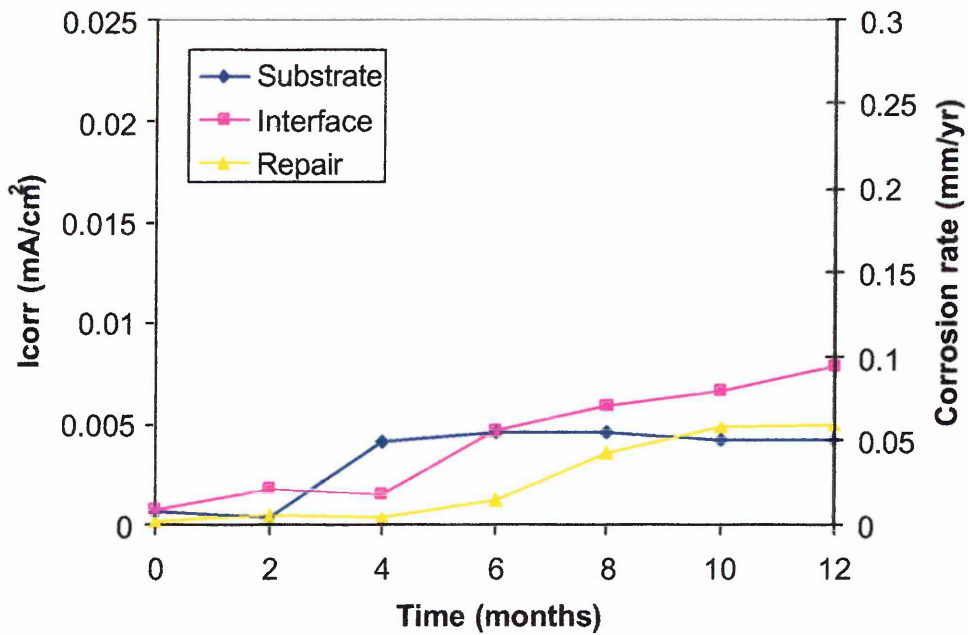


Figure 5.33 Material C with 0.4w/c substrate.

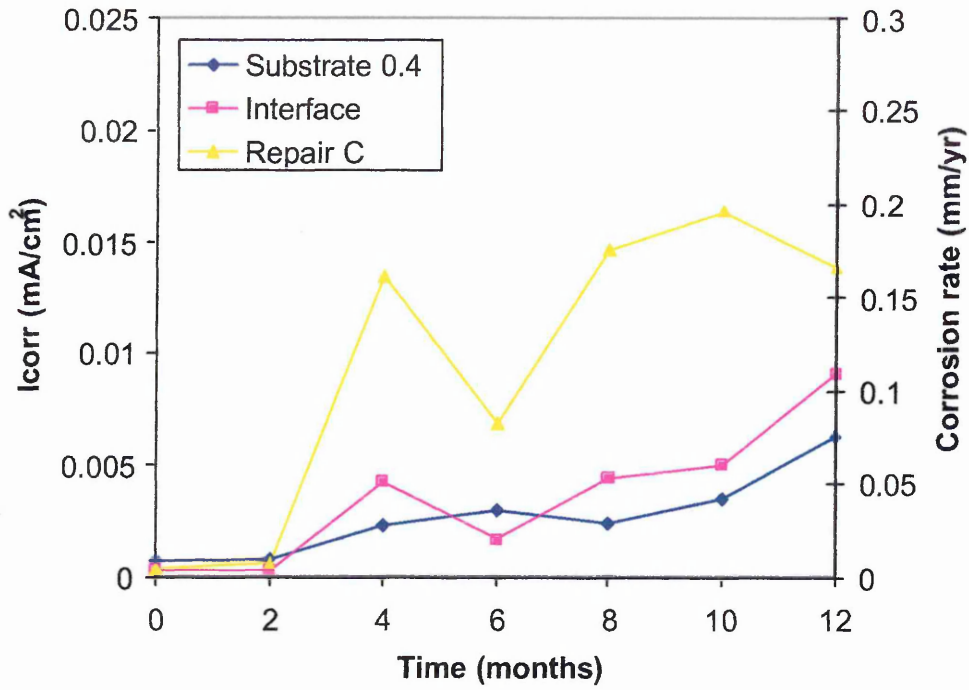


Figure 5.34 Material C with 0.8w/c substrate.

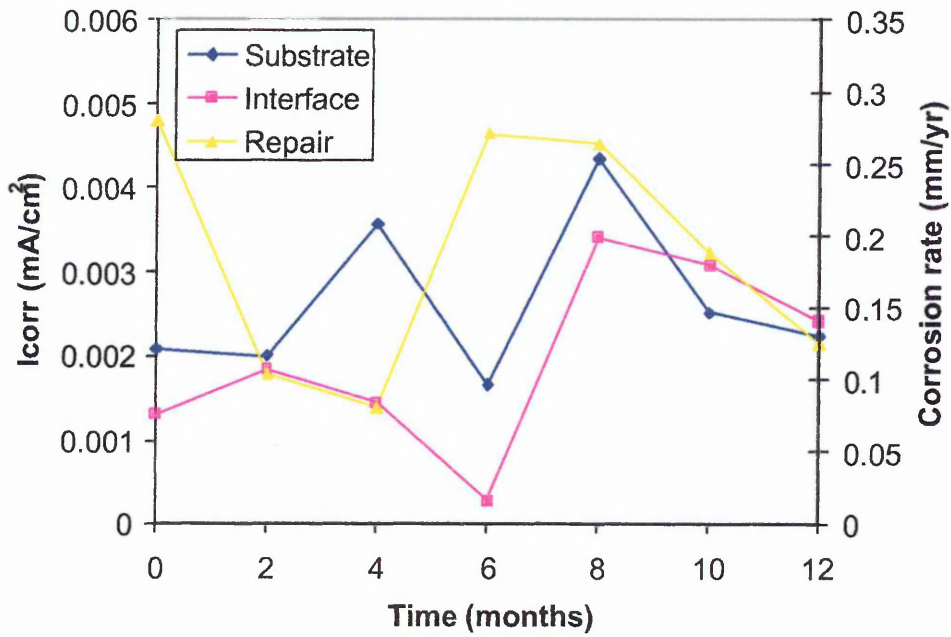
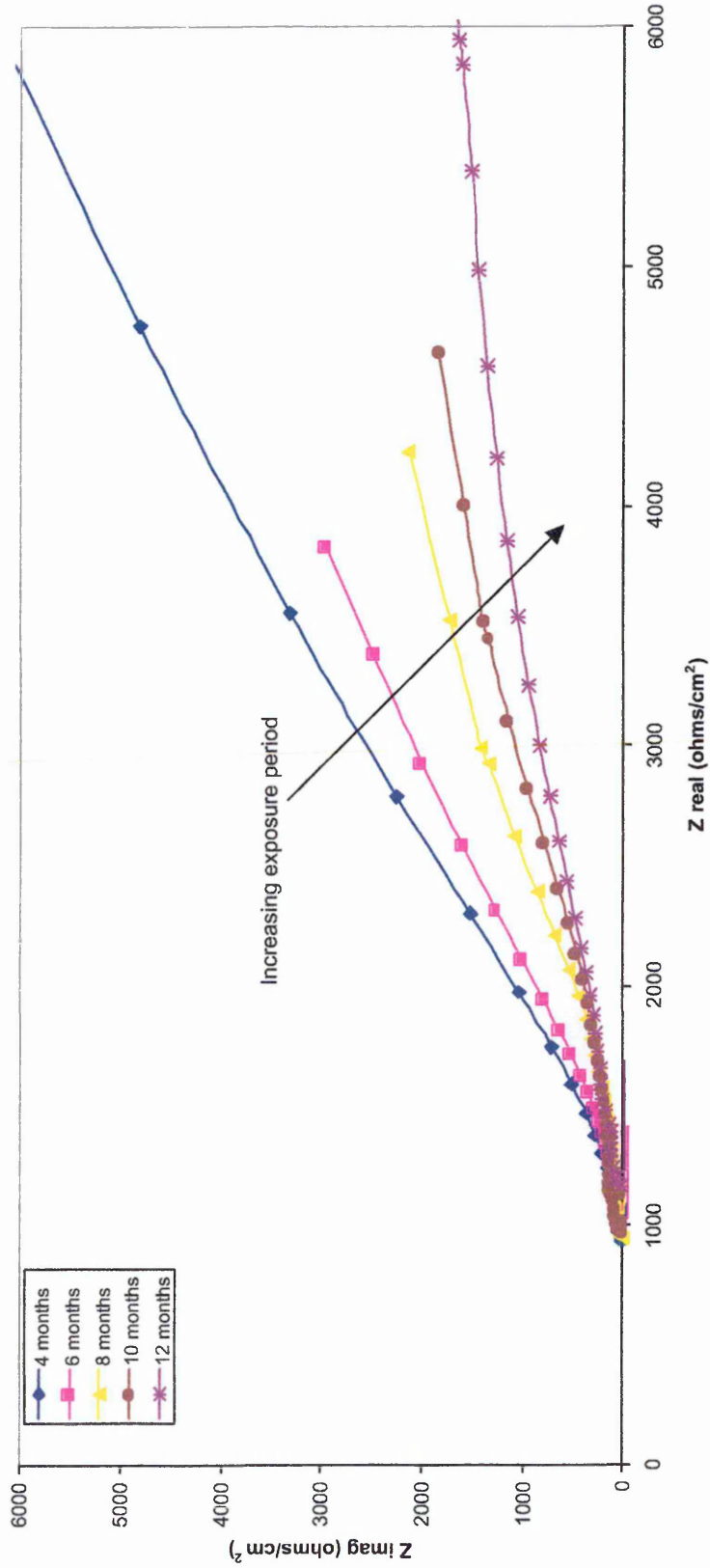


Figure 5.35 Nyquist plots for repair material B when combined with the 0.8w/c substrate.



5.4.5 Discussion

The analysis of the impedance data by equivalent circuits allowed the characterisation of the system. The use of constant phase elements in the circuit produced a good agreement between the experimental data and the equation derived for the circuit. However, the process of fitting the formula to the data was complex. This may account for the reason why much of the published work for impedance spectroscopy in concrete appears incomplete. Neither Wheat [210] or Sagoe-Crentsil et al [21] calculated R_{CT} or corrosion currents from the impedance data although they did present equivalent circuits to model the systems. Ping Gu et al [178] indicated that as the data did not intercept the real axis then estimation of R_{CT} would be subject to appreciable errors.

The data from the impedance spectroscopy measurements appears to be in general agreement with the LPR measurements taken and are within a factor of 3. This is the generally accepted accuracy limit for the technique. Overall the values predicted by impedance spectroscopy were lower than those from the LPR measurements. More importantly for the current work, the trends predicted were consistent between the two techniques. A comparison of the data from the two techniques will be considered further in the Section 5.7 on corrosion currents.

The use of equivalent circuit concept did not allow all characteristics of the cell to be determined as hoped. The complex nature of the formula calculated for the equivalent circuit meant there were a large number of variables to be fitted to the data. Equation 5.14 uses the following variables R_{SOL} , R_F , C_F , b_1 , α_1 , R_{CT} , C_{DL} , b_2 , α_2 and D from Z_W . It was not possible to achieve a fit with the experimental data, while keeping all the variables within a realistic range predicted from the physics of the model. The work

concentrated on achieving a fit for R_{CT} . in order to allow corrosion rates to be calculated.

To simplify matters values of α were set at 0.75 and b at 2 for both cases. The value of D used was obtained from the chloride diffusion results and allowed to vary by 2 decimal places. Values of R_F and C_F were kept constant for each material, but allowed to alter for different materials depending on the results of simulation runs. The solution resistance R_{SOL} was measured directly from the data. This effectively allowed only R_{CT} and C_{DL} to vary with each set of iterative simulations.

This process worked but removed the ability to study other physical processes within the cell such as diffusion. This, combined with the complexity of the technique made the use of simpler alternative techniques such as the fitting of semicircles more attractive. The use of semicircles yielded the same data as obtained from the software used to fit the formula but was quicker to obtain. The main problem was that the accuracy of this technique was suspect due to the curve having only one intercept on the real axis and also the validity of the technique was unconfirmed. The use of the Randles circuit (see section 5.4.5.2) confirmed the applicability of the technique to this situation. A comparison of results between the different techniques showed that the accuracy was no worse than any other technique (Figure 5.27). This provided confidence in the fitting of semicircles to the data to measure R_{CT} .

The results from the impedance data were combined to produce plots of the variation of corrosion current with time for each specimen type (Figures 5.30 to 5.35). This duplicates the work already completed for LPR measurements in Section 5.2 and allows a direct comparison between the two (see Chapter 5.7).

General trends within the specimens appear to be consistent between the two techniques. The low permeability repair materials such as material A with 0.8w/c substrate in Figure 5.30, have lower corrosion rates than the high permeability repair materials such as material C with 0.4w/c substrate in Figure 5.35. Specimens with a smaller disparity in permeability between the repair and the substrate appeared to exhibit lower corrosion rates. For instance, material B with the 0.8w/c substrate in Figure 5.33 and material C with the 0.8w/c substrate in Figure 5.35.

In only one situation does the trend predicted by the impedance spectroscopy measurements appear to be significantly different from the LPR results from Chapter 5.3. The interface for material A when combined with the 0.8w/c substrate has a high initial corrosion rate. This drops away with time following that of the substrate. This is the opposite to the trend detected from LPR measurements where the corrosion rate of the interface rises with time following the repair material. Otherwise, the general difference between the measurement techniques is that of magnitude of the readings. A more detailed discussion of the LPR and the impedance spectroscopy measurements is given in the Chapter 5.7 on corrosion currents.

The data showed a number features typical of concretes. Figure 5.36 shows a series of Nyquist plots for the same repair material (B) and how they vary with time. From this it can be seen that the low frequency curve due to diffusion decreases with time. This has been taken by some authors such as Dawson et al [60, 144] to indicate corrosion or a decrease in quality of the concrete. It possibly indicates the growth of a resistive film on the surface of the reinforcement, such as corrosion products. This is a significant finding in the impedance data as it would appear to confirm that the specimens were actively

corroding during the test period. With the low corrosion rates observed in some instances it was otherwise difficult to confirm if the reinforcement was corroding.

5.4.6 Conclusions

An equivalent circuit has been proposed for the impedance data. The equivalent circuit has some notable differences from the ones proposed by other authors. The circuit uses constant phase elements and a finite Warburg diffusion parameter to accommodate the depressed portion of the Nyquist Plot. A mathematical formula was developed to describe the circuit and obtain values for R_{CT} . Due to the large number of unknown variables, it was not possible to study other processes operating in the cell.

An alternative method of fitting semicircles to the data based on the Randles circuit was investigated to provide an easier method of analysing the data. Both methods produced good agreement with the LPR measurements. The fitting of semicircles is recommended for examining data due to ease of application.

The data showed a number of features that indicated that the specimens were corroding, such as the gradual fall in the low frequency arc of the spectrum with time.

5.5 RESISTIVITY

Resistivity as a technique is often used in conjunction with rest potentials to give an indication of corrosion rate [186]. It measures the resistance of the material to the flow of an electric current and gives an indication of the ease at which a corrosion cell can be produced in the cementitious material. A low resistivity would suggest the easy formation of corrosion cells and, therefore, a high rate of corrosion.

An empirical relationship has been found between resistivity and corrosion rate [186] (as seen in Table 5.11), and this is often used with the empirical relationship for rest potentials (Section 2.5 Electrochemical Test Methods, table 2.3) to assess the corrosion risk and the likely corrosion rate of steel embedded in concrete. For example, a material with a rest potential more negative than -350mV wrt Cu/CuSO_4 and a resistivity below $5\text{ k}\Omega\text{cm}$ would indicate a high risk of corrosion at a very high rate. With a higher resistivity the risk of corrosion would remain the same but the likely rate of corrosion would fall.

Table 5.11 Relationship between resistivity and corrosion rates.

Resistivity ($\text{k}\Omega\text{cm}$)	Corrosion Rate
< 5	Very High
5 – 10	High
10 – 20	Low/Moderate
> 20	Low

Previous studies of resistivity have shown it to be very dependent on water content and temperature [189]. Hunkler [4] found that resistivity was strongly related to pore

volume and relative humidity. The resistivity of the pore solution was affected by ionic concentration such as Cl^- concentration.

The empirical relationships for resistivity and half-cell potentials are not valid in all situations. A material that is saturated with water would have a low resistivity and a low half-cell potential due to the low oxygen concentration in the material. The empirical relationships for rest potential and resistivity would indicate a high risk of corrosion and a likely high rate of corrosion. However, corrosion would probably be low, controlled by the rate of oxygen diffusion [187].

The resistivity measurements in this study are used to compare differences in the resistivity of the different repair materials and substrates and to assess the likely impact on corrosion. The resistivity measurements can also be used to adjust for the IR drop in the LPR measurements for the different materials. Two techniques for measuring the resistivity of test materials were used. The first method was a commercially available hand held meter and the second technique involved solution resistance measurements from impedance spectroscopy tests.

5.5.1 Method

The specimen configuration and test materials are as described in Section 5.2. Resistivity readings were taken each time an LPR and impedance spectroscopy measurement was taken. The hand-held resistivity meter had 2 probes with a spacing of 5 cm between them. Four holes, 5mm depth and 5cm apart, were drilled into the side (in a vertical straight line along the 400mm height) of the cylindrical test specimens. Two holes were drilled in the repair and two in the substrate material. This allowed one resistivity reading in the substrate, one reading at the interface and one reading in the repair. After taking a set of readings the probes were reversed and a second set of

readings taken for each location. This allowed two readings for each location in each specimen. Two specimens for each repair/substrate combination were tested providing an average of four readings.

The impedance spectroscopy results presented in Chapter 5.4 also provide a measure of resistivity in the form of a solution resistance. The solution resistance was taken at the point where the first semi-circle of the Nyquist diagram first crosses the x -axis. This equates to the lowest impedance measured for the cell during the test. This is found at a high frequency (greater than 3000 Hz), when there is no contribution from the charge transfer resistance due to corrosion. Figure 5.21 shows a schematic Nyquist diagram and the point the R_{sol} measurement is taken. Figure 5.19 shows the equivalent point on an impedance frequency plot.

An R_{sol} value was measured for each impedance spectroscopy measurement. Two readings were taken at each measurement location (repair, substrate and interface) and two specimens for each repair/substrate combination. This produced a total of four readings at each measurement location (repair, substrate and interface) for each repair material/substrate combination. The readings were then averaged selectively; any reading with a deviation from the mean of 20% or greater was discarded from the average. This allows one set of readings for the repair, substrate and interface of each specimen at intervals of 2 months. The same measurement circuit was used for each reading. i.e. The R_{sol} reading taken at the repair material used the same measurement path as the repair readings for potential, impedance spectroscopy and LPR readings. The R_{sol} readings can, therefore, be conveniently used to compensate for IR drops in other measurements caused by the resistance of the concrete or repair material.

5.5.2 Results

The results of the resistivity and solution resistance measurements have been presented in the following figures:

Figure 5.37 Resistivity against time for repair material A with 0.4 w/c substrate.

Figure 5.38 Solution resistance against time for repair material A with 0.4 w/c substrate.

Figure 5.39 Resistivity against time for repair material A with 0.8 w/c substrate.

Figure 5.40 Solution resistance against time for repair material A with 0.8 w/c substrate.

Figure 5.41 Resistivity against time for repair material B with 0.4 w/c substrate.

Figure 5.42 Solution resistance against time for repair material B with 0.4 w/c substrate.

Figure 5.43 Resistivity against time for repair material B with 0.8 w/c substrate.

Figure 5.44 Solution resistance against time for repair material B with 0.8 w/c substrate.

Figure 5.45 Resistivity against time for repair material C with 0.4 w/c substrate.

Figure 5.46 Solution resistance against time for repair material C with 0.4 w/c substrate.

Figure 5.47 Resistivity against time for repair material C with 0.8 w/c substrate.

Figure 5.48 Solution resistance against time for repair material C with 0.8 w/c substrate.

5.5.3 Discussion

The changes in resistivity for the different repair substrate combinations show complicated relationships, with few clear trends. Repair materials appear to have different resistivity depending on the substrate to which they are connected. Figures 5.37 and 5.39 show the resistivity of material A when connected to the 0.4 and 0.8 w/c substrate respectively. The average resistivity of material A with the 0.4 w/c substrate is 17.3 kohm/cm and with the 0.8 w/c substrate it is 13.7 kohm/cm.

The same trend is not apparent with material B in Figures 5.41 and 5.43, which has a resistivity of 14 kohm/cm with both the 0.4 and 0.8w/c substrates. However, for material C in Figures 5.45 and 5.47 it is the substrate resistivity that changes. The 0.4

Figure 5.37 Resistivity values for repair material A with 0.4 w/c substrate.

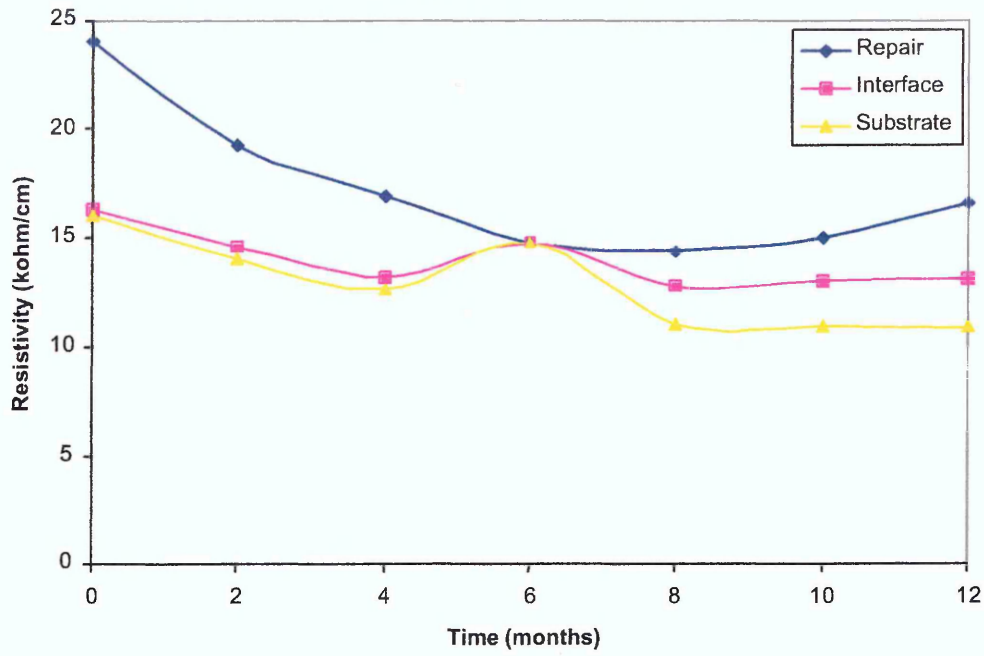


Figure 5.38 R_{sol} Values for Material A with 0.4 Substrate

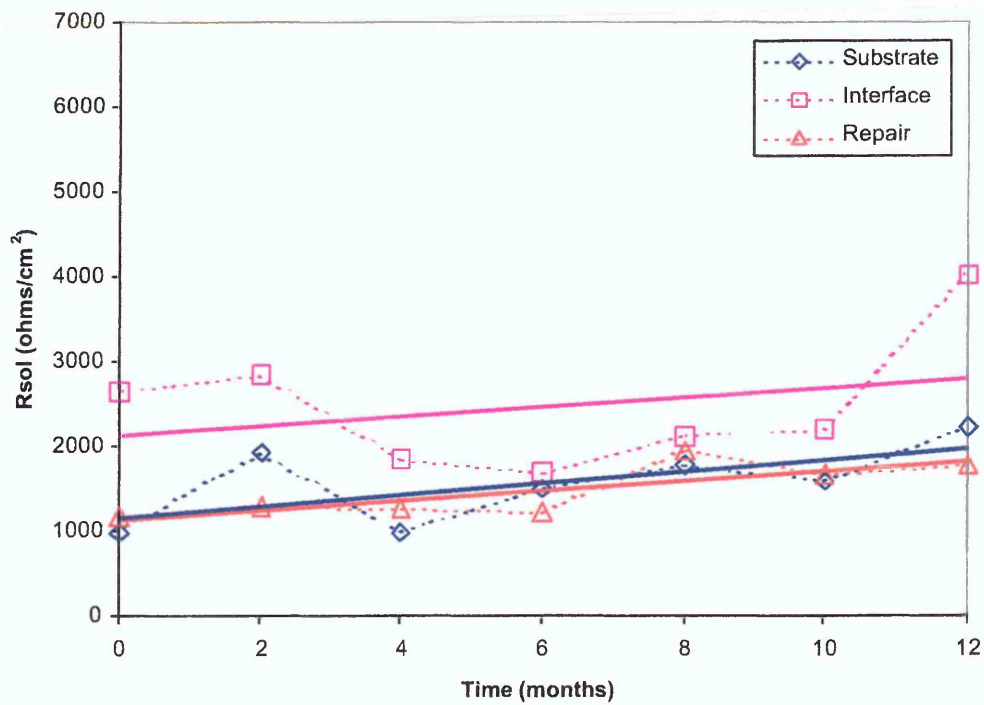


Figure 5.39 Resistivity values for repair material A with 0.8 w/c substrate

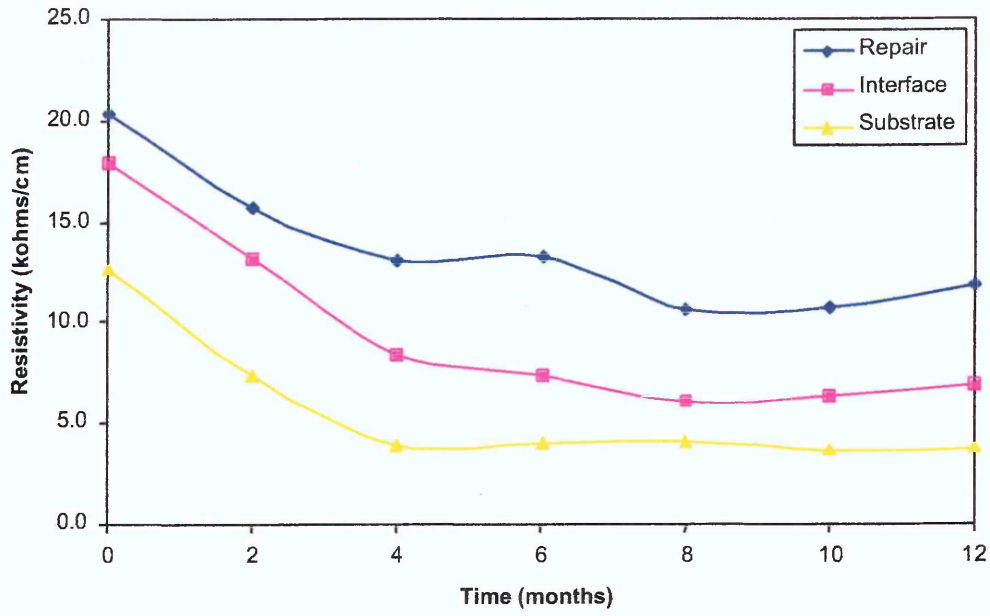


Figure 5.40 R_{sol} Values for Material A with 0.8 w/c Substrate.

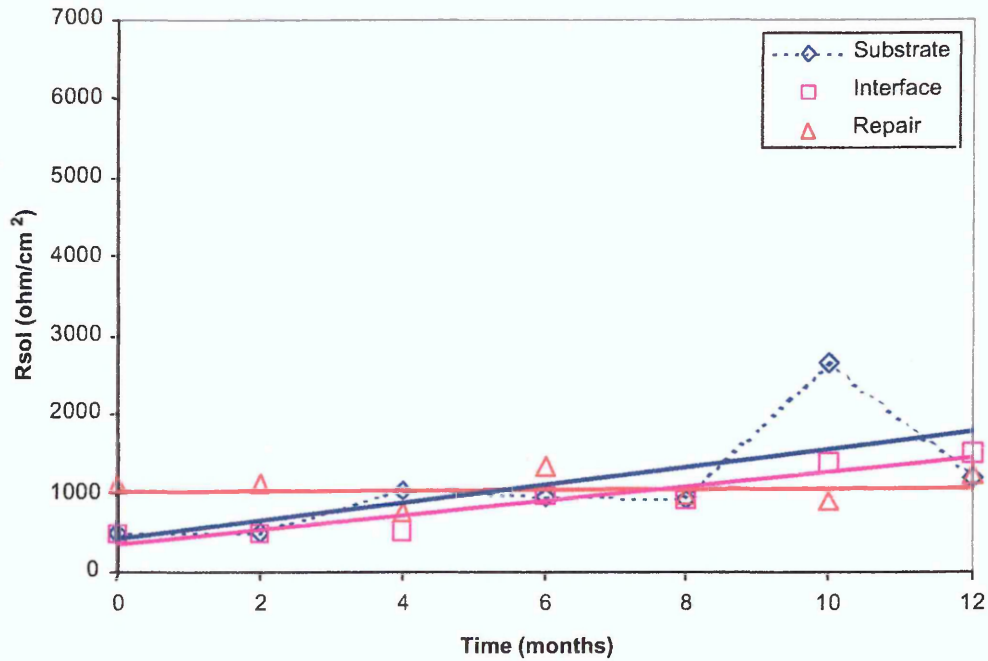


Figure 5.41 Resistivity values for repair material B with 0.4 w/c substrate

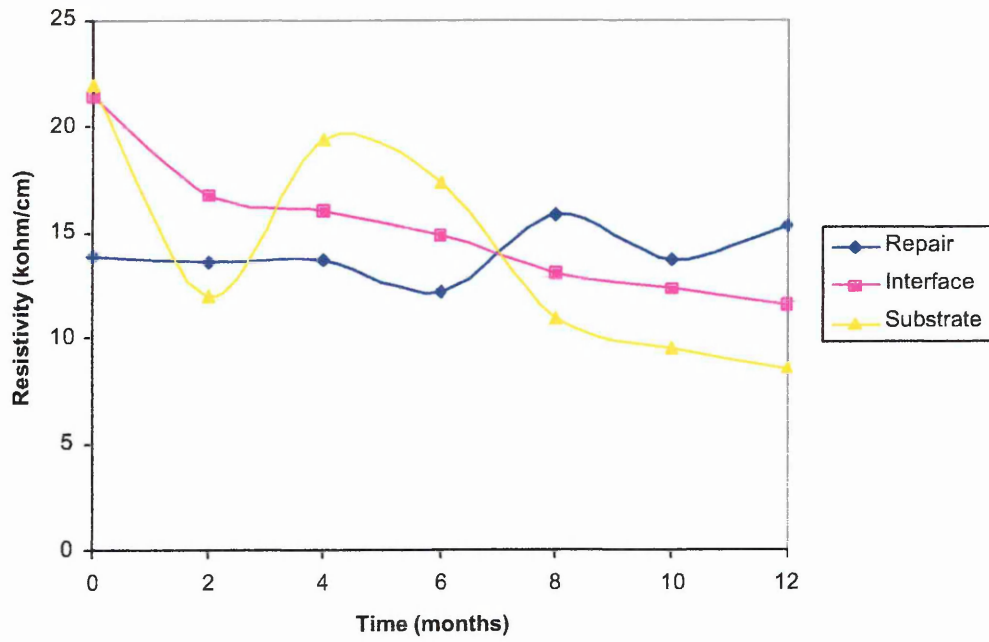


Figure 5.42 Rsol Values for Material B with 0.4 w/c Substrate

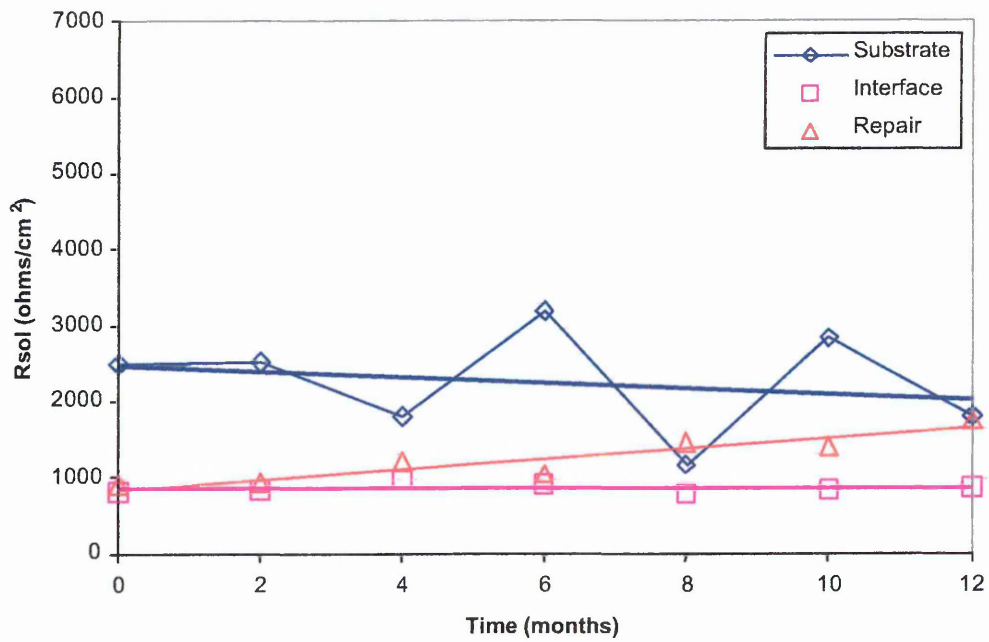


Figure 5.43 Resistivity values for repair material B with 0.8 w/c substrate

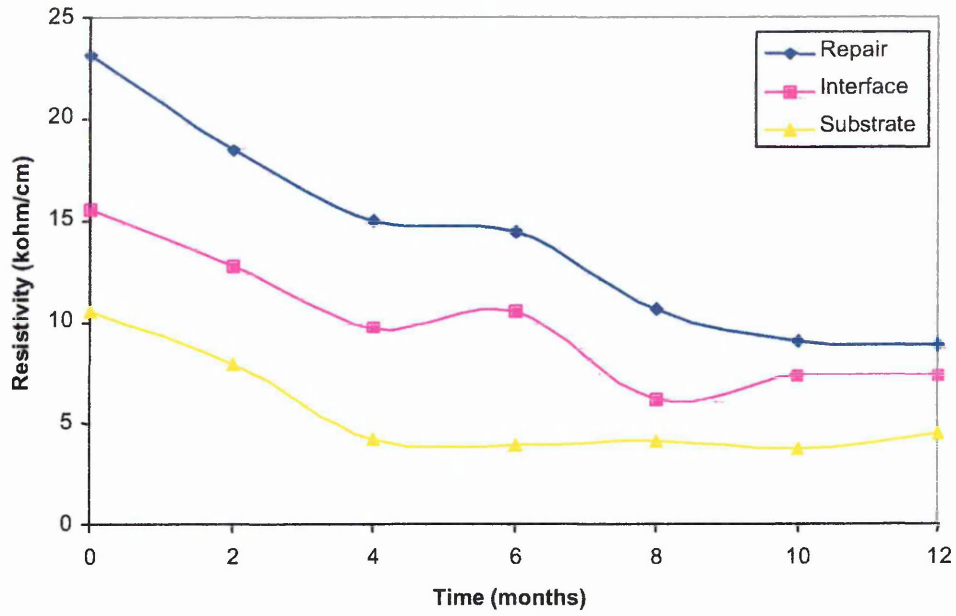


Figure 5.44 R_{sol} Values for Material B with 0.8 w/c Substrate

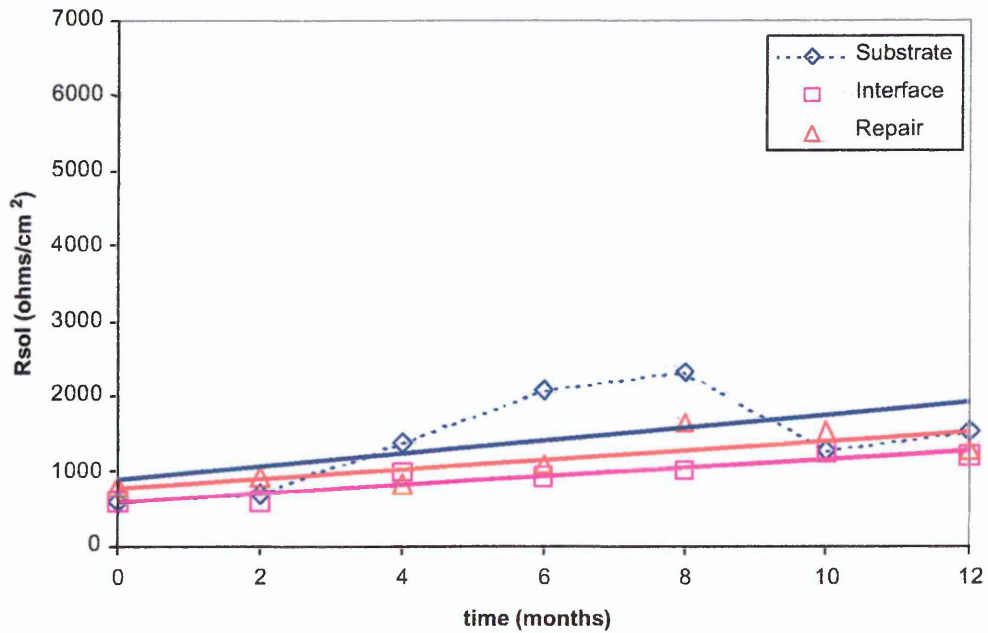


Figure 5.45 Resistivity values for repair material C with 0.4 w/c substrate

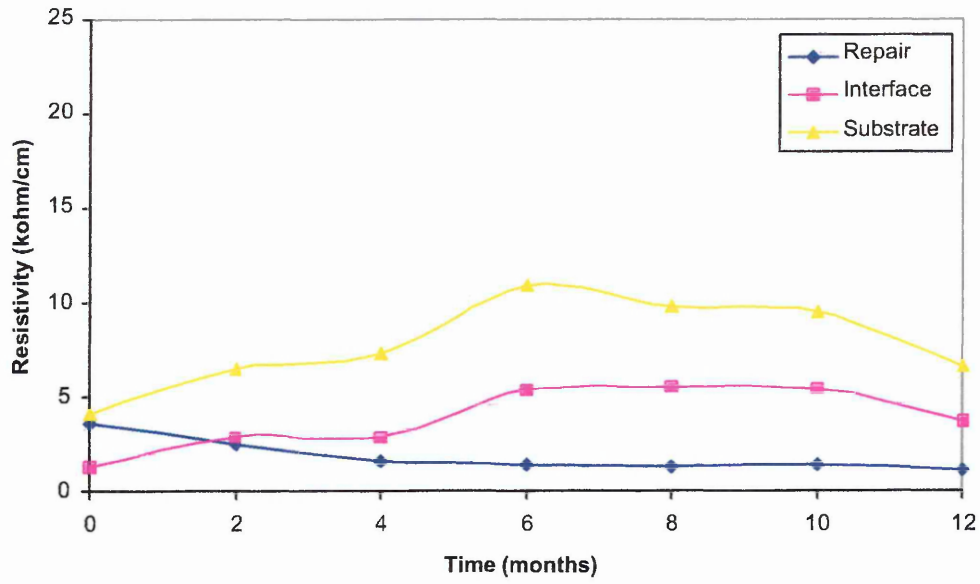


Figure 5.46 R_{sol} Values for Material C with 0.4 w/c Substrate

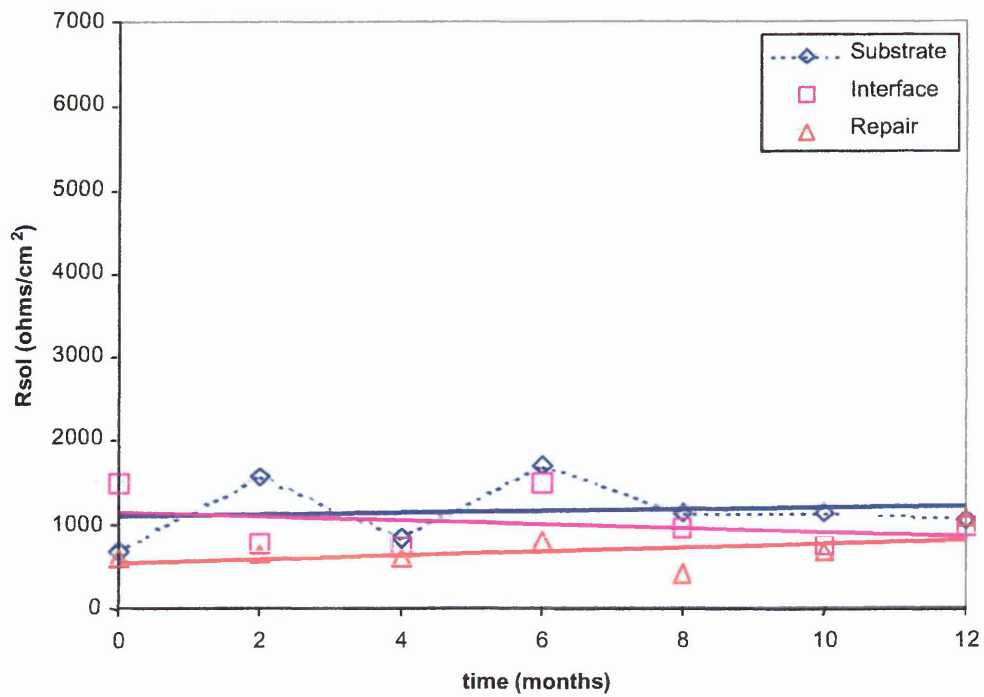


Figure 5.47 Resistivity values for repair material C with 0.8 w/c substrate

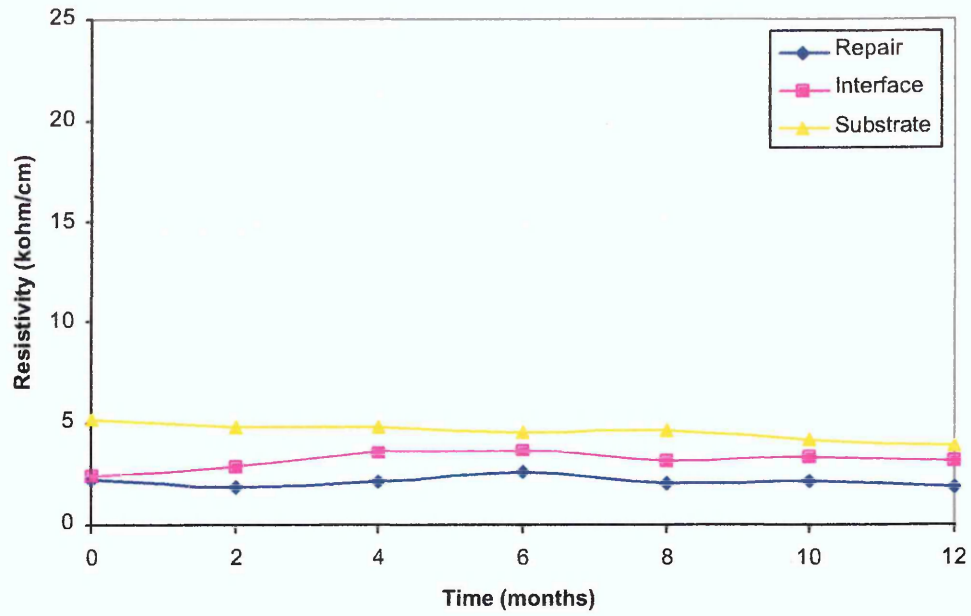
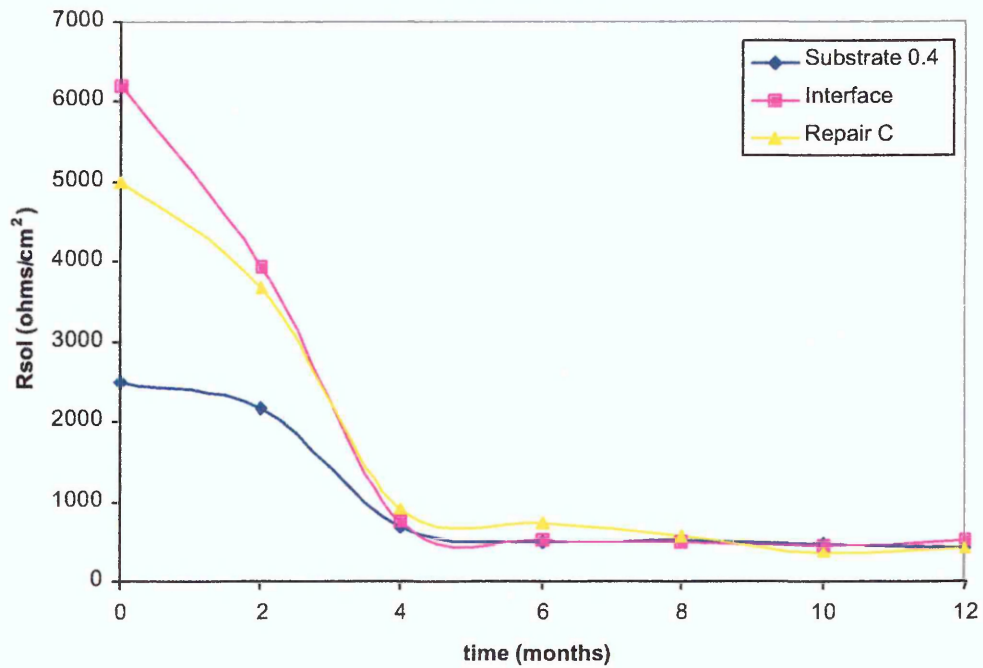


Figure 5.48 R_{sol} Values for Material C with 0.8 w/c Substrate



w/c substrate has an average of 7.8 kohm/cm with material C compared to about 14 kohm/cm with material A and B. For the 0.8 w/c substrate the average is approximately 4.6 kohms/cm compared to 5.6 kohm/cm for materials A and B.

It is unclear from the results how the different substrates effect the resistivity of repair material A, or how material C effects the resistivity of the substrates. It may be that there is movement of solution between the repair materials and substrate possibly by capillary flow. The resistivity falls over 12 months for most of the materials; only material B with the 0.8 w/c stayed constant and material C when combined with 0.4 w/c substrate showed a slight increase. However, material B has a similar permeability to the 0.8 w/c substrate, and so flow between the materials may be limited. Material C has a much higher permeability than the 0.4 w/c substrate and this would suggest a net flow from the repair material to the substrate.

The resistivity of the interface appears in all cases to be merely a function of the repair and substrate resistivity. The resistivity of the interface falls between that of the substrate and the repair material. The resistivity also develops in the same way as that of the substrate and repair material. The surface measurement of resistivity does not appear to be capable of detecting differences or changes in resistivity at the interface and so cannot be related to the structure of the interface.

Examining the graphs of the solution resistances obtained for each of the test specimens it can be seen that the variation in readings can be high on some specimens such as the 0.4 w/c substrate and low for repair material B as shown in Figure 5.41. The variation in the readings could result from changes not taken into account such as resistances at connections in the measurement circuit. The trend in the solution resistances appears to

be relatively stable with time showing only small changes over the 12 months exposure period.

The small differences in solution resistances between repair and substrate would indicate a feature in the test cell used to measure the solution resistance. The solution resistance measures the path of least resistance from the steel to the counter electrode at the surface of the specimen. This would include the interface between the steel and specimen. Any corrosion products on the steel would produce a high resistance barrier. It is possible that a high resistance film at the interface between the steel and concrete is the dominant feature in the measurement and masks changes in the resistance of the cementitious material. This would not apply to the surface resistivity as the probes for measuring the resistivity were located entirely across the material being studied.

The solution resistance results for material A combined with a 0.4 w/c substrate in Figure 5.38 show very small differences in solution resistance over 12 months. The solution resistance of the interface is higher than the substrate and the repair. For material A combined with the 0.8 w/c substrate in Figure 5.40 the solution resistance of the repair material is slightly lower to that measured with the 0.4 w/c substrate. The 0.8 w/c substrate initially has a lower solution resistance but increases with over time, until the trend indicates a solution resistance higher than that of the repair material. In Figure 5.40 the interface has a lower solution resistance than the substrate. The trends are not the same as for the resistivity measurements in Figure 5.39 where repair material A has a higher resistivity than the 0.4 w/c and the 0.8 w/c substrate. The difference in resistivity also appears to represent the difference in permeabilities of the materials, this does not appear to be the case for the solution resistance measurements.

For material B with the 0.4 w/c substrate (Figure 5.42) and the 0.8 w/c substrate (Figure 5.44) the trends are more predictable. The 0.4 w/c substrate has a higher solution resistance than the repair material this is the reverse of the resistivity results in Figure 5.41. For material B with the 0.8 w/c substrate the solution resistances of the substrate and the repair are similar. The permeabilities of the materials show material B to be similar to the 0.8 w/c substrate and, therefore, similar solution resistance values might be expected.

The trend seen for material C with the 0.4 w/c and 0.8 w/c substrates (Figures 5.46 and 5.48 respectively) is not predictable. Repair material C has a higher permeability than the substrate materials. However, solution resistances show the repair material C to have a slightly lower solution resistance than the 0.4 w/c substrate and a similar value to the 0.8 w/c substrate. Material C with the 0.8 w/c substrate in Figure 5.48 was the only set of measurements to show a rapid drop in solution resistance between 0 and 4 months.

The distribution of the solution resistance results in Figure 5.49 show that 90% of the results fall between 400 and 2400 ohms/cm². In this distribution there appears to be no trends to distinguish between different materials and solution resistance appears independent of the material type. This would tend to suggest that the solution resistance reading is relatively insensitive to changes in cementitious materials used in the study.

By comparison the distribution of the resistivity results show a greater spread of results over the range of measurements between 0 and 24 kohm/cm². The results show two peaks between 2 - 4 and 12 - 14 kohm/cm². These peaks correspond to values for the 0.8 w/c and the 0.4 w/c substrates as there were 3 more measurements taken for each of the

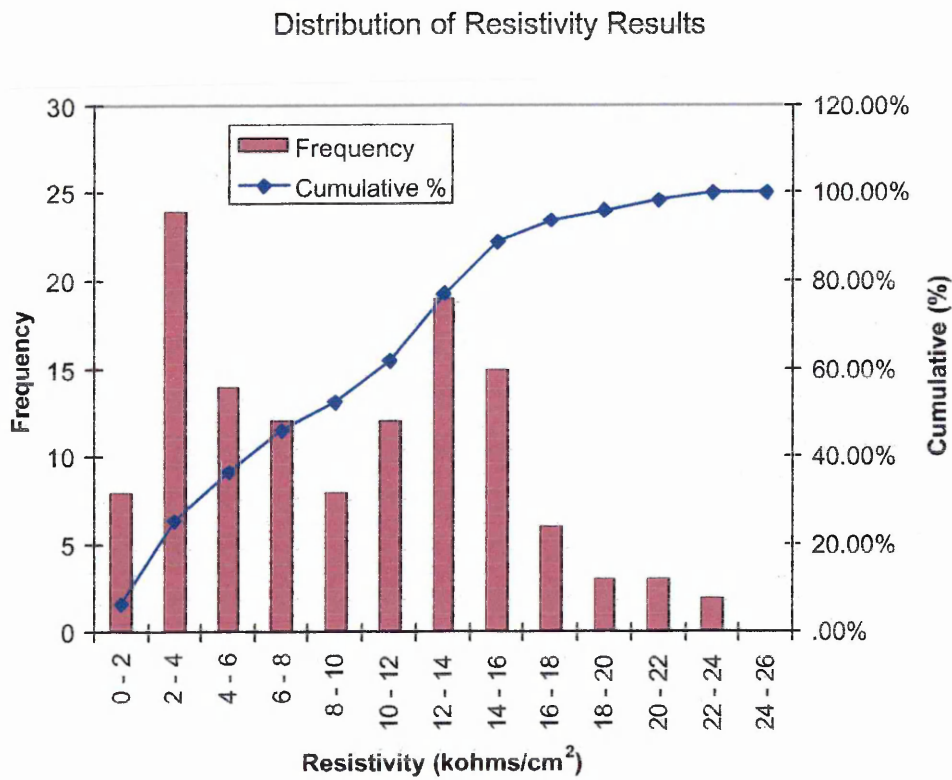
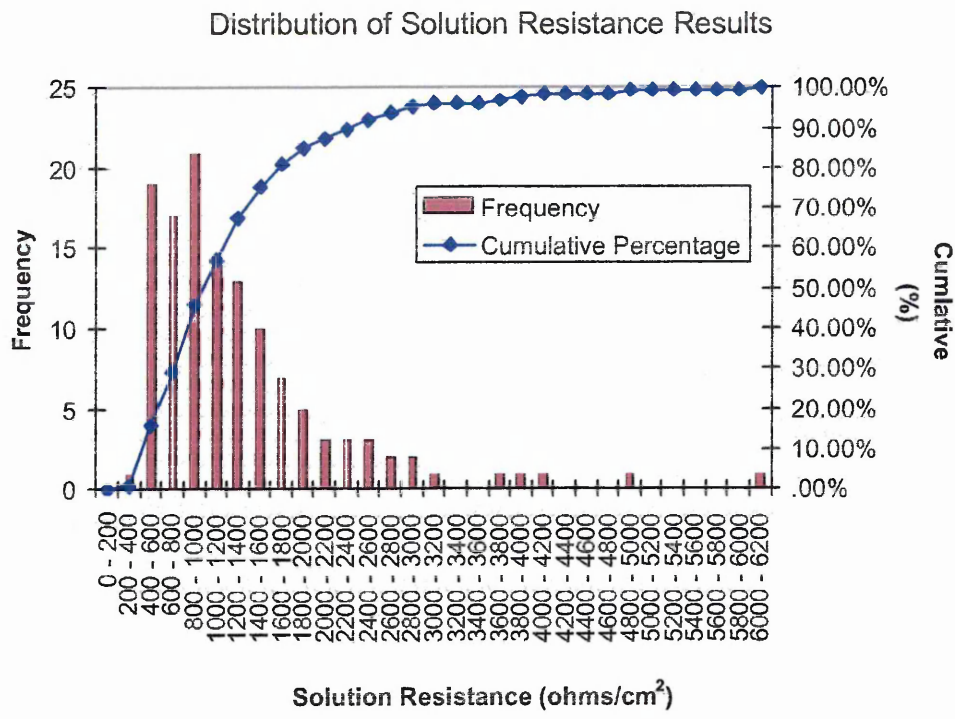
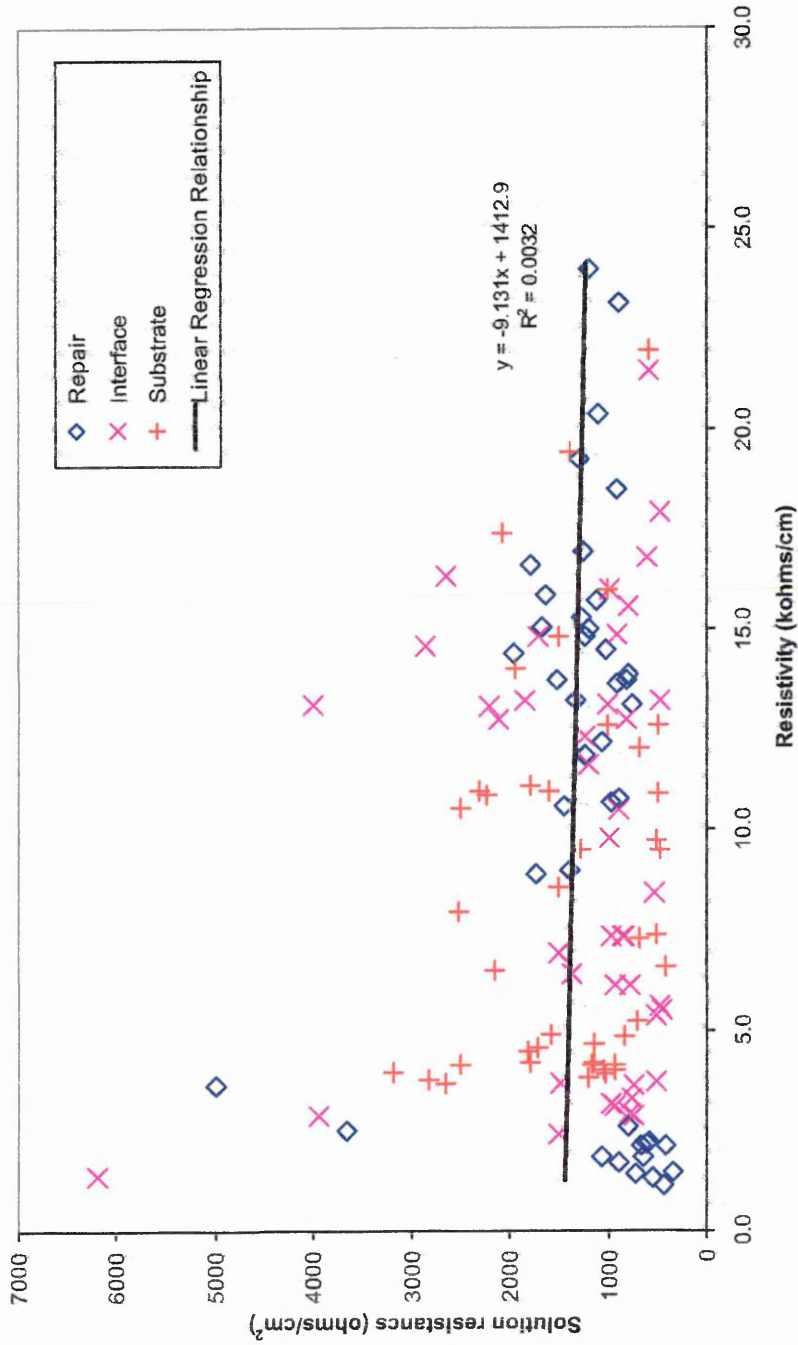


Figure 5.49 Distribution of solution resistance and resistivity results.

Figure 5.50 Relationship between Solution Resistance and Resistivity



substrates compared to the repair materials (9 readings compared to 6 for each repair material).

Figure 5.50 shows a graph of the solution resistance readings with the corresponding resistivity measurement. All the measurements taken at the repair, substrate and the interface are shown on the graph. However, no relationship is apparent from the graph. A linear regression line has been calculated for the results, the correlation coefficient for the line is very low indicating a poor fit to the results. The points appear to be randomly distributed between boundary levels of the measurements. This would appear to be between 400 and 2000 ohm/cm² for solution resistance and 1 to 24 kohm/cm for the resistivity measurements.

5.5.4 Conclusions

The resistivity measurements detect differences in the materials used in the study, but are insensitive to the interface between the two materials used in a test specimen.

The solution resistance results show high levels of variation, this masks changes and makes the measurements appear insensitive to differences in materials.

There is no detectable relationship between solution resistance and resistivity.

Solution resistance does mimic the measurement circuit for other readings taken and will allow a simple method of correcting for IR drop in the specimens.

5.6 Electrochemical Potential Measurements

In experimental studies of the reinforced concrete cell potential measurement is a commonly used technique mainly due to the ease of taking measurements [11, 50, 58, 63, 64, 68, 148 - 152]. Most studies do not carry out a rigorous interpretation of cell potentials, but use them as evidence of corrosion activity in conjunction with other techniques such as LPR or galvanic currents. A potential that becomes more negative with time is taken to show increased corrosion activity and the development of distinct differences in the potential between an anode and cathode to indicate macro-cell corrosion.

The ASTM standard C876 provides a method of relating potential measurements in certain ranges to the probability of corrosion (Section 2.5 Electrochemical Test Methods, table 2.3)[48, 135, 136, 137, 138, 145]. These measurements have been widely used for the assessment of corrosion damage to structures. The relationship of potential to corrosion is an empirical relationship, based on studies of the corrosion of concrete. This relationship has been shown not to be accurate for all situations and care is needed in the interpretation of potential measurements. An example of problems interpreting potential measurements in repaired structures is that dense low permeability repair patches can produce very negative half-cells readings (below -500mV) and still exhibit low corrosion rates. This is due to the low oxygen concentrations in dense repair patches [37], which result in lower half-cell potentials.

Potential measurements were conducted to provide a simple method of assessing the corrosion state of the reinforcement bars embedded in the repair and substrate materials. In addition the relative difference in potentials between the repair and substrate is important for determining the presence of galvanic corrosion cells in the specimens.

5.6.1 Method

The computer-controlled potentiostat automatically measured and recorded the rest potential of each test specimen prior to conducting the impedance spectroscopy measurements (Section 5.4). The experimental arrangement for measuring the rest potentials is as detailed in Figure 5.11. A calomel reference electrode was used to measure the cell potential at three locations along the test specimen corresponding to the repair material, the interface between repair and substrate and the substrate material.

Two rest potentials were measured for each specimen at each location. With two specimens for each repair/substrate combination, a total of four readings were taken for each location in a set of substrate/repair test specimens. The readings were treated in the same manner as the LPR readings. A selective average was taken for the rest potentials with any reading falling outside 25% of the other readings being discarded. However, the variation in rest potentials meant that if more than two readings varied by more than 25%, a non-selective average was taken to calculate the rest potential.

5.6.2 Results

The average potential measurements for each repair substrate combination were plotted as graphs of rest potentials against time.

Figure 5.51 Rest potentials for repair material A with 0.4 w/c substrate.

Figure 5.52 Rest potentials for repair material A with 0.8 w/c substrate.

Figure 5.53 Rest potentials for repair material B with 0.4 w/c substrate.

Figure 5.54 Rest potentials for repair material B with 0.8 w/c substrate.

Figure 5.55 Rest potentials for repair material C with 0.4 w/c substrate.

Figure 5.56 Rest potentials for repair material C with 0.8 w/c substrate.

Figure 5.51 Rest Potentials for Repair Material A with 0.4 w/c Substrate.

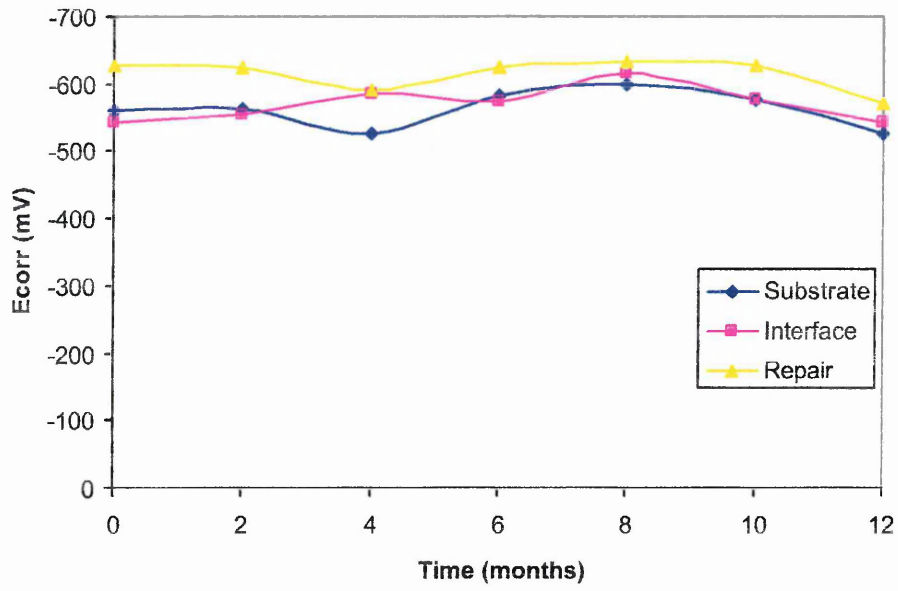


Figure 5.52 Rest Potentials for Repair Material A with 0.8 w/c Substrate

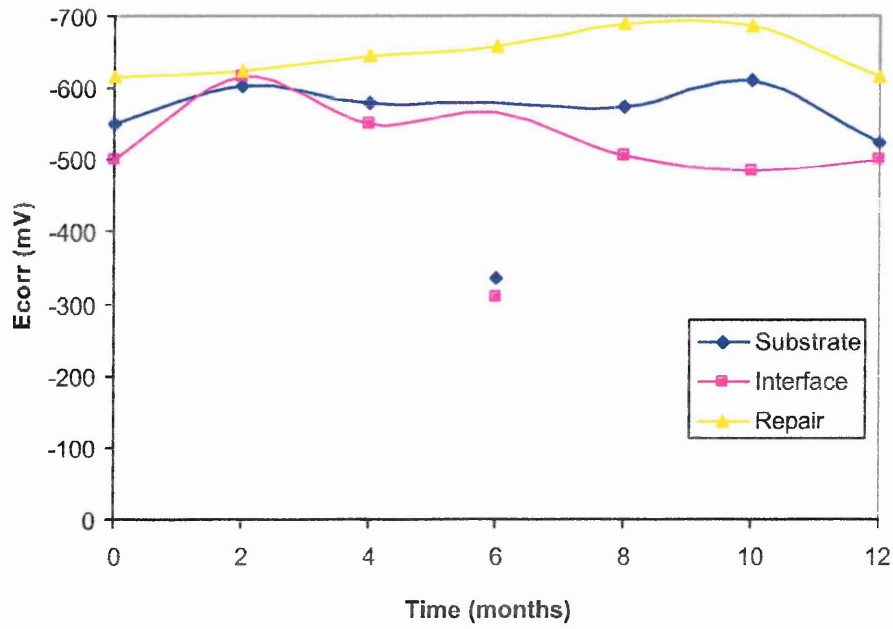


Figure 5.53 Rest Potentials for Material B with 0.4w/c Substrate

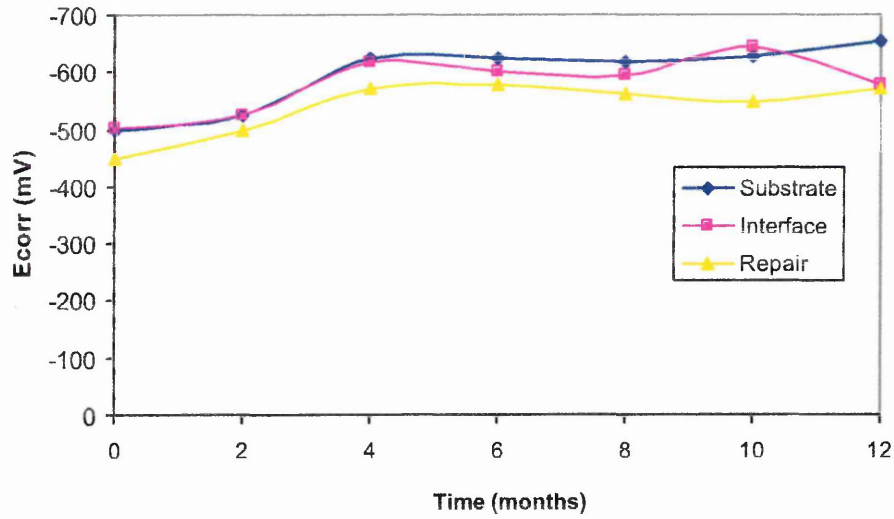


Figure 5.54 Rest Potentials for Repair Material B with 0.8 w/c Substrate

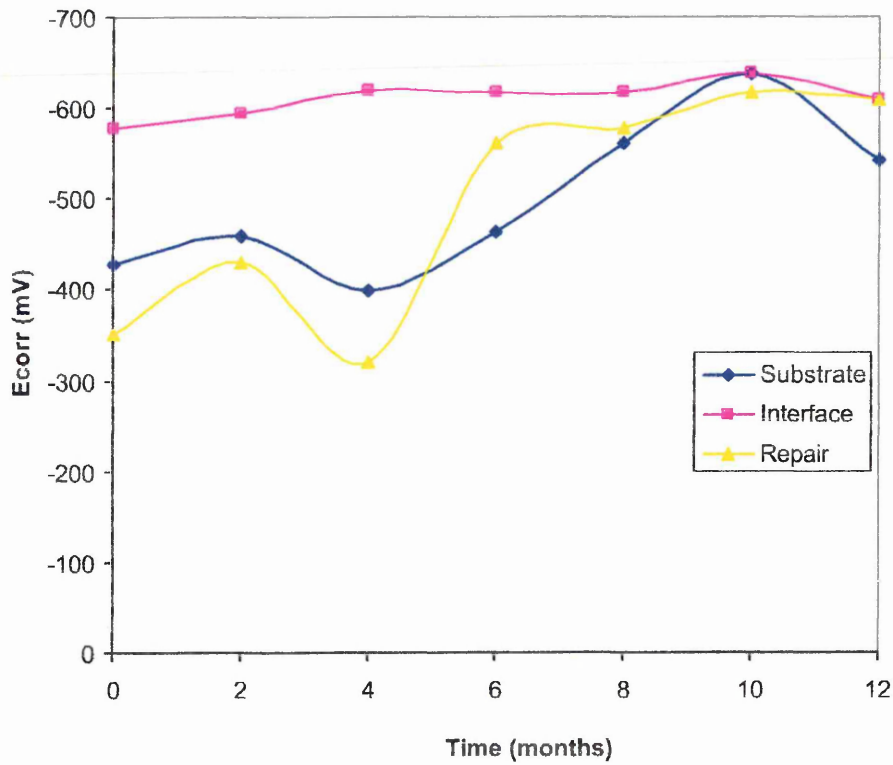


Figure 5.55 Rest Potentials for Repair Material C with 0.4 w/c Substrate

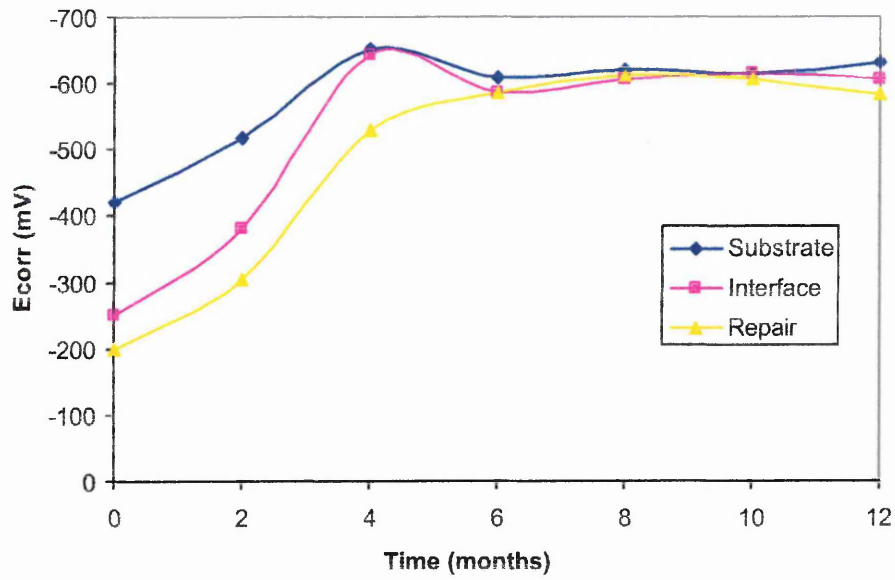
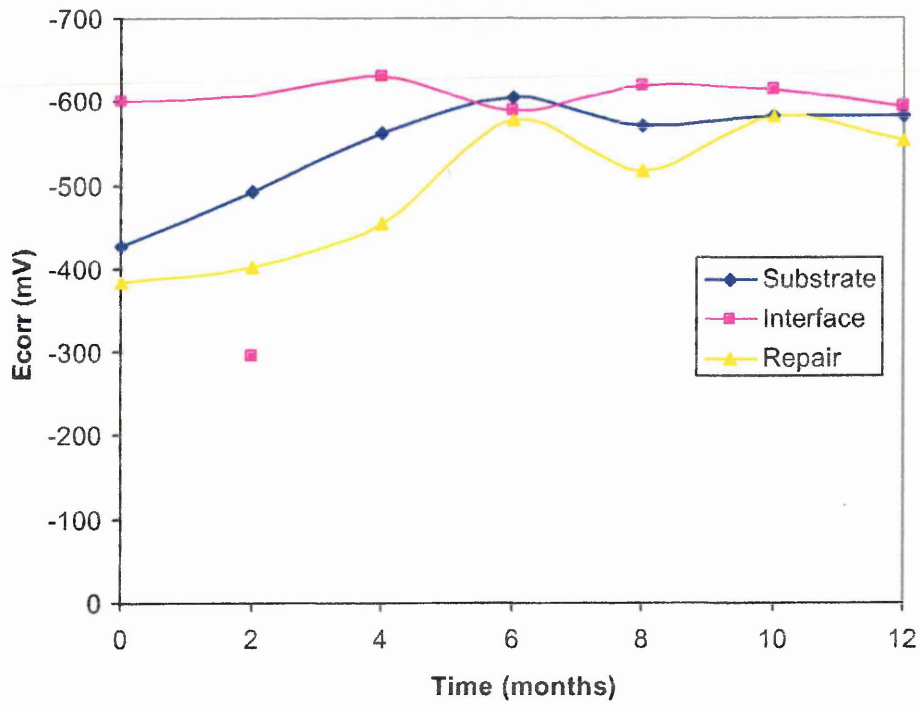


Figure 5.56 Rest Potentials for Repair Material C with 0.8 w/c Substrate



5.6.3 Discussion

The potentials measured vary from approximately -300mV to in excess of -600 mV . Such low potentials could be taken as an indication of a high level of corrosion activity according to ASTM C786. However, in this situation it is more likely that the specimens are fully saturated with water and this may result in a low oxygen concentration in the specimens. The actual potential value may not be a reliable indicator of the level of corrosion of the steel embedded in the repair and substrate materials. The Pourbaix diagram for the iron-water system (Section 2.2.1, Figure 2.5) indicates that any potential in the range -260 mV to -560mV wrt SCE may indicate general corrosion, assuming sufficient chloride is present to break down the passive film on the steel. However, as the flux rate of oxygen at the cathodic site will control the rate of corrosion, a low oxygen concentration would result in a low corrosion rate. All the potential values measured were within the range indicating that the steel embedded in the substrate and repair materials could be subject to general corrosion. Movements in the potential values, such as becoming more negative with time, may also indicate an actively corroding state. The potentials for repair materials B and C (Figures 5.53 to 5.56) became more negative with time, the values for material A (Figures 5.51 and 5.52) showed little change. The potentials measured indicate the possibility of corrosion in all specimens, but cannot provide information on the corrosion rate.

Another aspect to the interpretation of the potential measurements is to indicate if differences in potential exist due to combination of different repair and substrate materials. Differences in potential are required to develop macro corrosion cells. Therefore, if the large difference in physical properties between repair and substrate

materials results in the creation of a macro-cell, then a difference in the potential of the steel embedded in the two materials should be measurable.

In Figure 5.51 for repair material A with the 0.4 w/c substrate it can be seen that the repair material has a more negative potential than the 0.4 w/c substrate. Repair material A has a lower permeability than the 0.4w/c substrate. Material A would be expected to have a lower oxygen concentration and, therefore, a lower potential. The interface has a potential similar to the substrate. This would indicate that the oxygen concentration at the interface is similar to that at the substrate. Figure 5.52 represents material A combined with the 0.8 w/c substrate. The 0.8 w/c substrate has a higher permeability than the 0.4 w/c substrate and, therefore, a higher oxygen concentration than the 0.4 w/c substrate. It would be expected that the potential of the 0.8 w/c substrate in Figure 5.51 would be higher than the 0.4 w/c substrate in Figure 5.52. In addition, there is a much greater difference in rest potentials between material A and the 0.8 w/c substrate in Figure 5.52, compared with the 0.4 w/c substrate in Figure 5.51. The potential of material A would appear to be slightly higher with the 0.8 w/c substrate than with the 0.4 w/c substrate. It is unclear why this may be the case except that it may be due to natural variation of porosity within the material. In both cases there was a measurable difference in potential between the repair and substrate materials.

Material B is more permeable than the 0.4 w/c substrate. (Figure 5.53) and the rest potential of material B is higher (less negative) than that for the 0.4 w/c substrate. The interface occupies a position between the repair and the substrate. By comparison material B has a similar permeability to the 0.8 w/c substrate (Figure 5.54). Here the repair and substrate appear to have a broadly similar rest potential. The Potential of material B and the 0.8 w/c substrate start initially lower than previously recorded in

other specimens but after 12 months have similar values to those previously recorded. The potential at the interface is more negative than the repair material or the substrate suggesting that the interface is less porous than the parent materials.

For material C combined with the 0.4 w/c substrate in Figure 5.55 show the substrate to have a more negative rest potential than the repair material. This continues to follow the trend predicted by oxygen concentration. However, the difference between repair and substrate gets less with time and after 12 months the difference is smaller than might be expected in relation to the other specimens. It would seem that other factors besides oxygen concentration come into play with time. This may be the result of chloride diffusion into the repair material effecting the rest potential, assuming active corrosion has initiated. Figure 5.56 shows material C with the 0.8 w/c substrate, this also shows the substrate with a more negative rest potential than the repair. Again this is as would be predicted by permeability, material C has a higher permeability than either of the substrate materials. The difference between repair and substrate is less for material C with the 0.8w/c substrate as would be expected.

The results show a good consistency with predictions that would be made from permeability results for all test specimens i.e. the lower permeability material has the lowest (more negative) rest potential. However, it is difficult to predict if corrosion has initiated in the specimens. In all cases there was a measurable difference in potential between the repair and substrate materials. This suggests that corrosion macro-cell could exist between the repair and substrate materials.

The situation with the interface is uncertain, the rest potential can be in between the repair and substrate or more or less negative. There appears to be little consistency in

the results. It is likely that the actual condition of the interface plays a role, with the relative degree or ease of compaction of a repair material resulting in either a dense or porous interface. Variations in skill at placing the repair material or material workability could result in large differences in the physical condition of the interface. Unfortunately, these differences were not apparent from the porosity measurements carried out on samples during this study (presented in Chapter 4). Therefore, no evidence can be found to adequately explain the variation in rest potentials measured here.

5.6.4 Conclusions

The potentials measured were all approximately within the general corrosion range – 260 mV to -560mV wrt SCE, as indicated in the Pourbaix diagram for chloride contaminated iron water system [34]. However, due to the possible low oxygen levels in the water saturated specimens it could not be determined if the potentials measured indicated high corrosion levels from ASTM C876.

In all cases the material with the lowest permeability (and lowest oxygen concentration) had the lowest (more negative) potential.

There was a measurable difference in the potential between repair and substrate materials with different permeabilities.

When the repair and substrate had similar permeabilities, material B with the 0.8w/c substrate, the potential of steel embedded in the repair and substrate materials was similar.

5.7 COMPARISON OF CORROSION CURRENTS

5.7.1 Introduction

The earlier experimental work used two different techniques, impedance spectroscopy in Section 5.4 and linear polarisation resistance in Section 5.3. This produced two independent sets of measurements, the intention was to use the two techniques to corroborate the results obtained. This will be achieved in this Section by comparing and contrasting the trends in the two sets of results. The final stage will be to combine the results to produce a single set of measurements and to analyse the trends in corrosion in the repair/substrate combinations examined.

5.7.2 Analysis of Results

The two sets of measurements were taken on the same specimens at approximately the same time (the impedance measurements followed directly after the linear polarisation measurements). This should allow a direct comparison of measurements made using the two techniques. The two measurement techniques also have a number of similarities, both are electrochemical and non-destructive techniques. The measurements taken are used to calculate the polarisation resistance (for LPR) and a charge transfer resistance (for impedance spectroscopy). In each measurement, the resistance obtained is then converted to a corrosion current using the Stern Geary relationship (5.27).

$$i_{corr} = \frac{B}{R_p} \quad 5.27$$

i_{corr} = corrosion current density (A/cm²)

R_p = Polarisation Resistance (ohm/cm²)

B = Combined anodic and cathodic Tafel constants

The measurement of corrosion current offers a number of advantages. They are highly sensitive with resolutions far in excess of those possible by weight loss measurements. In addition the use of Faraday's law (5.28) allows the conversion of corrosion currents to a corrosion rate.

$$P = \frac{Mi_{corr}t}{\rho zF}$$

P = penetration (cm)
 t = time (s)
 ρ = density (g/cm^3) 5.28
 F = Faradays constant (96500 C/mol)
 M = molecular weight (g)
 z = number of electrons transferred per atom

The measurements are sensitive, but have a limited accuracy. The resistance is expressed in units of ohms/cm². The main assumption is that corrosion occurs over the entire surface of the electrode. It is difficult to identify the actual actively corroding area, particularly on an electrode embedded in concrete. The corroding area may be a lot smaller than the entire surface area of the electrode. Therefore, a small corrosion current may indicate a low corrosion rate over the whole electrode or a very high corrosion rate at a small area of the electrode. Generally these techniques are considered insensitive to localised corrosion such as pitting. Also the Stern Geary equation used to calculate the corrosion currents assumes a standard Tafel constant. Work by a number of authors into the use of polarisation resistance measurement technique [33, 134, 164, 165, 166] show that the corrosion current measured by these techniques, while being very sensitive, is not highly accurate and may be in error by as much as a factor of three. In this work Tafel constants were calculated from the potentiodynamic measurements made in Section 5.1 this has improved the potential accuracy to an approximate factor of two.

In this study the absolute accuracy of the results is less important than the assessment of trends. All the measurements reported represent an average from a maximum of four

readings taken from two specimens. Any measurement deviating from the mean by a factor of at least 10 was discarded from the results. The results presented here are an average for each technique.

Figures 5.57 to 5.62 show the corrosion currents measured for each repair material/substrate combination using both measurement techniques. Figure 5.57 shows the results for material A with the 0.4w/c substrate. This shows that both sets of measurements show similar trends in the results taken at particular locations such as at the repair, substrate and interface. However, the specific relationships between the measurement locations does show some differences, the LPR measurements for the repair is lower than the substrate and the interface whereas for impedance spectroscopy it tends to be higher. The impedance spectroscopy results also appear to be on average lower than the corresponding LPR results. Similar results can be seen in figures 5.60 and 5.62 for material B with the 0.8 w/c substrate and material C with the 0.8 w/c substrate.

There are some differences in the results from the different measurement techniques. In Figure 5.58 while the trends in the results are similar the initial impedance spectroscopy readings for the substrate are far higher than those measured using LPR. In Figure 5.59 for material B with 0.4w/c substrate, the trends appear different. Here the impedance spectroscopy results show the interface and substrate measurements decreasing with time, whereas the LPR measurements show them increasing with time. In Figure 5.61, for material C with the 0.4w/c substrate, the trends and relative positions of the measurement locations are the same, but the impedance measurements are higher than the corresponding LPR measurements.

This provides a confused picture of the relationships between the different measurement techniques and makes the identification of trends in the different specimens difficult. Figure 5.63 shows the relationship between the impedance data and the corresponding LPR measurements. The graph shows poor correlation between the two measurement sets. The accuracy limit normally accepted for these types of measurements is a factor of three [33, 134, 164, 165, 166], the lines in Figure 5.63 these limits representing a factor of 3 below and above the line of best fit. If the correlation of results is now compared within these limits of accuracy, it can be seen that the vast majority of the results fall within these lines. Figure 5.64 further considers the data in a frequency distribution bar chart for the differences between the results. The results in Figure 5.64 resemble a normalised distribution with values having a difference of 1 (identical) having the highest frequency. Over 80% of results are within the factor of 3 limit of accuracy for the techniques.

This seems strongly to indicate that the two sets of results are as similar as could reasonably be expected from the accuracy of the two techniques. To further examine trends in the corrosion currents measured for the repair/substrate combinations, each set of results were averaged to produce a single set of results. Therefore, for each repair/substrate combination, there is a single curve for each measurement location, in the repair, substrate and at the interface. These results can be seen in Figures 5.65 to 5.70. A second y axis has been added, showing the corrosion rate on each graph. This was calculated using Faraday's law (equation 5.28) and assumed that corrosion was uniform over the entire electrode surface. In reality it is more likely to be localised to discrete areas of the electrode. However, the corrosion rate is an easily understood parameter useful for showing trends in the specimens.

5.7.2.1 Comparison of corrosion currents in different repair substrate combinations.

Figures 5.65 and 5.66 show material A combined with the 0.4 and 0.8 w/c substrate respectively. Material A is the dense low permeability repair material. In both case the substrate starts with a high corrosion rate and falls with time. The corrosion rate of the repair material increases with time, in both specimens the corrosion rate for material A is very similar. In the case of the 0.8 w/c substrate in Figure 5.66 the corrosion rate of the substrate falls to a level below that of the repair after 12 months. However for the 0.4w/c substrate in Figure 5.65 the substrate always corrodes at a higher level than the repair. The interface appears to follow either the repair or the substrate.

The permeability of material B is between material A and C. Figures 5.67 and 5.68 show the corrosion rates of the two substrate combinations with material B. In both cases the substrate starts from a lower corrosion rate, which rises with time, as opposed to a high corrosion rate falling with time as for material A. The repair material shows similar behaviour to material A with corrosion rate rising with time. For the specimens made with material B the interface exhibits a higher corrosion rate than the repair or substrate.

Figures 5.69 and 5.70 show the corrosion rates for the specimens combining repair material C with the 0.4 and 0.8w/c substrates. Material C has the highest permeability of the three repair materials examined. Figure 5.69 shows material C combined with the 0.4w/c substrate. The repair material develops a higher corrosion rate than the substrate of approximately 0.2 mm/yr after 12 months. In comparison with the repair material the substrate reached a corrosion rate of 0.1 mm/yr after 12 months. Despite the errors

inherent in the Stern Geary equation used to calculate the corrosion currents, this difference appears significant. The interface readings follow those of the repair material.

Figure 5.70 shows material C combined with the 0.8w/c substrate. The repair material reaches a corrosion rate of 0.1 mm/yr after 12 months, this is approximately half that for material C when combined with the 0.4w/c substrate in Figure 5.69. In addition the 0.8w/c substrate also has a corrosion rate of 0.05 mm/yr, approximately half that of the 0.4w/c substrate when combined with material C. The corrosion rate of the 0.8w/c substrate is approximately twice that of repair material C in both figures 5.69 and 5.70, suggesting that the difference in corrosion rates between repair and substrate is significant. The interface between repair material C and the 0.8w/c substrate, follows the substrate as opposed to the repair material as in Figure 5.69.

Of the repair materials examined, the highest permeability material C has the highest corrosion currents after 12 months. The chloride diffusion results in Section 4.4 show that material C also had the highest chloride levels after 12 months. This suggests that the chloride levels are responsible for the highest corrosion of material C. However, material B has a slightly lower corrosion rate than material A after 12 months, even though the permeability (and chloride concentration) of material A is less than that of material B. A similar phenomenon can be seen in the substrates, the lower permeability 0.4w/c substrate has a higher corrosion rate after twelve months than the 0.8w/c substrate. In each substrate/repair combination the 0.8w/c substrate appears to have a corrosion rate of approximately 0.05mm/yr after twelve months compared with 0.1mm/yr for the 0.4w/c substrate. The interface appears to follow the results of either the repair or the substrate.

Figure 5.57 Corrosion currents measured using impedance spectroscopy and linear polarisation resistance for material A with 0.4 w/c substrate.

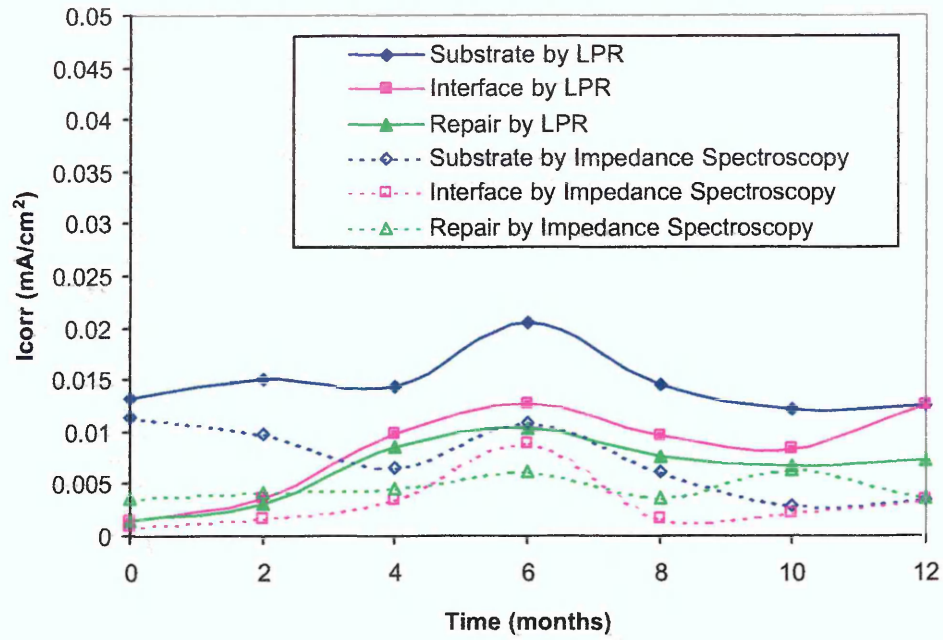


Figure 5.58 Corrosion currents measured using impedance spectroscopy and linear polarisation resistance for material A with 0.8 w/c substrate.

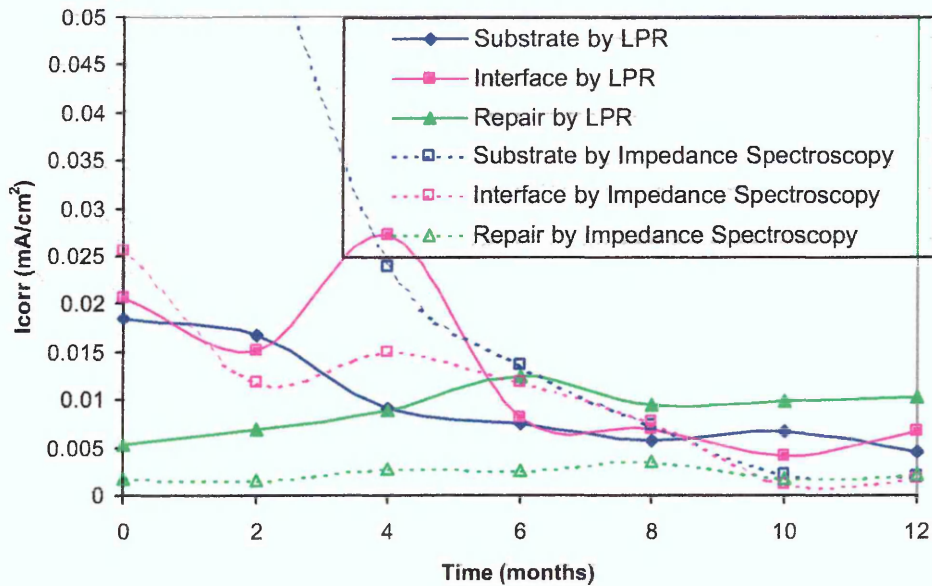


Figure 5.59 Corrosion currents measured using impedance spectroscopy and linear polarisation resistance for material B with 0.4 w/c substrate.

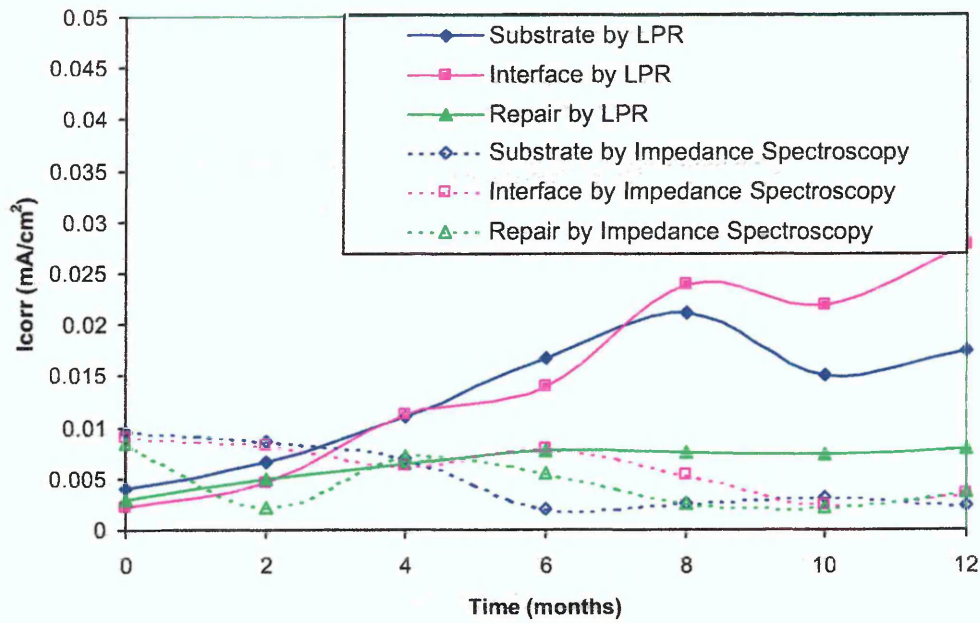


Figure 5.60 Corrosion currents measured using impedance spectroscopy and linear polarisation resistance for material B with 0.8 w/c substrate.

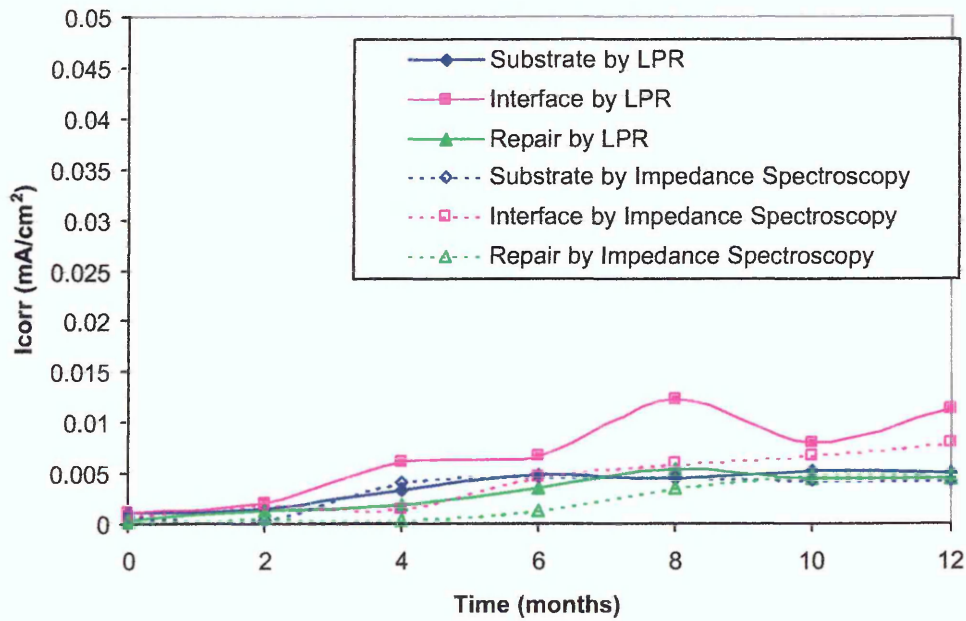


Figure 5.61 Corrosion currents measured using impedance spectroscopy and linear polarisation resistance for material C with 0.4 w/c substrate.

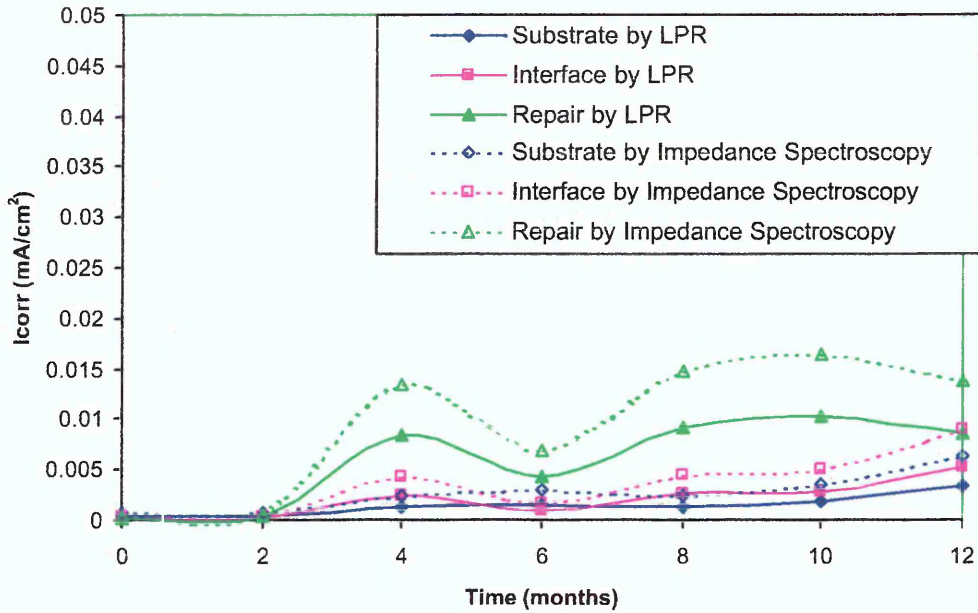


Figure 5.62 Corrosion currents measured using impedance spectroscopy and linear polarisation resistance for material C with 0.8 w/c substrate.

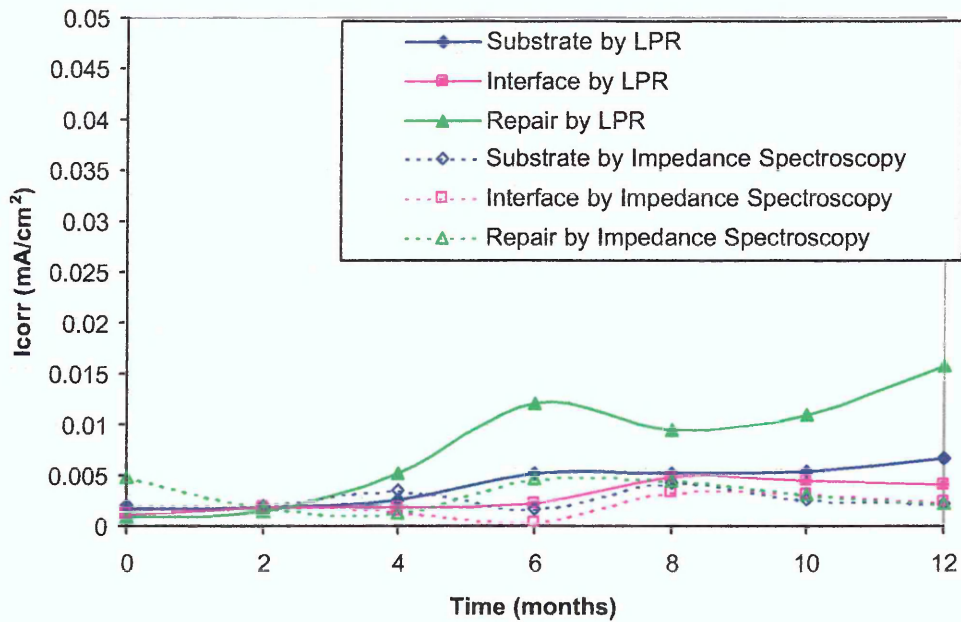


Figure 5.63 Comparison of corrosion currents obtained using linear polarisation resistance measurements and impedance spectroscopy measurements.

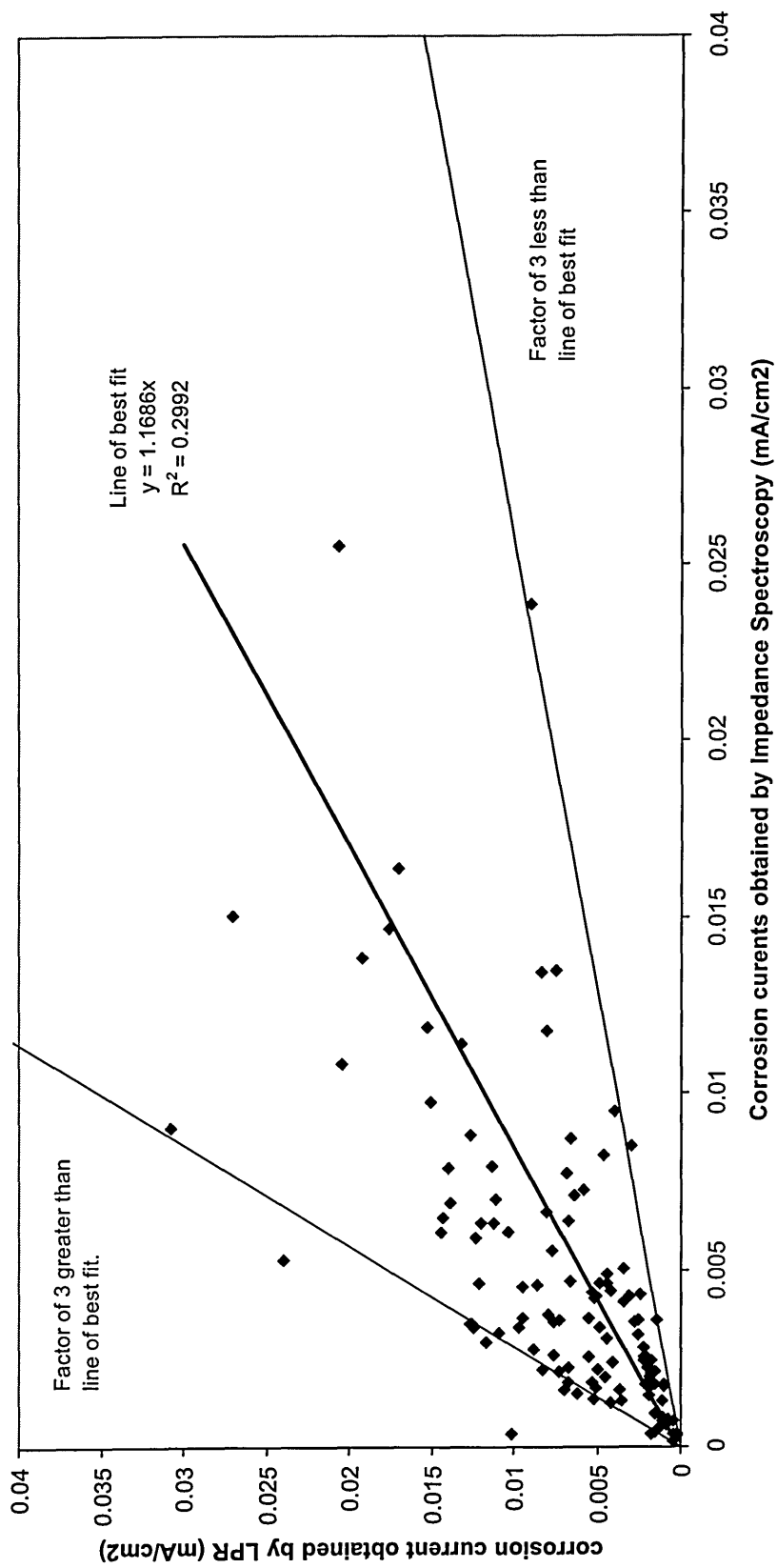


Figure 5.64 Distribution of the difference in magnitude of corrosion currents obtained using impedance spectroscopy and linear polarisation resistance.

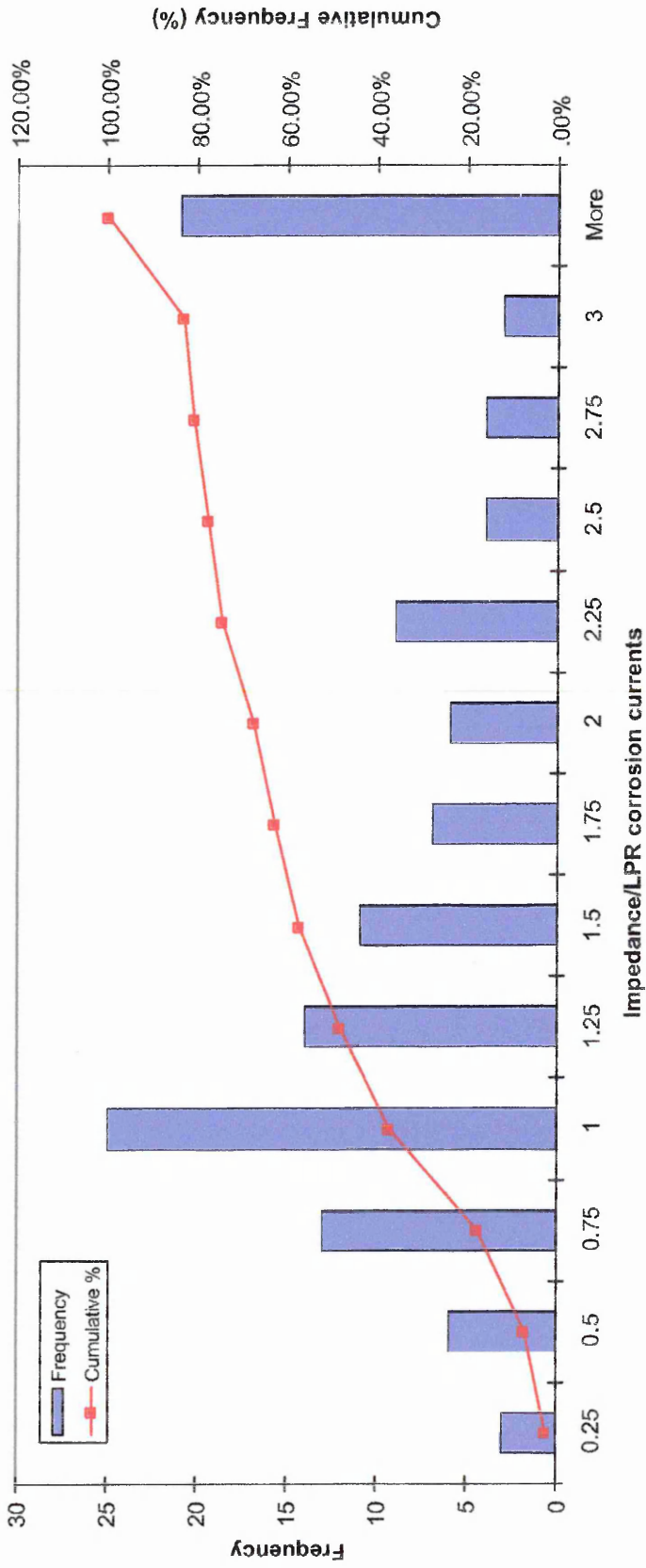


Figure 5.65 Corrosion rate with time relationship for repair material A with 0.4 w/c substrate.

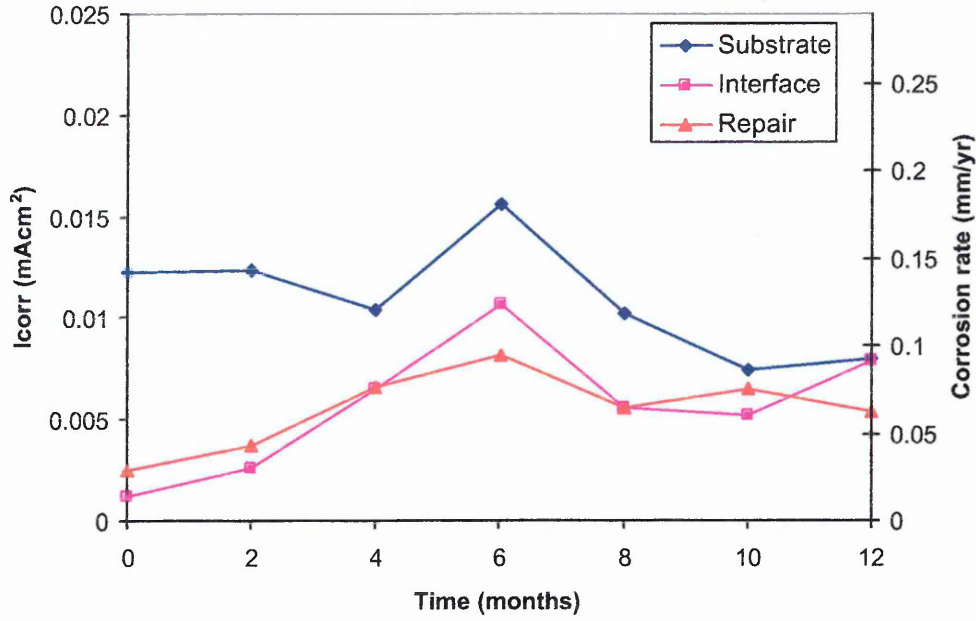


Figure 5.66 Corrosion rate with time relationship for repair material A with 0.8 w/c substrate.

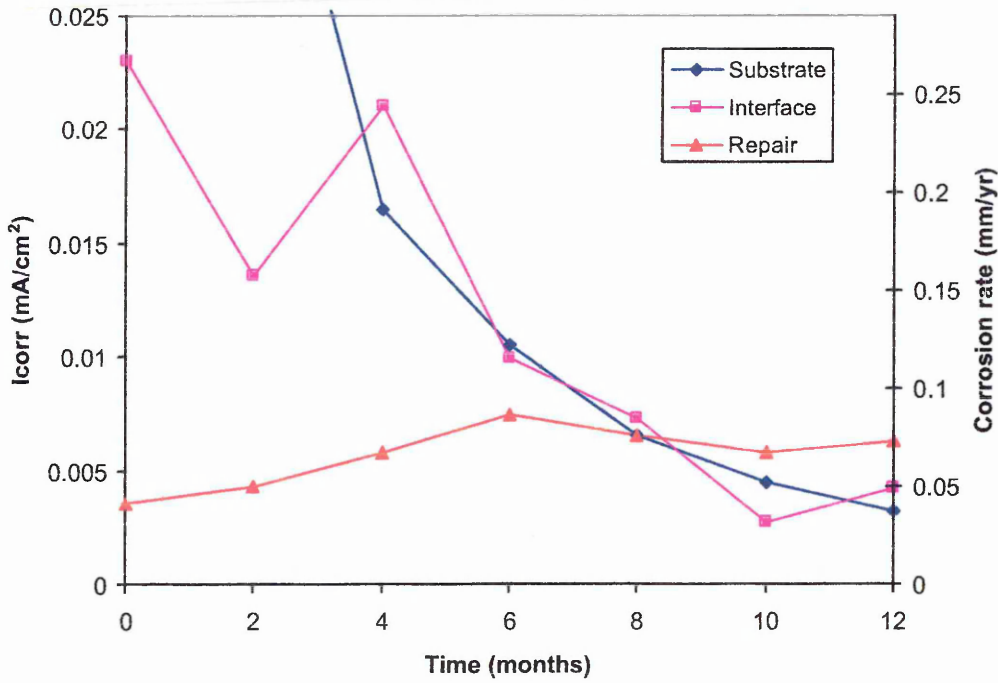


Figure 5.67 Corrosion rate with time relationship for repair material B with 0.4w/c substrate.

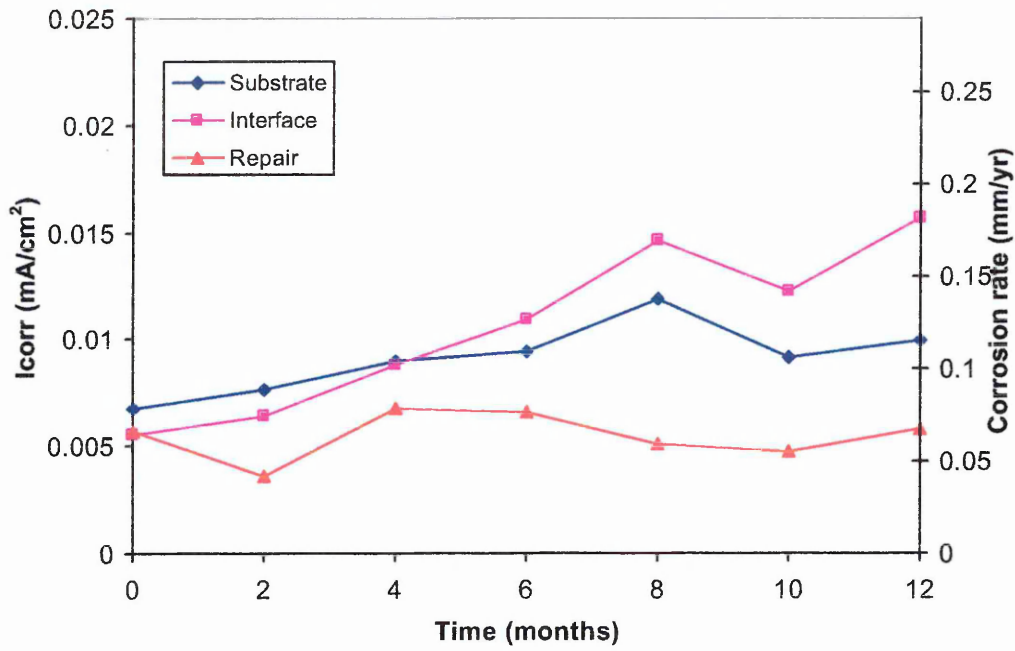


Figure 5.68 Corrosion rate with time relationship for repair material B with 0.8 w/c substrate.

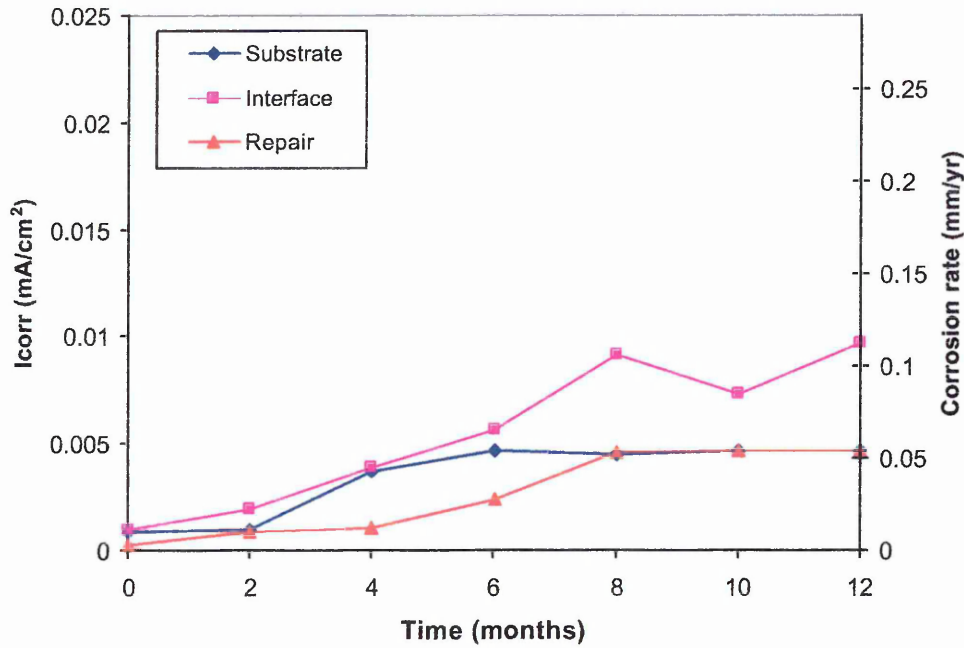


Figure 5.69 Corrosion rate with time relationship for repair material C with 0.4 w/c substrate.

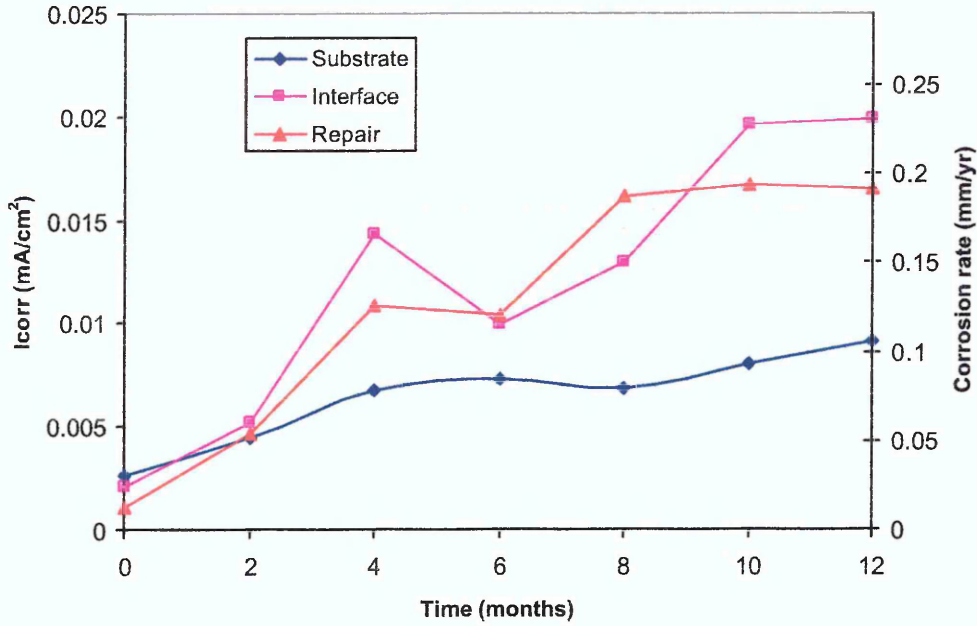
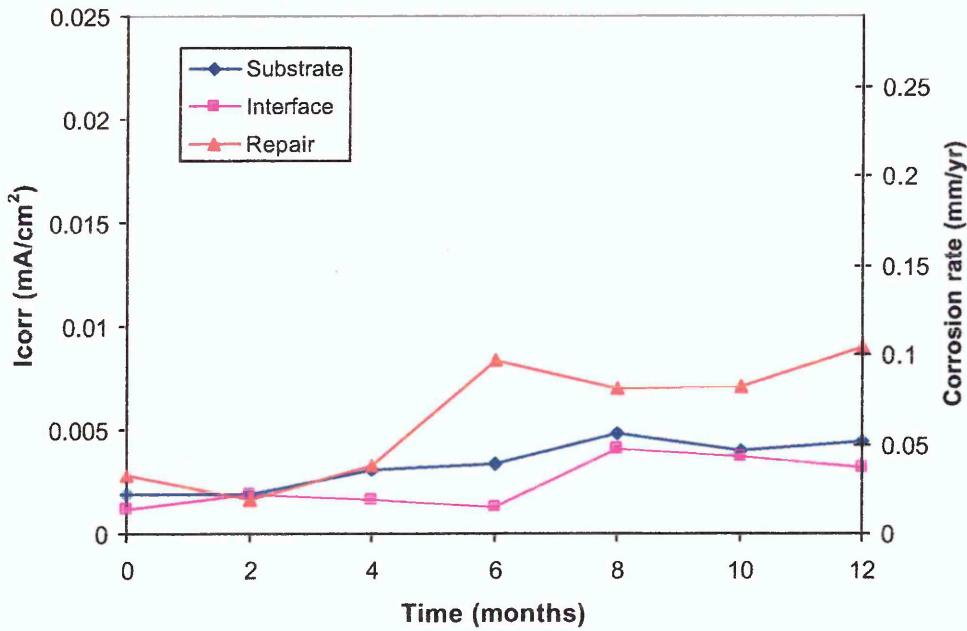


Figure 5.70 Corrosion rate with time relationship for repair material C with 0.8 w/c substrate.



5.7.3 Conclusions

The corrosion currents obtained by impedance spectroscopy are in most cases lower than those obtained by linear polarisation resistance. The trends in corrosion currents obtained using the two techniques are similar.

Over 80% of the impedance spectroscopy measurements produce corrosion currents within a factor of 3 of the corresponding linear polarisation resistance measurements. These are within the accuracy limits suggested by other authors for these techniques. This suggests that the two sets of measurements are the same and that it is valid to produce a single set of results from the average of the two measurements.

The averaged results from the two techniques showed that material A had a corrosion rate below the 0.8w/c substrate but higher than the 0.4w/c substrate after 12 months.

Material B had a corrosion rate similar or lower than both substrate materials. The corrosion rate of material C was higher than the substrate materials after 12 months. The difference in corrosion rate between repair and substrate materials was greater than a factor of 2 suggesting that the difference was significant, except for material A and B with the 0.8w/c substrate.

After 12 months the 0.4w/c substrate had a corrosion rate of approximately 0.1mm/yr, while the 0.8w/c substrate had a lower corrosion rate of approximately 0.05 mm/yr.

The interface between the repair and substrate follows either the repair or the substrate readings, except for material B with the 0.8w/c substrate.

6.0 Analysis of the effect of disparity in material properties on reinforcement corrosion.

6.1 INTRODUCTION

The experimental work reported in Chapter 5 combined different repair and substrate materials in test specimens and monitored corrosion of the reinforcement with time. The associated work on physical properties reported in Chapter 4 determined the properties of the repair and substrate materials used in the study. This chapter will combine these two areas of work to examine the effects of the disparity in properties between the repair and substrate materials on reinforcement corrosion.

The effect of differences in physical properties on the corrosion of steel embedded in cementitious materials has been investigated by a number of authors. Ping Gu et al [20, 230] examined the effect of porosity mismatch and proposed that due to differential aeration, corrosion could reinitiate in a lower porosity material when combined with a higher porosity material. This argument was developed into a theory for the electrochemical incompatibility of patch repairs in reinforced concrete. This work has influenced Emmons et al [22,23] to develop a system concept for concrete repairs. Cusson et al [21] recommend that porosity and resistivity of a repair material and the substrate material should be equal to ensure the durability of patch repairs. This work suggests that the durability of repair is related to the disparity in properties between the repair and substrate materials. However, work by Lambe et al [26] concluded that while it was important to view the region of repair as one electrochemical system, repair materials with lower diffusion rates for oxygen, chloride and moisture would provide

better protection for repair. This contradicts the idea of matching properties as a method of improving durability of the repair.

There is a lack of experimental work to investigate the likely effects of mismatches in properties. The current experimental work is intended to provide a further insight into the effect of disparities in physical properties of the repair and substrate materials on corrosion of reinforcement in repair patches. This is based on the three main measurements conducted in the corrosion testing work (Chapter 5), resistivity, electrochemical potential and corrosion currents. Resistivity provides a measure of the conductivity of the repair substrate environment. Electrochemical potential represents the thermodynamics of the corrosion cell and corrosion currents the kinetics of the corrosion reaction. These have been related to the main physical parameters determined in chapter 4, chloride content and permeability, for each of the repair and substrate materials.

6.2 EFFECT OF DISPARITY IN PROPERTIES ON RESISTIVITY

Resistivity is a measure of the conductivity and represents the ease of movement of an electric current in the cell. In the present work, conductivity of the repair and substrate materials would be expected to influence the rate of corrosion in the material. A high conductivity would allow high rates of corrosion and low conductivities the reverse. The Resistivity measurements in the current study were made against exposure time for all the specimens and have been discussed in detail in Chapter 5.3. Two techniques were used to assess the resistivity of concrete; a standard resistivity technique and solution resistance.

Previous resistivity measurements, conducted as part of the determination of the physical properties in Chapter 4, found that the level of water saturation and chloride content in the material was important in the resistivity value measured. This produced a strong relationship between the porosity of the material and resistivity value. The measurements were conducted on water saturated test specimens and the pore structure of the material was filled with water. Materials with higher porosity contained more water and had correspondingly lower resistivity. Therefore, resistivity measurements would be influenced by changes to the physical and chemical nature of the specimens during the test. Factors such as the diffusion of water through the material and temperature fluctuations would alter the resistivity measurements. To eliminate these the specimens were kept in a saturated condition at a constant temperature. Other factors that would influence resistivity, such as the diffusion of chlorides into the specimens and the refinement of the pore structure were not controlled in the experimental work.

Table 6.1 shows the averages for the solution resistance and resistivity measurements taken from Chapter 5.3 over 0-6 months, 6-12 months and 0-12 months. This is a simplification of the resistivity and solution resistance measurements taken, but provides an effective summary of the main conclusion from the work. Table 6.1 shows that for all the materials, resistivity fell from the first 6 months to the second six months of the study. By comparison solution resistance increased for all the materials except material C. This shows a contradiction between the two sets of measurements. However, the techniques differ in how the measurements were conducted. Resistivity measurements were taken from holes drilled through the surface of the specimen and the measurements made using a hand held resistivity meter. The readings consist of measurements made in the repair or substrate material only. Solution resistance was

measured as part of the impedance spectroscopy work in Chapter 5.4. Therefore, solution resistance measured the specific resistance of the cell used in the corrosion current measurements. It includes the repair or substrate material and the interface between the reinforcement and the material.

The decrease in resistivity indicates that all the materials (repair or substrate) became more conductive with time and, therefore, more corrosive. This is probably due to the diffusion of chloride into the materials with time.

The increase in solution resistance indicates an increase in resistance in the measuring circuit and, therefore, less corrosion. The most likely explanation is the formation of corrosion products on the reinforcement surface. This would form a high resistance film on the surface of the steel and increase the solution resistance. This suggests that the corrosion within the cells was under resistance control (see Evans diagram Figure 2.6). Eventually the formation of corrosion products could stop or slow corrosion by blocking the electrode surface from the electrolyte.

The two measurements together may indicate that the electrolyte (repair or substrate material) become more corrosive, but the reinforcement steel becomes less corrodible with time. However, resistivity or solution resistance do not provide a measure of the corrosion rate of the steel embedded in either repair or substrate materials. The kinetics of the corrosion reaction, obtained from the corrosion currents will be discussed later in this chapter.

Table 6.1 Average Resistivity and Solution Resistance Measurements

Material	Average Resistivity (k Ω cm)			Average Solution Resistance (Ω cm ²)		
	0-6	6-12	0-12	0-6	6-12	0-12
	Months	Months	Average	Months	Months	Average
A	17.17	13.22	15.20	1167.26	1424.58	1295.92
B	15.57	12.22	13.89	959.20	1506.611	1232.91
C	2.24	1.67	1.96	1616.26	581.32	1098.79
0.4 w/c	13.08	9.75	11.41	1337.178	1346.13	1341.65
0.8 w/c	6.16	4.08	5.12	1485.63	1548.76	1517.19

The relationship between resistivity and permeability coefficients for the repair and substrate materials is shown in Figure 6.1. This shows that materials with lower permeabilities tend to have a higher resistivity. Similarly, figure 6.2 shows that materials with higher chloride concentrations at the steel tend to have lower resistivity. In the work on the physical properties of the materials (Chapter 4), the chloride diffusion coefficient of a material was found to be related to the permeability. This would suggest a relationship between chloride concentration and permeability. Therefore, the relationships for resistivity with permeability and chloride concentration, shown in figures 6.1 and 6.2, should be the same. However, the relationship in Figure 6.2 is poorer than in Figure 6.1, due to the addition of chloride at mixing for the substrate concretes. This produced artificially high levels of chloride in the substrate materials in comparison to the repair materials.

Figure 6.1 Relationship between resistivity and permeability coefficients.

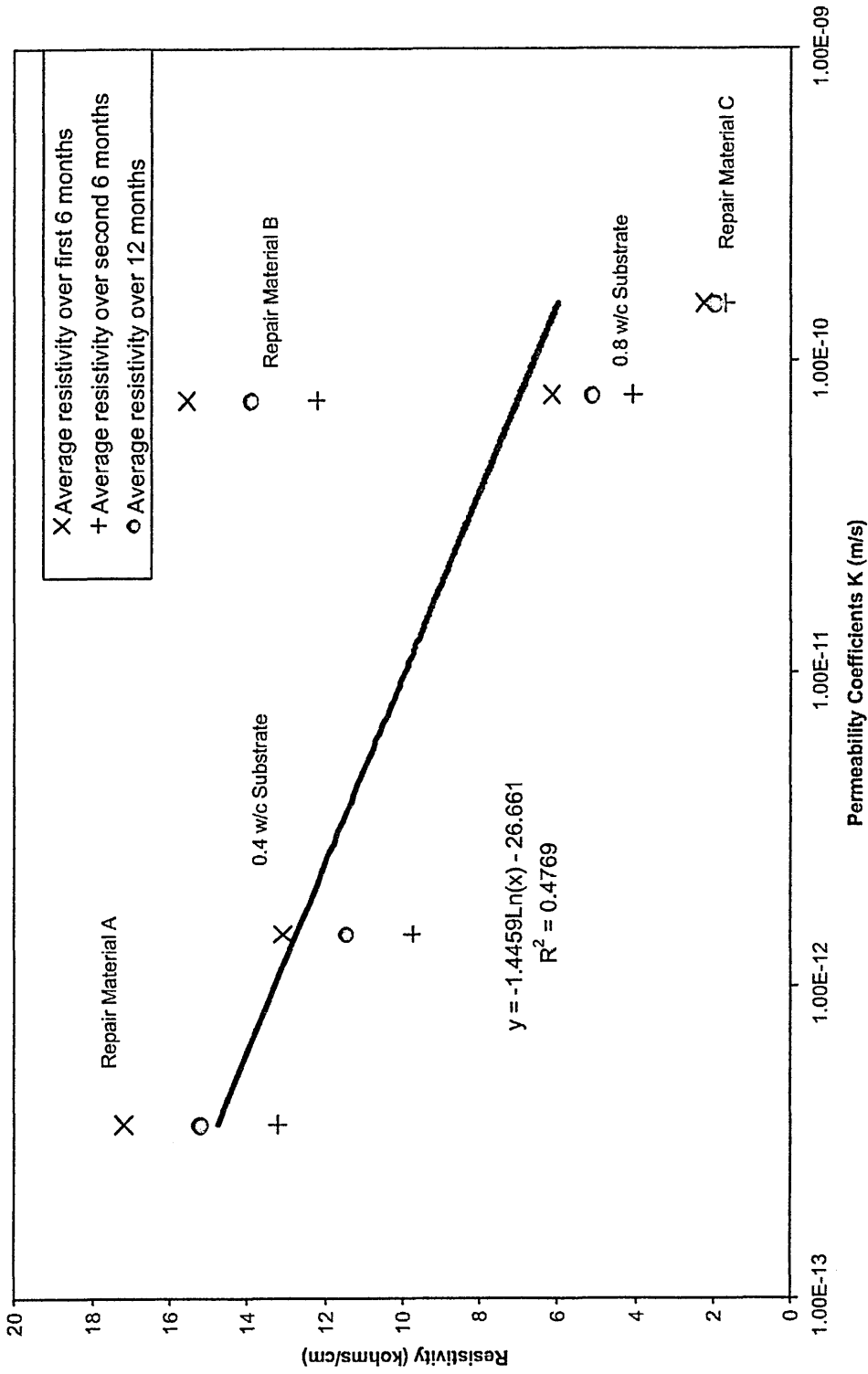


Figure 6.2 Relationship between resistivity and chloride concentration at steel surface

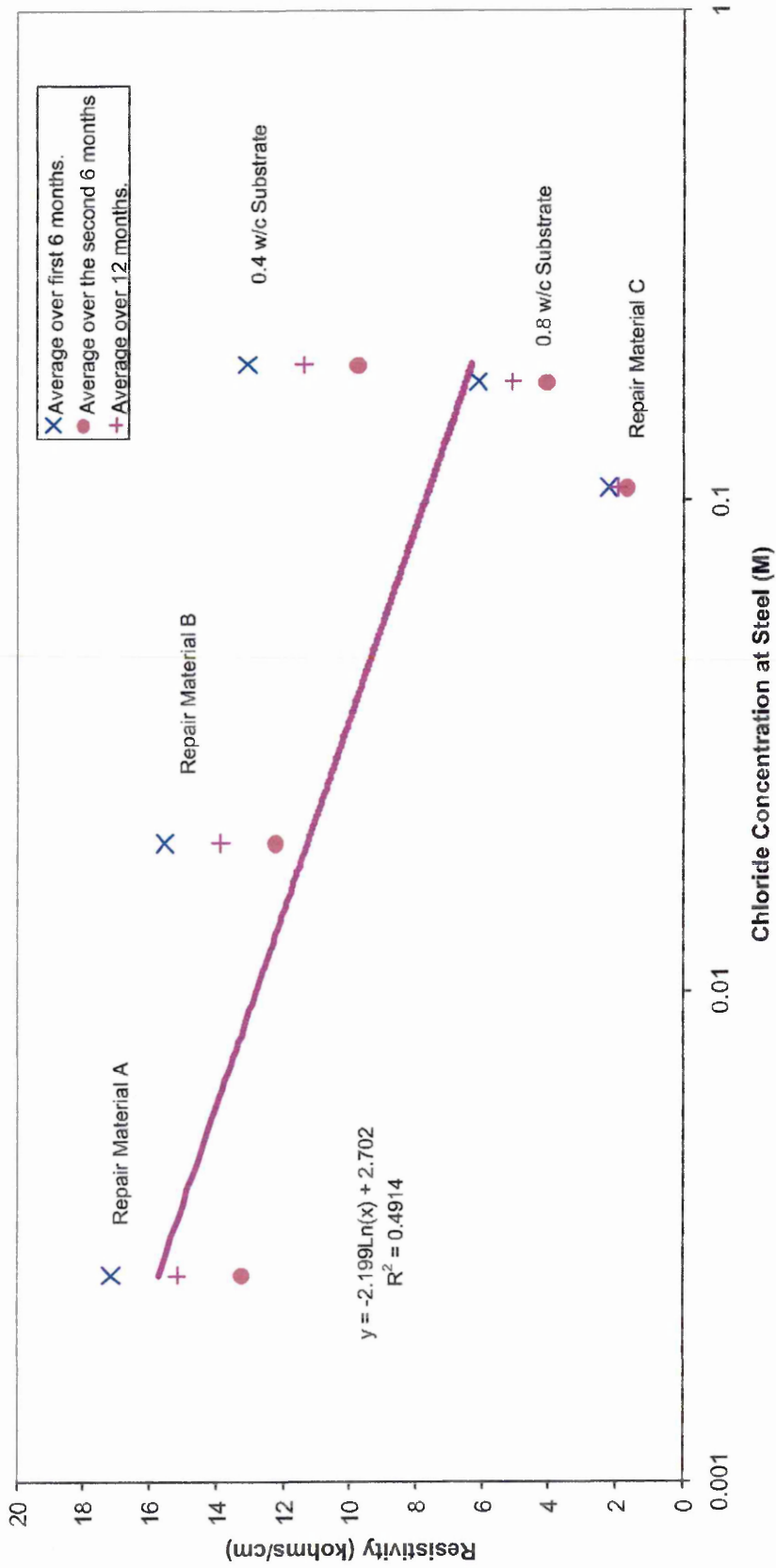


Figure 6.3 Relationship between solution resistance and permeability coefficients

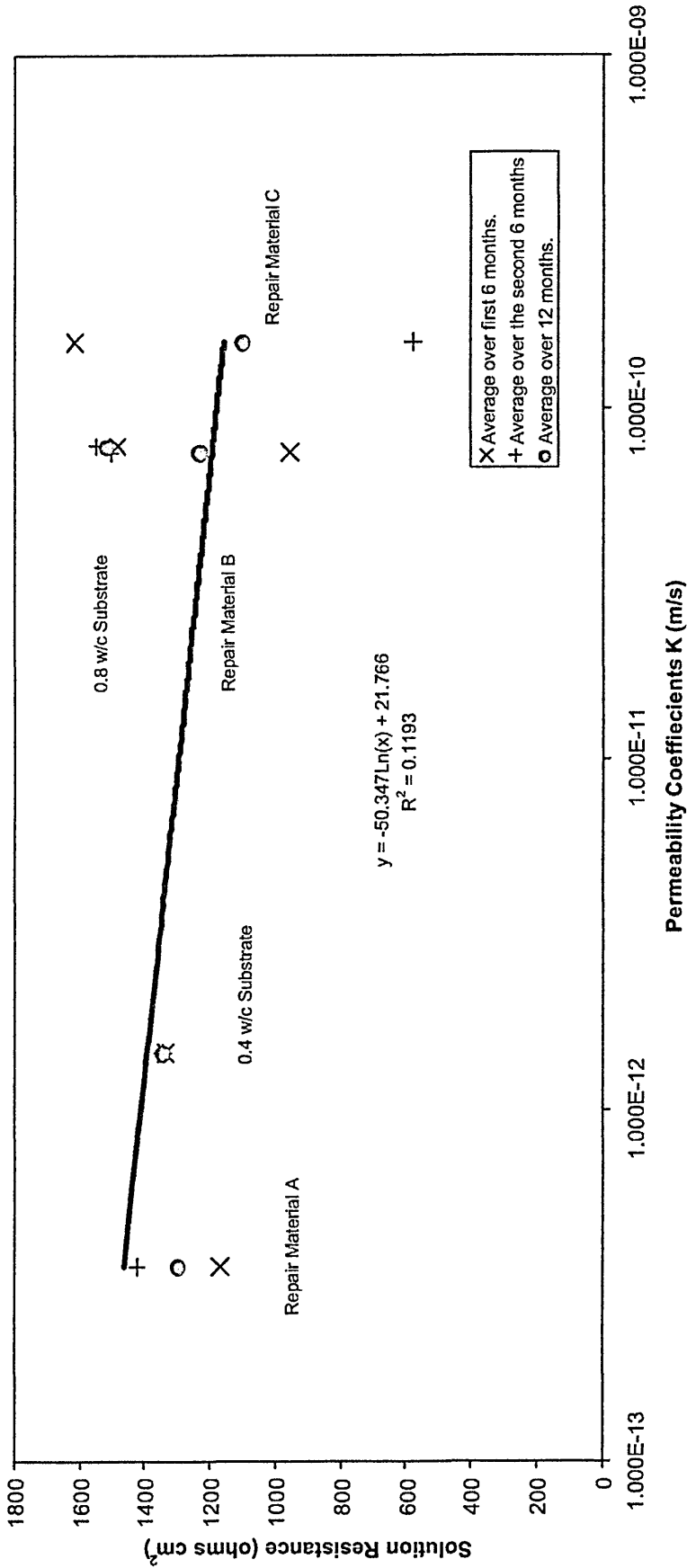
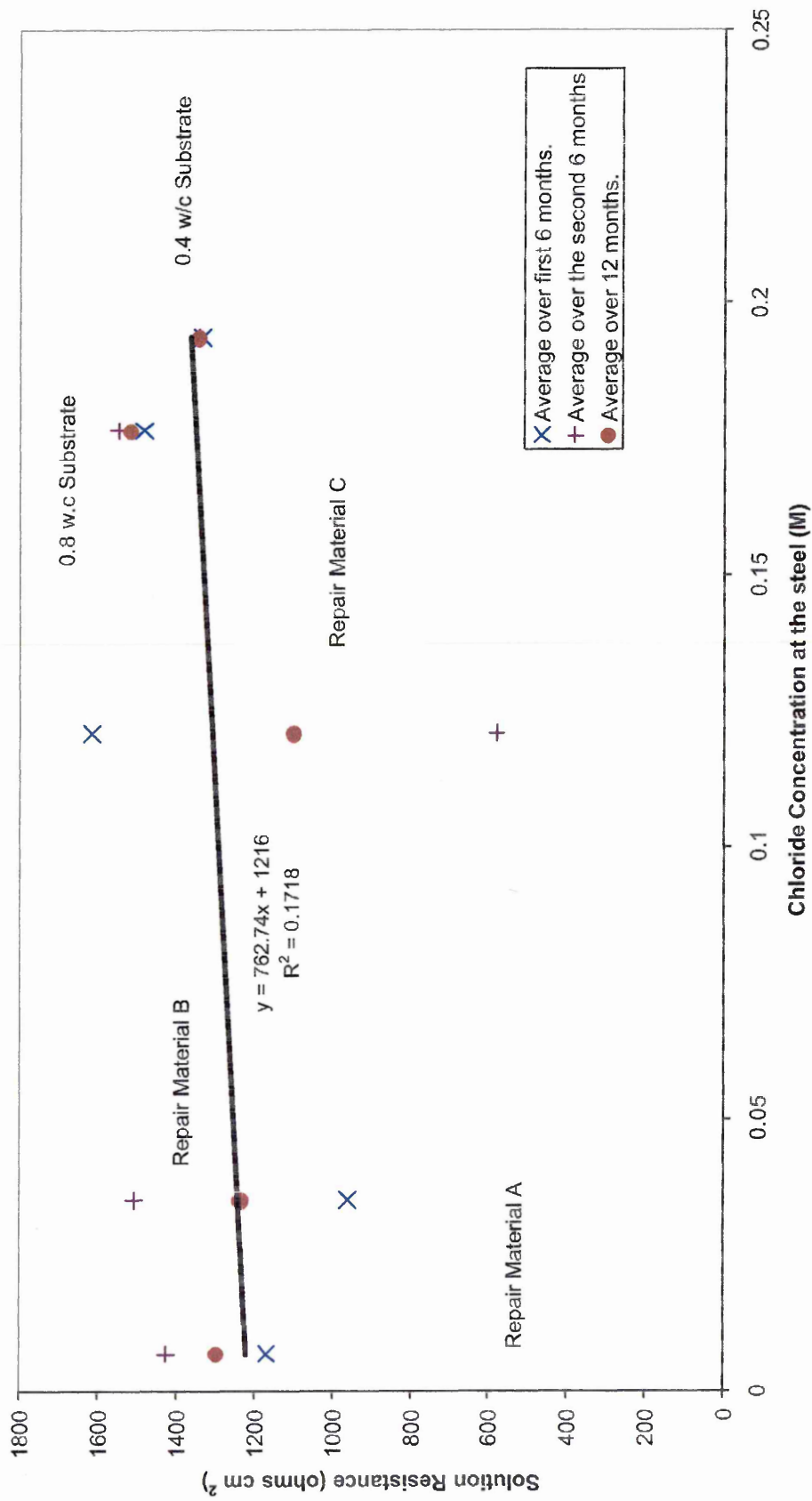


Figure 6.4 Relationship between solution resistance and chloride concentration



The relationships between solution resistance and permeability (Figures 6.3 and 6.4) are poorer than for resistivity (Figures 6.1 and 6.2). This is because solution resistance measurements are a function of the electrochemical cell and not a property of just the repair or substrate material being studied. Figure 6.3 shows that there is no strong relationship between solution resistance and permeability coefficients. The relationship of solution resistance with chloride content and is similar (Figure 6.4) to permeability. Overall solution resistance appears to be independent of either chloride content or permeability.

6.3 EFFECT OF DISPARITY IN MATERIAL PROPERTIES ON CORROSION POTENTIALS

6.3.1 Introduction

The electrochemical corrosion potentials of the repair and substrate materials in each test specimen were measured as part of the corrosion testing programme of work (see Chapter 5.6). The corrosion potential provides a measure of the electrochemical state of the metal in the particular environment. In this situation it was used to indicate the corrosion of the reinforcing steel embedded in the repair and substrate materials of the test specimen. In particular the difference in corrosion potentials between the repair and substrate materials is a measure of the development of macro-cells between the repair and substrate materials.

Table 6.2 shows the average corrosion potential measured for each material used in the study over the first and second six months of the study and the average over 12 months. All the corrosion potentials were in the range -429 mV to -634 mV wrt SCE, which are

within the potential range indicating a high risk of corrosion in accordance with ASTM C876 (1980). The corrosion potentials were lower (more negative) over the second six months of the study. This shows that the cell potentials for every material decreased (became more negative) with time. This would indicate that the steel embedded in the repair and substrate materials was actively corroding for the entire period of the study and became more active with time

Table 6.2 Average corrosion potentials of steel embedded in each cementitious material.

Material	Average Corrosion Potentials (mV wrt SCE)		
	0-6 months	6-12 months	0-12 months
0.4	-558.642	-607.753	-583.198
0.8	-523.114	-576.097	-549.605
A	-626.45	-642.042	-634.246
B	-469.207	-581.072	-525.139
C	-429.495	-575.853	-502.674

6.3.2 Effect of Permeability on Corrosion Potential

Table 6.2 also shows that materials with lower permeabilities have lower (more negative) corrosion potentials. This compares well with the corrosion potentials obtained from polarisation curves in Chapter 5.1, where the potentials showed a linear relationship with the log of the permeability coefficient for the material. Figure 6.5 plots the corrosion potentials from table 6.2 against the log of the permeability coefficient for the material. As with the data obtained from the polarisation curves (Chapter 5.5), there is a clear linear relationship between permeability of the material and corrosion

potential. The trend between cell potential and permeability coefficient from Figure 6.5, follows the empirical relationship given in equation 6.1.

$$E_{CORR} = 17.938 \ln(K) - 110.16 \quad 6.1$$

$$E_{CORR} = \text{Corrosion Potential (mV)}$$

$$K = \text{Permeability Coefficient (m/s)}$$

This empirical relationship between permeability and corrosion potentials fits the relationship expected for cell potential and concentration of reactants from the Nernst equation (equation 6.2) [36].

$$E = E_o + \frac{RT}{nF} \ln \left(\frac{\alpha[O]}{\alpha[R]} \right) \quad 6.2$$

Where:

E= Cell potential

E_o= Standard Electrochemical potential

α[O]= activity of oxidants

α[R]= activity of reductants

R= ideal gas constant

T= temperature (Kelvin)

F= Faraday's constant

n= number of moles of electrons transferred for a mole of reaction.

In the corrosion reaction for steel embedded in concrete the oxygen is reduced, therefore, from equation 6.2 the concentration of oxygen will alter the cell potential. The oxygen concentration will vary with the permeability of cementitious material.

Therefore a logarithmic linear relationship between permeability and electrochemical potential would be expected from the Nernst equation. It can be shown that by expressing the Nernst equation in terms of the oxygen reduction reaction:



The activity of oxygen in solution can be expressed in terms of the partial pressure of oxygen in equilibrium with the solution (PO_2/p°). Then the cell potential for the oxygen reduction reaction will be:

$$E = E_o + \frac{RT}{nF} \ln \left(\frac{[\text{OH}^-]^4}{[\text{OH}^-]^4} \right) \quad 6.3$$

Therefore, the lower the oxygen level the lower the oxygen reduction reaction potential. This will result in a lower measured potential for steel embedded in concrete with lower oxygen concentrations. This would confirm that oxygen concentration as the main factor controlling the potential of the steel embedded in the repair and substrate materials in the current work.

A number of authors have examined the effects of different cementitious materials on corrosion potentials. Ping Gu et al [137] measured lower cell potentials for dense patch repair materials compared to the higher porosity substrate material found during field surveys on structures. The lower potential was not, however, indicative of a higher corrosion rate in the repair patch. The conclusion drawn from this was that the lower oxygen concentration in the dense repair patch resulted in the lower cell potential. However, when a high porosity repair material was used with the low porosity substrate, the repair patch still had a lower potential than the substrate, but in this case the lower potential was found to indicate a higher corrosion rate in the repair patch. Ping Gu et al [137] explained this as being due to the ease of chloride penetration into the repair

patch. High chloride levels would move the half-cell potential of the steel to a lower value indicating active reinforcing steel and, therefore, an increased corrosion rate. In the current work permeability has been found to be a better measure of the diffusion characteristics of the material than porosity. However, both the current work and that by Ping Gu et al [137] indicate that dense repair patches will have lower cell potentials due to restricted oxygen diffusion.

A similar situation exists in water saturated concrete, which has also been found to restrict oxygen diffusion. Elsner et al [150] discussed factors affecting half-cell potentials from field surveys. They recognised that potentials for a column saturated in seawater would be lower than those found in corresponding structures that were not saturated due to lower oxygen concentrations in the saturated concrete. Grimaldi et al [136] also found lower potentials in water saturated concrete. This means that values indicated in the ASTM C876 (1980) standard would not be applicable for water saturated concrete. The ASTM Standard is now widely considered to be out of date and alternative approaches such as those given by the Concrete Society [146] are gaining favour.

6.3.3 Effect of Chloride Concentration on Corrosion Potential

In comparison to permeability the relationship between chloride concentration and cell potential in the repair and substrate materials is less clear. A plot of the half-cell potential and chloride concentration is shown in Figure 6.6. This shows that the higher the chloride concentration the higher (more positive) the half-cell potential for the repair materials. However, in Figure 6.6, the substrate materials do not fit this trend. Both

substrate materials had chlorides added during mixing. Whereas chloride diffusion occurred with time in the repair materials when the specimens were stored in the test solution.

A number of studies [28, 33, 48, 69, 78, 138] have shown a definite trend between cell potential and chloride concentration. The higher the chloride concentration the more negative the cell potential and this is the basis of the potential ranges given in ASTM C876 (1980) standard. This was not found in the current work. However, Figures 6.5 and 6.6, indicate that chlorides may influence but do not control the potential of the substrate and repair materials, since the main factor controlling both the potential and chloride concentration is permeability (Figure 6.5).

This would be expected, as the chlorides themselves are not directly involved in the corrosion reaction in that they are not oxidised or reduced. They are not, therefore, related to the cell potential in the Nernst equation (equation 6.2) as is the case with oxygen concentration. Chlorides are known to breakdown the passive film on steel embedded in concrete and thereby allow corrosion to initiate. What is found is that the higher the chloride concentration the smaller the region of potentials over which the steel is passive. The transpassive area is effectively lowered on the polarisation curve (Chapter 5.5). The implication of this with regards corrosion of reinforcement embedded in concrete is that a passive potential in a material with no chloride can exceed the critical pitting potential when chlorides are present. Pitting corrosion will then initiate on the steel. The critical pitting potential of the steel is a function of chloride concentration and will reduce with increasing chloride concentration.

Although the half-cell potential is unaffected by the chloride concentration, with higher chloride levels the passive region will disappear and the area of steel exposed will actively corrode. The actively corroding steel will have a lower (more negative) cell potential than passive steel. The tendency is for areas of the steel to become increasingly more active with higher chloride concentrations and therefore have lower (more negative) half-cell potentials. The chloride to hydroxide ratio has been found to be important with respect to reinforcement corrosion [49, 50, 51, 52, 138]. The repassivation of the steel surface by the hydroxide ions competes with the breakdown of passivity by the chloride ions. It would, therefore, be expected that the higher the chloride to hydroxide ratio, the less likely the steel will repassivate and stop corroding. However, it is clear that while chloride concentration can influence the half-cell potential, it is the ratio of the activity of oxidised and reduced species involved in the corrosion reaction which determine the cell potential.

6.3.4 Creation of Macro Cells due to Disparities in Properties

The difference in potentials between the steel embedded in the repair and substrate materials may allow the creation of a macro-cell between the two materials. This is analogous to the creation of galvanic cells by combining dissimilar metals such as, copper and steel. The more noble copper in the galvanic series (more +ve potential) will become cathodic and the more active steel (more -ve potential) anodic. Joining steel to copper will result in increased corrosion of the steel in preference to copper. The driving force for the reaction is given by the potential difference between the anodic and the cathodic sites.

In the situation of concrete repair the difference in potentials occurs between sites on the same piece of metal embedded in different materials. The site with the lowest cell potential would be anodic and the higher potential cathodic. Macro-cells result from differences in oxidants and reactants concentrations at the anodic and cathodic sites and for this reason are also called concentration cells. The most common form results from a difference in oxygen concentration between the anode and cathode and is called differential aeration. In reinforced concrete, macro-cells are also known to result from differences in chloride concentrations between the anode and cathode sites and this is called a chloride macro-cell. The site of higher chloride concentration will be more active and, therefore, have a lower cell potential than the site of lower chloride concentration. This will make the higher chloride site anodic and the lower chloride site cathodic. This is a common cause of macro-cell corrosion for steel embedded in concrete and has been investigated by a number of authors [28, 69, 71, 73, 231].

The current work has identified permeability as a controlling factor for the corrosion potential. This is caused by the relationship between permeability and oxygen concentration in the materials. Therefore, by combining two materials with different permeabilities it should be possible to produce a difference in corrosion potentials. A macro-cell created by this method would be a form of differential aeration. Specimens with a disparity in properties between repair and substrate were created, with differences in permeability and chloride concentration. The differences in chloride concentration have been further affected by adding chlorides to the substrate concrete at the time of mixing. The differences in potential between the repair and substrate combinations against the ratio of the permeability coefficients from the present study are shown in Table 6.2.

Table 6.3 Average corrosion potentials measured.

Specimen ID	Ratio of Substrate to Repair Permeabilities*	Average over whole study mV wrt SCE		
		Repair	Substrate	Difference
A04	4.1	-614	-563	51
A08	21.6	-655	-590	65
B04	0.02	-542	-601	-59
B08	1.0	-508	-508	0
C04	0.009	-503	-586	-83
C08	0.5	-503	-551	-48

*Ratio <1 indicates repair is more permeable than substrate.

*Ratio =1 indicates repair and substrate have the same permeability

*Ratio >1 indicates repair is less permeable than substrate

If the potential difference to create a macro-cell is possible from the disparity in permeabilities, then there should be a relationship between the difference in potential and the ratio of the repair-substrate permeabilities. The results follow an approximately linear relationship with a reasonable degree of correlation (see Figure 6.7). Equation 6.1 has also been used to examine the differences in potentials and show the correlation between the expected and actual results. A positive difference in potential indicates that the steel embedded in the repair material has a lower (more negative) potential than the steel embedded in the substrate materials. If the ratio of permeability coefficients is less than one then this indicates that the repair material is less permeable than the substrate.

Figure 6.5 Variation of potentials in repair and substrate materials against log of permeability

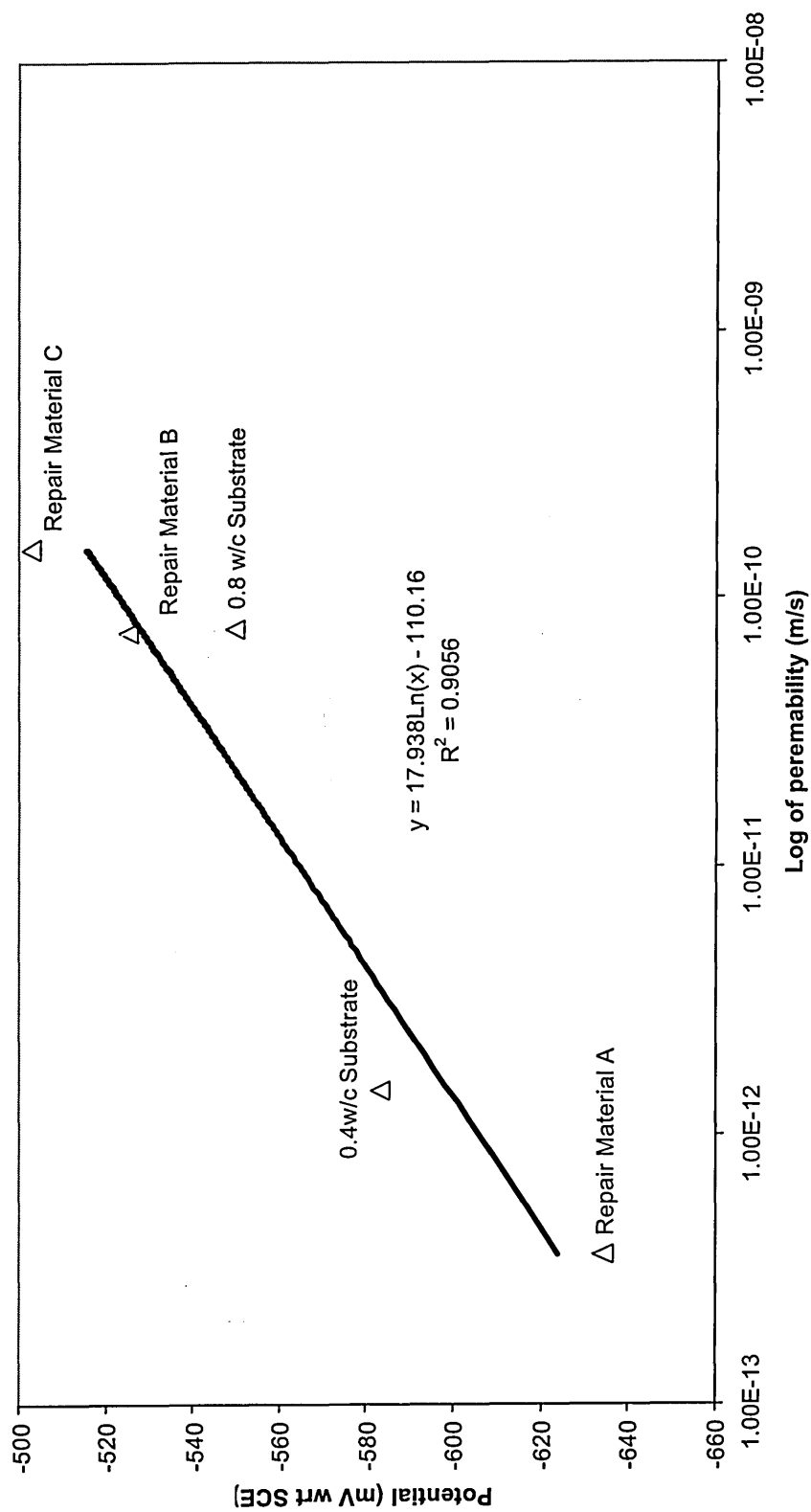


Figure 6.6 Ecorr against chloride concentration

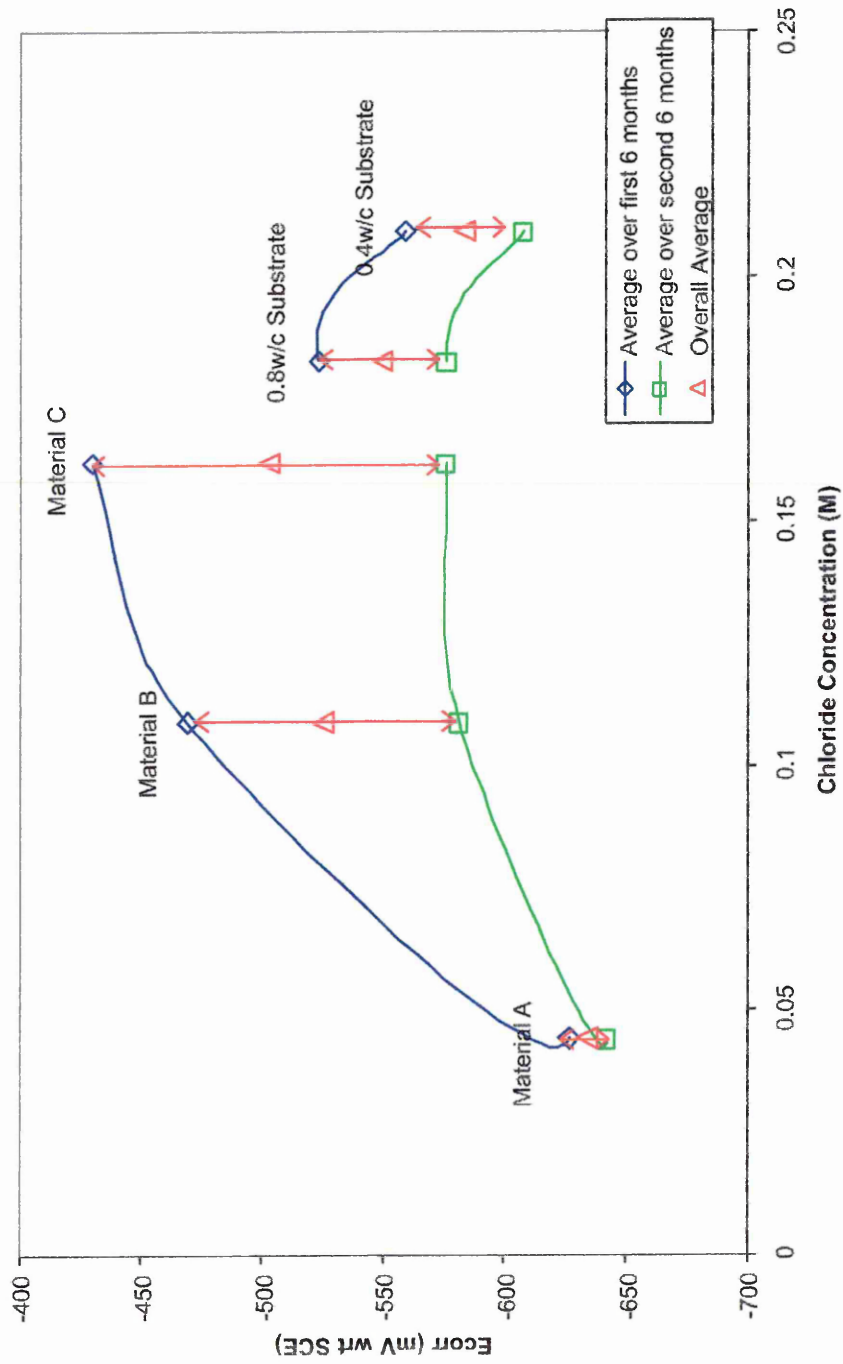
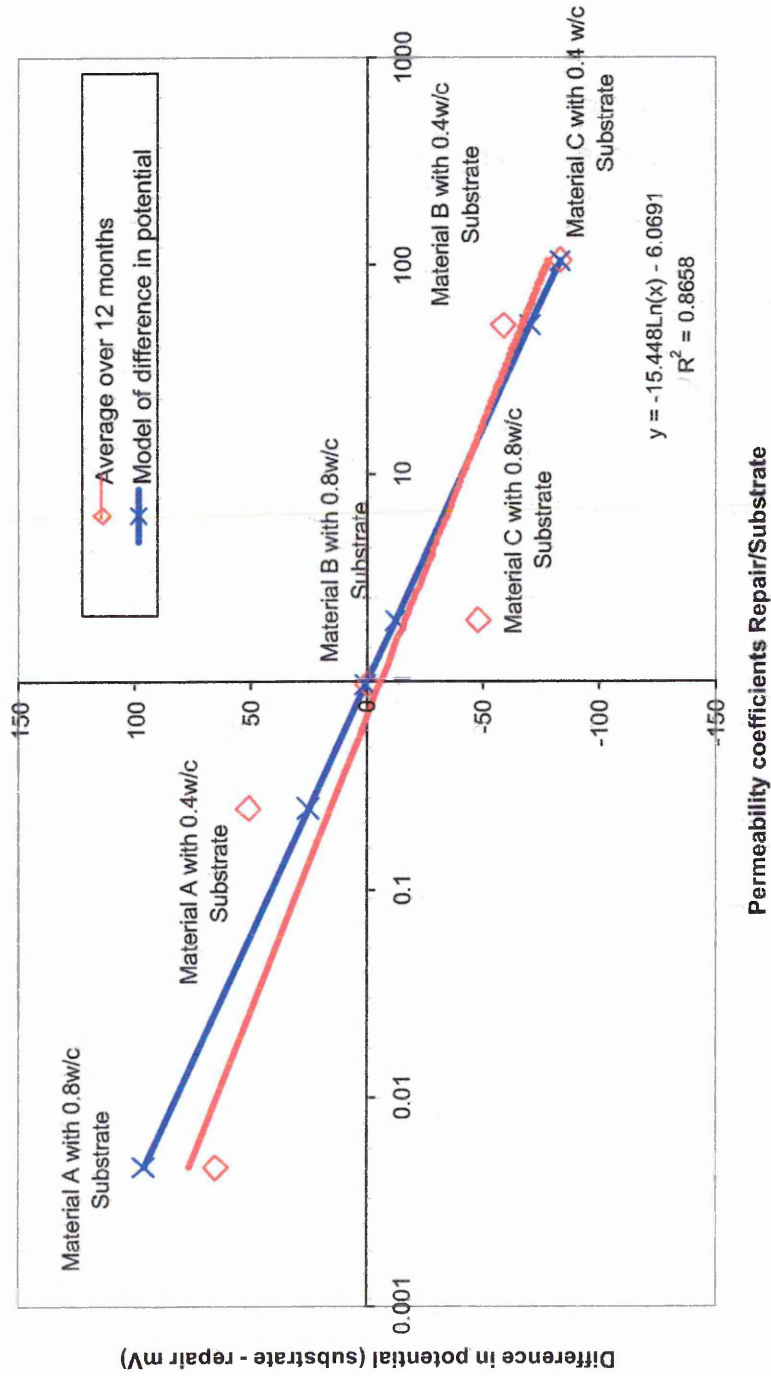


Figure 6.7 Difference in potentials between substrate material and repair against mismatch in permeability



Therefore, from equation 6.1 and Figure 6.7, for repair material A combined with the 0.8 w/c substrate, the repair material is less permeable than the substrate and there is a positive difference of approximately 100mV in potential (the steel embedded in the repair has a potential approximately 100mV more negative than the substrate). For material C with the 0.4 w/c substrate the situation is reversed, repair material C is more permeable than the substrate and correspondingly the difference in potentials is approximately -100mV (the steel embedded in the repair has a potential approximately 100mV more positive than the substrate).

It can be observed from figure 6.7, that the greater the difference in permeability between substrate and repair materials, the greater the difference in potential between the steel embedded in the substrate and repair materials. If the repair is less permeable than the substrate then the steel embedded in the repair will have a lower (more negative) potential and vice versa for when the repair is more permeable than the substrate. For the situation where there is little difference in permeability there is also little difference in potential. This suggests that the greater the difference in permeability between repair and substrate, the greater the driving force for establishing the macro cell.

6.4 EFFECT OF DISPARITY IN PROPERTIES ON CORROSION CURRENTS

Differences in potential do not necessarily indicate any difference in corrosion rate between the repair and substrate. Pourbaix [34] found that pH has a significant effect on the observed corrosion rates in differential aeration cells:

pH below 7: “abnormal operation”, aeration causes an increase in corrosion rate of aerated zones. There is only a small flow of current between aerated and non-

aerated zones and, therefore, only a small increase in the corrosion rate of the non-aerated zone.

pH 7 – 10: “normal operation”, passivation of the aerated zones and a large increase in corrosion rate in the non-aerated zones.

pH 10 – 13: “abnormal operation”, both aerated and non-aerated zones are passive and, therefore, no current flow.

pH above 13: “normal operation”, operation the same as at pH 7-10 , but less vigorous.

The pH for most cementitious materials is approximately 12.5 to 13, suggesting that differential aeration would only produce small galvanic currents. A mechanism that would decrease the pH of the steel into the critical zones indicated could lead to increased galvanic currents. From the work on corrosion potentials (Figure 6. 5), permeability and oxygen diffusion (aeration) are directly related. The effect of differences in permeability on corrosion rates is critical in defining the effect of differential aeration on the corrosion of steel embedded in repair and substrate materials.

Figure 6.8 shows the relationship between the corrosion potential E_{corr} and the corrosion current I_{corr} results from the present work. The results show a general relationship that the lower the potential (more negative) the higher the corrosion current. This indicates that the specimens were under anodic control (see Section 2.2.1 Electrochemistry of

Corrosion, Figure 2.6 Evans diagrams for types of corrosion control). This is accepted as the typical form of corrosion control found in reinforced concrete and is the basis of the ASTM standard on the significance of cell potentials in reinforced concrete structures. The results are in agreement with those presented by other authors such as Lambert et al [138].

Table 6.4 shows the average corrosion currents between 0 to 6 months, 6 to 12 months and 0 to 12 months. This shows that the average corrosion rate increased over the 6 to 12 month period when compared to the 0 to 6 month period. This was true for all repair materials and substrates except the 0.8 w/c substrate, where the corrosion rate decreased. This suggests that the test environment became more corrosive with time, probably due to the diffusion of chlorides into the materials. This would agree with the resistivity results in table 6.1, which, decreased with time indicating that the materials became more corrosive.

Table 6.4 Average corrosion rates

Material	Average Corrosion Rates ($\mu\text{A}/\text{cm}^2$)		
	0-6 months	6-12 months	0-12 months
A	5.26	6.02	5.64
B	3.42	4.91	4.17
C	5.39	12.05	8.72
0.4	8.74	8.97	8.85
0.8	11.22	4.60	7.91

Figure 6.9 is analogous to Figure 6.7 except that corrosion potential is replaced by corrosion current. The I_{corr} values can be expected to be related to the corrosion potentials with the material with the higher noble (less negative) potentials having the lowest corrosion current and the material with the more active lower potential (more negative) the highest corrosion current. This assumes that a differential aeration cell can operate in the high pH of a reinforced concrete structure. Figure 6.10 shows the average corrosion currents over twelve months, the relationships apparent in the graph are not well defined. The material with the highest permeability shows the highest corrosion current. Therefore, the most permeable material which should have the highest oxygen level, corrodes at the highest rate. This does not indicate the action of a galvanic cell, as from previous observations the low permeability material would be expected to be anodic (corroding) and the high permeability material cathodic (not corroding).

It is possible that chloride levels in the materials are controlling the corrosion currents. The substrate had chlorides added during mixing, and a high corrosion current would be expected for steel embedded in it. For the repair materials chlorides entered by diffusion from the electrolyte used. The chloride diffusion profiles (Chapter 4) show that significant level of chloride would have diffused to the steel embedded in material C over the twelve months of the study. Repair material C did show slightly higher average corrosion rates compared to either the 0.4w/c or the 0.8w/c substrates during the first six months.

In summary, the potentials measured indicate that the repair materials had lower (more negative) and, therefore, more active potentials. However, the corrosion currents measured suggest that the higher permeability materials, which were the substrates and

repair material C, corroded at a higher rate than the low permeability materials. These high permeability materials also had the highest chloride levels. This indicates that the materials with the highest chloride levels were corroding at the highest rates and no galvanic cell was established. These results are averages of all the results and hide relative changes in corrosion currents for changes in combinations of repair and substrate. The current work does not determine the area of the steel embedded in the specimen over which any macro cell is effective. It is possible the majority of the specimen would not be affected by a galvanic cell and corrosion is due to the influence of other factors such as chloride content.

Figure 6.10 shows the differences in corrosion currents (substrate – repair) against the ratio of permeability coefficients of repair to substrate. The behaviour of the specimens shows a distinct shift over the study period. The results show that the higher permeability material has the higher corrosion rate over the first six months compared to low permeability materials. However, this changes over the second six months of the study and the low permeability material corrodes at a higher rate than the high permeability material. The results appear to follow the difference in permeability with the specimen with the lowest difference in permeability showing the smallest difference in corrosion currents. For repair materials A and B a decrease in the difference in permeability between repair and substrate produces a corresponding change in the difference in corrosion currents. Only the results for material C do not fit this trend. This may be due to the high chloride levels that diffused into material C.

The experimental results indicate that the steel embedded in the repair and the substrate materials are corroding to some degree, as the currents measured are higher than the

exchange current densities expected for passive steel (1 to 3 $\mu\text{amps}/\text{cm}^2$). The trends in the corrosion currents may be indicative of the formation of a differential aeration cell between repair and substrate. This appears to develop with time and overcomes the differences in chloride concentration between the repair and substrate. However the actual differences in corrosion currents are small, in the order of 5 $\mu\text{amps}/\text{cm}^2$. It was not possible to determine how the cell initiated from the present work. For materials B and C the level of chloride contamination in the repair materials could allow corrosion to initiate and a differential aeration cells to develop. However, material A had no appreciable levels of chloride and the steel embedded in the material would have been expected to be passive. There are a number of possible mechanism for the activation of the steel embedded in material A and the creation of a differential aeration cells between the steel embedded in the repair and substrate materials.

The manufacturers of the repair materials design them to be of higher alkalinity (high pH above 12) compared to other cementitious materials (see chapter 3). An increase in pH above 13 would allow a limited differential aeration to operate [34]. This would fit the prediction from the work by Pourbaix [34] as only a small effect is shown by the present results. However, this would suggest different behaviour for different compositions depending on the composition and pH of the repair material, no evidence was found to support this in the current work.

An alternative process would be due to a local reduction in pH into the pH range 7-10. This would result in the depassivation of the steel allowing it to corrode. Gonzalez et al [78, 79] have proposed a mechanism for corrosion in reinforced concrete requiring the establishment of crevice corrosion conditions between the coarse aggregate and the

steel. This establishes a form of the differential aeration cell and the creation of the crevice corrosion cell results in the local acidification of the pore solution inside the crevice. The local acidification is due to the hydrolysis of metal ions at the anodic site. Gonzalez et al [78, 79] provide some experimental evidence for the crevice corrosion mechanism. The process is analogous to that at the anodic site, in this situation formed between repair and substrate materials. The galvanic current flow in the differential cell would reduce pH at the anodic site (repair or substrate material). This could drop below the pH that would depassivate the steel embedded in the material. This would allow active corrosion to initiate in the cell.

The role of chloride diffusion into the material also needs to be considered. Chloride ions would act to depassivate the steel allowing active corrosion and the creation of galvanic cells. In particular, it can act synergistically with local acidification of the material. Specifically, chloride ions may increase the pH at which the steel would depassivate, facilitating the creation of actively corroding sites. This could explain the change in behaviour with time, as chloride will diffuse into the repair material increasing concentration. At a particular pH and chloride ion concentration, the steel can depassivate, initiating galvanic corrosion. The rate at which this happened would depend on the chloride diffusion coefficient and the composition of the repair material. A number of authors have studied the effect of pH and chloride ion concentration on corrosion and have shown that the critical pH chloride ion ratio varies for different materials.

Figure 6.8 Graph of potentials against corrosion currents

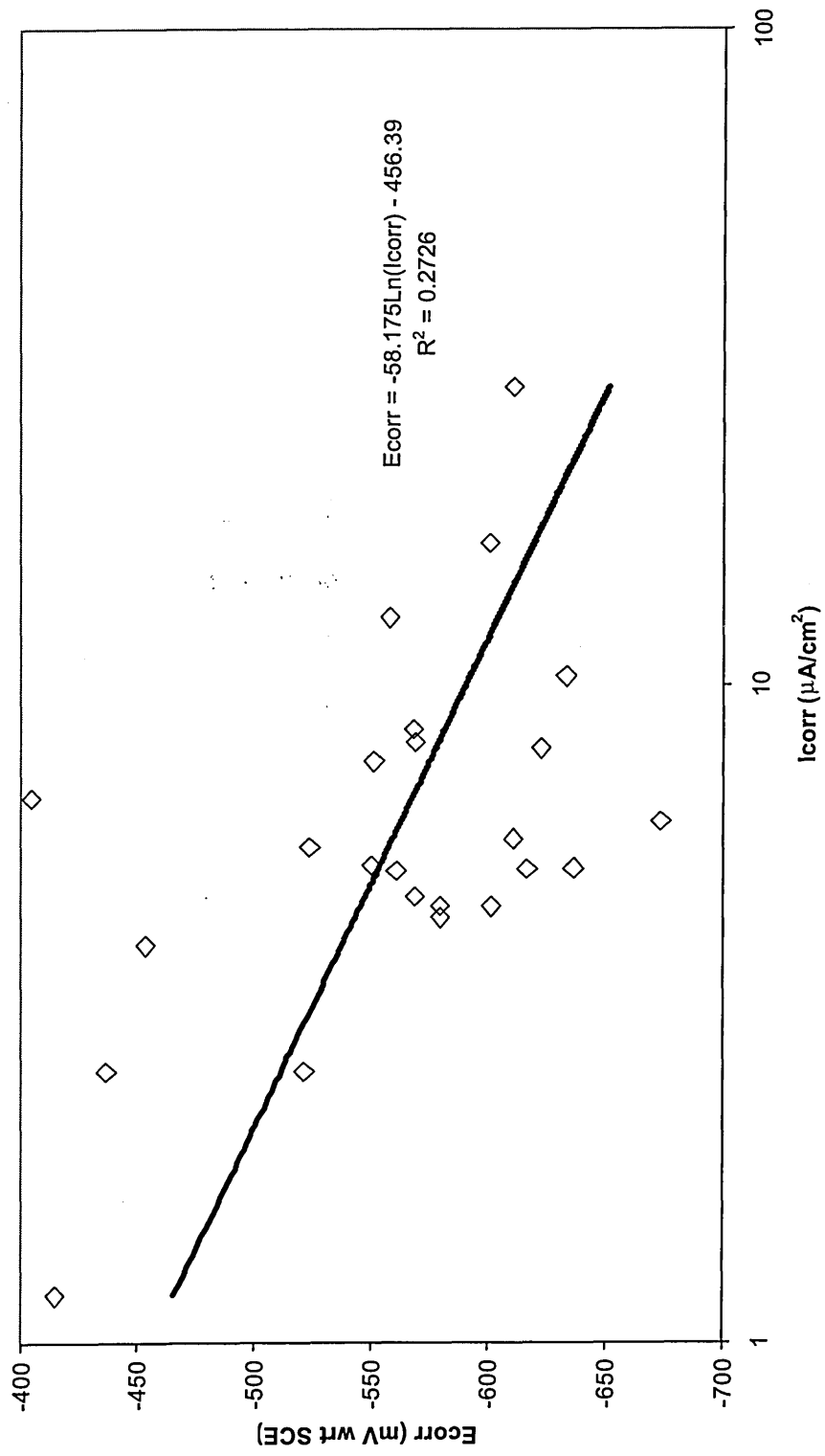


Figure 6.9 Variation in corrosion currents in repair and substrate materials against permeability

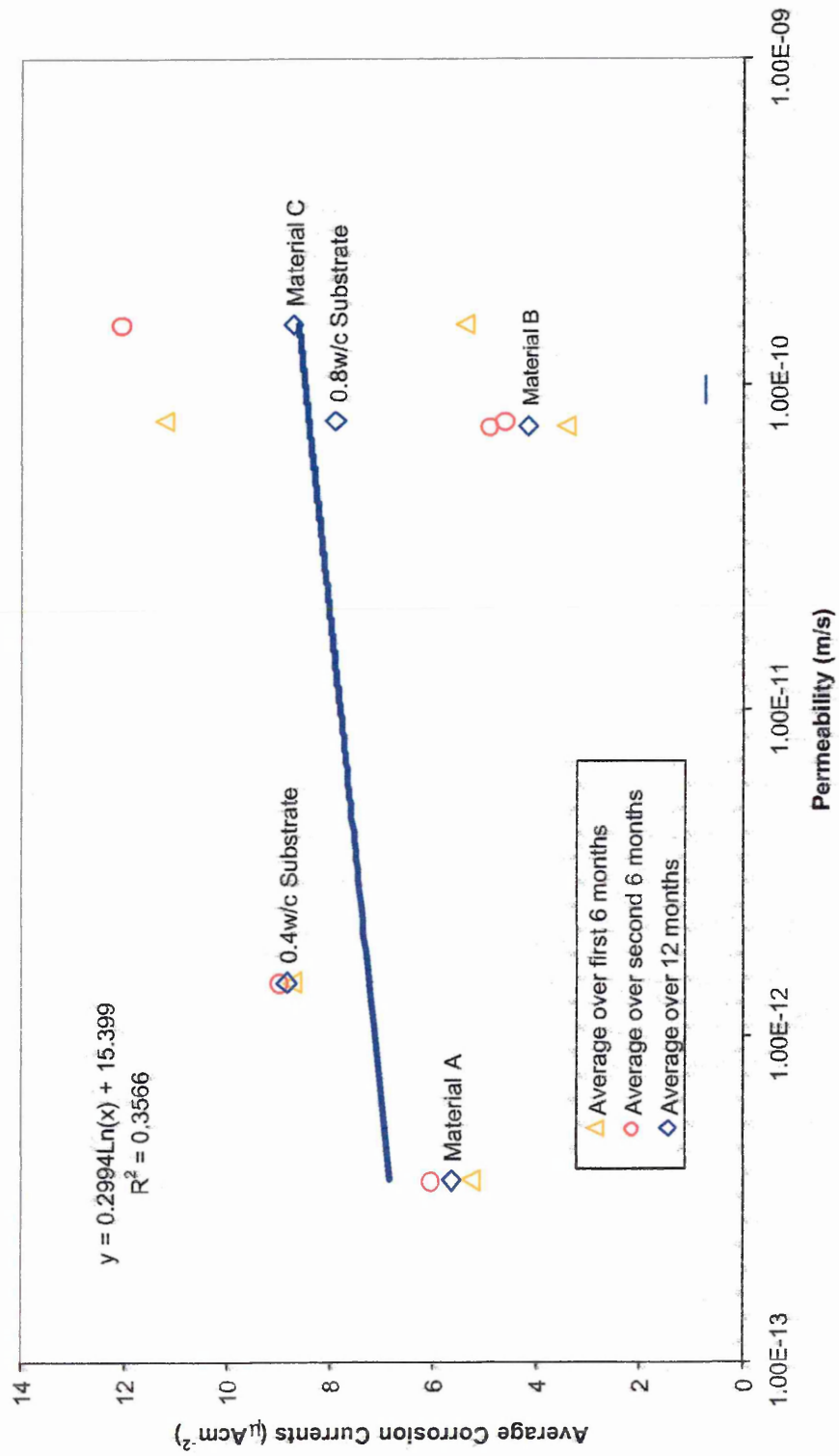
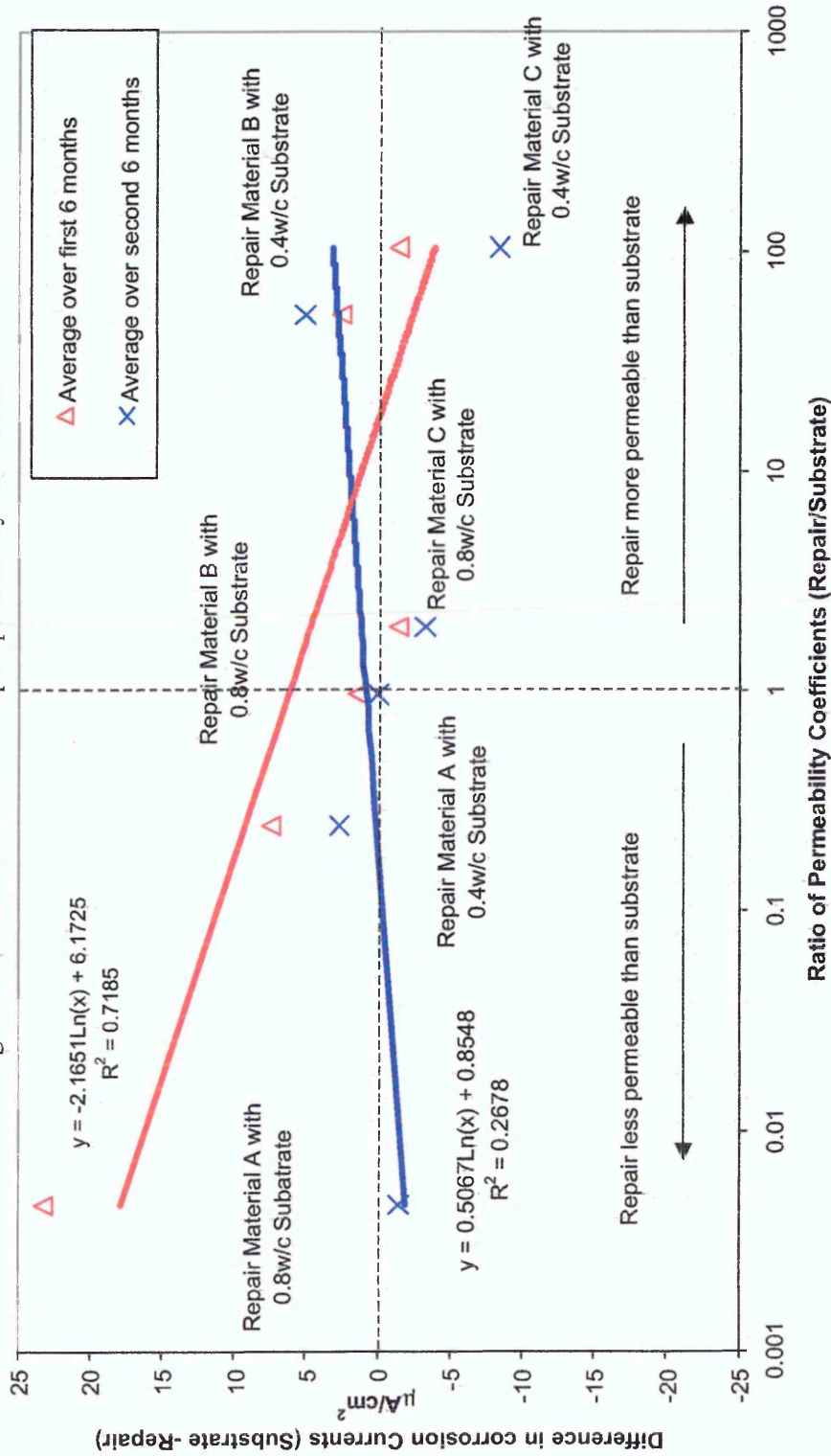


Figure 6.10 Difference in corrosion currents between repair and substrate against the ratio of substrate to repair permeability coefficients



6.5 CONCLUSIONS

A strong relationship exists between corrosion potentials and permeability. This is a logarithmic relationship that complies with the behaviour predicted by the Nernst equation.

The relationship confirms that the material with the lower permeability will tend to have the more active corrosion potential.

Examining differences in corrosion currents shows that over the first six months no galvanic cell was formed. The steel embedded in materials with higher corrosion potentials (high permeability) corrodes at a higher rate than steel embedded in the low corrosion potential (low permeability) materials.

Over the second six months of the study the relationship changes and the materials with the low corrosion potential (low permeability) appears to corrode at a higher rate than the material with the high corrosion potential (high permeability). This indicates the possibility of a very small galvanic effect. The maximum difference in corrosion currents was in the order of $5 \mu\text{amps}/\text{cm}^2$.

The resistivity measurements indicate that the electrolyte (repair or substrate material) become more corrosive, but the solution resistance measurements indicate that reinforcement steel becomes less corrodible with time.

7. Factors affecting the galvanic cell

7.1 INTRODUCTION

Chapter 6 examined the effect of a disparity in properties between the repair and substrate materials on the corrosion of the reinforcement. This showed a difference in corrosion potential between the repair and substrate with the steel embedded in the material with the lower permeability exhibiting the lower (more negative) potential. The implication of this is that a galvanic cell could be established, with the steel embedded in the low permeability material becoming the anode of the cell and the steel embedded in the higher permeability material the cathode. A very small corresponding difference in corrosion currents was found to suggest that such a cell had been established. However, results from the experimental work do not explain how the galvanic cell was initiated or the significance of such a cell to corrosion of steel embedded in repair substrate materials on reinforced concrete structures.

It is beyond the current work to show an initiation mechanism for the cell. However, using the assumption that cell has initiated between the steel embedded in the repair and substrate material, it is possible to model the effects of galvanic currents based on the results of the experimental work. The model proposed here is a simple one-dimensional model, extending on the work of other authors on chloride macro-cell corrosion. The aim is to study the broad implications of a disparity in properties between repair and substrate on the corrosion of the embedded reinforcement steel and how it could influence the repair of reinforced concrete structures.

A number of authors have modelled the galvanic currents from chloride macro-cells in concrete [21, 69, 71] and have used a similar approach in all cases. The galvanic cell is represented as a simple electrical circuit as in the diagram in figure 7.1.

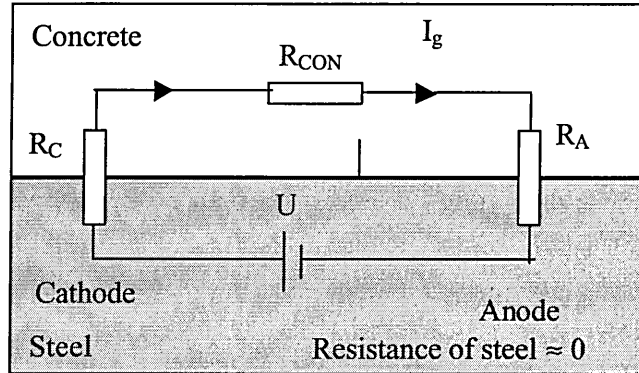


Figure 7.1 Simple electrical circuit to represent a galvanic cell [28]

U = Difference in rest potentials between anode and cathode

R_A = Polarisation resistance at the anode.

R_C = Polarisation resistance at the cathode.

R_{CON} = Resistance of the concrete.

I_g = Galvanic current flowing in the circuit

Ohms law can be applied to determine the current flowing in the circuit as follows:-.

$$I_g = \frac{U}{R_A + R_C + R_{CON}} \quad 7.1$$

This approach was used by Noggerath et al [69] and Gulikers et al [71]. Raupach [28] modified this approach by recognising that polarisation resistance of the anodes and cathodes was a function of the electrode area. This is inversely related to the polarisation resistance and so the larger the area of the anodes and cathodes the smaller the effective polarisation resistance for these sites. Equation 7.1 shows that the smaller the resistance the larger the galvanic current. Raupach [28] also included a factor to

represent the separation of the anode and cathode in the cell geometry. This would influence the magnitude of the concrete resistance and so influences the galvanic current flowing in the cell. Raupach [28] proposed the following equation for modelling the galvanic current.

$$I_g = \frac{U}{\frac{R_A}{A_A} + \frac{R_C}{A_C} + \frac{\rho_{CON}}{k}} \quad 7.2$$

Where:

A_A = Anodic acting steel surface area.

A_C = Cathodic acting steel surface area.

ρ_{CON} = Specific resistance of the concrete.

k = Cell constant geometry

7.2 MODELLING WORK FOR REPAIR MACROCELL

7.2.1 Theory

There are a number of limitations to the approach used by Raupach [28], Noggerath et al [69] and Gulikers et al [71] to model galvanic currents. The area of the anodes or cathodes cannot be determined directly from experimental measurements. In addition in concrete, the resistance will increase as the distance between anode and cathode increases and will in turn result in an IR drop between the anodic and cathodic sites. This will produce a drop in the potential difference between anode and cathode as the distance increases. As the voltage drops so will the galvanic current. Equation 7.2 takes this into account with the cell geometry factor k . However, it assumes that for a given cell the anodic polarisation resistance, cathodic polarisation resistance and concrete resistance are constant. This is not an accurate representation of the situation occurring in all macro-cells. For the situation involved in concrete repair it can be assumed that a single rebar runs from a repaired site to the substrate concrete. There will be a definite

interface between the repair and the substrate. This interface is the point where the potential difference between the two materials will be at its greatest.

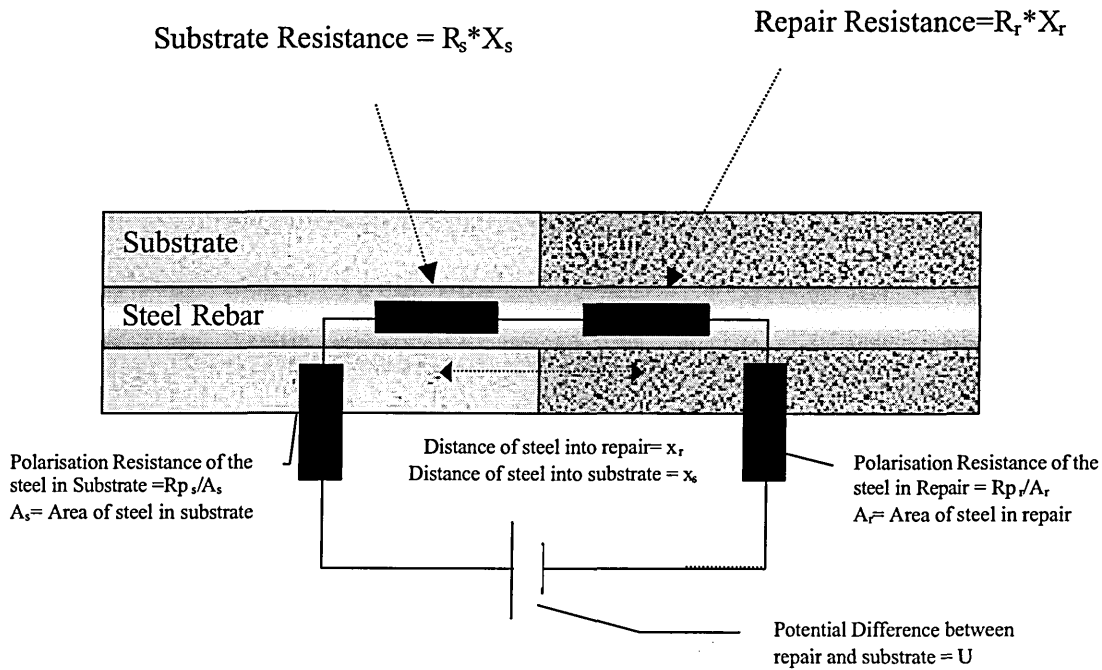


Figure 7.2 Schematic Diagram of Repair Macro-cell.

In this case an alternative schematic representation of the cell is given in figure 7.2. The area of steel in the repair or the substrate (A_r and A_s respectively from Figure 7.2) is equivalent to:

$$A = \pi d X \tag{7.3}$$

Where d = diameter of the rebar

X = distance into the repair or substrate (X_r or X_s).

The size of the polarisation resistance of the repair or substrate (R_{p_r} and R_{p_s} from figure 7.2) will vary with the area of the steel in the repair and substrate. This approximates to the length of rebar in the repair or substrate (X_r or X_s respectively from Figure 7.2) as follows:

$$\text{Polarisation Resistance} = \frac{R_p}{\pi l X} \approx \frac{R_p}{X} \quad 7.4$$

Assuming that $X_s = X_r = x$, using equation 7.2 applied to the situation shown in Figure 7.2, then for an incremental length of rebar dx in the repair and substrate the change in galvanic current δI_g will be:

$$\partial I_g = \frac{U}{R_r x + R_s x + R_{p_r} + R_{p_s}} \partial x \quad 7.5$$

Integrating equation 7.5 between 0 and x to find the total galvanic current I_g flowing in the cell gives:

$$I_g = \int \frac{U}{R_r X + R_s X + R_{p_r} + R_{p_s}} \partial x \quad 7.6$$

$$\therefore I_g = \frac{\ln[(R_s + R_r)x + R_{p_r} + R_{p_s}]}{R_s + R_r} U + c$$

From equation 7.5, when $x=0$, the total galvanic current I_g is given by:

$$I_g = \frac{U}{R_{p_r} + R_{p_s}} \quad 7.7$$

From equation 7.6 when $x=0$, the total galvanic current is also given by:

$$I_g = \frac{\ln(R_{p_r} + R_{p_s})}{R_s + R_r} U + c \quad 7.8$$

Combining 7.7 and 7.6 for the condition when $x=0$:

$$\frac{U}{R_{p_r} + R_{p_s}} = \frac{\ln(R_{p_r} + R_{p_s})}{R_r + R_s} U + c \quad 7.9$$

Rearranging equation to find c.

$$c = \frac{U}{Rp_r + Rp_s} - \frac{\ln(Rp_r + Rp_s)}{R_r + R_s} U \quad 7.10$$

The total galvanic current I_g flowing in the cell is given by combining equations 7.6 and 7.10:

$$I_g = \frac{\ln[(R_s + R_r)x + Rp_r + Rp_s]}{R_s + R_r} U - \frac{\ln(Rp_r + Rp_s)}{R_s + R_r} U + \frac{U}{Rp_r + Rp_s} \quad 7.11$$

Equation 7.11 was used to model the magnitude of galvanic current with increasing size of anodes and cathodes in different repair and substrate combinations. In addition to the total galvanic current, the distribution of current in the repair and substrate is of interest. This would allow the assessment of the effect of different combinations of repair and substrate materials on the corrosion of the reinforcement. A transmission line model (figure 7.3) was used to analyse the distribution of current.

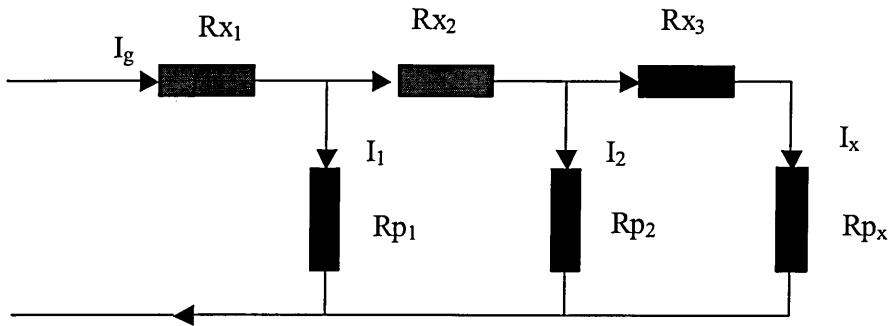


Figure 7.3. Transmission line model

The distribution of current through the circuit in figure 7.3 is inversely proportional to the resistance within the circuit.

$$I_x = \frac{(Rx + Rp_x)^{-1}}{\sum_0^x (Rx + Rp_x)^{-1}} I_g \quad 7.12$$

Using values of R and R_p for repair and substrate allows the distribution of current with the repair and substrate to be determined. The analyses of the experimental work provides values for R_r , R_s , R_{p_r} , R_{p_s} and U for each of the repair substrate combination investigated. Table 7.1 provides a summary of this work

7.2.2 Validity of Experimental Data

Table 7.1 provides a summary of values of polarisation resistance, solution resistance and potential difference between repair and substrate materials, obtained from the corrosion tests discussed in Chapter 5. These are the average values measured over the 2nd six months of the experimental study. The values for polarisation resistance and solution resistance in table 7.1 have been presented as the specific resistances in ohms per cm i.e. they have been adjusted for the diameter of rebar used in the test specimens. In addition the element (repair or substrate) with the lowest (most negative) half-cell potential has been identified as the anode and the other as the cathode.

Table 7.1 Summary of repair and substrate values from experimental work

Repair Material	Substrate Material	Anode	Cathode	U	(Ωcm)			
				(mV)	R_{p_r}	R_{p_s}	R_r	R_s
A	0.4 w/c	Repair	Substrate	51	3049.966	2212.737	15341.67	10958.33
A	0.8 w/c	Repair	Substrate	85	2866.328	3498.423	11100	3858.333
B	0.4 w/c	Substrate	Repair	-58	3907.172	1839.325	14950	9666.667
B	0.8 w/c	Substrate	Repair	-24	4431.306	3601.454	9491.667	4116.667
C	0.4 w/c	Substrate	Repair	-81	896.3167	2363.691	1316.667	8616.667
C	0.8 w/c	Substrate	Repair	-47	1924.297	3757.91	2025	4266.667

Equations 7.6, 7.11. and 7.12 have been used to model the current distribution in the specimens and the results can be seen in figures 7.4 to 7.10. To make the graphs clearer

Figure 7.4 Current distribution for material A combined with the 0.4 w/c substrate.

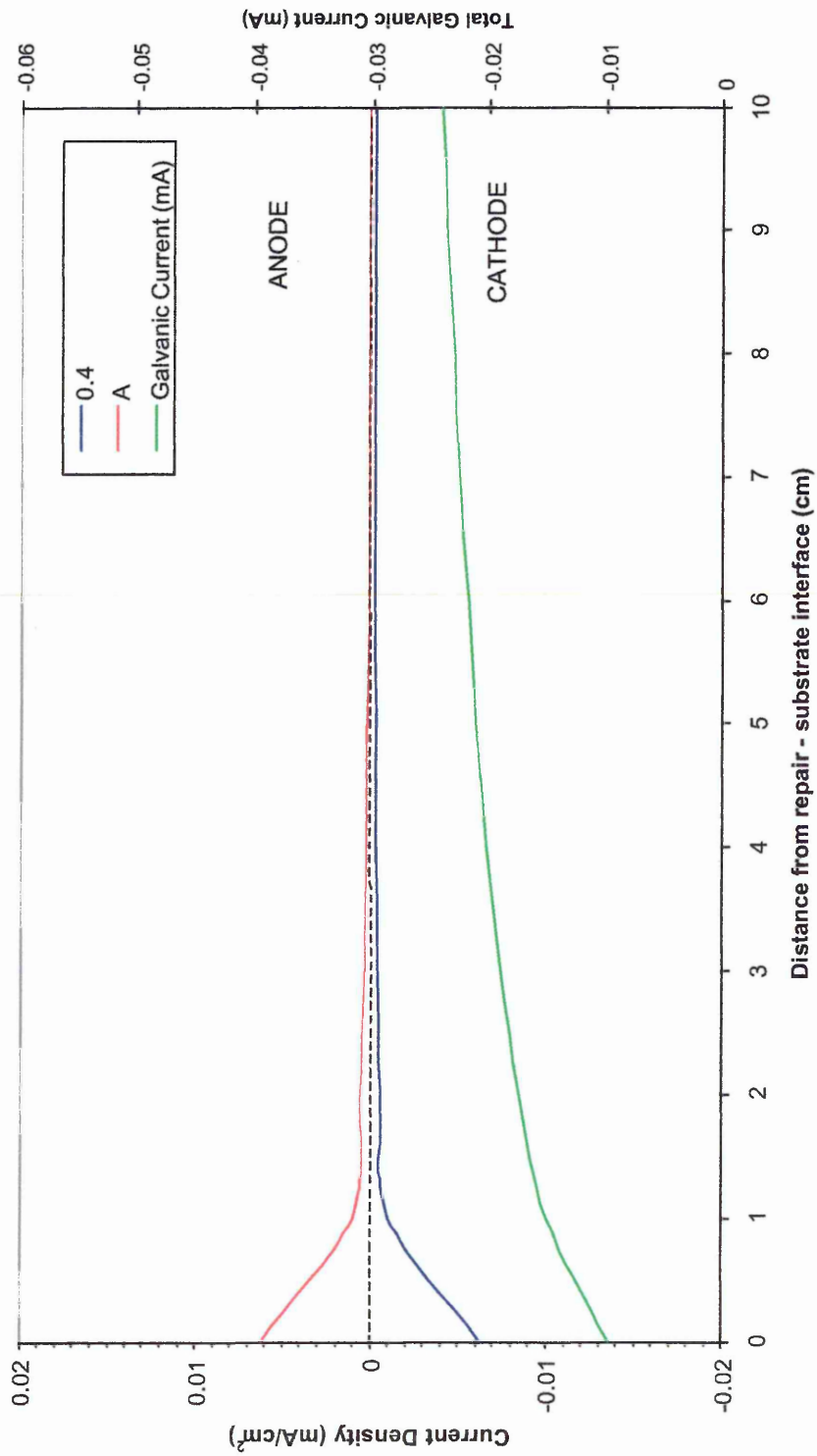


Figure 7.5 Current distribution for material A combined with 0.8w/c substrate

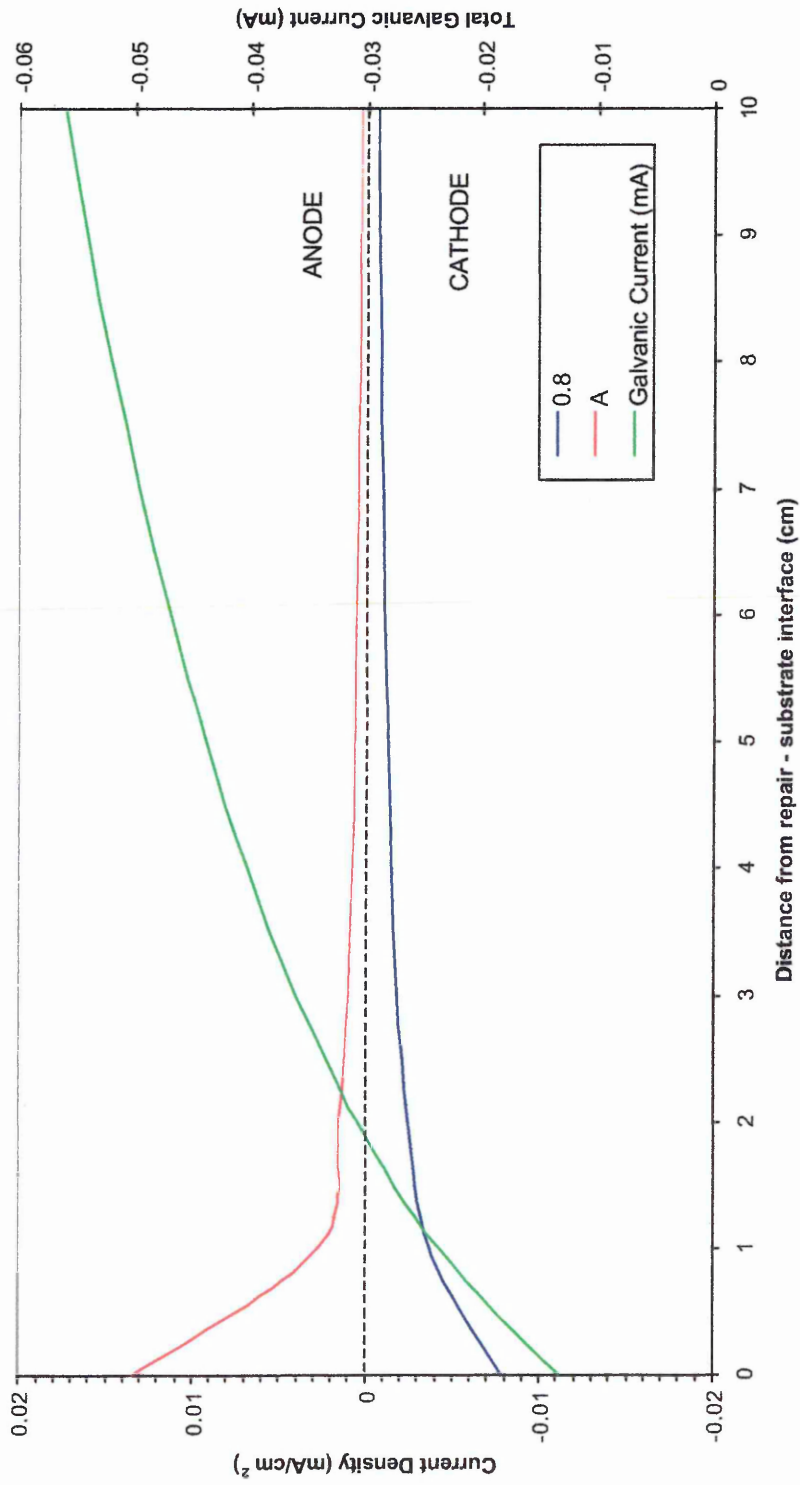


Figure 7.6 Current distribution for material B combined with 0.4 w/c substrate.

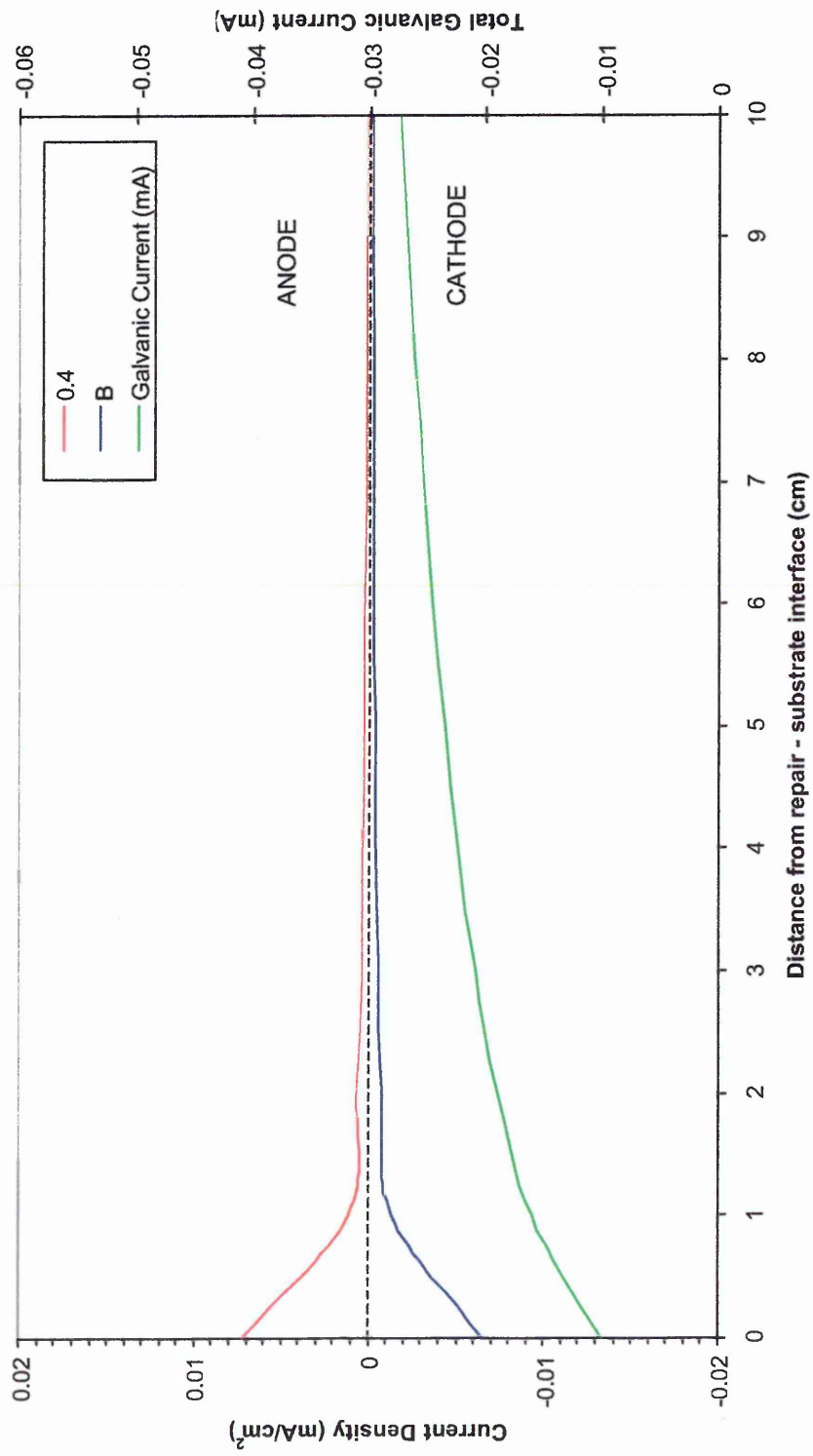


Figure 7.7 Current distribution for material B combined with 0.8 w/c substrate.

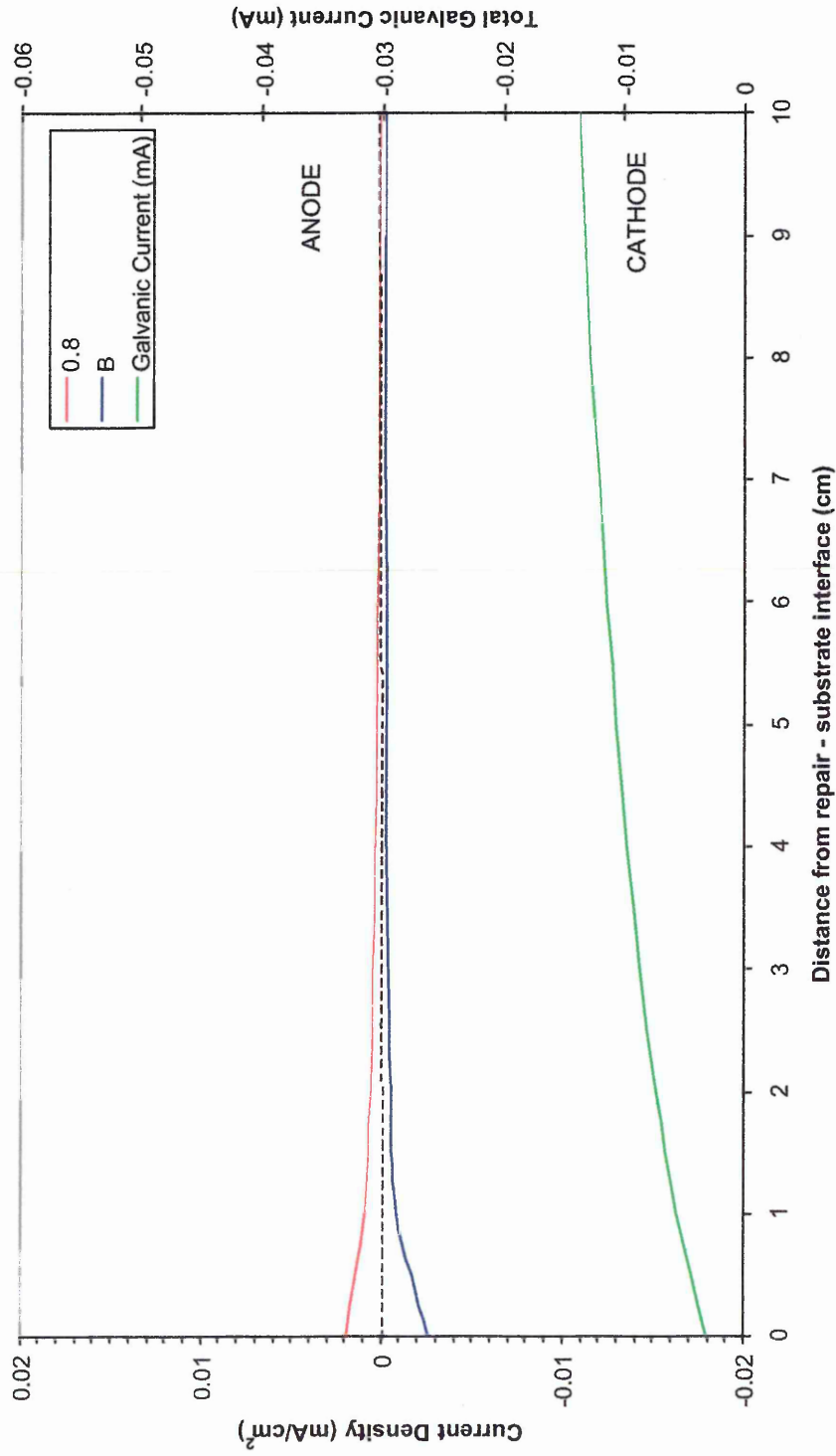


Figure 7.8 Current distribution for material C combined with 0.4 w/c substrate.

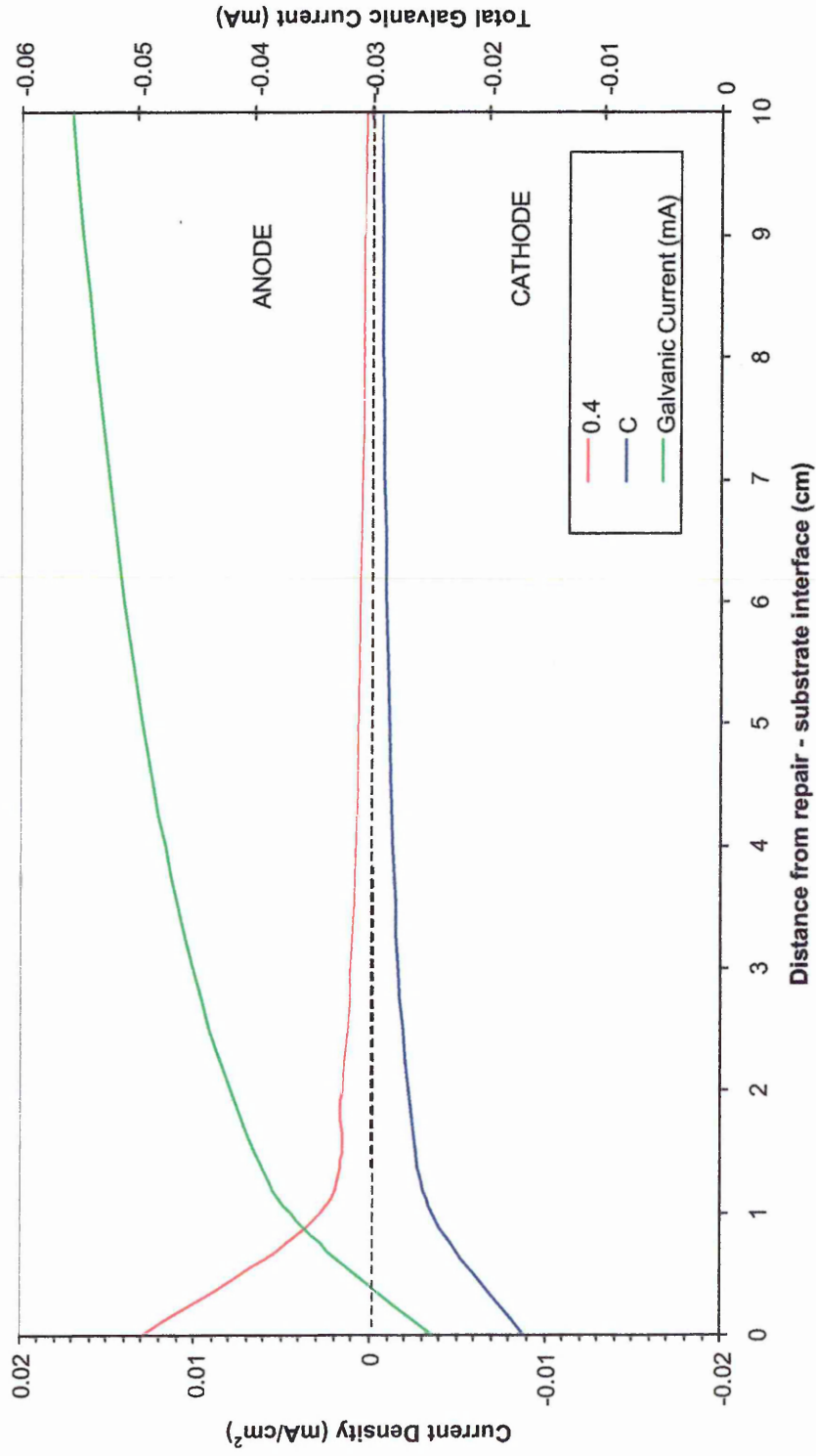


Figure 7.9 Current distribution material C combined with 0.8 w/c substrate.

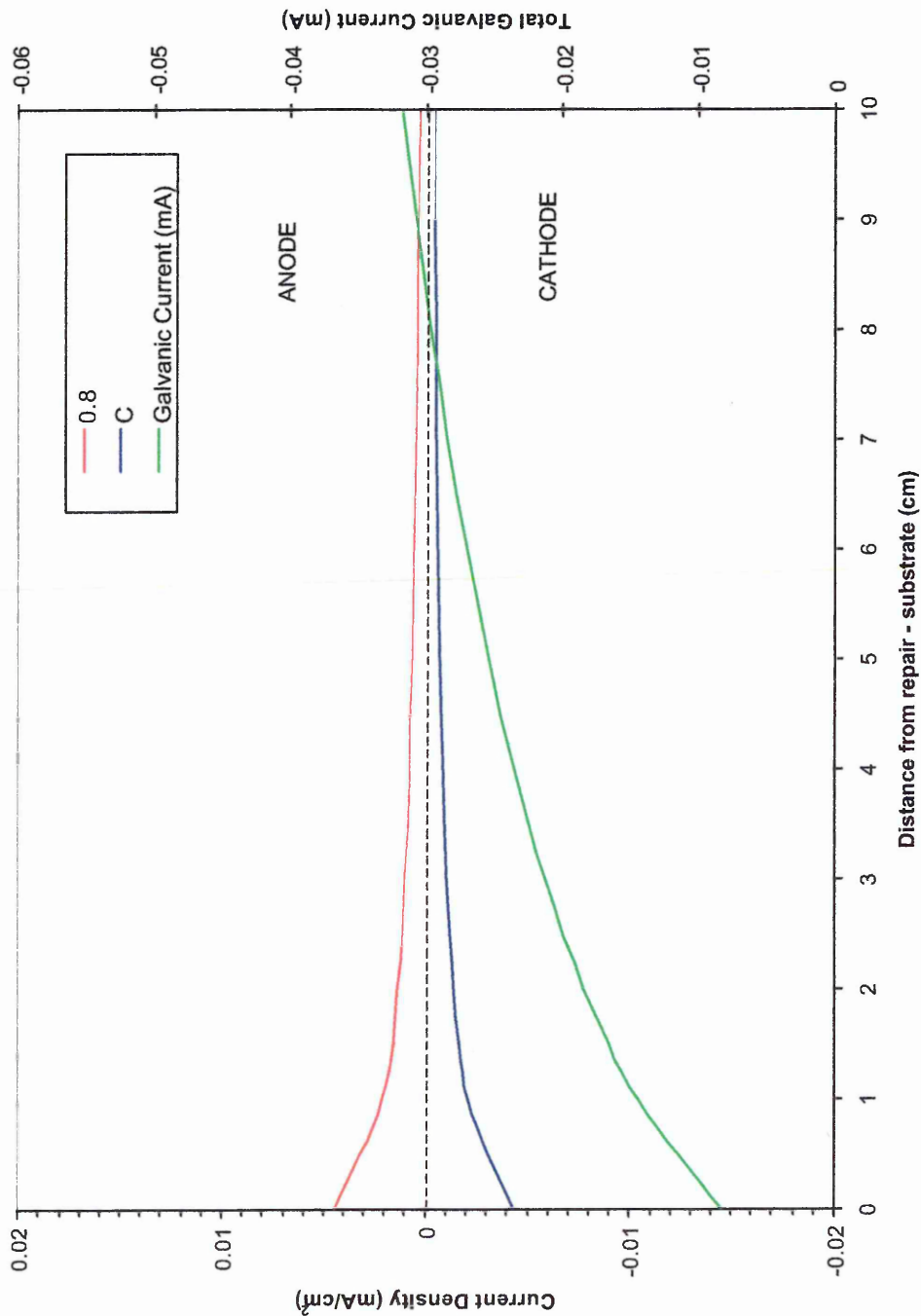


Figure 7.10 Average current densities for the anode and the interface of the repair-substrate combinations (over final six months of the study).

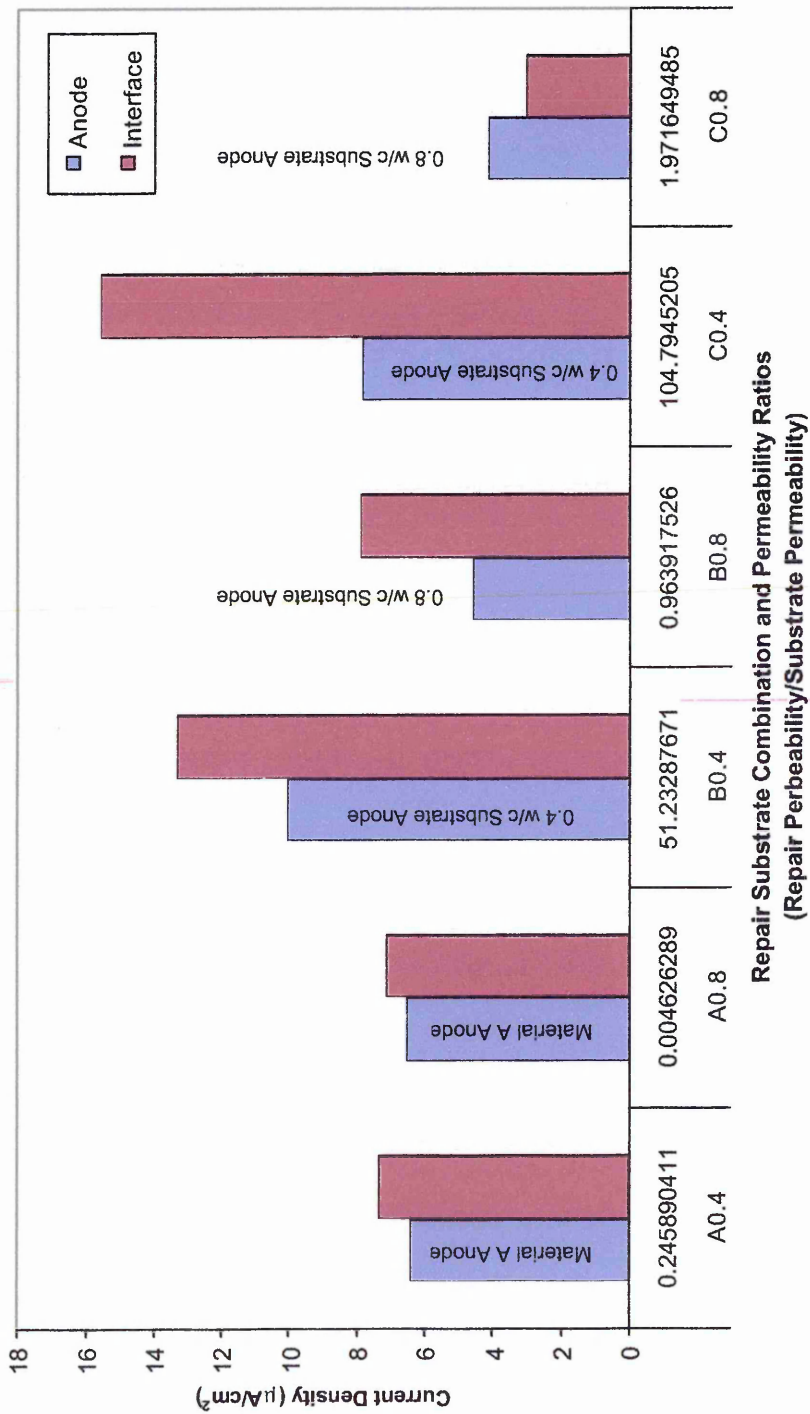


Figure 7.11 Effect of repair permeability on galvanic corrosion when combined with a high permeability substrate

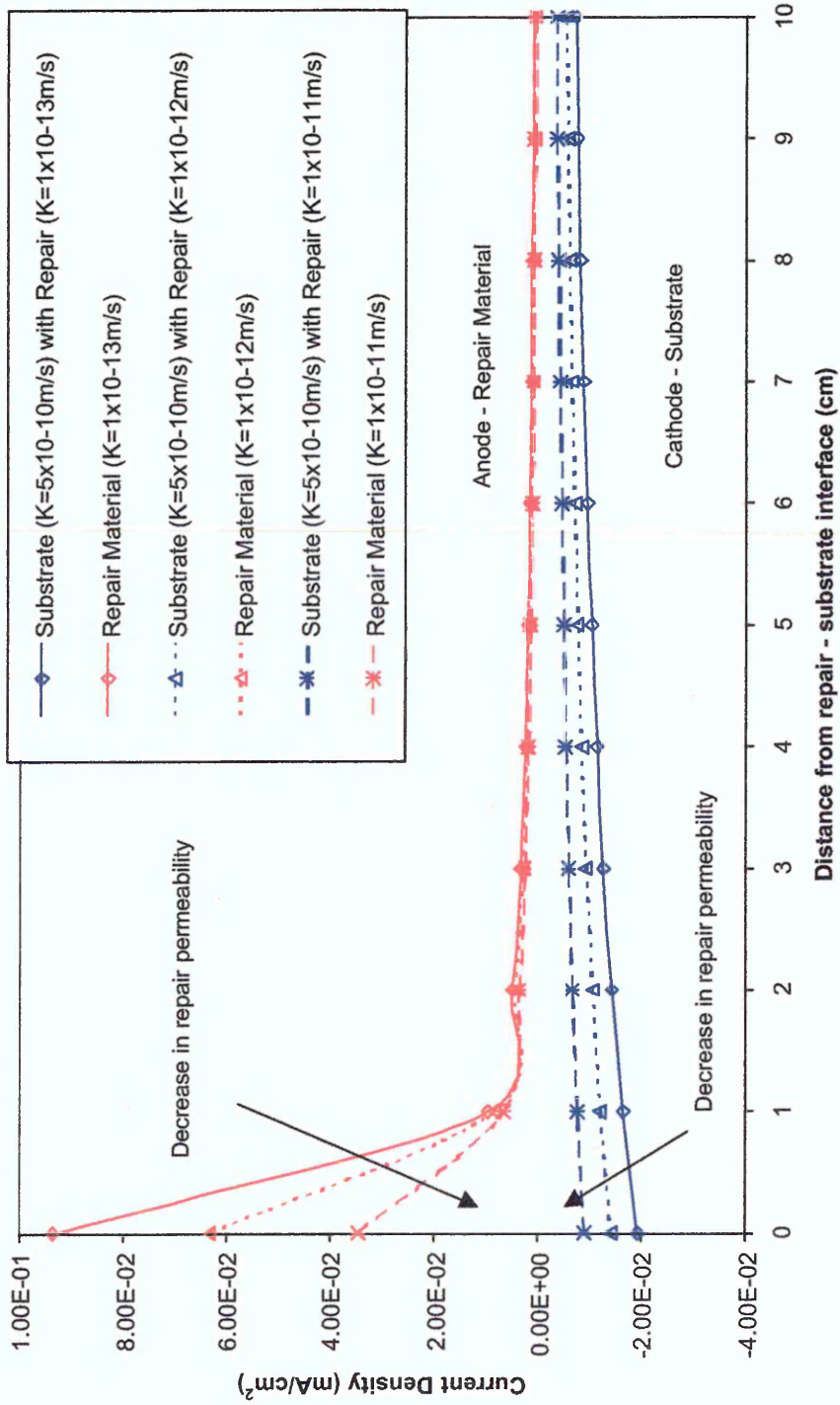


Figure 7.12 Comparison of low permeability and high permeability repair substrate combinations

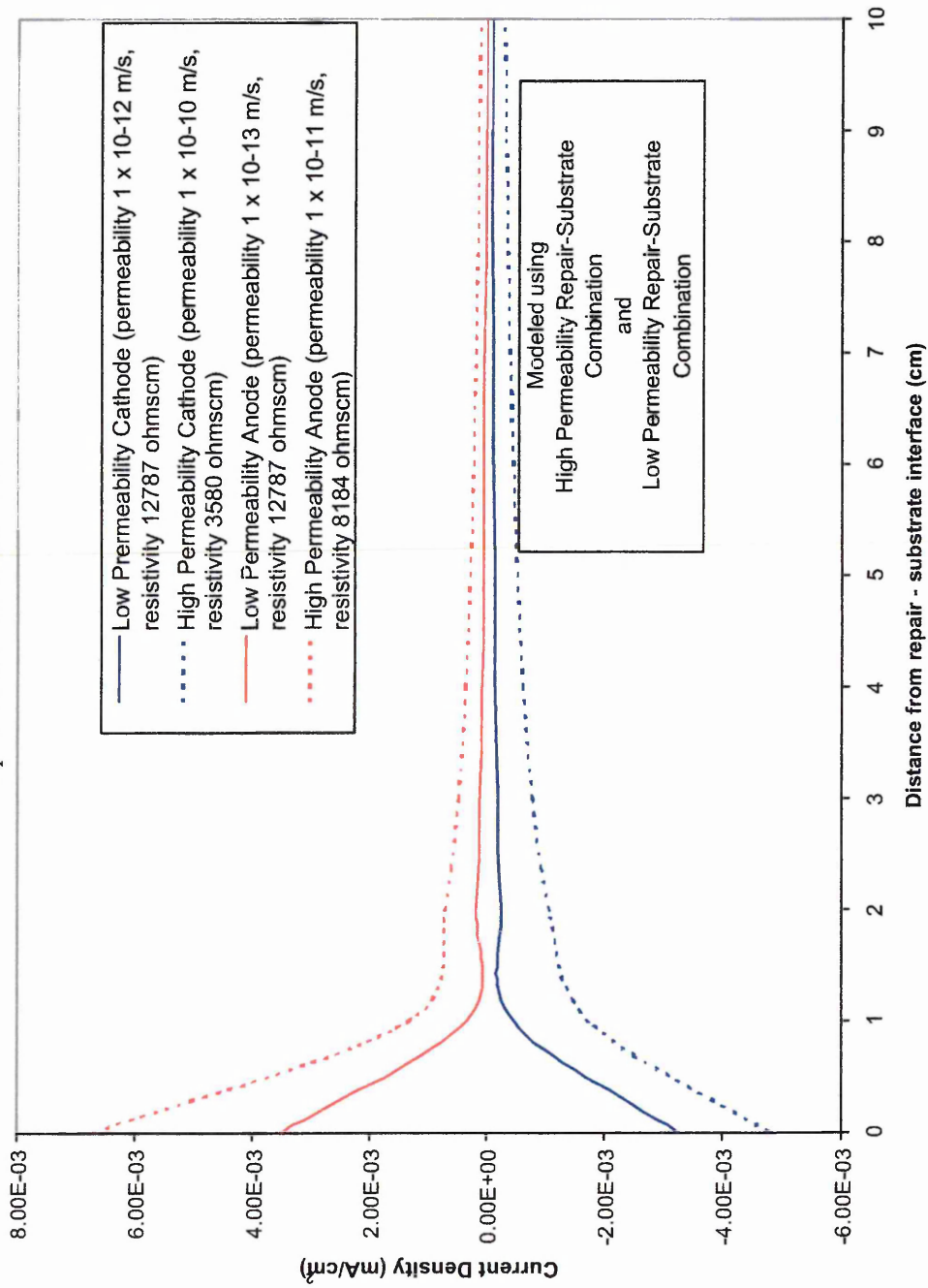
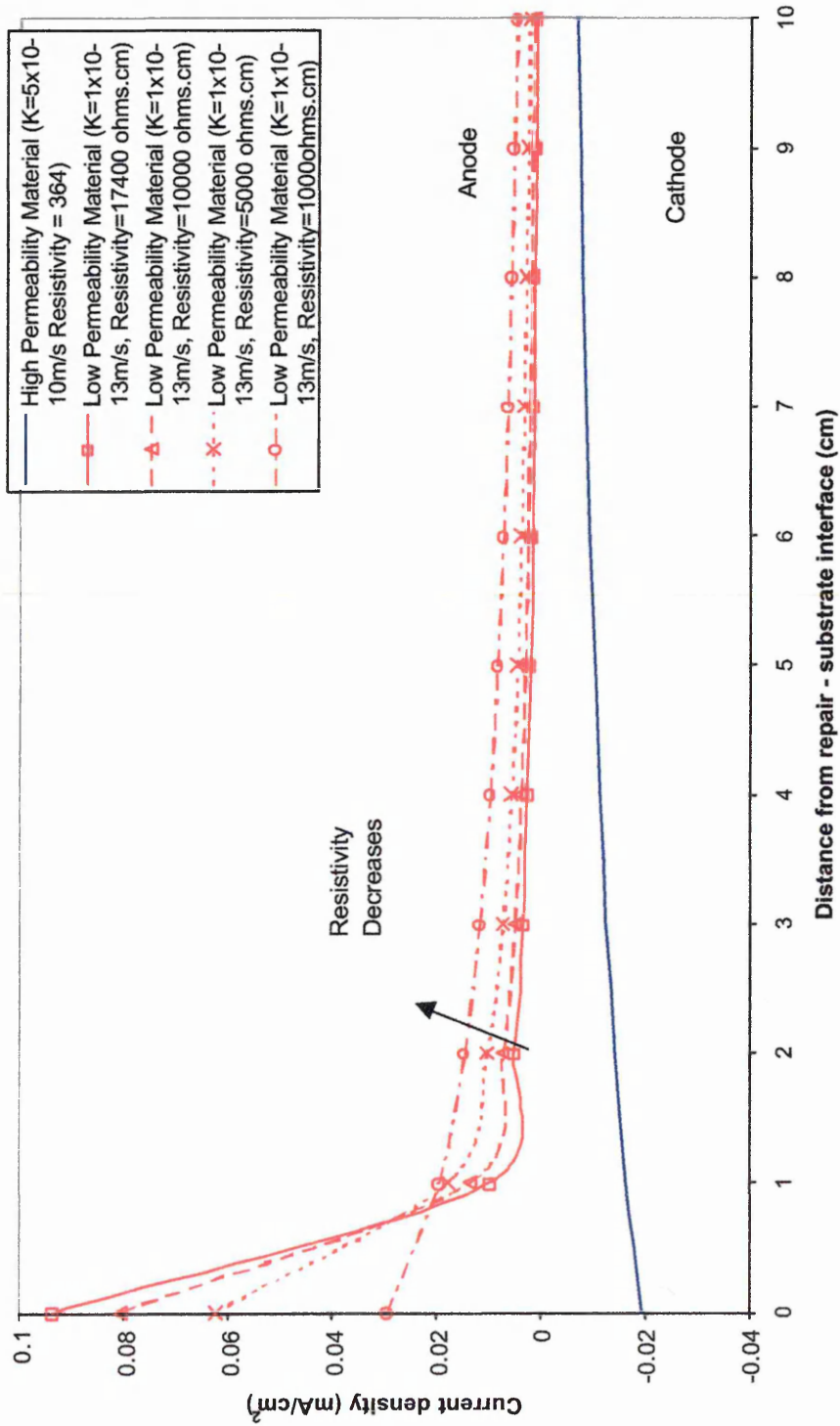


Figure 7.13 Effect of changes in resistivity of the anode on the distribution of galvanic current



a cathodic current is represented as a negative value and the anodic current is positive. As the cathodic site represents the site of oxygen reduction, the cathodic area controls the galvanic current flowing in the cell. Therefore the total galvanic current is also represented as a negative value.

Figures 7.4 and 7.5 show the results of the model of current distribution for material A when combined with the 0.4 w/c and the 0.8 w/c substrates. Material A has the highest resistivity and lowest permeability of all the materials examined during the experimental study. The cell potential of material A is, therefore, lower than either of the substrate materials, making it the anodic site and the substrate the cathodic site. The 0.4 w/c substrate has a lower permeability and higher resistivity than the 0.8 w/c substrate. This results in a lower half-cell potential for the 0.4 w/c substrate than the 0.8 w/c substrate. Therefore, the difference in potential between material A and substrate material increases depending on the substrate material (0.4 w/c or 0.8 w/c substrate). In addition the lower resistivity of the 0.8w/c substrate produces a lower IR drop in the substrate. This allows a larger cathodic area in the 0.8 w/c substrate than in the 0.4 w/c substrate. The potential difference is larger and operates over a bigger area in the 0.8 w/c substrate and will produce a correspondingly larger galvanic current. In addition, the current continues to increase over a larger distance from the repair in figure 7.5 for the 0.8w/c substrate compared to figure 7.4 for the 0.4 w/c substrate.

The larger galvanic current produced by the 0.8 w/c substrate produces a larger anodic current in material A. Therefore, the corresponding corrosion rate of steel embedded in material A will be higher when combined with the 0.8 w/c substrate as opposed to the 0.4 w/c substrate. However the anodic area appears to be similar in for both substrates, as the high resistivity of material A produces a large IR drop.

Although figures 7.4 and 7.5 show that the anodic current is higher in the 0.8 w/c substrate over the entire area of rebar examined in material A, the current quickly drops to a level below $3 \mu\text{A}/\text{cm}^2$ in both cases. A current of this magnitude can be considered to be insignificant with respect to corrosion rate. The galvanic current is concentrated in the first 2 to 3 cm of the anode. This results in extremely high anodic currents and hence corrosion rates at the interface between substrate and repair material A.

Figures 7.6 and 7.7 show the model results for material B combined with the 0.4 w/c and 0.8 w/c substrates. Material B has a higher permeability than either substrate and so the embedded steel is cathodic compared to steel in either substrate. For material B combined with the 0.8 w/c substrate (figure 7.7) the difference in permeability is small, and this has produced a correspondingly small difference in potential. As can be seen in figure 7.7, the total galvanic current and the corresponding cathodic and anodic currents are small in this case. In figure 7.6, the 0.4w/c substrate and material B combination produces a significantly higher galvanic current. This results in higher cathodic current densities for steel in material B and higher anodic current densities for steel in the 0.4 w/c substrate. The anodic current densities for the steel in the 0.4 w/c and 0.8 w/c substrates are concentrated at the interface within the first centimetre from the repair. However, material B which, contains the cathode has a higher resistivity than both the substrates which contain the anodic sites. This was due to the addition of chloride to the substrate at mixing. It would therefore be expected that the cathodic site would be smaller in area than if the resistivity was lower. This appears to be the case in figure 7.7, where the cathodic current densities between 0 and 1 cm from the interface between the repair and substrate are higher than the corresponding anodic current density.

Material C combined with the 0.4 w/c and 0.8 w/c substrates shows the same trends as for materials A and B, as shown in figures 7.8 and 7.9. Material C has the highest permeability and lowest resistivity of the repair materials examined and the steel embedded in it is, therefore, cathodic. The 0.8 w/c substrate had a closer match of permeability to material C and, therefore, the difference in cell-potentials was also less. Correspondingly the galvanic current generated by the 0.8w/c substrate combined with material C was lower than for the 0.4 w/c combination. The largest anodic and cathodic current densities are within 2 cm of the repair substrate interface. As the distance from the interface increases the current density drops quickly and after approximately 3 cm from the interface is insignificant.

For all the materials studied the anodic current densities predicted by the model were higher at the interface than in the bulk material. One method of validating the model is to compare the experimental corrosion rates measured from the interface for each specimen with the corrosion rates measured from the anodic sites of the specimens. Figure 7.10 shows the average corrosion currents measured over the final six months of the study for the interface and the anodic site. In all cases except one, the corrosion current at the interface is higher than at the anodic site. This appears to support the findings from the model.

7.3 SIGNIFICANCE OF MODELING WITH RESPECT TO CONCRETE

REPAIR

The model used in this study is one-dimensional and so cannot be considered sufficiently sensitive or sophisticated to provide life predictions for concrete repairs. However, the model can provide guidance on the general effect of certain generic repair substrate combinations on the corrosion of embedded steel reinforcement. Three basic scenarios have been modelled here:

- Effect of a large disparity in permeability between repair and substrate
- Effect of a match in permeability between repair and substrate
- Effect of repair and substrate resistivity on size of cell.

7.3.1 Effect of A Large Disparity in Permeability of Repair and Substrate

The difference in size of half-cell potentials between the repair and substrate is significant in determining the galvanic corrosion current produced. The greater the difference in half-cell potentials, the larger the galvanic corrosion current generated. This study has identified that the difference in permeabilities between repair and substrate is a key factor generating an associated difference in half-cell potential. In the experimental work the 0.8 w/c substrate and material B combination shows the smallest disparity in permeabilities and, therefore, the smallest difference in half-cell potentials and hence the lowest galvanic current (see figure 7.8).

By using equation 6.1 from chapter 6, the empirical relationship between permeability and cell potential from the experimental data, it is possible to determine the potential of a material based on its permeability. This can be used in the model to examine the effect of different repair substrate combinations. However, in order that the permeability value chosen was consistent with data for actual cementitious materials, figure 4.5 from chapter 4 was used, this showed the variation in coefficient of permeability and the water cement ratio of the material. From examining this data it is apparent that the practical range of permeability coefficients is from 1×10^{-14} m/s to 1×10^{-10} m/s for cementitious materials in use on actual structures. A permeability coefficient of 1×10^{-10} m/s represents a substrate with a water cement ratio between 0.7 and 1.2, this would be

similar to repair material C from the experimental work. A value of 1×10^{-14} m/s would be equivalent to a low permeability repair material similar to material A.

The effect of different combinations of repair and substrate permeabilities on cell potentials is shown in Table 7.2. This indicates that the maximum practical difference in potential that could be expected from a difference in permeability between repair and substrate is approximately 150 mV. As the difference in permeability decreases so does the difference in potentials. Figure 7.11 shows the results of the combination of a substrate with a permeability of 5×10^{-10} m/s to repair materials of differing permeabilities. However, the higher permeability substrate also has a lower resistivity than the repair material. Therefore, the cathodic area is larger than the anodic area. The greater the difference in permeability the greater the current generated. The higher resistivity of the repair material means that the current is concentrated in the first 2 cm of the repair. The effect of a lower permeability repair material is to produce high rates of corrosion in the repair material at the interface between repair and substrate. As the difference in permeability decreases, the anodic current at the interface in the repair material also decreases. Figure 6.2 from Chapter 6 shows that resistivity of the material will fall with increasing permeability the presence of chlorides also has an effect the resistivity. A higher permeability substrate would tend to produce a greater galvanic current than a lower permeability substrate, as the cathodic area is larger. A higher permeability repair has a larger anodic area than a lower permeability repair material. Beyond the interface between repair and substrate materials the current becomes similar irrespective of the difference in permeabilities (figure 7.11). This indicates that the potential difference between the repair and substrate is critical in determining the level of galvanic current.

Table 7.2 Theoretical half-cell potentials and resistivity values for a repair materials combined with a high permeability substrate

Material	Permeability Coefficient (m/s)	Half-cell potential of embedded steel (mV wrt SCE)	Difference in embedded steel potential (mV wrt SCE)	Resistivity (Ωcm)
Substrate	5×10^{-10}	-494	-	3580
Repair	1×10^{-13}	-647	153	17400
Repair	1×10^{-12}	-606	112	12800
Repair	1×10^{-11}	-523	70	8180

7.3.2 Effect of a match in permeability between repair and substrate

Another method of examining the effect of mismatch is to look at two different repair substrate combinations that produce comparable differences in potentials. Figure 7.12 shows two such combinations, one of a high permeability repair and substrate, the other of a low permeability repair and substrate. Both combinations result in a difference in potentials between repair and substrate of 41mV. The lower resistivity of the high permeability material produces a bigger cathodic area and consequently higher corrosion at the interface between repair and substrate. The conclusion from this is that it is preferable to have a low permeability repair substrate combination than a high permeability combination

The present industry practice is to use a repair material of low permeability in all situations, assuming low permeability acts to mitigate corrosion. This work suggests

that it may be inappropriate to apply a low permeability material to a high permeability substrate, as it could result in high corrosion rates of the steel embedded in the repair at the interface with the substrate. However, a structure with a permeability coefficient as high as the 5×10^{-10} m/s, used in the present example, would suffer more serious corrosion problems due to general corrosion from chloride diffusion or carbonation. Galvanic corrosion of the repair is unlikely to be a problem in this situation. The general rule would appear to remain that low permeability cementitious materials mitigate corrosion of the steel.

7.3.3 Effect of repair and substrate resistivity on the size of cell.

The final situation under consideration is when a low permeability substrate material has a higher resistivity than the high permeability repair material. An example of this would be a high permeability repair material applied to a chloride contaminated, low permeability substrate. In this situation the steel within the chloride contaminated substrate would be the anode and that within the repair the cathode. In figure 7.13 a high permeability repair material ($K=5 \times 10^{-10}$ m/s) is joined to a low permeability material substrate ($K= 1 \times 10^{-13}$ m/s). This produces a difference in potential between repair and substrate of 152 mV. The graph shows the effect of decreasing the resistivity of the low permeability substrate by chloride contamination. Steel embedded in the high permeability material forms the cathodic site and is unaffected by the change in resistivity of the low permeability material. Therefore, the current produced is the same irrespective of the change in resistivity of the low permeability material. The factor controlling the size of the current is the area of steel within the high permeability material. In this instance, this equates to the size of the repair, i.e. the larger the repair, the larger the galvanic current. The effect of reducing the resistivity at the anode is to

alter the distribution of current. With high resistivity the current is concentrated at the interface in the first 1 to 2 cm of the low permeability material. As the resistivity is reduced, the current density at the interface falls, but the current density rises further into the substrate. Therefore a more even distribution of the current is achieved through the low permeability material and the effect is to produce a lower maximum corrosion rate effective over a larger area of steel.

In the repair-substrate cells the anode always has a lower permeability than the cathodic site. This would typically mean that the repair has a lower permeability than the substrate. One effect of this is that the cathode generally has a lower resistivity than the anode and that the area of the cathode is therefore bigger than the anode. The ratio of anode and cathode size will be equivalent to the ratio of resistivity of the anode to the cathode. It is recognised that a large cathode to anode area ratio will produce high corrosion rates at the anode, as the current generated by the cathode is focused on a smaller area.

The mechanism of galvanic corrosion between repair and substrate materials is similar to the creation of chloride macro-cells in concrete. When a chloride macro-cell is created the higher chloride level at the anode compared to the cathode implies that the resistivity at the anode will be lower than at the cathode. Therefore, the anode would generally be expected to have a larger area than the cathode in such circumstances. This is not as serious a situation as predicted by this model for repair substrate combinations, where high current densities and hence corrosion rates can be produced in small areas.

7.3.4 Practical Consequences of the Modelling work

Care must be taken in interpreting the significance of these results. While there is a significant difference in potential produced by extreme combinations of low and high permeability materials, this does not necessarily mean that it will be a significant cause of corrosion at concrete repair sites. The difference in potential is smaller than may be expected from the combination of two dissimilar metals, which is recognised as a significant source of corrosion problems. For example, the combination of steel and copper causes significant galvanic corrosion and would result in a potential difference of approximately 300mV. When the potential difference is below 50mV the level of galvanic corrosion is considered insignificant. It is only at the extreme combinations the effect of the disparity in permeabilities is likely to produce a potential difference that would suggest significant levels of galvanic corrosion. The model assumes that a galvanic corrosion cell has been initiated and models the distribution of currents within the cell. If the conditions are not established to initiate the galvanic cell then the disparity in properties will have no effect on corrosion of the steel embedded in the repair and substrate. No attempt is made to model the distribution of corrosion currents with time or any initiation period associated with the development of a galvanic cell.

It should also be appreciated that it may not be practical to match the permeability of repair material to the substrate material. Permeability is a function of the pore structure and will change and refine with age. A match at mixing, may not be a match after several years in service. The significance of this work to commercial concrete repair situations is to suggest that a repair material alone cannot be considered a totally effective form of corrosion prevention. The application of other protection methods needs to be considered to prevent premature failure of repair sites from corrosion. One

method is to use cathodic protection systems on the structure. This removes any differences in potentials from variations in chloride concentration and cover depth and is insensitive to differences in permeability between repair and substrate materials. This can be expensive and simpler alternatives are available in the form of barrier coatings and corrosion inhibitors. These can be applied to the surface of the substrate and repair materials, or applied to the reinforcement to mitigate any corrosion that may be initiated post-repair. This work indicates that any galvanic corrosion initiated by a mismatch between the repair and substrate is effective for only a few centimetres either side of the interface. Therefore, protection methods could be concentrated on the interface between the repair and the substrate. This would be more cost effective than applying the protection method to the entire surface of the structure.

7.4 SUMMARY AND CONCLUSIONS

The permeability of a material has been shown to be significant in controlling the half-cell potential of steel embedded in the material. The difference in half-cell potentials between the steel embedded in the repair and substrate materials is one of the main factors in terms of the magnitude of the galvanic current produced in a cell.

Steel embedded in the lower permeability material will have a lower cell potential and therefore be anodic. The reinforcement in the higher permeability material will be cathodic. The maximum potential difference likely from the use of cementitious materials with different permeabilities is of the order of 150mV.

Combinations of lower permeability repair and substrate materials produce lower galvanic currents than combinations of higher permeability materials for the same difference in potential.

Resistivity in the cells was found to control the effective area of steel in the anodic and cathodic sites. The area of the anode will increase as the resistivity of the material at the anode decreases and the area of the cathode will increase as the resistivity of the material at the cathode decreases. The larger the cathodic area, the larger the galvanic current generated. The smaller the anode, the higher the corrosion rates at the anodic sites.

Generally, the lower permeability material, which will be at the anodic site, will also have a higher resistivity. This means that the area of anodic steel will be smaller than the area of cathodic steel.

The highest corrosion rates will be at the interface between the repair and substrate. If the resistivity at the anode falls the current density at the interface will drop and correspondingly, the current density will rise further into anodic material.

Concrete repair alone cannot be considered to be a method of corrosion protection. The model supports the traditional view that low permeability materials produce lower corrosion rates. The model also supports the view that the better the match in permeability the lower the potential difference and therefore the lower the corrosion rate.

The model shows that the area of the steel affected by a galvanic cell caused by a disparity in permeability between repair and substrate is unlikely to be greater than a few centimetres either side of the repair.

It is not practical to match the permeabilities of repair and substrate materials. The present work suggests that barrier coatings on the steel or surface of the repair or substrate would only need to be employed at the interface to mitigate this form of corrosion.

8.0 Conclusions

The aim of this project was to examine the effect of combining repair and substrate materials with different physical properties on the corrosion of reinforcement embedded in these materials. This was accomplished by relating the physical properties of selected repair and substrate materials and measuring how corrosion developed with time in specimens made of different repair substrate material combinations. The following conclusions have been drawn from this work.

8.1 PHYSICAL AND ELECTROCHEMICAL PROPERTIES OF REPAIR AND SUBSTRATE MATERIALS

The permeability and chloride diffusion coefficient were related to the pore structure of the materials and the measurements independent of the constituents used in the different materials. This was not the case for resistivity and porosity measurements.

There was a clear relationship between permeability and chloride diffusion coefficients for the materials examined during the study.

Of the properties examined, permeability of the materials provided the most meaningful method of comparing the mismatch between repair and substrate materials.

All the materials produced similar polarisation curves indicating that the steel was in a similar chemical environment in all the materials.

Materials with lower permeability coefficients had lower corrosion potentials for the steel embedded in the material. This followed the behaviour expected from the Nernst

equation. This suggested that the lower permeability materials had lower oxygen levels, resulting in the lower potentials.

There was also a relationship between the log of the permeability coefficient, the anodic Tafel constant. This showed that the higher the permeability coefficient, the lower the anodic Tafel constant, suggesting that the materials with higher permeability coefficients were more active.

No corresponding relationship was found with the cathodic Tafel constant, which was relatively constant for all the materials examined in this study.

8.2 CORROSION OF THE TEST SPECIMENS

The potentials measured were all approximately within the general corrosion range -260 mV to -560 mV wrt SCE, indicating a high probability of corrosion according to ASTM C876.

However, potential was found to vary with permeability in the water saturated specimens, due to the low oxygen levels. The actual corrosion state of the steel was uncertain from the potential measurements.

The material with the lower permeability had the lower, more active, electrochemical potential.

No clear relationship was found between chloride concentration and electrochemical potential.

The lower the electrochemical potential measured the lower the corrosion current measured this indicates that the specimens were under anodic control for the duration of the study.

The average corrosion rate for the test specimens increased over the 12 months. This was true for all repair materials and substrate except the 0.8 w/c substrate, where the corrosion rate decreased.

The average resistivity for all the materials fell between 0 to 6 months and 6 to 12 months of the study caused by chloride diffusion with time.

By comparison solution resistance increased for all the materials except material C due to the corrosion of the reinforcing steel, producing a high resistance surface film.

It was concluded from this that resistivity was a function of the repair or substrate material and the condition solution resistance the resistance of the measuring circuit, including the embedded reinforcing steel.

This indicates that the test materials became more corrosive to steel with time, probably due to the diffusion of chlorides into the materials.

The reinforcement steel becomes less corrodable with time due to the formation of corrosion products on the surface of the bar.

8.3 DISPARITY IN PROPERTIES BETWEEN REPAIR AND SUBSTRATE MATERIALS ON CORROSION OF THE REINFORCEMENT STEEL.

The corrosion potentials showed similar trends to the corrosion potentials measured from the polarisation curves. This was a logarithmic relationship between electrochemical potential and permeability that complied with the Nernst equation.

The larger difference in permeability between the repair and substrate, the greater the difference in electrochemical potentials between the two materials.

This indicates that a difference in half-cell potentials between the steel embedded in the repair and substrate materials that could initiate a galvanic corrosion cell.

The material with lowest permeability (most negative potential) would be anodic and the material with the highest permeability cathodic.

During the first six months the lower permeability material corroded at a lower rate than the high permeability material. This indicated that no galvanic cell was in action and the material with easier oxygen access and higher chloride levels was corroding at a higher rate than the denser low chloride material.

During the second half of the study the relationship reversed and the corrosion current of the material identified as anodic by half-cell potentials was higher for larger mismatch in permeability. This indicated a higher corrosion rate in the anodic material for substrate repair combinations that result in large differences in half-cell potentials.

The increase in corrosion current was small, of the order of $5 \mu\text{Acm}^2$, but was taken to suggest that a galvanic cell was formed. The results did not provide evidence for an initiation mechanism for the galvanic cell.

8.4 MODELLING THE EFFECT OF DISPARITY

A mathematical model was proposed to examine the difference in potential caused by the mismatch in permeability between repair and substrate material to the size of galvanic current generated.

$$I_g = \frac{\ln[(R_s + R_r)x + Rp_r + Rp_s]}{R_s + R_r} U - \frac{\ln(Rp_r + Rp_s)}{R_s + R_r} U + \frac{U}{Rp_r + Rp_s}$$

The resistivity of the material controlled the distribution of current due to the IR drop within the cell. This defined the area of the anode or cathode within the cell.

In a low resistivity material the galvanic current will affect a larger area of the steel than in a high resistivity material.

The highest anodic current densities and therefore corrosion rates would be found at the interface between anodic and cathodic sites, located in the anodic material.

Generally the lower permeability material also has a higher resistivity. The area of anodic steel is therefore smaller than the area of cathodic steel. The higher resistivity of the material the smaller the anodic area and the higher the corrosion rate at the interface.

The permeability of the material controlled the electrochemical potential of steel embedded in the material. This determined the magnitude of the galvanic current produced in a cell.

The maximum potential difference likely from the use of cementitious materials of different permeabilities in the conditions considered in the model is of the order of 150mV.

Combinations of lower permeability materials would produce lower galvanic currents than combinations of higher permeability materials for the same difference in potential.

The model supports the traditional perception that low permeability materials produce lower corrosion rates. The model also supports the view that the better the match in permeability the lower the potential difference and therefore the lower the corrosion rate.

It is only at the extreme combinations the effect of a disparity in permeability is likely to produce a potential difference that could produce significant levels of galvanic corrosion.

However, the model is one-dimensional and assumes that a galvanic corrosion cell has been initiated. No attempt was made to model any initiation period for corrosion.

It should also be appreciated that it may not be practical to match the permeability of repair material to the substrate material and that repair materials alone cannot be considered a totally effective form of corrosion prevention.

9.0 Further Work

The current work has investigated the effect of a mismatch in permeability between a repair and substrate material on the corrosion of the steel embedded in the material. This has concentrated on the effect of galvanic corrosion cells between the repair and substrate. This shows a small effect on corrosion, particularly at the interface between the two materials.

It is debatable whether the effect on corrosion is significant in terms of other corrosion mechanisms occurring within a reinforced concrete structure. Therefore the practical benefit from further work studying the effect of differences in properties between repair and substrate materials appears limited. However there are a number of areas, which the current work has not been able to investigate and these could provide some scope for further work.

The modelling work was developed from the results of the experimental work. The model was one-dimensional and assumed that the galvanic cell had already initiated. The current work did not examine the initiation of the cell. It is possible that the results are an aberration of the experimental method and environment used in the study. Further work is required to determine if the galvanic cells due to a mismatch in permeability between repair and substrate can be produced in practical situations on reinforced concrete structures. The mechanism and time for initiation of the galvanic cell need to be investigated.

The existence of a difference in potential does not in itself prove that a galvanic cell has been created. The high pH of cementitious materials would act to maintain the steel in a passive state, and the application of a potential difference would not make the steel active. None of the experimental measurements conducted in this study can provide information on the

initiation of corrosion of the steel in these galvanic cells. This is particularly true for the low permeability material A, where the chloride concentrations measured after the 12 month exposure period were still below a level expected to destroy the passive film on the steel. A possible explanation could be local acidification of the steel mortar interface from exposure to the potential difference. It is not clear from literature whether this is possible in cementitious material with the buffering of high pH from calcium hydroxide. Further work to investigate this would technically be difficult.

The current work has examined the implication of differences in permeability on the electrochemical potential and corrosion of the steel reinforcement. This concluded that the maximum likely difference in potential was 150 mV. Other factors, such as, cover depth can effect oxygen levels and therefore electrochemical potential of steel. Differences in cover depth would also produce differences in electrochemical potential. This area was examined in the current study.

This work has concluded that the use of repair materials alone cannot be considered a form of corrosion protection. Repair systems would also need to include corrosion protection methods, such as; barrier coatings, both on reinforcement and the surface of cementitious materials, inhibitors and cathodic protection. The use of sacrificial anodes at the interface between the repair and substrate could also act to mitigate this form of corrosion. The effectiveness of many of these techniques is not fully accepted and allows considerable scope for further work.

The results from the experimental work were difficult to interpret and further work using different experimental techniques might clarify some of the results obtained. In the current

study corrosion current measurements were made to study the creation of galvanic cells. An alternative approach would have been to make galvanic current measurements using a zero resistance ammeter. This would have provided a direct measurement of the size of galvanic current and the area of the steel over which the cell operated. The current work produced a model of the effect of a mismatch in permeability on corrosion and these extra measurements would be useful to fully validate the model.

The type of model employed in this study could also be used to look at chloride macro-cell corrosion. This work could provide an alternative approach to the study of chloride induced macro-cells, particularly in identifying the area over which a macro-cell would be active in a structure. This could also be beneficial in further investigating incipient corrosion on structures. Here, the anodic site is shifted down a structure from one high chloride area to the next by progressive repair. The current work indicates macro-cells produced by repair would only be effective over a few centimetres of the structure. This could be valuable work in identifying repair and maintenance strategies for structures.

10.0 References

- 1 O'BRIEN, T.P. Concrete deterioration and repair. *Proceedings of Institution of Civil Engineers Part 1*, August 1980, vol. 68, p. 399-408.
- 2 ALLEN, R.T.L. and FORRESTER J.A. Choosing a concrete repair system. *Construction repairs & maintenance*, September 1986, p. 10-12.
- 3 TROCONIS De RINCON O. and ROMERO De CARRUYO A. The importance of diagnosing before repairing reinforced concrete structures. *Materials Performance*, October 1998, p. 69-76.
- 4 THE WORKING PARTY OF THE CONCRETE SOCIETY Concrete Society Technical Report 36: Patch repair of reinforced concrete subject to reinforcement. *Corrosion Concrete Society*, 1991.
- 5 KAY, E.A. and DAVIES, H. The European standard on concrete repair principles. *Construction Repair*, vol. 6, 1997, p. 52-55.
- 6 ROBERY, P.R. Maintenance and repair strategies. *Construction Repair*, vol 6, 1997. p. 633-638.
- 7 LITTLE, D. Effective repair and protection of concrete. *Construction Repairs & Maintenance*, September 1986, p. 23-25.
- 8 STANFIELD, R.F. Waterborne maintenance systems for concrete structures. *Construction Repair*, May/ June 1996, p.10-16.
- 9 GRANTHAM, M. and GRAY, M. Patch repairs and cathodic protection. *Construction Repairs*, vol. 6, 1997, p.42-45.
- 10 McCURRICH, L.H., KEELEY, C., CHERITON, L.W. and TURNER, K.J. Mortar repair systems - Corrosion protection for damaged reinforced concrete. *Corrosion of Reinforcement in Concrete Construction*, Publisher: Ellis, H., Editor: Crane, A., 1983, p. 235-253.
- 11 WHEAT, H.G. and ELIEZER, Z. Comments on the identification of a chloride threshold of steel in concrete. *Corrosion*, 1987, vol. 43, no. 2, p.127-128.

- 12 ALLEN, R.T.L. and FORRESTER, J.A. The investigation and repair of damaged reinforced concrete structures. *Corrosion of Reinforcement in Concrete Construction*, Publisher: Ellis, H., Editor: Crane, A., 1983, p.223-234.
- 13 OHAMA, Y. DEMURA, Polymer based materials for repair and improved durability: Japanese experience. *Construction and Building Materials*, 1996, vol. 10, no. 1, p.77-82.
- 14 OHAMA, Y. DEMURA, Pore size distribution and oxygen diffusion resistance of polymer-modified mortars. *Cement and Concrete Research*, 1991, vol. 21, p.309-315.
- 15 KOBAYASHI, K. and SHUTTOH, K. Oxygen diffusivity of various cementitious materials. *Cement and Concrete Research*, 1991, vol. 21, p.273-284.
- 16 PARROTT, L.J. Some effects of cement and curing upon carbonation and reinforcement corrosion in concrete. *Materials and Structures*, April 1996, vol. 29, p.164-173.
- 17 NILSSON, L.O., POULSEN, E., SANDBERG, P., SORENSEN, H.E. and KLINGHOFFER, O., Chloride penetration into concrete. *State of the art transport processes corrosion initiation test methods and penetration models*, Danish Road Directorate, Publisher: HETEK, 1996.
- 18 KEER, J.G., CHADWICK, J.R. and THOMPSON, D.M. Protection of reinforcement by concrete repair materials against chloride induced corrosion. *Corrosion of reinforcement in concrete*, Publisher: Elsevier Applied Science, Editor: Page, C.L., Treadaway, K.W.J. and Bamforth, P.B., 1990, p.420-432.
- 19 PING GU, ZHONGZI XU, PING XIE and BEAUDOIN, J.J. Application of ac impedance techniques in studies of porous cementitious materials. *Cement and Concrete Research*, 1993, vol. 23, p.531-540.
- 20 PING GU, BEAUDOIN, J.J., TUMIDAJSKI, P.J. and MAILVAGANAM N.P. Electrochemical incompatibility of patches in reinforced concrete. *Concrete International*, August 1997, p.68-72.
- 21 CUSSON, D. and MAILVAGANAM Durability of repair materials. *Concrete International*, March 1996, p.34-38.
- 22 EMMONS, P.H. and VAYSBURD, A.M. The total system concept - necessary for improving the performance of repaired structures. *Concrete International*, March 1995, p.31-36.

- 23 EMMONS, P.H. and VAYSBURD, A.M. System concept in design and construction of durable concrete repairs. *Construction and Building Materials*, 1996, vol. 101, p. 69-75.
- 24 PAGE, C.L. and LAMBERT, P. Kinetics of oxygen diffusion in hardened cement pastes. *Journal of Materials Science*, 1987, vol. 22, p.942-946.
- 25 WHEAT, H.G. Corrosion rate determination on repaired reinforced concrete specimens Corrosion rates of steel in concrete. Publisher: ASTM, Editor: Burke, N.S. Chaker, V. and Whiting, D., 1990, p. 52-65.
- 26 LAMBE, R.W., HUMPHREY, M.J. and WATKINS, T.F. Development of materials for repair and protection of reinforced concrete. *Corrosion of reinforcement in concrete*, Publisher: Elsevier Applied Science, Editor: Page, C.L. Traedaway, K.W.J. and Bamforth, P.B., 1990, p.471-485.
- 27 SCHIESSL, P. and BREIT, W. Local repair measures at concrete structures damaged by reinforcement corrosion - aspects of durability. *Corrosion of Reinforcement in Concrete Construction*, Publisher: SCI, Editor: Page, C.L. Bamforth, P.B. and Figg, J.W., 1996, p.525-534.
- 28 RAUPACH, M. Chloride-induced macrocell corrosion of steel in concrete - theoretical background and practical consequences. *Construction and Building Materials*, 1996, vol. 105, p.329-338.
- 29 HOLLINSHEAD, K., BIGLAND, D.J. and PETTIFER, R.J. Natural exposure in UK of repaired specimens in BRITE project 3291. *Corrosion of Reinforcement in Concrete Construction*, Publisher: SCI, Editor: Page, C.L. Bamforth, P.B. and Figg, J.W., 1996, p.535-545.
- 30 PAGE, C.L. and TREADAWAY, K.W.J. Aspects of the electrochemistry of steel in concrete. *Nature*, 1982, vol. 297, p.109-114.
- 31 Corrosion of Steel in Concrete. *Report of the Technical Committee 60-CSC RILEM*, Publisher: Chapman and Hall, Editor: Schiessl, P., 1988.
- 32 GLASS, G.K. HASSANEIN, A.M. and BUENFELD, N.R. Monitoring the passivity of steel in concrete induced by cathodic protection. *Corrosion Science*, 1997, vol. 39, no. 8, p. 1451-1458.
- 33 ANDRADE, C. and ALONSO, C. Corrosion rate monitoring in the laboratory and on site. *Construction and Building Materials*, 1996, vol. 105, p. 315-328.

- 34 POURBAIX, M. *Atlas of electrochemical equilibria*. Publisher: Pergamon, Editor: Franklin J.A., 1966, p 307-321
- 35 BAZANT P.Z. Physical model for steel corrosion in concrete sea structures – Theory. *Journal of the Structural Division ASCE*, 1979, vol. 105, no. 6, p. 1137-1153.
- 36 BRET, C.M.A. and BRET, A.M.O. *Electrochemistry principles methods and applications*. Oxford Science Publications, 1993.
- 37 LEEK D.S. The passivity of steel in concrete. *Quarterly Journal of Engineering Geology*, 1991, vol. 24, p. 55-66.
- 38 BAZANT, Z.P. Physical model for steel corrosion in concrete sea structures – Application. *Journal of the Structural Division ASCE*, 1979, vol. 105, no. 6, p. 1155-1166.
- 39 ANDRADE, C. ALONSO, M.C. GONZALEZ, J.A. and FELIU S. Similarity between atmospheric/ underground corrosion and reinforced concrete corrosion. *Corrosion of Reinforcement in Concrete*, Publisher: Elsevier Applied Science, Editor: Page, C.L. Traedaway, K.W.J. and Bamforth, P.B., 1990, p. 39-48.
- 40 ESCALANTE, E. The effect of soil resistivity and soil temperature on corrosion of galvanically coupled metals in soil. *Galvanic Corrosion*, Publisher: ASTM, Editor: Hack, H.P.1986, p. 193-202.
- 41 ARUP, H. The mechanisms of the protection of steel by concrete. *Corrosion of Reinforcement in Concrete Construction*, Publisher: Ellis, H., Editor: Crane A.P., 1983, p. 151-158.
- 42 KRUGER, J. Passivity of metals - A materials science perspective. *International Materials Review*, 1988, vol. 33, no. 3, p.113-129.
- 43 MARTIN, F. and OLEK J. The nature of passivity of reinforcing steel. *Materials for the New Millennium 4th Materials Eng. Conf. Washington*, 10-14 Nov 1996, p.1111-1120.
- 44 GONZALEZ, J.A., ALGABA, S. and ANDRADE, C. Corrosion of reinforcing bars in carbonated concrete. *British Corrosion Journal*, 1980, 15, 3, p.135-139.
- 45 HOUST, Y.F. and WITTMANN, H. Influence of porosity and water content on the diffusivity of CO₂ and O₂ through hydrated cement paste. *Cement and Concrete Research*, 1994, vol.24, no.6, p.1165-1176.

- 46 GURASAMMY K. *PhD. Thesis*, Aberdeen University 1987.
- 47 BRE Digest no.444, 2000.
- 48 WHEAT, H.G. and ELIEZER, Z. Some electrochemical aspects of the corrosion of steel in concrete. *Corrosion*, 1985, vol. 41, no. 11, p.640-645.
- 49 PAGE, C.L., LAMBERT, P. and VASSIE, P.R.W. Investigations of reinforcement corrosion. 1. The pore electrolyte phase in chloride-contaminated concrete. *Materials and Structures*, 1991, vol. 24, p. 243-252.
- 50 MANGAT, P.S. and MOLLOY, B.T. Factors influencing chloride-induced corrosion of reinforcement in concrete. *Materials and Structures*, 1992, vol. 25, p. 404-411.
- 51 MANGAT, P.S. and GURASAMY, K. Pore fluid composition under marine exposure of steel fibre reinforced concrete. *Cement and Concrete Research*, 1987, vol. 17, p. 734-742.
- 52 KAYYALI, O.A. and HAQUE, M.N. The Cl/ OH ratio in chloride contaminated concrete a most important criterion. *Magazine of concrete research*, 1995, vol. 47, no. 172, p. 235-242.
- 53 YONEZAWA, ASHWORTH, V. and PROCTER, R.P.M. Pore solution composition and chloride effects on the corrosion of steel in concrete. *Corrosion*, 1988, vol. 44, no. 7, p. 489-499.
- 54 TANG, L. and NILSSON, L.O. Chloride binding capacity and binding isotherms of OPC pastes and mortars. *Cement and Concrete Research*, 1993, vol. 23, p. 247-253.
- 55 MANGAT, P.S. MOLLOY, B.T. Chloride binding in concrete containing PFA GBS or silica fume under sea water exposure. *Magazine of Concrete Research*, 1995, vol. 47, no. 171, p. 129-141.
- 56 SURYAVANSHI, A.K., SCANTLEBURY, J.D. and LYON, S.B. Mechanisms of Friedel's salt formation in cements rich in tricalcium aluminate. *Cement and Concrete Research*, 1996, vol. 26, no. 5, p. 7171-727.
- 57 HAWKINS, C. and MCKENZIE, M. Environmental effects on reinforcement corrosion rates. Corrosion of reinforcement in concrete construction. SCI, Page C.L. Bamforth P.B. Figg J.W. 1996, p. 167-175.

- 58 MANGAT, P.S., KHATIB, J.M. and MOLLOY, B.T. Microstructure chloride diffusion and reinforcement corrosion in blended cement paste and concrete. *Cement and Concrete Composites*, 1994, vol. 16, p. 73-81.
- 59 CAO, H.T. and SIRIVIVATNANON, V. Corrosion of steel in concrete with and without silica fume. *Cement and Concrete Research*, 1991, vol. 21, p. 316-324.
- 60 DAWSON, J.L., JOHN, D.G., JAFAR, M.I., HLADKY, K. and SHERWOOD L. Electrochemical methods for inspection and monitoring of corrosion of reinforcing steel in concrete. *Corrosion of Reinforcement in Concrete*, Publisher: Elsevier Applied Science, Editor: Page, C.L. Traedaway, K.W.J. and Bamforth, P.B., 1990, p. 358-371.
- 61 WILKINS, N.J.M. and LAWRENCE, P.F. The corrosion of steel reinforcements in concrete immersed in seawater. *Corrosion of Reinforcement in Concrete Construction*, Publisher: Ellis, H., Editor: Crane, A., 1983, p.119-142.
- 62 RAUPACH, M. Corrosion of steel in the area of cracks in concrete: laboratory tests and calculations using a transmission line model. *Corrosion of Reinforcement in Concrete Construction*, Publisher: SCI, Editor: Page, C.L. Bamforth, P.B. and Figg, J.W., 1996, p. 13-23.
- 63 BERKE, N.S DALLAIRE, M.P. HICKS, M.C. and HOOPES, R.J. Corrosion of steel in cracked concrete. *Corrosion*, November 1993, p. 934-943.
- 64 BERKE, N.S., DALLAIRE, M.P., HICKS, M.C. and HOOPES, R.J. Corrosion of steel in cracked concrete - Reply to Discussion. *Corrosion*, 1994, vol. 50, no. 10, p. 781-784
- 65 SUZUKI, K., OHNO, Y., PRAPARNTANATORN, S. and TAMURA, H Mechanism of steel corrosion in cracked concrete. *Corrosion of Reinforcement in Concrete in Concrete Construction*, Publisher: SCI, Editor: Page, C.L. Bamforth, P.B. and Figg, J.W., 1996, p. 24-32.
- 66 OHNO, Y., PRAPARNTANATORN, S. and SUZUKI, K. Influence of cracking and water cement ratio on macrocell corrosion of steel in concrete. *Corrosion of Reinforcement in Concrete Construction*, Publisher: SCI, Editor: Page, C.L. Bamforth, P.B. and Figg, J.W., 1996, p. 24-32.
- 67 PING, GU, ELLIOT, S., HRISTOVA, R., BEAUDOIN, J. J., BROUSSEAU, R. and BALDOCK, B. A study of corrosion inhibitor performance in chloride contaminated concrete by electrochemical impedance spectroscopy. *ACI Materials Journal*, Sept/Oct 1997, p. 385-395.

- 68 GOUDA, V.K. and HALAKA, W.Y. Corrosion and corrosion inhibition of reinforcing steel - II. Embedded in concrete. *British Corrosion Journal*, Sept 1997, vol. 05, p. 204-208.
- 69 NOGGERATH, J. and BOHNI, H Macro cell corrosion of steel in chloride containing concrete. *Materials Science Forum*, 1992, vol. 111-112, p. 659-676.
- 70 SCHIESEL, P. and RAUPACH, M, Chloride induced corrosion of steel in concrete - Investigation with a concrete corrosion cell, *Corrosion of Reinforcement in Concrete Construction*, Publisher: SCI, Editor: Page, C.L. Bamforth, P.B. and Figg, J.W., 1996,p. 226-231.
- 71 GULIKERS, J. and SCHLANGEN, E. Numerical analysis of galvanic interaction in reinforcement corrosion. *Corrosion of Reinforcement in Concrete Construction*, Publisher: SCI, Editor: Page, C.L. Bamforth, P.B. and Figg, J.W., 1996, p. 3-12.
- 72 GULIKERS, J. Development of a galvanic corrosion probe to Assesss the corrosion rate of steel reinforcement. *Corrosion of Reinforcement in Concrete Construction*, Publisher: SCI, Editor: Page, C.L. Bamforth, P.B. and Figg, J.W., 1996, p. 327-336.
- 73 ARYA, C. and VASSIE, P.R.W. Effective cathode to anode ratio and reinforcement corrosion in concrete corrosion of reinforcement in concrete. *Corrosion of Reinforcement in Concrete Construction*, Publisher: SCI, Editor: Page, C.L. Bamforth, P.B. and Figg, J.W., 1996, p. 33-42
- 74 *Impedance Spectroscopy - Emphasizing Solid Materials And Systems*. Publisher: John Wiley & Sons Inc, Editor: MacDonald J.R., 1987.
- 75 RAUPACH, M. Investigations on the influence of oxygen on corrosion of steel in concrete - Part 1, *Materials and Structures*, April 1996, vol. 29, p. 174-184.
- 76 RAUPACH, M. Investigation on the influence of oxygen on corrosion of steel in concrete - Part 2. *Materials and Structures*, April 1996, vol. 29, p. 226-232.
- 77 GONZALEZ, J.A, LOPEZ, W. and RODRIGUEZ, P. Effects of moisture availability on corrosion kinetics of steel embedded in concrete. *Corrosion*, vol 49, December, 1993, vol 49, No 12, p. 1004-1010.
- 78 GONZALEZ, J.A., MOLINA A., OTERO, E. and LOPEZ, W. On the mechanism of steel corrosion in concrete: the role of oxygen diffusion. *Magazine of Concrete Research*, 1990 vol. 42, no. 150, p. 23-27.

- 79 GONZALEZ, J.A., OTERO, E., FELIU, S., BAUTISTA, A., RAMIREZ, E., RODRIGUEZ, P. and LOPEZ, W. Some considerations on the effect of chloride ions on the corrosion of steel reinforcements embedded in concrete structures. *Magazine of Concrete Research*, 1998, vol. 50, no. 3, p. 189-199.
- 80 SUZUKI, K., OHNO, Y., PRAPANTANATORN, S. and TAMURA, H. Some phenomena of macrocell corrosion. *Corrosion of Reinforcement in Concrete*, Publisher: Elsevier Applied Science, Editor: Page, C.L. Traedaway, K.W.J. and Bamforth, P.B., 1990, p. 87-95.
- 81 KIEGER, P and LAMOND, J.F. Concrete Testing. *ASTM Special Publication 169c*, 1994.
- 82 TECHNICAL REPORT No31, Permeability Testing of Site Concrete. *Concrete Society*, 1987.
- 83 GRATTAN-BELLEW, P.E. Microstructural investigation of deteriorated Portland cement concretes. *Construction and Building Materials*, 1996, vol. 10, no. 1, p. 3-16.
- 84 KRUS, M., HANSEN, K.K. and KUNZEL, H.M. Porosity and liquid absorption of cement paste, *Materials and Structure*, Aug/Sept 1997, vol. 30, p. 394-398.
- 85 MANGAT, P.S. and EL-KHATIB, J.M. Influence of initial curing on pore structure and porosity of blended cement concrete. *Istanbul Conference SP 132-45*, 1992, p. 814-833.
- 86 GARBOCZI, E.J. and BENTZ, D.P. Computer simulation of diffusivity of cement based materials. *Journal of Materials Science*, 1992, vol. 27, p. 2083-2092.
- 87 GARBOCZI, E.J. and BENTZ D.P. Modelling of the microstructure and transport properties of concrete. *Construction and Building Materials*, 1996, vol. 105, p. 293-300.
- 88 GARBOCZI, E.J., SCHWARTZ, L.M. and BENTZ, D.P. Modelling the influence of the interfacial zone on the DC electrical conductivity of mortar. *Advanced Cement Based Materials*, 1995, vol. 2, p. 169-181.
- 89 BASHEER, P. A review of measurement of permeation properties of concrete on site. *Non-Destructive Testing in Civil Engineering*, Publisher: British Inst of NDT, Editor: Bungey, J.H., 1993, vol.1, p. 273-300.
- 90 XI, Y., BAZANT, Z.P., MOLINA, L. and JENNINGS H.M. Moisture Diffusion in cementitious materials. *Advanced Cement Based Materials*, 1994, vol. 1, p. 258-266.

- 91 XI, Y., BAZANT, Z.P. and JENNINGS, H.M. Moisture diffusion in cementitious materials. adsorption isotherms. *Advanced Cement Based Materials*, 1994, vol. 1, p. 248-257.
- 92 BUTLER, A. Capillary absorption by concrete. *Concrete*, July/Aug 1997, p. 23-25.
- 93 LAMBERT, P. Controlling Moisture. *Construction Repair*, vol. 6, 1997, p. 29-32.
- 94 DHIR, R.K., BYARS, E.A., CHAN, Y.N. and SHAABAN, I.G. ISAT prediction of concrete durability. *Non-Destructive Testing in Civil Engineering*, Publisher: British Inst of NDT, Editor: Bungey, J.H., 1993, vol.1, p. 301-314.
- 95 BROOMFIELD, J.P. The Assessment of corrosion of reinforcing steel on highway bridges. *Non-Destructive Testing in Civil Engineering*, Publisher: British Inst of NDT, Editor: Bungey, J.H., 1993, vol. 2, p. 551-566.
- 96 BASHEER, P., LONG, A.E. and MONTGOMERY, F.R. The autoclam permeability system for measuring the in-situ permeation properties of concrete. *Non-Destructive Testing in Civil Engineering*, Publisher: British Inst of NDT, Editor: Bungey, J.H., 1993, vol.1, p. 235-260.
- 97 LEEMING, M.B.A surface air permeability test for concrete and surface treatments on concrete *Non-Destructive Testing in Civil Engineering*, Publisher: British Inst of NDT, Editor: Bungey, J.H., 1993, vol.1, p. 261-272
- 98 DINKU, A. and REINHART, H.W. Gas permeability coefficient of cover concrete as a performance control. *Materials and Structures*, August-September 1997, vol. 30, p. 387-393.
- 99 HEARN, N. and MILLS, R.H. A simple permeater for water or gas flow. *Cement and Concrete Research*, 1991, vol. 21, p. 257-261.
- 100 LYDON, F.D. Effect of coarse aggregate and water/cement ratio on intrinsic permeability of concrete subject to drying. *Cement and Concrete Research*, 1995, vol. 25, no. 8, p. 1737-1746.
- 101 HEARN, N. and MORLEY, C.T. Self-sealing property of concrete - Experimental evidence. *Materials and Structures*, Aug/Sept 1997, vol. 30, p. 404-411.
- 102 KHATRI, R.P. and SIRIVIVATNANON, V. Methods for the determination of water permeability of concrete. *ACI Materials Journal*, May/June 1997, p. 257-261.

- 103 BAMFORTH, P.B. The relationship between permeability coefficients for concrete obtained using liquid and gas. *Magazine of Concrete Research*, 1987, vol. 39, no. 138, p. 3-11.
- 104 ANDRADE, C. and WHITINGS, D. A comparison of chloride ion diffusion coefficients derived from concentration gradients and non steady state accelerated ionic migration. *Materials and Structures*, October 1996, vol. 29, p. 476-484.
- 105 DHIR, R.K. JONES, M.R. AHMED, H.E.H. and SENEVIRATNE, A.M.G. Rapid estimation of chloride diffusion coefficient in concrete. *Magazine of Concrete Research*, 1990, vol. 42, no. 152, p. 177-185.
- 106 YU, S.W. and PAGE, C.L. Diffusion in cementitious materials: 1. Comparative study of chloride and oxygen diffusion in hydrated cement pastes. *Cement and Concrete Research*, 1991, vol. 21, p. 581-588.
- 107 ATKINSON, A. and NICKERSON, A.K. The diffusion of ions through water-saturated cement. *Journal of Materials Science*, 1984, vol. 19, p. 3068-3078.
- 108 TANG, L. Concentration dependence of diffusion and migration of chloride ions, Part 1: Theoretical considerations. *Cement and Concrete Research*, 1999, vol. 29, p. 1463-1468.
- 109 TANG, L. Concentration dependence of diffusion and migration of chloride ions, Part 2: Experimental evaluation. *Cement and Concrete Research*, 1999, vol. 29, p. 1469-1474.
- 110 JENSEN, O.M. HANSEN, P.F. COATS, A.M. and GLASSER, F.P. Chloride ingress in cement paste and mortar. *Cement and Concrete Research*, 1999, vol. 29, p. 1497-1504.
- 111 AZARI, M.M., MANGAT, P.S. and TU, S.C. Chloride ingress in microsilica concrete. *Cement and Concrete Composites*, 1993, vol. 15, p. 215-221.
- 112 MANGAT, P.S. and GURUSAMY, K. Chloride diffusion in steel fibre reinforced marine concrete. *Cement and Concrete Research*, 1987, vol. 17, p. 385-396.
- 113 HONG, K. and HOOTON, R.D. Effects of cyclic chloride exposure on penetration of concrete cover. *Cement and Concrete Research*, 1999, vol. 29, p. 1379-1386.
- 114 LIANG, M.T., WANG, K.L. and LIANG, C.H. Service life predictions of reinforced concrete structures. *Cement and Concrete Research*, 1999, vol. 29, p. 1411-1418.

- 115 THOMAS, M.D.A. and BAMFORTH, P.B. Modelling chloride diffusion in concrete effect of fly ash and slag. *Cement and Concrete Research*, 1999, vol. 29, p. 487-495.
- 116 DHIR, R.K. JONES, M.R. and AHMED, H.E.H. Concrete durability: estimation of chloride concentration during design life. *Magazine of Concrete Research*, 1991, vol. 43, no.154, p. 37-44.
- 117 DHIR, R.K., JONES, M.R. and NG, S.L.D. Prediction of total chloride content profile and concentration/time-dependent diffusion coefficients for concrete. *Magazine of Concrete Research*, 1998, vol. 50, no.1, p. 37-48.
- 118 JOHANSEN, V., GOLTERMANN, P. and THAULOW, N. Chloride transport in concrete. *Concrete International*, July 1995, p. 43-44.
- 119 MANGAT, P.S. and MOLLOY, B.T. Prediction of long term chloride concentration in concrete. *Materials and Structures*, 1994, vol. 27, p. 338-346.
- 120 MANGAT, P.S. and MOLLOY, B.T. Prediction of free chloride concentration in concrete using routine inspection data. *In publication*.
- 121 BERKE, N.S. and HICKS, H.C. Predicting times to corrosion from field and laboratory chloride data. *Techniques to Assess the Corrosion Activity of Steel Reinforced Concrete Structures ASTM STP 1276*, Publisher ASTM, Editor Berke, N.S. Escalante, E. Nmai, C.K. Whiting, D., 1996, p. 42-57.
- 122 BENTZ, E.C., EVANS, C.M. and THOMAS, M.D.A. Chloride diffusion modelling for marine exposed concretes. *Corrosion of Reinforcement in Concrete Construction*, Publisher: SCI, Editor: Page, C.L. Bamforth, P.B. and Figg, J.W., 1996, p. 136-145.
- 123 SAGUES, A.A. and KRANC, S.C. Effect of structural shape and chloride binding on time to corrosion of steel in concrete in marine service. *Corrosion of Reinforcement in Concrete Construction*, Publisher: SCI, Editor: Page, C.L. Bamforth, P.B. and Figg, J.W., 1996, p. 105-114.
- 124 POLDER, B. Laboratory testing of five concrete types for durability in a marine environment. *Corrosion of Reinforcement in Concrete Construction*, Publisher: SCI, Editor: Page, C.L. Bamforth, P.B. and Figg, J.W., 1996, p. 114-123.
- 125 HANSSON, C.M. Oxygen diffusion through Portland cement mortars. *Corrosion Science*, 1993, vol. 35, no.5-8, p. 1551-1556.

- 126 TUUTTI, K. Corrosion of steel in concrete. *Swedish Cement and Concrete Research Institute*, 1982.
- 127 BALABANIC, G., BICANIC, and N. DUREKOVIC, A. Mathematical modelling of electrochemical steel corrosion in concrete. *Journal of Engineering Mechanics*, December 1996, p. 1113-1122.
- 128 LIU, Y. and WEYERS, R.E. Time to cracking for chloride induced corrosion in reinforced concrete. *Corrosion of Reinforcement in Concrete Construction*, Publisher: SCI, Editor: Page, C.L. Bamforth, P.B. and Figg, J.W., 1996, p. 88-104.
- 129 HAUSMANN, D.A. A probability model of steel corrosion in concrete. *Materials Performance*, October 1998, vol 37, p. 64-68.
- 130 GLASS, G.K. and BUENFELD, N.R. Theoretical basis for designing reinforced concrete cathodic protection systems. *British Corrosion Journal*, 1997, vol. 32, no.11, p. 179-183.
- 131 KORETSKY, M.D., ABOOAMERI, F. and WESTALL, J.C. Effect of concrete pore saturation on cathodic protection of steel - Reinforced concrete bridges. *Corrosion*, 1999, vol. 55, no.1, p. 52-64.
- 132 ANDRADE, C. and ALONSO, C. Progress on design and residual life calculation with regards to rebar corrosion of reinforced concrete. *Techniques to Assess the Corrosion Activity of Steel Reinforced Concrete Structures ASTM STP 1276*, Publisher ASTM, Editor Berke, N.S. Escalante, E. Nmai, C.K. Whiting, D., 1996 p. 23-39.
- 133 MANGAT, P.S. and LIMBACHIYA, M.C. Effect of initial curing on chloride diffusion in concrete repair. *Cement and Concrete Research*, 1999, vol. 29, p. 1475-1485.
- 134 RODRIGUEZ, P., RAMIREZ, E. and GONZALEZ, J.A. Methods for studying corrosion in reinforced concrete. *Magazine of Concrete Research*, 1994, vol. 46, no.167, p. 81-90.
- 135 STRATFULL, R.F. Comments on the identification of a chloride threshold in the corrosion of steel in concrete. *Corrosion*, 1987, vol. 43, no.8, p. 483-485.
- 136 GRIMALDI, G. and RAHARINAIVO, A. Measuring the half-cell potential of steel embedded in immersed concrete: principles and application. *Corrosion of Reinforcement in Concrete Construction*, Publisher: SCI, Editor: Page, C.L. Bamforth, P.B. and Figg, J.W., 1996, p. 313-319.
- 137 PING GU, CARTER, P., BEAUDOIN, J.J., and ARNOTT, M. Validation of half-cell potential data from bridge decks. *Construction Repair*, May/June 1996, p. 18-20.

- 138 LAMBERT, P., PAGE, C.L., and VASSIE, P.R.W. Investigations of reinforcement corrosion. 2. Electrochemical monitoring of steel in chloride-contaminated concrete. *Materials and Structures*, 1991, vol. 24, p. 351-358
- 139 MEITZ J. and ISECKE B. Electrochemical potential monitoring on reinforced concrete using anodic pulse techniques. *Non-Destructive Testing in Civil Engineering*, Publisher: British Inst of NDT, Editor: Bungey, J.H., vol. 2, p. 567-578
- 140 FRANCOIS, R. and ARGIGUIE, G. Measurement of electrode potential of concrete reinforcing bars using a bi-electrode system. *Non-Destructive Testing in Civil Engineering*, Publisher: British Inst of NDT, Editor: Bungey, J.H., 1993, p. 597-604
- 141 JONES, M.R., MCCARTHY, M.J., and DHIR, R.K. Half-cell potential to estimate chloride-induced corrosion rates in structural concrete. *Non-Destructive Testing in Civil Engineering*, Publisher: British Inst of NDT, Editor: Bungey, J.H., 1993, vol. 2, p. 605-620.
- 142 NAGAYAMA, M., TAMURA, H. and SHIMOZAWA, K. Corrosion monitoring of rebars in an existing concrete structure. *Non-Destructive Testing in Civil Engineering*, Publisher: British Inst of NDT, Editor: Bungey, J.H., 1993, vol. 2, p. 621-632.
- 143 NAISH, C.C., HARKER, A. and CARNEY, R.F.A. Concrete inspection: Interpretation of potential and resistivity measurements. *Corrosion of reinforcement in concrete*, Publisher: Elsevier Applied Science, Editor: Page, C.L. Traedaway, K.W.J. and Bamforth, P.B., 1990, vol. 314-332.
- 144 DAWSON, J.L. Corrosion monitoring of steel in concrete. *Corrosion of Reinforcement in Concrete Construction*, Publisher: Ellis Horwood, Editor: Crane A.P, 1983, p. 175-191.
- 145 VASSIE, P.R. The half-cell potential method for locating corroding reinforcement in concrete structures. *Transport and Road Research Laboratory Application Guide AG9*, TRRL, 1991.
- 146 Half-cell potential inspection technique for steel in concrete. *Concrete Society Current Practice Guide No 120*, July/August 2000, p. 43-45.
- 147 KRIVAN, L. Meaning and measurement of corrosion potential. *British Corrosion Journal*, 1991, vol. 26, no.3, p. 191-104
- 148 LORENTZ, T. and FRENCH, C. Corrosion of reinforcing steel in concrete: Effect of materials mix composition and cracking. *ACI Materials Journal*, March/April 1995, p. 181-189.

- 149 CARASSITI, F., PROERBO, E. and VALENTE, T. Corrosion state evaluation of steel in concrete by resistivity and polarisation measurement. *Materials Science Forum*, 1992, vol. 111-112, p. 647-658.
- 150 ELSENER, B. and BOHNI, H. Electrochemical methods for the inspection of reinforcement corrosion in concrete structures - Field experience. *Materials Science Forum*, 1992, vol. 111-112, p. 635-646.
- 151 GONI, S., ANDRADE, C. and PAGE, C.L. Corrosion behaviour of steel in high alumina cement mortar samples: Effect of chloride, *Cement and Concrete Research*, 1991, vol. 21, no.4, p. 635-646.
- 152 CIGNA, R., PROVERBIO, E. and ROCCHINI, G. A study of reinforcement behaviour in concrete structure using electrochemical techniques. *Corrosion Science*, 1993, vol. 35, no.5-8, p. 1579-1584.
- 153 KATWAN, M.J., HODGKIESS, T. and ARTHUR, P.D. Electrochemical noise technique for the prediction of corrosion rate of steel in concrete *Materials and Structures*, 29 June 1996, p. 286-294.
- 154 HARDON, R.G., LAMBERT, P. and PAGE C.L. Relationship between electrochemical noise and corrosion rate of steel in salt contaminated concrete. *British Corrosion Journal*, 1988, vol. 23, no.4, p. 225-228.
- 155 CIGNA, R., GARCIA, O., ROCCHINI, G. and BROGLIA, M. Use of polarisation curves in the study of the corrosion mechanism of the steel in concrete. *Materials Science Forum*, 1992, vol. 111-112, p. 667-688.
- 156 GONZALEZ, J.A., FELIU, S., RODRIGUEZ, P., LOPEZ, W., RAMIREZ, E., ALONSO, C. and ANDRADE, C. Some questions on the corrosion of steel in concrete. Part II Corrosion mechanism and monitoring service life prediction and protection methods. *Materials and Structures*, March 1996, vol 29, p. 97-104.
- 157 VIDEM, K. and MYRDAL, R. Electrochemical Behaviour of steel in concrete and evaluation of the corrosion rate. *Corrosion*, 1997, vol. 53, no.9, p. 734-742.
- 158 RODRIGUEZ, J., ORTEGA, L.M. and GARCIA, A.M. On-site corrosion measurements in concrete structures. *Construction Repair*, November/December 1995, p. 27-30
- 159 GOWERS, K.R., MILLARD, S.G., GILL, J.S. and GILL, R.P. Programmable linear polarisation meter for determination of corrosion rate of reinforcement in concrete structures. *British Corrosion Journal*, 1994, vol. 29, no.1, p. 25-32

- 160 CARASSITI, F., PROVERBIO, E. and VALENTE T. Corrosion state evaluation of steel in concrete by resistivity and polarisation resistance measurement. *Materials Science Forum*, 1992, vol. 111-112, p. 647-658.
- 161 NEWHOUSE, W. Time to corrosion cracking. *Techniques to Assess the Corrosion Activity of Steel Reinforced Concrete Structures ASTM STP 1276*, Publisher ASTM, Editor Berke, N.S. Escalante, E. Nmai, C.K. Whiting, D., 1996, p. 4-22.
- 162 ANDRADE, C., MACIAS, A., FELIU, S., ESCUDERO, M.L. and GONZALEZ, J.A. Quantitative measurement of the corrosion rate using a small counter electrode in the boundary of passive and corroded zones of a long concrete beam. *Techniques to Assess the Corrosion Activity of Steel Reinforced Concrete Structures ASTM STP 1276*, Publisher ASTM, Editor Berke, N.S. Escalante, E. Nmai, C.K. Whiting, D., 1996, p. 134-142
- 163 Mansfeld, F. Bertocci, U., Electrochemical corrosion testing: a symposium sponsored by ASTM committee G1 on Corrosion of Metals, *ASTM*, San Francisco, 21 -23 May, 1979
- 164 GONZALEZ, J.A., MOLINA, A., ESCUDERO, M.L. and ANDRADE, C. Errors in the electrochemical evaluation of very small corrosion rates - 1. Polarization resistance method applied to corrosion of steel in concrete. *Corrosion Science*, 1985, vol. 25, no.10, p. 917-930.
- 165 FLIS, J., PICKERING, H.W. and OSSEO-ASARE, K. Assessment of data from three electrochemical instruments for evaluation of reinforcement corrosion rates in concrete bridge components, *Corrosion*, August 1995, vol 51, No 8, p. 602-609.
- 166 SAGUES, A.A. and KRANE, S.C. Computer modelling of corrosion macrocells on measurement of corrosion rate of reinforcing steel in concrete. *Corrosion of Steel in Structures ASTM*, 1996, p. 58-73.
- 167 BERKE, N.S., SHEN, D.F. and SUNDBERG, K.M. Comparison of the polarization resistance technique to the macrocell corrosion technique. *Corrosion Rates of Steel in Concrete ASTM*, 1996, p. 38-51.
- 168 ELSENER, B., WOJTAS, H. and BOHNI, H. Inspection and monitoring of reinforced concrete structures - Electrochemical methods to detect corrosion. *Non-Destructive Testing in Civil Engineering*, Publisher: British Inst of NDT, Editor: Bungey, J.H., 1993, vol. 2, p. 579-596.
- 169 HOLZE, R. Electrode impedance measurements a versatile tool for electrochemists. *Bulletin of Electrochemistry*, 1994, vol. 10, no.1, p. 56-67.

- 170 MANSFELD, F. Evaluation of corrosion protection methods with electrochemical impedance spectroscopy. *Corrosion* 87, NACE, 1987, vol. 481.
- 171 WALTER, G.W. A review of impedance plot methods used for corrosion performance analysis of painted metals. *Corrosion Science*, 1986, vol. 26, no.9, p. 681-703.
- 172 HLADKY K. CALLOW L.M. and DAWSON, J.L. Corrosion rates from impedance measurements an introduction. *British Corrosion Journal*, 1980, vol. 15, no.1, p. 20-25.
- 173 LEMOINE, L., WEGER, F. and GALLAND, J. Study of the corrosion of concrete reinforcement by electrochemical impedance measurement. *Corrosion rates of steel in concrete*, ASTM STP 1065, 1990, p. 118-133.
- 174 HACHANI, L., FIAUD, C., TRIKI, E. and RAHARINAIVO, A. Characterisation of steel/concrete interface by electrochemical impedance spectroscopy. *British Corrosion Journal*, 1994, vol. 29, no.2, p. 122-127.
- 175 PECH-CANUL, M.A., SAGUES, A.A. and CASTRO, P. Influence of counter electrode positioning on solution resistance in impedance measurements of reinforced concrete. *Corrosion*, 1998, vol. 54, no.8, p. 663-667.
- 176 COVERDALE, R.T., CHRISTENSEN, B. J., JENNINGS, H.M., MASON, T. O., BENTZ, D.P. and GARBOCZI E.J Interpretation of impedance spectroscopy of cement paste via computer modelling. *Journal of Materials Science*, 1995, vol. 30, p. 712-719.
- 177 COVERDALE, R.T., CHRISTENSEN, B.J., MASON, T. O., JENNINGS, H.M. and GARBOCZI, E.J. Interpretation of the impedance spectroscopy of cement paste via computer modelling Part II Dielectric response. *Journal of Materials Science*, 1994, vol. 29, p. 4984-4992.
- 178 GU, P. and BEAUDOIN, J.J. Estimation of steel corrosion rate in reinforced concrete by means of equivalent circuit fittings of impedance spectra. *Advances in Cement Research*, 1998, vol. 10, no.2, p. 43-56.
- 179 BRANTERVIK, K. and NIKLASSON, G.A. Circuit models for cement based materials obtained from impedance spectroscopy. *Cement and Concrete Research*, 1991, vol. 21, p. 496-508.
- 180 SAGOE-CRENTSIL, K.K., GLASSER, F.P. and IRVINE, J.T.S. Impedance Spectroscopy characteristics of reinforced concrete. *British Corrosion Journal*, 1992, vol. 27, no.2, p. 113-118.

- 181 JOHN, D.G., COOTE, AT., TREADAWAY, K.W.J. and DAWSON, J.L. The repair of concrete - A laboratory and exposure site investigation. *Corrosion of Reinforcement in Concrete Construction*. Publisher: Ellis Horwood, Editor: Crane A.P, 1983, p. 263-286.
- 182 LEE, S.L., WONG, S.F., SWADDIWUDHIPOG, S., WEE, T.H. and LOO, Y.H. Accelerated test of ingress of chloride ions in concrete under pressure and concentration gradients. *Magazine of Concrete Research*, 1996, vol. 48, no.174, p. 15-25.
- 183 MATSUOKA, K., KIHIRA, H., ITO, S. and MURATA, T. Corrosion monitoring for reinforcing bars in concrete. *Techniques to Assess the Corrosion Activity of Steel Reinforced Concrete Structures ASTM STP 1276*, Publisher ASTM, Editor Berke, N.S. Escalante, E. Nmai, C.K. Whiting, D., 1996, p. 103-117.
- 184 AGUILAR, A., SAGUES, A.A., and POWERS, R.G. Corrosion measurements of reinforcing steel in partially submerged concrete slabs. *Corrosion Rates of Steel in Concrete ASTM STP 1065*, publisher ASTM, 1990, p. 67-85.
- 185 DUNSTER, A.M., BIGLAND, D.J., HOLLINSHEAD, K. and CRAMMOND, N.J. Studies of carbonation and reinforcement corrosion in high alumina cement concrete. *Corrosion of Reinforcement in Concrete Construction*, Publisher: SCI, Editor: Page, C.L. Bamforth, P.B. and Figg, J.W., 1996, vol. 191-199.
- 186 GOWERS, K.R., MILLARD, S.G. and BUNGEY, J.H. The influence of environmental conditions upon the measurement of concrete resistivity for the Assessment of corrosion durability. *Non-Destructive Testing in Civil Engineering*, Publisher: British Inst of NDT, Editor: Bungey, J.H., 1993, vol. 2, p. 633-660.
- 187 FELIU, S., ANDRADE, C., GONZALEZ, J.A. and ALONSO, C.A new method for in-situ measurement of electrical resistivity of reinforced concrete. *Materials and Structures*, July 1996, vol. 29, p. 362-365.
- 188 BURCHLER, D., ELSENER, B. and BOHNI, H. Electrical resistivity and dielectric properties of hardened cement paste and mortar. *Corrosion of Reinforcement in Concrete Construction*, Publisher: SCI, Editor: Page, C.L. Bamforth, P.B. and Figg, J.W., 1996, p. 283-293.
- 189 FIORE, S., POLDER, R.B. and CIGNA, R Evaluation of the concrete corrosivity by means of resistivity measurements. *Corrosion of Reinforcement in Concrete Construction*, Publisher: SCI, Editor: Page, C.L. Bamforth, P.B. and Figg, J.W., 1996, p. 273-282
- 190 McCARTER, W.J., EMERSON, M. and EZIRIM, H. Properties of concrete in the cover zone: development in monitoring techniques. *Magazine of Concrete Research*, 1995, vol. 47, no.172, p. 243-251

- 191 HUNKELER, F. The resistivity of pore water solution - a decisive parameter of rebar corrosion and repair methods. *Construction and Building Materials*, 1996, vol. 10, no.5, p. 381-389.
- 192 RODRIGUEZ, P. and GONZALEZ, J.A. Use of the coulometric method for measuring corrosion rates of embedded metal in concrete. *Magazine of Concrete Research*, 1994, vol. 46, no.167, p. 91-97.
- 193 GLASS, G.K., PAGE, C.L., SHORT, N.R. and YU S. W. An investigation of galvanostatic transient methods used to monitor the corrosion rate of steel in concrete. *Corrosion Science*, 1993, vol. 35, no.5-8, p. 1585-1592.
- 194 MESZAROS, L., MESZAROS, G. and LENGYEL, B. Application of harmonic analysis in the measuring technique of corrosion. *Journal of the Electrochemical Society*, 1994, vol. 141, no.8, p. 2068-2071.
- 195 SATHIYANARAYANAN, S. and BALAKRISHNAN, K. Critique of harmonic analysis for corrosion rate measurement. *British Corrosion Journal*, 1994, vol. 29, no.2, p. 152-155
- 196 GONZALEZ, J.A. MOLINA A. ESCUDERO M.L. and ANDRADE C. Errors in the electrochemical evaluation of very small corrosion rates - II. Other electrochemical techniques applied to corrosion of steel in concrete. *Corrosion Science*, 1985, vol. 25, no.7, p. 519-530.
- 197 BERTHIER, F., DIARD, J.P., Le GORREC, B. and MONTELLA, C. Method for determining the Faradaic impedance of an electrode reaction: Application to metal corrosion rate measurements. *Corrosion*, 1995, vol. 51, no.2, p. 105-115.
- 198 GULIKERS, J.J.W. and Van MIER, J.G.M. The influence of patch repairs on corrosion of carbonated reinforced concrete. *Non-Destructive Testing in Civil Engineering*, Publisher: British Inst of NDT, Editor: Bungey, J.H., 1993, vol. 2, p. 719-740.
- 199 GONZALEZ, J.A., BENITO, M., FELIU, S., RODRIGUEZ P. and ANDRADE C. Suitability of Assessment methods for identifying active and passive zones in reinforced concrete, *Corrosion*, 1985, vol. 51, no.2, p. 145-152.
- 200 MILLARD, S.G., GHASSEMI, M.H., BUNGEY, J.H. and JAFAR, M.I. Assessing the electrical resistivity of concrete structures for corrosion durability studies. *Corrosion of reinforcement in concrete*, Publisher: Elsevier Applied Science, Editor: Page, C.L. Traedaway, K.W.J. and Bamforth, P.B., 1990, p. 303-313.

- 201 MCCARTER, W.J. A parametric study of the impedance characteristics of cement aggregate systems during early hydration. *Cement and Concrete Research*, 1994, vol. 24, no.6, p. 1097-1110.
- 202 De LEVIE, R. Electrochemical Response of Porous and Rough Electrodes. *Advances in Electrochemistry and Electrochemical Engineering*, 1996, p. 329-397
- 203 McCARTER, W.J. and EZIRIM, H.A.C. Impedance profiling within cover zone concrete: influence of water and ionic ingress. *Advances in Cement Research*, 1998, vol. 10, no.2, p. 57-66.
- 204 SUDA, K., MISRA S. and MOTOHASHI, K. Corrosion products of reinforcing bars embedded in concrete. *Corrosion Science*, 1993, vol. 35, no.5-8, p. 1543-1549.
- 205 MacQUEEN, R.C., MIRON, R.R. and GRANATA, D. Method for corrosion inhibitor mechanism studies in epoxy coated aluminium. *Journal of Coatings Technology*, 1996, vol. 68, no.857, p. 75-82.
- 206 ENOS, D.G., WILLIAMS, A.J. and SCULLY, J.R. Long-term effects of cathodic protection on prestressed concrete structures: Embrittlement of prestressing steel. *Corrosion*, 1997, vol. 53, no.11, p. 891-908.
- 207 GONZALEZ, J.A., FELIU S., RODRIGUEZ, P., RAMIREZ, E., ALONSO, C. and ANDRADE, C. Some questions on the corrosion of steel in concrete - Part 1: When how and how much steel corrodes. *Materials and Structures*, 1996, vol. 29, p. 40-46
- 208 BROUSSEAU, R., ARNOTT, M. and BALDOCK, B. Laboratory performance of zinc anodes for impressed current cathodic protection of reinforced concrete. *Corrosion*, 1995, vol. 51, no.8, p. 639-644.
- 209 NAGATAKI, S., NOBUASKI, O., TIONG-HUAN, W. and NAKASHITA, K. Condensation of chloride ion in hardened cement matrix materials and on embedded steel bars. *ACI Materials Journal*, July-August 1993, vol 90, No 4, p. 323-332.
- 210 KHATIB, J.M. and MANGAT, P.S. Absorption characteristics of concrete as a function of location relative to casting position, *Cement and Concrete Research*, 1995, vol. 25, no.5, p. 999-1010.
- 211 CASTRO, P., MALDONADO, L. and DeCOSS, R. Study of chloride diffusion as a corrosive agent in reinforced concrete for tropical marine environment. *Corrosion Science*, 1993, vol. 35, no.5-8, p. 1557-1562.

- 212 PAPADAKIS, V.G., VAYENAS, C.G. and FARDIS, M.N. Fundamental modelling and experimental investigation of concrete carbonation. *ACI Materials Journal*, July-August 1991, p. 363-373
- 213 CHATTERJI, S. Transportation of ions through cement based materials. Part 2. Adaptation of the fundamental equations and relevant comments. *Cement and Concrete Research*, 1994, vol. 24, no.6, p. 1010-1014
- 214 PING GU, BEAUDOIN, J.J. and BROUSSEAU, R. Flat aggregate Portland cement paste interfaces 1. Electrical conductivity models. *Cement and Concrete Research*, 1991, vol. 21, p. 515-522.
- 215 TULLMIN, M.A.A., HANSSON, CM and ROBERGE, P.R. Electrochemical techniques for measuring reinforcing steel corrosion, <http://www.intercorr.com>, 1997.
- 216 SHIESSL, P. and RAUPACH, M. Non-Destructive Permanent Monitoring of the Corrosion risk of concrete. *Non-Destructive Testing in Civil Engineering*, Publisher: British Inst of NDT, Editor: Bungey, J.H., 1993, vol. 2, p. 661-674.
- 217 CHANG, T.P., HWANG, C.L., LIN, C.Y. and CHIOU, I.C. Evaluation of concrete cracking on the corrosion rate for steel reinforcement by AC impedance method. *Non-Destructive Testing in Civil Engineering*, Publisher: British Inst of NDT, Editor: Bungey, J.H., 1993, vol 2, p. 675-696.
- 218 DHIR, R.K., JONES, M.R. and NG, S.L.D. Prediction of total chloride content profile and concentration/time dependent diffusion coefficients for concrete. *Magazine of Concrete Research*, 1998, vol. 501, p. 37-48.
- 219 WILKINS, N.J.M. and SHARP, J.V. Localised corrosion of reinforcement in marine concrete. Corrosion of reinforcement in concrete. *Corrosion of reinforcement in concrete*, Publisher: Elsevier Applied Science, Editor: Page, C.L. Treadaway, K.W.J. and Bamforth, P.B., 1990, p. 3-18.
- 220 SCHIESSL, P. and RAUPACH, M. Influence of concrete composition and microclimate on critical chloride composition. *Corrosion of reinforcement in concrete*, Publisher: Elsevier Applied Science, Editor: Page, C.L. Treadaway, K.W.J. and Bamforth, P.B., 1990, p. 49-58.
- 221 SAGOE-CRENTSIL, K.K. and GLASSER, F.P. Analysis of the steel: Concrete interface. *Corrosion of reinforcement in concrete*, Publisher: Elsevier Applied Science, Editor: Page, C.L. Treadaway, K.W.J. and Bamforth, P.B., 1990, p. 74-85.

- 222 BAMFORTH, P.B. and POCOCK, D.C. Minimising the risk of chloride induced corrosion by selection of concreting materials. *Corrosion of reinforcement in concrete*, Publisher: Elsevier Applied Science, Editor: Page, C.L. Treadaway, K.W.J. and Bamforth, P.B., 1990, p. 119-131.
- 223 RENDELL, F. and MILLER, W. Macrocell corrosion of reinforcement in marine structures. *Corrosion of reinforcement in concrete*, Publisher: Elsevier Applied Science, Editor: Page, C.L. Treadaway, K.W.J. and Bamforth, P.B., 1990, p. 167-177.
- 224 THOMAS, M.D.A., MATTHEWS, J.D. and HAYNES, C.A. Effect of cement composition on corrosion of reinforcing steel in concrete. *Corrosion of reinforcement in concrete*, Publisher: Elsevier Applied Science, Editor: Page, C.L. Treadaway, K.W.J. and Bamforth, P.B., 1990, p. 213-226.
- 225 RASHEEDUZZAFAR AL-SAADOUN, S.S., DAKHIL, F.H. and AL-GAHTANI, A.S. The influence of pfa on proportion of free chlorides in salt contaminated concrete. *Corrosion of reinforcement in concrete*, Publisher: Elsevier Applied Science, Editor: Page, C.L. Treadaway, K.W.J. and Bamforth, P.B., 1990, p. 227-236.
- 226 Van Der WEGEN, G. and BIJEN, J. Diffusion of various ions from sea water into polymer modified cement paste. *Corrosion of reinforcement in concrete*, Publisher: Elsevier Applied Science, Editor: Page, C.L. Treadaway, K.W.J. and Bamforth, P.B., 1990, p. 246-257.
- 227 ANDRADE, C., SARRIA, J. and ALONSO, C. Statistical study on simultaneous monitoring of rebar corrosion rate and internal humidity in concrete structures exposed to the atmosphere. *Corrosion of Reinforcement in Concrete Construction*, Publisher: SCI, Editor: Page, C.L. Bamforth, P.B. and Figg, J.W., 1996, p. 233-242.
- 228 HAWKINS, C. and MCKENZIE, M. Environmental effects on reinforcement corrosion rates. *Corrosion of Reinforcement in Concrete Construction*, Publisher: SCI, Editor: Page, C.L. Bamforth, P.B. and Figg, J.W., 1996, p. 166-175.
- 229 ANDRADE, C., SARRIA, J. and ALONSO, C. Statistical study on simultaneous monitoring of rebar corrosion rate and internal relative humidity in concrete structures exposed to the atmosphere. *Corrosion of Reinforcement in Concrete Construction*, Publisher: SCI, Editor: Page, C.L. Bamforth, P.B. and Figg, J.W., p. 233-242.
- 230 GU, P., FU, F., XIE, P. and BEAUDOIN, J.J. Effect of uneven porosity distribution in cement paste and mortar on reinforcing steel corrosion. *Cement and Concrete Research*, 1994, vol. 24, no.6, p. 1055-1064.

- 231 SCHIESSL, P. Durability of reinforced concrete structures. *Construction and Building Materials*, 1996, vol. 10, no.5, p. 289-292.
- 232 ESTES, A.C. and FRANGOPOL, D.M. Lifetime repair optimisation of highway bridges based on system reliability and cost. *Buildings to Last - Proc. Structures Congress XV APR 13-16 Portland Oregon*, ASCE, 1997, p. 243-247
- 233 MORGAN, D.R. Compatibility of concrete repair materials and systems, *Construction and Building Materials*, 1996, vol. 10, no.1, p. 57-67.
- 234 MOUKWA, M., YOUN, D. and HASSSANALI, M. Effects of degree of polymerisation of water soluble polymers on concrete properties. *Cement and Concrete Research*, 1993, vol. 23, p. 122-130
- 235 ARMSTRONG, R.D., BELL, M.F. and METCALFE, A.A. The ac impedance of complex electrochemical reactions. *Electrochemistry*, Chemical Society, 1976, p. 98-127.
- 236 FORD, S.J. and MASON, T.O. Combined bulk and interfacial studies of the cement steel system by impedance spectroscopy. *Techniques to Assess the corrosion activity of steel reinforced concrete structures*, Publisher: ASTM, Editor: Berke, S., Escalante, E., Nmai, K. and Whiting, D., 1996, p. 147-155.
- 237 DHIR, R.K. and JONES, R.M. Influence of PFA on proportion of free chlorides in salt contaminated concrete. *Corrosion of reinforcement in concrete*, Publisher: Elsevier Applied Science, Editor: Page, C.L. Treadaway, K.W.J. and Bamforth, P.B., 1990, p. 227-236.
- 238 ABRAMOWITZ, M. and STEGUN, I.D., Handbook of mathematical functions with formulas, graphs and mathematical tables, National Bureau of Standards, 1972
- 239 VANAKEN, D., Engineering Concepts: The Error Function and Carburization. www.Industrialheating.com, 2000